Univerzita Karlova

2. lékařská fakulta

Doktorský studijní program: Biochemie a patobiochemie

Mgr. Monika Zouharová

Studium vazebných partnerů a modulace funkčních vlastností kalmodulinu
a jeho fúzních proteinových variant

Study of binding partners and modulation of calmodulin functional properties
and its fusion protein variants

Disertační práce

Školitel: RNDr. Kristýna Boušová, Ph.D.

Praha, 2024

Prohlášení:

Prohlašuji, že jsem závěrečnou práci zpracovala samostatně a že jsem řádně uvedla a citovala všechny použité prameny a literaturu. Současně prohlašuji, že práce nebyla využita k získání jiného nebo stejného titulu.

Souhlasím s trvalým uložením elektronické verze mé práce v databázi systému meziuniverzitního projektu Theses.cz za účelem soustavné kontroly podobnosti kvalifikačních prací.

V Praze, 27. 5. 2024

Monika Zouharová

………………………………………

Poděkování:

Na tomto místě bych ráda poděkovala své školitelce RNDr. Kristýně Boušové, Ph.D. za odborné vedení, motivaci a všestrannou podporu v průběhu mého doktorského studia. Velké poděkování patří prof. RNDr. Jiřímu Vondráškovi, CSc. za četné odborné konzultace a aktivní zapojení do rozvoje studované tématiky a Ing. Janu Teisingerovi, CSc. za laskavé vedení a početné odborné diskuze v počátcích mého doktorského studia. Dále děkuji všem spoluautorům publikací, na jejichž podkladě byla disertační práce sepsána, i celému kolektivu skupiny Bioinformatika z Ústavu Organické Chemie a Biochemie AV ČR za vytvoření motivujícího a přátelského pracovního prostředí. V neposlední řadě děkuji své rodině, která mě všestranně podporovala v průběhu celého studia.

Studium vazebných partnerů a modulace funkčních vlastností kalmodulinu a jeho fúzních proteinových variant

Abstrakt

Disertační práce se zabývá studiem kalmodulin (CaM) - dependentní modulace podrodiny iontových kanálů TRPM, zapojených do patogeneze kardiovaskulárních, neurodegenerativních či nádorových chorob. Celkem bylo na iontových kanálech TRPM4, TRPM5, TRPM6 a TRPM7 detailně charakterizováno pět nových vazebných epitopů pro CaM. Výsledky molekulového modelování a dokování prokázaly dobrou přístupnost vazebných epitopů pro interakci s CaM. Formace komplexů s CaM byla podmíněna přítomností bazických reziduí, typických pro nekovalentní interakce CaM s iontovými kanály rodiny TRP. V případě TRPM5, TRPM6 a TRPM7 se jedná o první studie poukazující na potencionální modulaci kanálů prostřednictvím CaM. CaM byl dále studován s ohledem na možnou optimalizaci vlastností molekuly v rámci fúzních proteinových konstruktů. Spojením CaM s vnitřně neuspořádanou C-koncovou doménou proteinu ameloblastinu (AMBN-Ct) byla získána inovativní fúzní molekula CaM/AMBN-Ct. Spektroskopie cirkulárního dichroismu (CD) a vazebné studie prokázali zachování požadovaných strukturně-funkčních vlastností CaM v CaM/AMBN-Ct. Výsledky sedimentačních analýz i spektroskopie CD poukázaly na komunikaci fúzních partnerů. Vzájemné kontakty mezi CaM a AMBN-Ct ve fúzní molekule vedly k signifikantnímu navýšení teplotní stability CaM. Fúzní konstrukt CaM/AMBN-Ct tak může být základem designu stabilnějších biomedicínsky/biotechnologicky využitelných molekul založených na unikátních vlastnostech molekuly CaM.

Klíčová slova

Ameloblastin, fúzní proteiny, iontové kanály TRPM, kalmodulin, proteinové inženýrství, vnitřně neuspořádané proteiny

Study of binding partners and modulation of calmodulin functional properties and its fusion protein variants

Abstract

The thesis studies calmodulin (CaM)-dependent modulation of the TRPM ion channel subfamily involved in the pathogenesis of cardiovascular, neurodegenerative diseases or cancer. In total, 5 new CaM-binding epitopes were characterized in detail in TRPM4, TRPM5, TRPM6, and TRPM7. The results of molecular modeling and docking showed good accessibility of the binding epitopes for an interaction with CaM. The presence of basic residues, typical for non-covalent CaM interactions with TRP, was required for the formation of complexes with CaM. As regards TRPM5, TRPM6, and TRPM7, this is the first study that indicates their potential modulation by CaM. Furthermore, CaM was studied in terms of possible optimization of the properties of the molecule in fusion protein constructs. The innovative fusion molecule CaM/AMBN-Ct was obtained by fusing CaM and an intrinsically disordered C-terminal domain of ameloblastin (AMBN-Ct). As shown by circular dichroism (CD) spectroscopy and binding studies, the required structural and functional properties of CaM are preserved in CaM/AMBN-Ct. The results of sedimentation analyses and CD spectroscopy indicated communication between the fusion partners. Mutual contacts between CaM and AMBN-Ct in the fusion molecule resulted in a significant increase in thermal stability of CaM. The CaM/AMBN-Ct fusion construct thus may be used for the design of more stable molecules based on unique CaM properties, for biomedical and biotechnological applications.

Keywords

Ameloblastin, calmodulin, fusion proteins, intrinsically disordered proteins, protein engineering, TRPM ion channels

Seznam použitých zkratek

|	
AMBN	Ameloblastin
AMBN-Ct	C-koncová doména ameloblastinu
AMPs	Antimikrobiální peptidy
ASEC	Analytická gelová chromatografie
CaM	Kalmodulin
CaM/AMBN-Ct	Fúzní protein tvořený kalmodulinem a C-koncovou doménou ameloblastinu
CD	Cirkulární dichroismus
GFP	Zelený fluorescenční protein
F_B	Podíl vazebných epitopů v interakci
Fc	Konstantní oblast imunoglubulinu
FDA	Dozorový orgán federální vlády USA pro potraviny a léčiva, z angl. Food and Drug Administration
FRET	Försterovův rezonanční přenos energie
IDP	Vnitřně neuspořádaný protein
IDPRs	Proteiny s rozsáhlými vnitřně neuspořádanými oblastmi
K_D	Rovnovážná disociační konstanta
MHR	Melastatinové homologní oblasti
Mw	Molekulová hmotnost
PIP2	Fosfatidylinositol-4,5-bisfosfát
PIRT	Regulátor TRP kanálů interagující s fosfoinositidy
$S_{20,w}$	sedimentačních koeficient přepočítaný na standardní podmínky (20 °C, čistá voda)
Tm	Teplota tání proteinu
TNF-α	Tumor nekrotizující factor α
TRP	Rodina iontových kanálů "transient receptor potential"
TRPM	Podrodina iontových kanálů "transient receptor potential melastatin"
TRPV	Podrodina iontových kanálů "transient receptor potential vanilloid"

OBSAH

1. ÚVOD

1.1. Kalmodulin

1.1.1. Obecná charakteristika

Kalmodulin (CaM) je malý (16,7 kDa) intracelulární protein přítomný ve všech eukaryotických buňkách. Klíčovou funkcí molekuly CaM je monitoring změn koncentrace volných vápenatých iontů uvnitř buňky a následná regulace rozličných komponent signálních drah zapojených do řízení proliferace, diferenciace, apoptózy či autofagie (Berchtold and Villalobo, 2014). Modulace esenciálních buněčných procesů je spjata s enormní evoluční konzervovaností CaM v rámci celé linie obratlovců (Halling et al., 2016). Lidský genom obsahuje tři neidentické geny *CALM 1-3* s odlišnými 5′ a 3′ nepřekládanými regulačními oblastmi, kódující totožný protein CaM (Fischer et al., 1988). CaM je klíčovým regulátorem řady kardiomyocytárních iontových kanálů, jako jsou kalciové kanály typu L, sodíkové a draslíkové kanály nebo Ryanodinové receptory (Ben-Johny et al., 2015). Mutace v jediném ze tří genů *CALM*, měnící aminokyselinou sekvenci nebo regulaci exprese CaM, může vést k závažným kongenitálním srdečním onemocněním, souhrnně označovaným jako kalmodulinopatie (Crotti et al., 2019, Friedrich et al., 2009). Mutace postihující CaM jsou vzhledem k silnému selekčnímu tlaku proti změnám v proteinové sekvenci velmi vzácné a potenciální souvislost s jinými než srdečními patologiemi je předmětem budoucího výzkumu (Jensen et al., 2018).

Molekula CaM tvoří α-helikální protein o celkové délce 148 aminokyselin. Jeho N- i C-koncová globulární doména obsahuje vždy 2 motivy tzv. EF-ruky, zajišťující interakci s ionty Ca^{2+} (**Obr. 1 A-B**) (Barbato et al., 1992, Kuboniwa et al., 1995). Motiv EF-ruky tvoří dva α-helixy spojené krátkou acidickou smyčkou o délce 12 aminokyselin (Biekofsky et al., 1998). Atomy kyslíku potřebné pro vazbu iontů Ca^{2+} typicky poskytují postranní řetězce reziduí 1, 3, 5 a 12 společně s karbonylovou skupinou peptidového řetězce rezidua 7 (Kretsinger and Nockolds, 1973). Globulární domény CaM jsou odděleny vysoce flexibilním linkerem o délce 26 reziduí (Barbato et al., 1992). V průběhu vazby Ca^{2+} probíhá reorientace α-helixů v motivu EF-ruky a dochází k vystavení hydrofobních motivů pro interakci s cílovými proteiny na povrch molekuly CaM (**Obr. 1 A-B**).
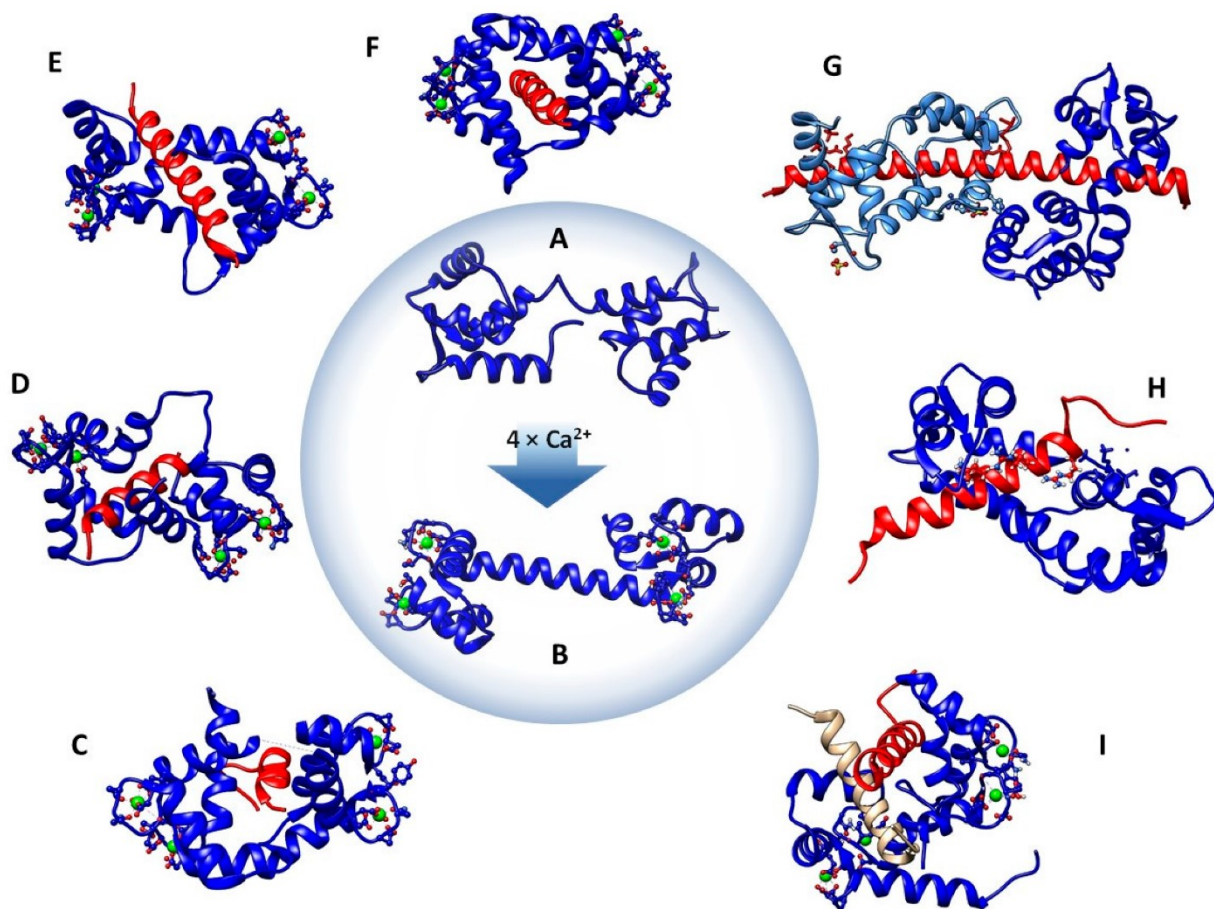
Obr. 1: Konformační plasticita molekuly CaM, převzato z (Andrews et al., 2020). (**A**) Molekula CaM (modře) v prostředí bez Ca^{2+}, <u>PDB:</u> 1cfd. (**B**) CaM s navázanými ionty Ca^{2+} (zeleně), <u>PDB:</u> 4bw8. (**C**) Komplex CaM/Ca^{2+}/epitop MARCKS (myristoylated alanine-rich C-kinase substrat): N-koncová doména CaM se neúčastní interakce, <u>PDB:</u> 1iwq. (**D**) Komplex CaM/Ca^{2+}/epitop CaMKIIα: kompaktní molekula CaM s vazebným módem 1-5-10, <u>PDB:</u> 1cm1. (**E**) Komplex CaM/Ca^{2+}/epitop RyR1: kompaktní molekula CaM s netypickým vazebným módem 1-17, <u>PDB:</u> 2bcx. (**F**) Komplex CaM/Ca^{2+}/epitop kinázy lehkého řetězce myozinu, <u>PDB:</u> 1cdl. (**G**) CaM/epitop myosinu V: vazebná stechiometrie 2:1, <u>PDB:</u> 2ix7. (**H**) CaM/epitop IQCG (IQ motif containing G) proteinu: protáhlejší molekula CaM, <u>PDB:</u> 4lzx. (**I**) CaM/Ca^{2+}/epitopy řetězce B a C dekarboxylázy glutamátu, <u>PDB:</u> 1nwd.

1.1.2. Vazebné vlastnosti

Interakce s CaM byla popsaná u více než tří set různých proteinů (Sorensen et al., 2013). Enormní spektrum jeho vazebných partnerů může být dáno (1) vysokou flexibilitou molekuly CaM, umožňující ustavení preferovaného vazebného módu, či (2) odlišnou vazebnou afinitou jednotlivých motivů EF-ruky k iontům Ca^{2+}, podmiňující existenci různých konformačních stavů CaM v závislosti na aktuální koncentraci Ca^{2+} (Liu et al., 2017, Liu et al., 2019b). Extrémní konformační plasticitu molekuly CaM dokumentuje široký rozptyl vazebných módů (**Obr. 1 C-I**), zahrnující vysoce kompaktní konformace CaM s globulárními doménami v těsné blízkosti i natažené konformace, kdy globulární domény atakují vzdálenější vazebné oblasti (Fallon and Quiocho, 2003, Johnson et al., 2018).

Proteinové sekvence vazebných motivů pro CaM se vyznačují diverzitou a neexistuje pro ně pouze jediná snadno identifikovatelná konsenzuální sekvence (Yap et al., 2000). První popsané komplexy CaM s cílovým proteinem byly formovány v závislosti na zvýšení intracelulární koncentrace iontů Ca^{2+}. Přítomnost vazebných epitopů pro komplex CaM/Ca^{2+} je predikována na základě výskytu biochemických a biofyzikálních charakteristik, jako je amfipatický charakter sekvence, obsahující alespoň dva hydrofobní aminokyselinové zbytky s vmezeřenými bazickými rezidui, společně s tendencí k tvorbě α-helikálních struktur (Bahler and Rhoads, 2002). Vazebné epitopy pro CaM jsou na základě pozice klíčových hydrofobních zbytků řazeny do dvou hlavních (1-10, 1-14) a čtyř minoritních (1-3, 1-16,1-17,1-18) skupin (Rhoads and Friedberg, 1997, Grant et al., 2020). Řadu cílových molekul rozpoznává CaM také při klidových intracelulárních koncentracích Ca^{2+} prostřednictvím vazby ke konsenzuální sekvenci IQ motivu (IQXXXRGXXXR) (Rhoads and Friedberg, 1997). Vznik takových komplexů může být podkladem nejen pro regulaci cílových proteinů v nepřítomnosti Ca^{2+}, ale i pro modulaci vazebné dynamiky CaM a iontů Ca^{2+} (Putkey et al., 2003). Interakce s IQ motivy cílových proteinů tak mohou posílit citlivost CaM k náhlým a přechodným změnám intracelulární koncentrace Ca^{2+} a vylepšit tak jeho funkci kalciového senzoru.

Vzhledem k vysoké sekvenční diverzitě vazebných epitopů pro CaM může být úspěšnost jejich identifikace v laboratorních podmínkách nejistá a finančně ztrátová. S ohledem na nezastupitelnou roli těchto interakcí v klíčových buněčných procesech probíhá implementace moderních metod strojového učení do predikčních softwarů s cílem rozšířit spektrum popsaných

vazebných epitopů pro CaM (Abbasi et al., 2017, Li et al., 2018, Andrews et al., 2020). Regulace prostřednictvím interakcí s CaM byla popsána u řady různorodých cytoplazmatických i transmembránových proteinů, jako jsou CaM – dependentní fosfatázy a kinázy, neuronální i srdeční napěťově řízené iontové kanály, aquaporinové kanály, ryanodinové receptory či zástupci nejpočetnější rodiny iontových kanálů – transient receptor potential (TRP) kanálů (Liu, 2009, Reddy Chichili et al., 2013, Tan et al., 2002, Nemeth-Cahalan and Hall, 2000, Zalk et al., 2007, Zhu, 2005).

1.2. TRP kanály

Rodina TRP kanálů zahrnuje polymodálně aktivované kationtové kanály integrující exogenní i endogenní stimuly fyzikálního nebo chemického charakteru. Klíčovou roli hrají zejména při nocicepci nebo jako senzory detekující teplo, chlad, sladkou, hořkou nebo umami chuť (Clapham, 2003). Kromě senzorických funkcí zajišťují TRP kanály také synchronizaci procesů imunitní odpovědi nebo osmoregulaci (Khalil et al., 2018, Bessac and Fleig, 2007). Prvním popsaným zástupcem rodiny TRP kanálů byl fotoreceptor rodu *Drosophila* (Minke, 1977). Majorita TRP kanálů má funkci neselektivních kationtových kanálů propustných pro ionty Ca^{2+}. Vzhledem k zásadní roli TRP kanálů v řízení životně důležitého procesu vápníkové homeostázy byly mutace postihující geny pro TRP kanály asociovány s rozvojem řady onemocnění včetně nádorových, kardiovaskulárních, neurodegenerativních, imunitních nebo metabolických poruch (Nilius, 2007).

TRP kanály jsou velmi heterogenní rodinou iontových kanálů s celkovou sekvenční identitou menší než 20 % (Palovcak et al., 2015). Lidské TRP kanály jsou na základě sekvenční homologie děleny do 6 podrodin: TRPC (canonical), TRPV (vanilloid), TRPM (melastatin), TRPML (mucolipin), TRPPP (polycystin) a TRPA (ankyrin) (**Obr. 2**) (Samanta et al., 2018). Nejpočetnější a zároveň nejrůznorodější podrodinou, spojenou s řadou patologických procesů, je podrodina TRPM.
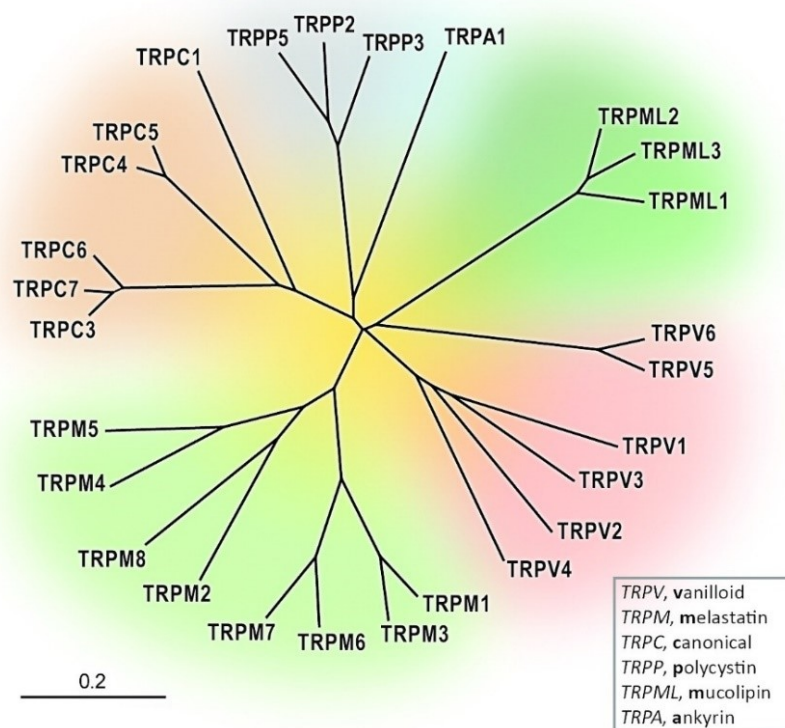
Obr. 2: Fylogenetický strom zástupců lidské rodiny TRP kanálů členěný do šesti podrodin, převzato z (Stoerger and Flockerzi, 2014). Měřítko ukazuje stupeň genetické rozmanitosti v arbitrárních jednotkách. Pseudogen *TRPC2* byl vyloučen z analýzy.

1.2.1. Podrodina TRPM

Podrodinu TRPM tvoří 8 iontových kanálů (TRPM1 až TRPM8), exprimovaných v širokém spektru tkání včetně srdce, plic, ledvin, střev, pankreatu nebo v buňkách imunitního systému (Fonfria et al., 2006, Perraud et al., 2004). Na základě sekvenční homologie jsou členové podrodiny TRPM řazeni do 4 podskupin: TRPM1/TRPM3, TRPM2/TRPM8, TRPM4/TRPM5 a TRPM6/TRPM7 (Harteneck, 2005). Majorita TRPM kanálů má homotetramerní, případně heterotetramerní strukturu, kdy každá podjednotka obsahuje 6 transmembránových segmentů (S1 až S6) a S5 společně s S6 a linkerem S5–S6 tvoří pór iontového kanálu (**Obr. 3**) (Huang et al., 2020). Typickým rysem TRPM kanálů jsou velmi dlouhé N-koncové cytoplazmatické konce, obsahující 4 melastatinové homologní oblasti (MHR 1–4). Cytoplazmatický C-konec je tvořen TRP doménou s klíčovou funkcí v regulaci aktivity

TRP kanálů i tetramerizace jejich podjednotek, následovanou doménou typu coiled-coil, podílející se rovněž na asociaci podjednotek TRPM. (Garcia-Sanz et al., 2007, Rohacs et al., 2005, Tsuruda et al., 2006). U řady členů podrodiny TRPM se dále vyskytuje vysoce variabilní C-koncová doména (CTD). V případě TRM2, TRPM6 a TRPM7 má CTD funkci enzymatickou, přičemž TRPM2 disponuje doménou homologní k mitochondriální pyrofosfatáze adenosindifosfát ribózy a TRPM6 i TRPM7 serin/threonin kinázovou doménou (Perraud et al., 2001, Ryazanova et al., 2001).
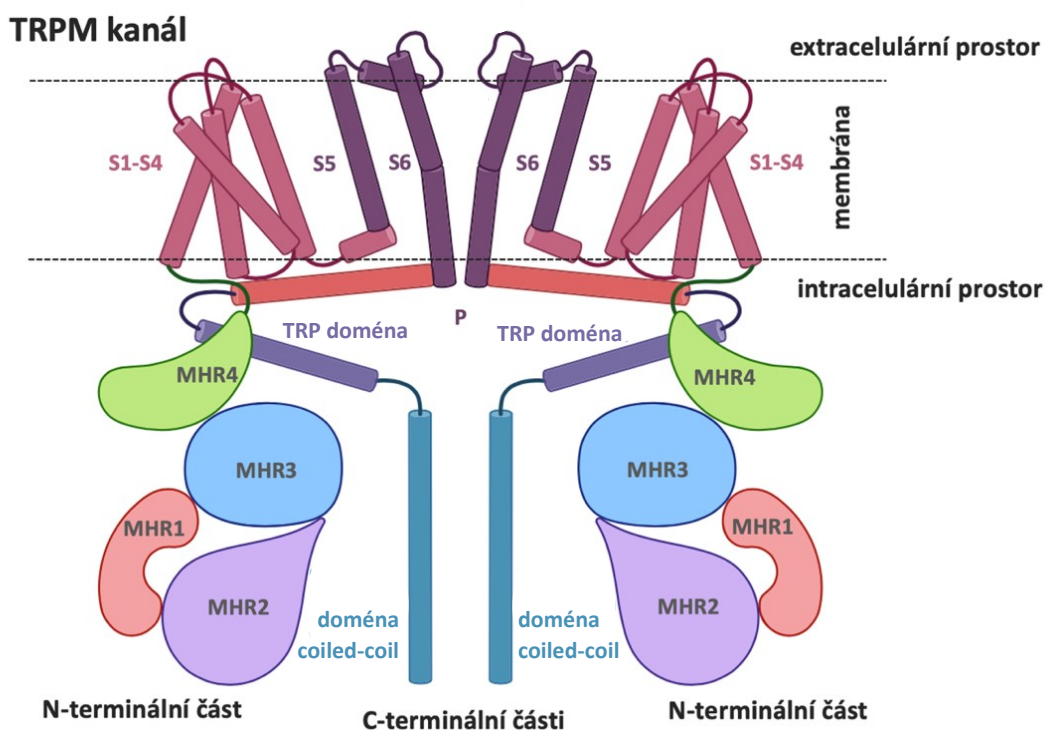
Obr. 3: Membránová topologie dimeru TRPM kanálu, převzato z (Bousova et al., 2021b); upraveno. Intracelulární N-koncová část obsahující MHR 1-4, transmembránová oblast s integrálními α-helikálními segmenty (S1-S6) a kratším helixem v oblasti póru (P) a intracelulární C-koncová část s TRP doménou a doménou typu coiled-colid.

Abnormální exprese nebo aktivace TRPM kanálů má vzhledem k širokému expresnímu profilu podrodiny TRPM enormní patofyziologický dopad (Jimenez et al., 2020). Modulace jejich aktivity představuje významný terapeutický cíl a stává se předmětem intenzivního vývoje nových léčiv. Typickou vlastností podrodiny TRPM je polymodální regulace exogenními i endogenními stimuly včetně tepla (TRPM2, TRPM4, TRPM5), chladu (TRPM8), tlaku (TRPM4), napětí (TRPM8, TRPM4), přítomnosti chemických látek jako mentol, icilin (TRPM8), neurosteroid pregnenolon sulfát (TRPM3) nebo změny pH (Zheng, 2013, Earley et al., 2004, Wagner et al., 2008). Mezi nejrozšířenější modulátory aktivity TRPM kanálů patří oscilace intracelulární koncentrace iontů Ca^{2+} (Hasan and Zhang, 2018). TRPM kanály mohou být regulovány přímou interakcí s Ca^{2+}, avšak ve většině případů je efekt změny hladiny Ca^{2+} zprostředkován proteiny navazujících signálních drah (Vangeel and Voets, 2019). Tímto způsobem dochází zejména k aktivaci fosfolipázy C a štěpení regulační molekuly fosfatidylinositol-4,5-bisfosfátu (PIP2) nebo k aktivaci proteinů vázajících vápník, především molekul CaM. Aktuální výzkumy ukazují zásadní roli CaM v rámci regulace aktivity členů podrodiny TRPM.

1.2.1.1. CaM-dependentní regulace podrodiny TRPM

V rámci celé rodiny TRP kanálů byla popsána pozitivní i negativní modulace zprostředkovaná molekulou CaM (Hasan and Zhang, 2018). Funkcí CaM nemusí být pouze aktivace nebo inhibice daného TRP kanálů, ale může docházet k přepínání mezi aktivačním a inhibičním módem molekuly (Hasan et al., 2017). Na strukturní úrovni byla regulace prostřednictvím CaM popsána v případě TRPV6 (Singh et al., 2018a). V komplexu CaM/TRPV6 interaguje CaM s celkem 6 různými vazebnými oblastmi na TRPV6 a klíčovou roli hraje interakce s ústím iontového póru TRPV6, zprostředkovaná lyzinem (K115) C-terminální domény CaM a tryptofany (W583) podjednotek TRPV6. U podrodiny TRPM byla prokázána přímá regulace molekulou CaM v případě TRPM4 nebo TRPM2, avšak u většiny členů TRPM byly identifikovány vazebné oblasti pro CaM, jejichž funkční význam zbývá ověřit, případně popis vazebných epitopů pro CaM dosud chybí (Nilius et al., 2005, Tong et al., 2006).

V rámci podskupiny TRPM1/TRPM3 poukazují vazebné studie na možnost regulace kanálu TRPM3 prostřednictvím CaM. TRPM3 je teplotně senzitivní nociceptor, podílející se také na regulaci sekrece insulinu v β-buňkách pankreatu (Thiel et al., 2017). Mezi nejznámější aktivátory TRPM3 patří extracelulární neurosteroid pregnenolon sulfát nebo membránový fosfolipid PIP2 (Wagner et al., 2008, Toth et al., 2015). Při aktivaci TRPM3 dochází ke vstupu iontů Ca^{2+} s potenciálem poskytovat negativní zpětnou vazbu (Grimm et al., 2003). U TRPM3 bylo identifikováno 5 různých vazebných epitopů pro CaM, které poukazují na možnost kooperativní vazby CaM (podobně jako v případě CaM/TRPV6) a zapojení CaM do zpětnovazebné regulace TRPM3 (Przibilla et al., 2018, Holakovska et al., 2012, Holendova et al., 2012). Zastoupení jednotlivých vazebných míst pro CaM se mezi různými izoformami TRPM3 liší a může představovat mechanismus zajišťující buněčně/tkáňově specifickou odpověď na změnu hladiny Ca^{2+} (Przibilla et al., 2018).

Regulace aktivity prostřednictvím CaM byla potvrzena u obou zástupců podskupiny TRPM2/TRPM8. TRPM2 je termosenzitivní neselektivní iontový kanál, aktivovaný zejména prostřednictvím adenosindifosfát ribózy v odpověď na oxidativní stres (Miller and Cheung, 2016). Nárůst intracelulární koncentrace Ca^{2+} následně aktivuje CaM k pozitivní zpětnovazebné modulaci TRPM2 (Tong et al., 2006). V rámci TRPM2 byly identifikovány dva fyziologicky významné vazebné epitopy pro CaM. Jeden se nachází na cytoplazmatickém N-konci TRPM2, zatímco druhý je součástí domény podobné nudix hydroláze 9 (NUDT9H) na jeho C-konci (Tong et al., 2006, Gattkowski et al., 2019). Vazebné místo v doméně NUDT9H se stává dostupným pro interakci s CaM v důsledku strukturních změn při zvýšení teploty nad 35 °C a pravděpodobně se podílí na teplotní regulaci TRPM2. Neselektivní iontový kanál TRPM8 naopak umožňuje vnímání chladových podnětů včetně mentolu, eukalyptu nebo kafru (McKemy et al., 2002). Nárůst intracelulární koncentrace Ca^{2+} spouští negativní zpětnovazebnou regulaci TRPM8, která zahrnuje přímou vazbu Ca^{2+} k TRPM8, štěpení pozitivního regulátoru PIP2 aktivovanou fosfolipázou C i aktivaci CaM (Diver et al., 2019, Rohacs et al., 2005, Sarria et al., 2011). Mechanismus desenzitizace TRPM8 prostřednictvím CaM/Ca^{2+} nebyl dosud objasněn. CaM/Ca^{2+} může modulovat TRPM8 buď prostřednictvím přímé vazby nebo zprostředkovaně přes PIRT (phosphoinositide-interacting regulator of TRP) (Sisco et al., 2020). PIRT funguje jako negativní regulátor lidského TRPM8, snižující dostupnost PIP2 pro aktivaci TRPM8 (Sisco et al., 2019). PIRT interaguje také s CaM a

v prostředí s Ca^{2+} dochází ke snížení vazebné afinity komplexu (Sisco et al., 2020). Aktivace CaM ionty Ca^{2+} tak může vést k disociaci komplexu CaM/PIRT a uvolnění PIRT pro negativní modulaci TRPM8.

Podskupinu TRPM4/TRPM5 tvoří neselektivní iontové kanály propustné pouze pro monovalentní kationty. Aktivace TRPM4 i TRPM5 je podmíněna nárůstem intracelulární koncentrace Ca^{2+} a v případě TRPM4 je Ca^{2+}-dependentní regulace spojena také s molekulou CaM (Hofmann et al., 2003, Nilius et al., 2005). TRPM4 se nachází v širokém spektru tkání a představuje potenciální terapeutický cíl při léčbě kardiovaskulárních, neurologických i onkologických onemocněních (Wang et al., 2018, Schattling et al., 2012, Borgstrom et al., 2021). Citlivost TRPM4 vůči zvýšené intracelulární koncentraci Ca^{2+} je významně modulována prostřednictvím CaM, který interaguje s TRPM4 a umožňuje jeho aktivaci při fyziologických hladinách Ca^{2+} (Nilius et al., 2005). U dvou vazebných epitopů odvozených z N-konce a jednoho z C-konce TRPM4 bylo detailně popsáno vazebné rozhraní komplexu s CaM a potvrzena charakteristická role bazických a hydrofobních aminokyselin při jejich interakci (Bousova et al., 2018, Bousova et al., 2020). Zatímco fyziologický význam vazebných epitopů odvozených z N-konce TRPM4 zbývá ověřit, vazebné místo na C-konci TRPM4 se překrývá s dříve popsaným fragmentem TRPM4 nezbytným pro jeho regulaci závislou na molekule CaM (Nilius et al., 2005). Tento vazebný epitop má navíc schopnost vázat PIP2, který rovněž pozitivně moduluje citlivost TRPM4 k Ca^{2+} (Bousova et al., 2020, Nilius et al., 2006). TRPM5 je na rozdíl od TRPM4 exprimován ve značně omezeném souboru buněčných typů a nachází se zejména v chuťových buňkách typu II, kde se podílí na vnímání hořké, sladké či umami chuti nebo v β-buňkách pankreatu (Prawitt et al., 2003, Dutta Banik et al., 2018). Vzhledem k zapojení do regulace sekrece inzulinu představuje TRPM5 potenciální terapeutický cíl při léčbě diabetes mellitus typu II (Vennekens et al., 2018). TRPM5 je aktivován přímou vazbou iontů Ca^{2+} a jeho citlivost k Ca^{2+} je pozitivně modulována prostřednictvím PIP2 (Hofmann et al., 2003, Liu and Liman, 2003). Přítomnost vazebného epitopu pro CaM na N-konci TRPM5 poukazuje na možné zapojení molekuly CaM do Ca^{2+}-dependentní regulace TRPM5 (Bousova et al., 2022).

Podskupina TRPM6/TRPM7 zahrnuje klíčové regulátory homeostázy iontů Mg^{2+}. Jejich typickým rysem je přítomnost kinázové domény, která může fosforylovat vlastní iontový kanál

i další cílové molekuly (Clark et al., 2008a, Clark et al., 2008b). Zatímco TRPM7 je všudypřítomný iontový kanál, exprese TRPM6 je typická zejména pro střeva nebo ledviny a jeho dysfunkce vede k rozvoji primární hypomagnezemie se sekundární hypokalcemií (Voets et al., 2004, Zou et al., 2019) Kromě Mg^{2+} propouští TRPM6/TRPM7 také další bivalentní kationty včetně Ca^{2+} (Voets et al., 2004, Monteilh-Zoller et al., 2003). Nárůst intracelulární koncentrace Mg^{2+} i štěpení PIP2 vede k inaktivaci TRPM6/TRPM7 (Voets et al., 2004, Nadler et al., 2001, Xie et al., 2011, Runnels et al., 2002). Lokalizace vazebných míst pro CaM na intracelulárním N-konci TRPM6 i TRPM7 poukazuje na potenciální Ca^{2+}-dependentní regulaci prostřednictvím CaM (Zouharova et al., 2019, Bousova et al., 2021b).

Ačkoli v rámci celé rodiny TRP kanálů patří CaM mezi široce využívané regulační molekuly, zůstávají poznatky ohledně CaM-dependentní modulace podrodiny TRPM stále velmi omezené. Podrodina TRPM je spojena s rozvojem řady závažných onemocnění včetně kardiovaskulárních chorob (Inoue et al., 2019, Watanabe et al., 2008), neurodegenerativních poruch, (Duitama et al., 2020) či chorob spojených s endokrinním systémem (Liu et al., 2022). Vzhledem k širokému patofyziologickému dopadu dysregulace TRPM představuje detailní objasnění mechanismů jejich regulace klíčový krok pro vývoj moderních terapeutik. Unikátní charakter molekuly (konformační změny indukované vazbou Ca^{2+}, enormní konformační plasticita nebo existence množství vazebných partnerů) činí z CaM navíc ideální výchozí molekulu pro design nových/vylepšených biotechnologicky i biomedicínsky významných proteinových molekul.

1.3. Proteinové inženýrství

Prvním krokem k širokému biomedicínskému i biotechnologickému využití proteinů byl vznik technologie rekombinantní DNA, který umožnil rozvoj rutinní a efektivní laboratorní produkce požadovaných proteinů. Od roku 1982, kdy dozorový orgán federální vlády USA pro potraviny a léčiva Food and Drug Administration (FDA) schválil Humulin (rekombinantní lidský inzulin), se proteinová terapeutika stala zásadní inovací farmakologického výzkumu (Walsh, 2014). Využití proteinů je často limitováno zejména nedostatečnou stabilitou a aktivitou v důsledku transferu do podmínek odlišných od fyziologického prostředí. Metody proteinového inženýrství však umožnily modifikaci klíčových vlastností proteinů a tím rozvoj proteinových technologií v biomedicínských oblastech (**Obr. 4**).
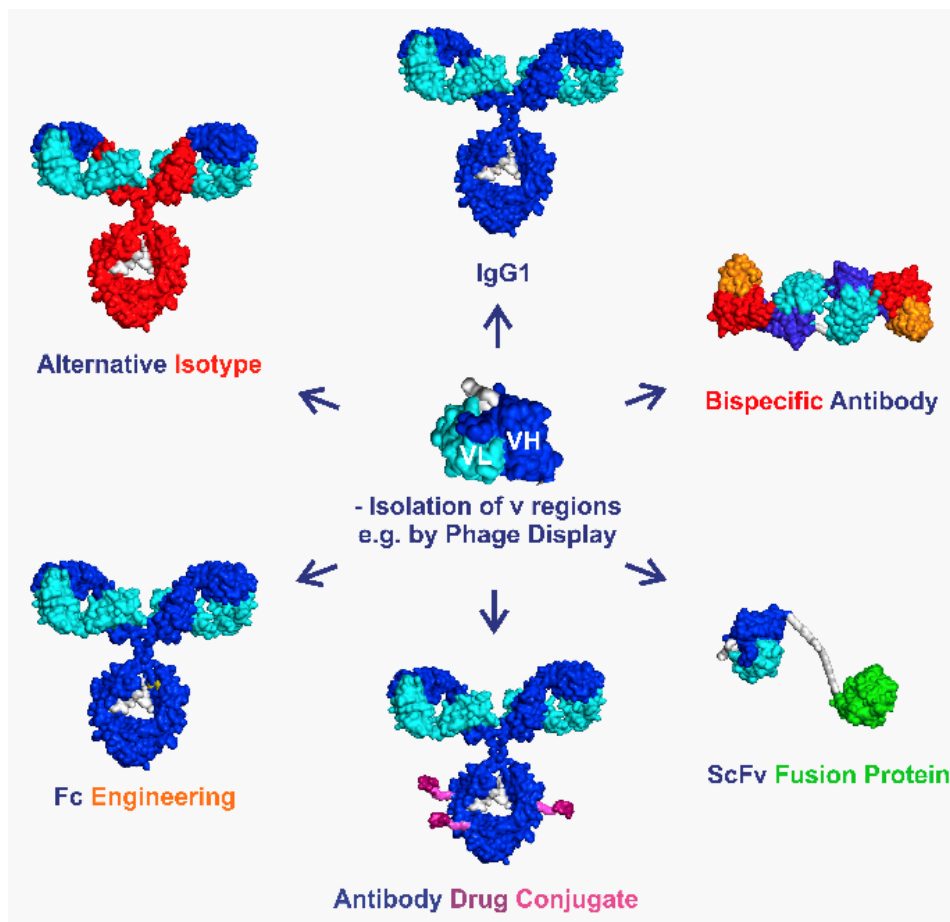
Obr. 4: Grafický přehled strategií proteinového inženýrství protilátek, převzato z (Humpe and Peipp, 2017). S využitím vybraných variabilních oblastí protilátek a navazujících technik proteinového byly připraveny nové molekuly s efektorovými funkcemi optimalizovanými pro konkrétní klinickou aplikaci. Metody proteinového inženýrství umožnily modifikovat konstantní oblasti protilátek a generovat alternativní isotypy nebo optimalizovat stávající fragment Fc. Dále mohou být protilátky konjugovány s léčivem nebo fúzovány s dalšími proteiny či variabilními protilátkovými oblastmi za vniku bispecifických protilátek.

Proteinové inženýrství je rychle se rozvíjející obor, zabývající se návrhem a modifikacemi proteinů za účelem vytvoření nových nebo vylepšení stávajících funkcí. (Lutz, 2010, Lutz and Iamurri, 2018). Oblast definuje několik přístupů proteinového inženýrství: řízená evoluce, racionální design a výpočetní metody *De novo* (Sinha and Shukla, 2019, Singh

et al., 2018b). Řízená evoluce zahrnuje vytvoření knihovny proteinových variant a výběr těch, které vykazují požadovanou funkci (Pongsupasa et al., 2022, Lutz, 2010). Tento přístup nevyžaduje hluboké pochopení struktury a funkce proteinu, ale spoléhá na náhodné mutace a následnou selekci proteinů s novými nebo vylepšenými funkcemi. Racionální design naopak na základě propojení detailní znalosti strukturně-funkčních vlastností proteinu a *in silico* predikčních modelů identifikuje konkrétní mutace asociované s požadovanými vlastnostmi (Liu et al., 2019a). Výpočetní metody *De novo* zahrnují použití výpočetních algoritmů a modelů v kombinaci s aktuálními přístupy strojového učení k navrhování a predikci funkce nových proteinů (Yang et al., 2019). Výpočetní metody *De novo* tak kombinují prvky jak racionálního designu, tak řízené evoluce (Korendovych and DeGrado, 2020). Celkově je proteinové inženýrství velkým příslibem pro vývoj nových terapeutik či biomateriálů a pravděpodobně bude i v následujících letech nezbytnou součástí vývoje nových léčiv.

1.3.1. Syntetické fúzní proteiny

Příprava nových molekul prostřednictvím proteinových fúzí náleží mezi nejlukrativnější oblasti biofarmaceutického výzkumu. Fúzí dvou či více nukleotidových sekvencí, kódujících původně samostatné proteiny/proteinové domény, lze získat bi/multi-funkční rekombinantní proteiny nebo modulovat konkrétní vlastnost fúzního partnera. Pro úspěšný design bioaktivních fúzních proteinů je kritická volba vhodných peptidových linkerů, umožňujících vznik požadovaných mezi-doménových interakcí (flexibilní linkery), redukujících sterické zábrany (flexibilní i rigidní linkery) nebo zajišťujících oddělení domén v místě určení *in vivo* (rozštěpitelné linkery). Optimalizací sekvence linkeru lze vylepšit bioaktivitu, farmakokinetické vlastnosti i expresi proteinu (Chen et al., 2013). Mezi hlavní faktory úspěšného designu fúzních proteinů patří také kompatibilita vlastností molekul nebo delece jejich neesenciálních částí pro zlepšení prostupnosti zejména nádorových tkání. Například studium fúzních konstruktů založených na doméně PDZ3 lidské *Zonula Occludens* a syntetickém miniproteinu Trp-cage navíc ukazuje i vliv vzájemné orientace fúzních partnerů na ustavení mezi-doménové komunikace a výslednou strukturu/stabilitu fúzních molekul (Bousova et al., 2021a).

1.3.1.1. Fúzní proteiny v biomedicíně

Prvním a zároveň komerčně úspěšným lékem z kategorie syntetických fúzních terapeutik byl inhibitor tumor nekrotizujícího faktoru α (TNF-α) Enbrel schválený FDA v roce

1998 (Huang, 2009). Během následujících let pomohly fúzní konstrukty odstranit řadu limitujících faktorů proteinových terapeutik. Krátký cirkulační poločas terapeuticky významných proteinů (např. cytokinů) lze významně navýšit prostřednictvím fúzí s konstantní částí (fragment Fc) imunoglobulinu G1, lidským sérovým albuminem, transferinem nebo nestrukturovaným polypeptidem XTEN (Strohl, 2015). Biologický poločas je v rámci fúzních konstruktů ovlivněn díky omezenému přístupu proteolytických enzymů k terapeutiku, sníženému vylučování v ledvinách v důsledku navýšení velikosti molekuly nebo potlačení lysozomální degradace v odpověď na vazbu Fc fragmentu či sérového albuminu k neonatálnímu Fc receptoru (Chen et al., 2013).

Klíčovou vlastností moderních fúzních terapeutik je efektivní cílení do místa určení *in vivo*, založené zejména na vysoké afinitě a specifitě vazby protilátka-antigen. Tímto lze minimalizovat toxické a pleiotropní účinky léčiv a zajistit jejich bezpečnější systémové podání. Protilátky/fragmenty protilátek jsou často fúzovány s cytokiny a nové molekuly imunocytokinů nachází uplatnění při léčbě chronických zánětlivých nebo nádorových onemocněních (Mansurov et al., 2021). Nádorová terapie využívá cílení imunostimulačních cytokinů do specifického nádorového mikroprostředí. Uplatnění nachází především fúze cytokinů s protilátkami proti komponentám extracelulární matrix, jako jsou izoformy fibronektinu asociované s neovaskularizací, nebo buněčným onkoproteinům např. receptoru 2 pro lidský epidermální růstový faktor (HER2) (Lee et al., 2020, Han and Lu, 2017). Využití imunocytokinů pro léčbu chronických zánětlivých/autoimunitních onemocněních je ve srovnání s aplikacemi v nádorové terapii méně pokročilé. Preklinické studie ukazují pozitivní efekt cílení protizánětlivých imunocytokinů do zánětlivých ložisek při léčbě artritidy, aterosklerózy, idiopatických střevních zánětů, chronických zánětů kůže nebo endometriózy (Bootz and Neri, 2016).

Kromě imunocytokinů jsou na přesném cílení terapeutik založeny také imunotoxiny nebo fúze protilátka/enzym. Molekulu imunotoxinu tvoří protilátkový fragment a cytotoxická složka, nejčastěji toxin inhibující proteosyntézu (bakteriální diptheria toxin, exotoxin A *Pseudomonas aeruginosa*, rostlinný ricin, saporin či lidské RNázy) (Akbari et al., 2017). Imunotoxiny nachází uplatnění zejména v terapii nádorových onemocnění, avšak pozitivních výsledků mohou dosahovat také při léčbě infekčních onemocnění (Spiess et al., 2016). Klinické

využití imunotoxinů je podmíněno mimimalizací obecně vysoké imunogenicity, dané především jejich cytotoxickou složkou. Exogenní molekuly toxinů jsou modifikovány odstraněním imunogenních epitopů nebo nahrazovány endogenními lidskými proteiny, jako jsou RNázy nebo proapoptotické proteiny (granzym B, TRAIL (apoptózu indukující ligand příbuzný TNF), Fas-ligand) (Mathew and Verma, 2009, Mazor and Pastan, 2020). Dalšího snížení imunogenicity lze u fúzních proteinů založených na protilátkách dosáhnout změnou aminokyselinové sekvence protilátky či posttranslační modifikace (Harding et al., 2010).

Terapeutické aplikace proteinových konstruktů typu protilátka/enzym jsou založeny buď na přímých fúzích protilátek s enzymaticky aktivním léčivem nebo na konstruktech protilátka/enzym konvertujících následně podané proléčivo na farmakologicky aktivní léčivo. Do první kategorie lze zařadit enzymaticky aktivní zástupce imunocytokinů (nejčastěji imunoRNázy) nebo konstrukty pro substituční enzymatickou terapii, nahrazující disfunkční mutované enzymy (Andrady et al., 2011). Cílením funkčních enzymů lze zajistit degradaci lysozomálního i cytosolárního glykogenu u pacientů s Pompeho chorobou nebo vylepšit katabolizmus glykosaminoglykanů u mukopolysacharidóz (Yi et al., 2017, Fecarotta et al., 2018). Výhodou druhé skupiny enzymatických fúzních terapeutik, založených na postupném podání konstruktu protilátka-enzym a příslušného proléčiva, je stále přesnější cílení terapeutik, spojené s maximalizací léčebných účinků a minimalizací toxických a systémových efektů zejména nádorové terapie (Mishra et al., 2018).

Klinicky významnou skupinu fúzních konstruktů tvoří tzv. decoy receptory, zahrnující také známý inhibitor TNF-α Enbrel. Přípravek Enbrel obsahuje léčivou látku Etanercept, tvořenou extracelulární vazebnou doménou receptoru p75 pro TNF-α a fragmentem Fc lidského IgG1 (Goffe and Cather, 2003). Etanercept funguje jako kompetitivní inhibitor prozánětlivého cytokinu TNF-α, jehož patologická produkce je spojena s rozvojem chronických zánětlivých onemocnění jako revmatoidní nebo psoriatická artritida (Choy and Panayi, 2001, Gottlieb and Antoni, 2004). Decoy receptory cílí také na procesy onkogeneze, nejčastěji prostřednictvím receptoru pro epidermální růstový faktor (EGFR) nebo vaskulární endoteliální růstový faktor (VEGFR). Fúzní bispecifické decoy receptory mají potenciál simultánně inhibovat buněčnou proliferaci i neovaskularizaci (např. konstrukt VEGFR/IgG1-Fc/EGFR) nebo synergní působení angiogenních signalizačních kaskád, zahrnujících VEGFR a receptor pro fibroblastový růstový

faktor 2 (FGFR) (konstrukt VEGFR1/VEGFR2/FGFR/IgG1-Fc) (Guo et al., 2022, Jiang et al., 2018).

Pokročilý design cílených proteinových terapeutik umožňuje transport nových léčiv také přes hematoencefalickou bariéru nebo placentu. Průchod hematoencefalickou bariérou zprostředkovávají inzulinové (IR) nebo transferinové receptory (TfR), na které cílí protilátková část fúzního terapeutika (Pardridge and Boado, 2012). Design řady rekombinantních proteinů byl modernizován s ohledem na zajištění průchodnosti hematoencefalickou bariérou. V rámci fúzních konstruktů jde o substituční enzymatická terapeutika pro léčbu neurologických symptomů mukopolysacharidóz nebo první fúzní terapeutikum schválené FDA – inhibitor TNF-α Enbrel (Boado et al., 2008, Boado et al., 2010). Fúzní inhibitory prozánětlivých cytokinů mají potenciál při terapii akutních traumatických poškození mozku i chronických neurodegenerativních onemocnění (Sumbria et al., 2012, Zhou et al., 2011b). Účinná léčba by zejména v případě Alzheimerovy nemoci umožnila snížit enormní růst nákladů na péči o pacienty s pokročilou fází choroby. Slibné výsledky v terapii Alzheimerovy choroby může přinést kombinatorní léčba, postihující více úrovní patogeneze onemocnění (Cummings et al., 2019). S využitím fúzních proteinů lze do mozkové tkáně cílit protizánětlivé inhibitory, protilátky proti amyloidním plakům nebo neurotrofní faktory (Zhou et al., 2011a, Sumbria et al., 2013, Zhou et al., 2010).

1.3.1.2. Fúzní proteiny založené na molekule CaM

Design fúzních konstruktů odvozených od CaM využívá zejména konformačních změn molekuly CaM při interakci s ligandy. Fúzí CaM s vhodným reportérovým systémem lze získat rychlé a citlivé biosenzory pro detekci stanovovaných analytů. Typickým příkladem jsou biosenzory monitorující koncentraci iontů Ca^{2+}, založené na fúzi CaM a zeleného fluorescenčního proteinu (GFP) nebo jeho spektrálních variant. První fluorescenční biosenzory byly založeny na Försterově rezonančním přenosu energie (FRET) a obsahovaly dva fluorofory fúzované s molekulou CaM a vazebným epitopem pro CaM (doména M13 myosin kinázy lehkého řetězce) (Miyawaki et al., 1997). Interakce mezi CaM/Ca^{2+} a vazebným epitopem vedla k vzájemnému přiblížení fluoroforů a emisi fluorescence o dané vlnové délce. Široce rozšířené jsou také biosenzory využívající jediný fluorofor, který na strukturní změny postihující fúzovanou molekulou CaM a vazebný epitop pro CaM reaguje změnou své konformace a

fluorescenčních vlastností (Nakai et al., 2001). Zatímco FRET biosenzory nachází uplatnění při kvantifikaci signálu Ca^{2+}, biosenzory s jedním fluoroforem jsou vhodnější pro studium jeho dynamiky (Lohr et al., 2021). Design zástupců z obou skupin biosenzorů byl optimalizován s ohledem na vylepšení jejich citlivosti, poměru signálu k šumu, stability, spektrálních charakteristik, cílení do intracelulárních kompartmentů nebo nežádoucích efektů exprese biosenzorů v buňce (zejména abnormální jaderná akumulace a narušení fyziologické signalizace ionty Ca^{2+}) (Nakai et al., 2001, Horikawa et al., 2010, Tallini et al., 2006, Palmer et al., 2006, Yang et al., 2018). Biosenzory založené na molekule CaM nachází využití při studiu gastrulace, neurální okruhů v motorickém a somato-senzorickém kortexu, neurálních změn v hipokampu při behaviorálních studiích nebo v retině oka během světelné expozice (Shindo et al., 2010, Tian et al., 2009, O'Connor et al., 2010, Dombeck et al., 2010, Borghuis et al., 2011).

Konformační plasticita CaM může tvořit také základ designu biosenzorů pro detekci nových farmakologicky významných molekul. Příkladem je fúzní protein odvozený z CaM a mutované varianty GFP – EGFP (enhanced GFP) (Dikici et al., 2003). Při aktivaci biosenzoru ionty Ca^{2+} dochází k zpřístupnění vazebných kapes pro fenothiazinové deriváty a příbuzná tricyklická antidepresiva v molekule CaM. Důsledkem rozsáhlých konformačních změn při jejich následné interakci s molekulou CaM/Ca^{2+} je zhášení fluorescenčního signálu fúzovaného EGFP. Biosenzory založené na molekule CaM lze využít jako rychlou a levnou high-throughput technologii pro farmakologicky atraktivní ligandy CaM. Psychofarmaka založená na antagonistech CaM modulují aktivitu řady klíčových proteinů signalizačních kaskád, například CaM-dependentní protein kinázy II regulující uvolňování neurotransmiterů a synaptické transmise (Vertessy et al., 1998, Barbiero et al., 2007). Kromě antidepresiv a antipsychotik mohou inhibitory CaM nacházet využití také při léčbě bolesti, v nádorové terapii pro potlačení chemoterapeutické rezistence či angiogeneze, v terapii neurodegenerativních onemocnění jako Alzheimerova nebo Huntingtonova choroba, případně při eradikaci mykotických biofilmů (Olah et al., 2007, Mayur et al., 2006, Jung et al., 2010, O'Day, 2020, Ceballos Garzon et al., 2020).

Charakteristické vlastnosti molekuly CaM lze kromě designu biosenzorů uplatnit také při optimalizaci rekombinantní produkce terapeuticky významných proteinů. Prostřednictvím fúze s CaM bylo v buňkách *E. coli* dosaženo dostatečné exprese solubilních antimikrobiálních

peptidů (AMPs), ačkoli samostatné peptidové sekvence vykazují značnou cytotoxicitu a citlivost k endogenním proteázám (Ishida et al., 2016). AMPs typicky sdílí vysoký stupeň podobnosti s vazebnými motivy pro CaM. Jedná se o amfipatické sekvence s motivy hydrofobních a bazických aminokyselin, které v rámci fúzního konstruktu interagují s molekulou CaM, čímž dochází k maskování jejich cytotoxicity i ochraně před proteolytickou degradací. Rekombinantní produkce AMPs umožňuje finančně výhodnější inkorporaci nepřirozených aminokyselin nebo izotopové značení sekvencí pro detailní studium jejich strukturně-funkčních vlastností. Maskování sekvencí molekulou CaM poskytlo také expresi solubilních transmembránových sekvencí nebo lidského makrofágového zánětlivého proteinu 3α (Ishida et al., 2016, Ramamourthy et al., 2019). Fúzní expresní systémy mohou molekulu CaM využívat rovněž jako univerzální purifikační kotvu pro hydrofobní interakční chromatografii, kdy přídavek chelatačního činidla vyváže ionty Ca^{2+} z CaM, konformační změny skryjí hydrofobní motivy uvnitř molekuly a fúzní konstrukt založený na CaM se uvolní z matrice kolony.

Fúzní konstrukty využívající vlastností CaM byly studovány i z hlediska potenciální aplikace v nádorové terapii při tzv. nádorovém pretargetingu. Principem nádorového pretargetingu je postupné podání dlouho cirkulujícího protilátkového konjugátu proti tkáni nádoru a malé radioaktivní molekuly s krátkým cirkulačním časem (Patra et al., 2016). Po dosažení optimální koncentrace protilátkového konjugátu v nádorové tkáni a eliminaci nadbytečných molekul z těla následuje podání menší radioaktivní molekuly s vysokou afinitou k protilátkovému konjugátu akumulovanému v nádoru. Rychlá farmakokinetika radioaktivní molekuly umožňuje minimalizaci vedlejších účinků radioterapie na zdravé tkáně. Chimerický protein scFv(L19)-CaM, navržený pro nádorový pretargeting, obsahuje protilátkový fragment scFv(L19) proti izoformě fibronektinu asociované s nádorovou angiogenezí a CaM (Melkko et al., 2002). Pro rychlé cílení terapeutických/diagnostických radionuklidů byly zvoleny peptidové ligandy molekuly CaM. Ačkoli v rámci konstruktu scFv(L19)-CaM zůstávají vazebné vlastnosti scFv(L19) i CaM zachovány, cílení do místa nádoru *in vivo* bylo neúspěšné. Příčinou může být velmi nízký isoelektrický bod CaM, zabraňující prostupu scFv(L19)-CaM do perivaskulárního prostoru. Potenciální řešení nabízí tkáňově specifické cílení scFv(L19)-CaM do kalveol endoteliálních buněk, zprostředkovávajících transcytózu terapeutik přes endoteliální bariéru (Marchetti et al., 2019).

Na unikátních vlastnostech CaM lze založit design širokého spektra fúzních konstruktů s využitím od detekčních systémů až po proteinová terapeutika. Základní vlastnosti aplikačně významných molekul včetně CaM jsou často modifikovány pro dosažení optimálních charakteristik v rámci odvozených fúzních makromolekul. Univerzálně žádanou modifikací je navýšení stability pro použití v suboptimálních podmínkách. Stabilitu proteinových molekul lze navýšit prostřednictvím mutací vytipovaných aminokyselin nebo alternativně fúzí se stabilizačním proteinem (Pucci et al., 2022, Morimoto et al., 2022). Vysoký modulační potenciál nabízí fúze s vnitřně neuspořádanými proteinovými sekvencemi, kdy na podkladě jejich enormní flexibility a konformační dynamiky dochází k vzájemné komunikaci mezi fúzními partnery (Zouharova et al., 2021).

## 1.4. Strukturní neuspořádanost proteinových molekul

Přibližně 44 % lidských kódujících genů tvoří geny pro vnitřně neuspořádané proteiny (IDPs) nebo proteiny s rozsáhlými vnitřně neuspořádanými oblastmi (IDPRs) (Pentony and Jones, 2010). Mezi IDPs/IDPRs řadíme vysoce flexibilní proteinové sekvence, které ve svém nativním stavu spontánně nezaujímají stabilní 3D strukturu. Typický je pro ně obsáhlý soubor vzájemně přecházejících konformačních stavů, zahrnujících natažené i kompaktní formy (Uversky and Dunker, 2010). U některých vnitřně neuspořádaných proteinových sekvencí indukuje interakce s vazebným partnerem sbalovaní do 3D struktur, jiné zůstávají a plní funkci v nestrukturovaném stavu (van der Lee et al., 2014). V obou případech však interakce ovlivňuje konformační dynamiku a výslednou funkci molekul.

Enormní soubor možných konformačních stavů umožňuje široké zapojení IDPs/IDPRs do regulace i integrace klíčových signalizačních kaskád řídících transkripci, translaci i průběh buněčného cyklu (Wright and Dyson, 2015). Dosud popsané IDPs/IDPRs překvapivě nenachází uplatnění během řízení signalizačních kaskádách závislých na iontech Ca^{2+}. Vnitřně neuspořádané vazebné sekvence pro ionty Ca^{2+} se vyskytují spíše u skladovacích proteinů endoplazmatického retikula (kalretikulin) a především u proteinů zapojených do procesu biomineralizace jako je starmaker, amelogenin nebo ameloblastin (AMBN) (Shivarov et al., 2014, Wojtas et al., 2015, Yamakoshi et al., 2001, Vetyskova et al., 2020).

1.4.1. Ameloblastin

AMBN byl původně popsán jako druhý nejpočetnější protein extracelulární matrix nejtvrdší tkáně lidského těla – zubní skloviny. Během odontogeneze ovlivňuje proliferaci, polaritu a diferenciaci ameloblastů (Fukumoto et al., 2004). Společně s amelogeninem vytváří supramolekulární organickou matrici pro orientovaný růst hydroxyapatitových krystalů (Wald et al., 2017). Mutace genu pro AMBN souvisí rozvojem dědičné hypoplázie zubní skloviny Amelogenesis imperfekta (Poulter et al., 2014). Kromě mineralizace zubní skloviny se AMBN podílí na regulaci osteogeneze i osteoklastogeneze a zajišťuje rychlou reparaci kostních fraktur (Iizuka et al., 2011, Lu et al., 2013, Lu et al., 2016). Zvýšená exprese AMBN navozuje tumor supresivní fenotyp a chemosenzitivitu osteosarkomu a může představovat nový prognostický marker či terapeutický cíl (Ando et al., 2017).

AMBN patří do nepočetné skupiny IDPs interagujících s ionty Ca^{2+}. Molekulu AMBN tvoří dvě domény – bazická N-koncová doména (AMBN-Nt) a acidická C-koncová doména (AMBN-Ct) (Wald et al., 2011). Sestavování supramolekulárních struktur AMBN řídí evolučně konzervovaný oligomerizační motiv v AMBN-Nt (**Obr. 5)** (Wald et al., 2013). Fosforylace nebo delece této oblasti potlačuje nejen oligomerizaci AMBN, ale i schopnost interakce s ionty Ca^{2+} (Stakkestad et al., 2017, Vetyskova et al., 2020). Vazba molekul Ca^{2+} probíhá zřejmě v acidické AMBN-Ct, které však sama o sobě nemá oligomerizační potenciál a interakci s ionty Ca^{2+} poskytuje pouze ve spojení s oligomerizační funkcí AMBN-Nt (Vetyskova et al., 2020). Monomerní charakter samostatné AMBN-Ct společně s její kompletní vnitřní neuspořádaností z ní činí vhodného kandidáta pro modulaci proteinových molekul v rámci fúzních konstruktů, například terapeuticky a biotechnologicky zajímavé cílové molekuly CaM. V této disertační práci se proto mimo jiné zabýváme fúzní molekulou tvořenou CaM a AMBN-Ct s cílem zjistit, zda dojde k ovlivnění vlastností molekuly CaM.
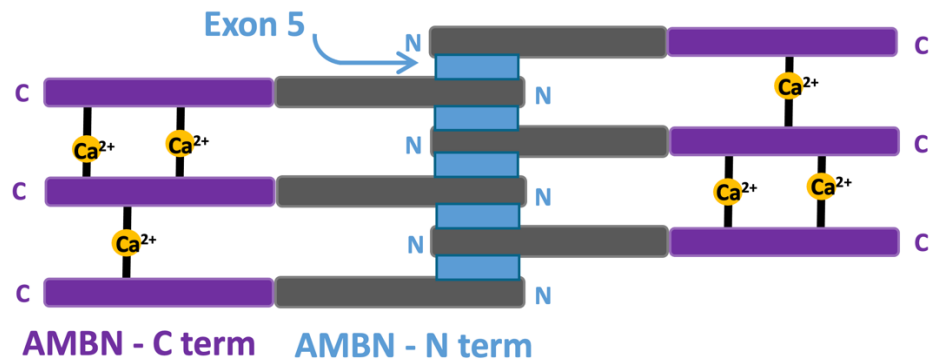
Obr. 5: Schematické znázornění předpokládaného oligomerizačního mechanismu molekul AMBN, převzato z (Vetyskova et al., 2020); upraveno. N-koncová doména AMBN (šedě) obsahuje motiv kódovaný exonem 5 indukující oligomerizaci (modře) monomerů AMBN. Oligomerizace molekul AMBN umožňuje interakci C-koncové domény AMBN (fialově) s ionty Ca^{2+} (žlutě).

2. CÍLE DISERTAČNÍ PRÁCE

Disertační práce se zabývá studiem široce rozšířeného kalciového senzoru CaM, regulujícího aktivitu stovek cílových proteinů zapojených do klíčových fyziologických procesů. Vlastnosti CaM jsou navíc uplatňovány při designu biomedicínsky/biotechnologicky významných proteinů, využívaných zejména pro detekci změn hladiny iontů Ca^{2+}. Cílem první části disertační práce bylo studium CaM s ohledem na možné zapojení do regulace medicínsky významných členů podrodiny iontových kanálů TRPM. Druhá část disertační práce se zabývá modulací vlastností CaM v rámci fúzních proteinových konstruktů, které by mohly nacházet uplatnění při designu nových proteinových konstruktů pro oblast biomedicíny či biotechnologií.

<u>Část 1</u>: Identifikace a charakterizace vazebných míst pro CaM u podrodiny iontových kanálů TRPM

Současné poznatky ohledně CaM-dependentní modulace TRP kanálů indikují značnou komplexitu interakcí CaM/TRP kanál. Jednotlivé TRP kanály mohou obsahovat více vazebných epitopů pro CaM, které se spolupodílejí na vazbě regulační molekuly CaM. Identifikace jednotlivých vazebných epitopů pro CaM tak může vést k pochopení komplexního průběhu interakce CaM/TRP. Jelikož CaM představuje rozšířenou modulační molekulu v rámci rodiny TRP kanálů, předpokládáme existenci podobných vazebných míst pro CaM také u podrodiny TRPM, kde zůstávaly poznatky ohledně CaM-dependentní regulace limitované.

Cílem práce je:
- Lokalizace a charakterizace nových vazebných epitopů pro CaM na intracelulárních koncích vybraných členů podrodiny TRPM (TRPM4, TRPM5, TRPM6 a TRPM7)
- Ověření charakteristické role bazických aminokyselinových zbytků v zajištění vazby molekuly CaM
- Konstrukce modelu CaM v interakci s nově identifikovanými vazebnými epitopy podrodiny TRPM

<u>Část 2:</u> Modulace vlastností CaM prostřednictvím proteinových fúzí

Vlastnosti aplikačně významných molekul mohou být optimalizovány prostřednictvím metod proteinového inženýrství. Mezi účinné přístupy patří např. design fúzních proteinových konstruktů za účelem vylepšení stávajících nebo zisku nových vlastností fúzovaných molekul. Univerzálními modulátory fúzních partnerů jsou zejména flexibilní vnitřně neuspořádané proteinové domény, schopné dynamicky reagovat na změny ve svém okolí. Fúzním partnerem CaM byla zvolena proteinová doména tvořící C-konec ameloblastinu (AMBN-Ct). Vzhledem ke kompletně vnitřně neuspořádanému charakteru AMBN-Ct předpokládáme vznik mezi-doménové komunikace mezi fúzovanými molekulami CaM a AMBN-Ct, která může pozitivně ovlivnit např. teplotní stabilitu struktury CaM.

Cílem práce je:

- Design a příprava fúzní molekuly založené na CaM a kompletně vnitřně neuspořádané doméně AMBN-Ct
- Potvrzení nativní struktury CaM v molekule CaM/AMBN-Ct
- Ověření zachovaných vazebných funkcí CaM v CaM/AMBN-Ct prostřednictvím interakce s dříve popsaným vazebným epitopem pro CaM odvozeným z iontového kanálu podrodiny TRPM
- Studium vlivu mezi-doménové komunikace na teplotní stabilitu CaM v CaM/AMBN-Ct

3. MATERIÁL A METODY

3.1. Exprese a purifikace proteinů

3.1.1. CaM

CaM byl exprimován z vektoru pET3a v buňkách *E. coli* Bl-21. Exprese byla indukována při teplotě 25 °C přídavkem 0,5 mM IPTG. Buňky byly kultivovány při 25 °C/150 rpm a po 18 hod. resuspendovány v lyzačním pufru (50 mM Tris-HCl pH7,5, 2 mM EDTA, 2 mM 2-Merkapto-EtOH, 0,2 mM PMSF), a dezintegrovány sonikací. CaM byl purifikován ze solubilní frakce pomocí hydrofobní chromatografie na Phenyl Sepharose CL-4B (GE Healthcare, Chicago, IL, USA) podle standardního purifikačního protokolu (Bousova et al., 2018) a převeden do finálního pufru 50 mM Tris-HCl pH 7,5, 250 mM NaCl, 2 mM CaCl$_2$ (studium komplexů CaM s vazebnými epitopy odvozenými od TRPM) nebo 10 mM Tris-HCl pH 7,5, 100 mM NaCl, ± 10 mM CaCl$_2$ (studium fúzního konstruktu CaM/AMBN-Ct).

3.1.2. CaM/AMBN-Ct

Exprese CaM/AMBN-Ct probíhala z vektoru pET28b v buňkách *E. coli* Bl-21. Buněčná suspenze byla v logaritmické fázi růstu zchlazena na 15 °C a přídavkem IPTG do koncentrace 0,5 mM indukována exprese proteinu. Po kultivaci při 15 °C/150 rpm/18 hod. byly buňky resuspendovány v lyzačním pufru (50 mM Tris-HCl pH 8,0, 50 mM NaCl, 2 mM 2-Merkapto-EtOH, 2 mM EDTA). Po sonikaci buněk byl CaM/AMBN-Ct purifikován pomocí hydrofobní chromatografie dle totožného protokolu jako molekula CaM. Následně byl CaM/AMBN-Ct dialyzován do 50 mM Tris-HCl pH 7,5, 500 mM NaCl a proteázou TEV při 4 °C/24 hod odštěpena sekvence 6xHis. Po přídavku EDTA do koncentrace 10 mM byl CaM/AMBN-Ct převeden do finálního pufru (10 mM Tris-HCl pH 7,5, 100 mM NaCl, ± 10 mM CaCl$_2$) na koloně Superdex 200 Increase 10/300 GL (GE Healthcare, Chicago, IL, USA).

3.1.3. AMBN-Ct

Podmínky pro expresi AMBN-Ct byly totožné jako u CaM/AMBN-Ct. Po resuspendaci buněk v lyzačním pufru (50 mM Na$_2$HPO$_4$ pH 8,0, 50 mM NaCl, 2 mM 2-Merkapto-EtOH) a sonikaci buněk byla k solubilní frakci přidána močovina do koncentrace 8M. CaM/AMBN-Ct

byl purifikován s využitím Chelating Sepharose Fast Flow s navázanými ionty Ni^{2+} (GE Healthcare, Chicago, IL, USA). AMBN-Ct byl z elučního pufru (50 mM Tris-HCl pH 7,5, 600 mM NaCl, 8 M močovina, 600 mM imidazol) dialyzován do 50 mM Tris-HCl pH 7,5, 500 mM NaCl a štěpen proteázou TEV při 4 °C/24 hod. Štěpná směs byla nanesena na Chelating Sepharose Fast Flow s navázanými ionty Ni^{2+} (GE Healthcare, Chicago, IL, USA) a slabě navázaný AMBN-Ct byl eluován do 10 mM Tris-HCl pH 7,5, 100 mM NaCl, 100 mM imidazol. Po přídavku EDTA do koncentrace 10 mM byl AMBN-Ct převeden na koloně Superdex 200 Increase 10/300 GL (GE Healthcare, Chicago, IL, USA) do finálního pufru (10 mM Tris-HCl pH 7,5, 100 mM NaCl, ± 10 mM $CaCl_2$).

3.2. Fluorescenční spektroskopie

Časově rozlišená anizotropie fluorescence byla měřena na spektrofluorimetru K2 (ISS Inc., Champaign, IL, USA) při teplotě 25 °C. Vazebné epitopy pro CaM označené fluoresceinem byly titrovány přídavky CaM, CaM/AMBN-Ct nebo AMBN-Ct. Fluorescence byla excitována při 490 nm a hodnoty časově rozlišené anizotropie fluorescence (r) zaznamenány při 530 nm. Podíl vazebných epitopů v interakci (fraction bound, F_B) byl stanoven dle rovnice (1):

$$F_B = (r - r_{min})/[(r_{max} - r)\, Q + (r - r_{min})],$$

kde je r hodnota anizotropie při jednotlivých koncentracích ligandu, r_{min} anizotropie samotného vazebného epitopu, r_{max} anizotropie při saturační koncentraci ligandu a Q je korekční faktor (poměr kvantového výtěžku vázané a volné formy studovaného epitopu). Hodnota rovnovážné disociační konstanty (K_D) komplexu byla stanovena z proložení závislosti F_B na koncentraci ligandu rovnicí (2):

$$F_B = \frac{K_D + [P1] + [P2] - \sqrt{(K_D + [P1] + [P2])^2 - 4[P1][P2]}}{2[P1]},$$

kde [P1] je koncentrace vazebného epitopu a [P2] koncentrace ligandu. K vyhodnocení dat byl použit software Sigmaplot 11.0 (Systat software, San Jose, CA, USA).

3.3. Analytická ultracentrifugace

Sedimentační rychlost molekul byla měřena s využitím analytické ultracentrifugy ProteomeLab XL-I (Beckman Coulter, Indianapolis, IN, USA). Experimenty byly provedeny při 48 000 rpm/20 °C s využitím rotoru An50-Ti. Pro měření byly použity proteiny o koncentracích: 2,8 mg.ml^{-1} (CaM), 1,1 mg.ml^{-1} (AMBN-Ct) a 1,3 mg.ml^{-1} (CaM/AMBN-Ct) v pufru 10 mM Tris-HCl pH 7,5, 100 mM NaCl. Absorbance vzorků byla detekována při 280 nm v intervalu 3-6 minut. Při vyhodnocení dat byly použity softwary Sednterp a Sedfit (Philo, 2023, Schuck, 2000).

3.4. Spektroskopie cirkulárního dichroismu

Spektra cirkularního dichroismu (CD) byla studována s využití spektropolarimetru Jasco-1500 a Peltierova termostatu PTC-517 (JASCO, Easton, MD, USA). Spektra CD byla měřena v teplotním gradientu 10-90 °C ve vzdálené (195–280 nm) i blízké (240–350 nm) UV oblasti. Měření v blízké UV oblasti probíhalo v 1 mm křemenné kyvetě s teplotním přírůstkem 10 °C. K experimentům byly použity proteiny o koncentracích: 160 μM (CaM), 65 μM (CaM/AMBN-Ct) a 47 μM (AMBN-Ct) v pufru 10 mM Tris-HCl pH 7,5, 100 mM NaCl. Pro měření ve vzdálené UV oblasti byla použita 0,5 mm křemenná kyveta, teplotní přírůstek 5 °C a koncentrace proteinů 10x nižší než v případě experimentů v blízké UV oblasti. Finální data byla vyhodnocena v software Sigmaplot 12.5 (Systat software, San Jose, CA, USA) a vyjádřena v jednotkách molární elipticity (θ).

3.5. Molekulové modelovaní a molekulová dynamika

Struktura CaM bez Ca^{2+} byla převzata z NMR modelu (PDBID: 1CFD) (Kuboniwa et al., 1995). Trojrozměrná struktura CaM s Ca^{2+} byla modelována podle kompaktní struktury získané rentgenovou krystalografií (PDBID: 1PRW) (Fallon and Quiocho, 2003). N-koncová i C-koncová doména CaM byly stabilizovány potenciálem omezujícím vzdálenost extrahovaným z experimentálních modelů. Vzdálenosti všech vazeb v rozmezí 1-2 nm byly limitovány harmonickým potenciálem se silovou konstantou 240 kJ·mol^{-1}·nm^{-2}. N-koncová doména (A5-T79) a C-koncová doména (S81-K148) CaM byly kalkulovány nezávisle, proto jejich vzájemná orientace zůstala neomezená. K molekule CaM s i bez vázaných iontů Ca^{2+} byly připojeny extendované konformace flexibilního linkeru (GGGGSS) a C-koncové domény

AMBN (L223-P447, číslované podle sekvence AMBN). Minimalizace energií získaných struktur byla provedena v softwaru GROMACS (Abraham et al., 2015).

Simulace dynamického chování molekul byly provedeny v GROMACS (v. 5.1.1) (Abraham et al., 2015) s použitím stochastického dynamického integrátoru s časovým krokem 20 fs a inverzní konstantou tření 20 ps při 300 K. Molekulární dynamika byla propagována na 100 milionů kroků. Každý systém byl kalkulován v 5 nezávislých simulacích za účelem odhadu konvergence vzorkování a intervalů spolehlivosti.

4. VÝSLEDKY

4.1. Identifikace a charakterizace vazebných míst pro CaM u podrodiny iontových kanálů TRPM

### 4.1.1. Identifikace vazebných epitopů pro CaM

Vazebné motivy pro CaM byly predikovány *in silico* s využitím softwaru „Calmodulin target database" (Yap et al., 2000). Pro další studium byly vybrány potenciální nové vazebné epitopy pro CaM odvozené z lidských iontových kanálů TRPM4, TRPM5, TRPM6 a TRPM7 (**Tab. 1**). Sekvence obsahující typické motivy hydrofobních a bazických aminokyselin byly syntetizovány jako krátké peptidy a využity ve vazebných studiích s molekulou CaM. Detailní data z charakterizace vazebných epitopů budou ukázána na příkladu iontového kanálu TRPM6 (**Obr. 6 A**).

Tab. 1: Přehled nových vazebných epitopů pro CaM u podrodiny TRPM. Bazické aminokyseliny s potenciální rolí při formování komplexu s CaM jsou zvýrazněny oranžově. Zkratkou K_D jsou označeny rovnovážné disociační konstanty komplexů s CaM, SD definuje směrodatnou odchylku.

Vazebný epitop	Lokalizace vazebného epitopu na TRPM kanálu	Syntetizovaná sekvence vazebného epitopu pro CaM	$K_D \pm SD$
TRPM4np	Intracelulární N-konec	$_{627}$FGECY**R**SSEVRAA**R**LLL**RR**CPL$_{648}$	1,3 ± 1,8
TRPM4cp	Intracelulární C-konec	$_{1078}$PFIVISHL**R**LLL**R**QLC**RR**PRS$_{1098}$	2,6 ± 0,5
TRPM5np	Intracelulární N-konec	$_{83}$WL**R**DVL**RK**GLV**K**$_{94}$	1,0 ± 0,1
TRPM6np	Intracelulární N-konec	$_{520}$LIGRAY**R**SNYT**RK**HF**R**$_{535}$	14,87 ± 0,7
TRPM7np	Intracelulární N-konec	$_{523}$TY**R**CTYT**RKR**F**R**L$_{535}$	6,1 ± 0,4

Vazebná afinita CaM k novým vazebným epitopům podrodiny TRPM byla určena pomocí měření anizotropie při ustálené fluorescenci. Fluorescenčně značené peptidy odvozené z TRPM kanálů byly titrovány přídavky CaM. Z nárůstu fluorescenční anizotropie v důsledku vazby CaM k značeným epitopům byl stanoven podíl vazebných epitopů v interakci s CaM (fraction bound, F_B). Rovnovážné disociační konstanty byly určeny z proložení závislosti F_B na koncentraci CaM rovnicí 2 (3. Materiál a metody, 3.2. Fluorescenční spektroskopie) (**Obr. 6**

B, Tab. 1). Měření anizotropie při ustálené fluorescenci potvrdilo interakci mezi CaM a studovanými vazebnými epitopy podrodiny TRPM.
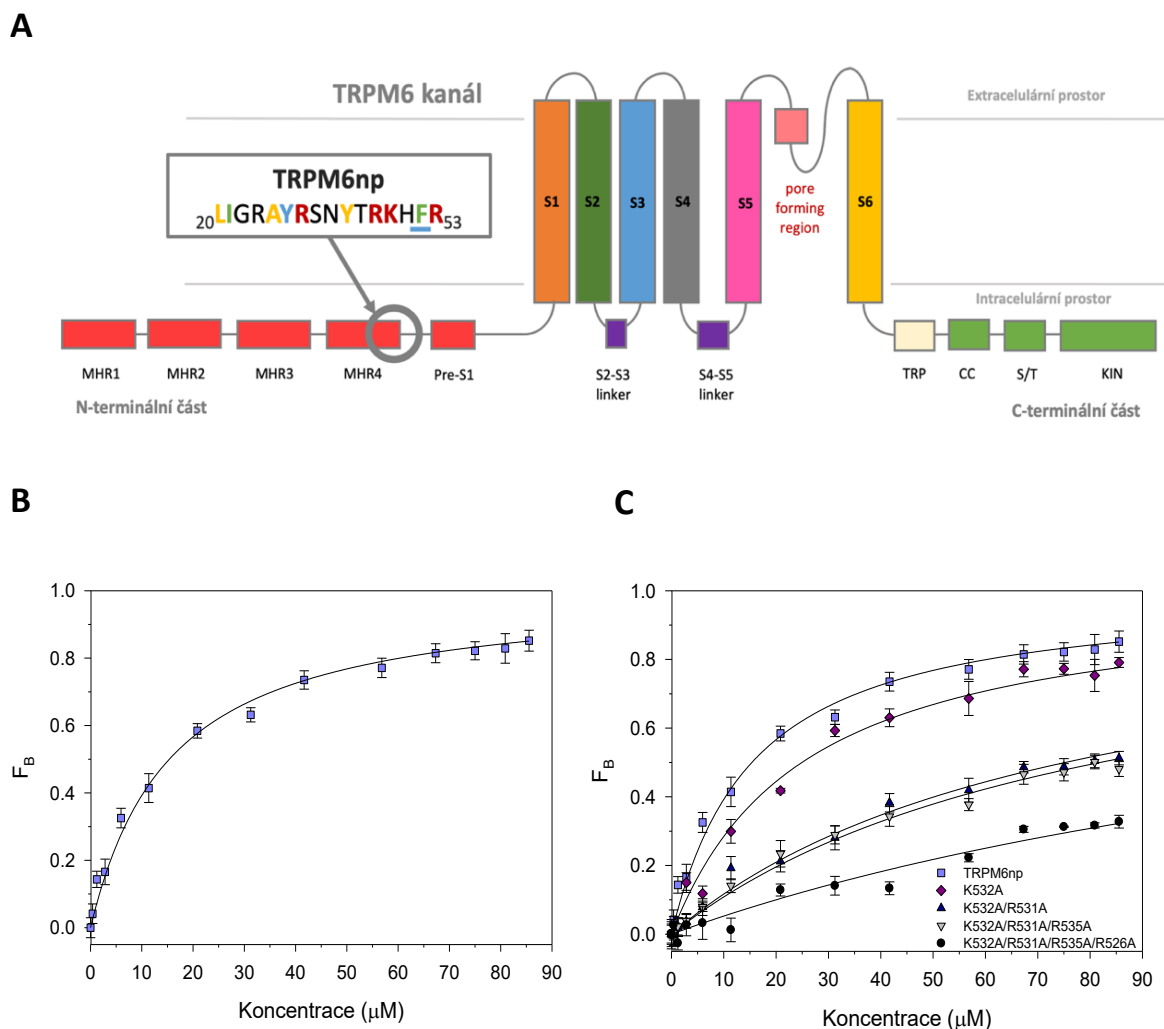
Obr. 6: Charakterizace vazebného epitopu TRPM6np. (**A**) Lokalizace TRPM6np na iontovém kanálu TRPM6. Intracelulární N-konec TRPM6 obsahuje 4 domény MHR a pre-S1 doménu. Transmembránovou část tvoří 6 α-helikálních segmentů (S1-S6), přičemž pór iontového kanálu je formován mezi S5 a S6. Součástí C-konce TRPM6 je TRP doména, doména typu coiled-coil, doména bohatá na serin/threonin a α-kinázová doména. Lokalizace TRPM6np je vyznačena kružnicí v N-terminální části proteinu. (**B**) Podíl molekul vazebného epitopu TRPM6np v interakci s CaM. (**C**) Podíl mutovaných forem TRPM6np vázajících CaM.

### 4.1.2. Role bazických aminokyselin při formování komplexů CaM/TRPM

Formace komplexů CaM/TRP probíhá na základě vzájemných hydrofobních interakcí a vzniku solných můstků mezi bazickými zbytky vazebných epitopů pro CaM a negativně nabitými aminokyselinami CaM. Vazebné epitopy odvozené od TRPM4, TRPM5 a TRPM6 byly syntetizovány v mutované formě se záměnou potenciálních klíčových bazických reziduí za alanin (**Tab. 2**). Měření anizotropie při ustálené fluorescenci potvrdilo výrazný pokles vazebné afinity mezi CaM a mutovanými epitopy odvozenými z TRPM4, TRPM5 i TRPM6. Průběh závislosti F_B jednotlivých mutovaných vazebných epitopů na koncentraci CaM je zobrazen na příkladu TRPM6np (**Obr. 6 C**). Vazebné studie s mutovanými formami vazebných epitopů potvrdily specifitu interakce mezi CaM a nově identifikovanými vazebnými epitopy.

Tab. 2: Role bazických aminokyselinových zbytků vazebných epitopů při tvorbě komplexu s CaM. Vybrané bazické aminokyseliny (oranžově) byly nahrazeny alaninem (červeně). Následně byly stanoveny hodnoty K_D komplexů mutovaných vazebných epitopů s CaM. Zkratkou SD je označena směrodatná odchylka.

| Vazebný epitop	Sekvence	$K_D \pm SD$
TRPM6np	LIGRAYRSNYTRKHFR	14,87 ± 0,70
K532A	LIGRAYRSNYTRAHFR	22,44 ± 1,22
K532A/R531A	LIGRAYRSNYTAAHFR	74,74 ± 2,36
K532A/R531A/R535A	LIGRAYRSNYTRKHFR	81,40 ± 2,17
K532A/R531A/R535A/R526A	LIGRAYASNYTAAHFA	179,04 ± 9,44
TRPM4np	FGECYRSSEVRAARLLLRRCPL	1,3 ± 1,8
R632A	FGECYASSEVRAARLLLRRCPL	27,2 ± 5,0
R640A	FGECYASSEVRAAALLLRRCPL	17,0 ± 2,0
R640A/R644A/R645A	FGECYASSEVRAAALLLAACPL	80,0 ± 20,0
TRPM4cp	PFIVISHLRLLLRQLCRRPRS	2,6 ± 0,5
R1086A/R1090A	PFIVISHLALLLAQLCRRPRS	bez interakce
R1094A/R1095A	PFIVISHLRLLLRQLCAAPRS	bez interakce
TRPM5np	WLRDVLRKGLVK	1,0 ± 0,1
R85A/R89A/K90A/K94A	WLADVLAAGLVA	13,6 ± 0,5

4.1.3. Homologní modelování TRPM kanálů a molekulové dokování

Konstrukce homologního modelu iontového kanálu podrodiny TRPM a dokování získané struktury studovaného vazebného epitopu do molekuly CaM do je zobrazeno na příkladu iontového kanálu TRPM6. Homologní model TRPM6 byl připraven v softwaru SWISS-MODEL podle známé struktury příbuzného myšího iontového kanálu TRPM7 (PDB: 5ZX5) (Duan et al., 2018a). Vazebný epitop TRPM6np byl lokalizován na cytoplazmatické části iontového kanálu TRPM6, kde je dobře přístupný pro interakci s CaM (**Obr. 7**).
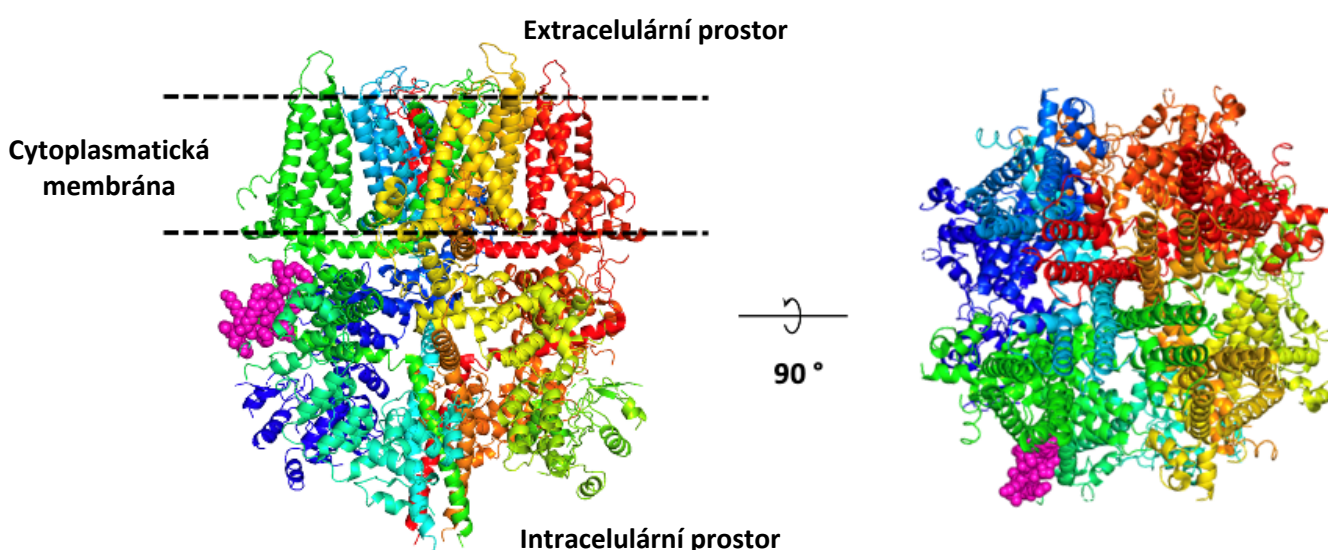
Obr. 7: Homologní model iontového kanálu TRPM6. TRPM6 s vyznačenou lokalizací vazebného epitopu TRPM6np (růžově). (**A**) Boční pohled na TRPM6 zanořený v cytoplazmatické membráně. (**B**) Pohled na TRPM6 z intracelulární strany membrány. Molekulový model byl připraven v programu ChimeraX-1.3 (Pettersen et al., 2021).

Část získané struktury TRPM6 odpovídající oblasti vazebného epitopu TRPM6np byla dokována do molekuly CaM v softwaru ClusPro2.0 (**Obr. 8**) (Kozakov et al., 2017). *In silico* analýza komplexu CaM/TRPM6np potvrdila vhodnou orientaci studovaných bazických aminokyselin TRPM6np pro interakci s CaM a koreluje s výsledky předchozích vazebných studií. Analogickým způsobem bylo studování vazebné rozhraní komplexu CaM s TRPM4np, TRPM4cp, TRPM5np i TRPM7np a podpořena role vytipovaných bazických aminokyselin při interakci s CaM.
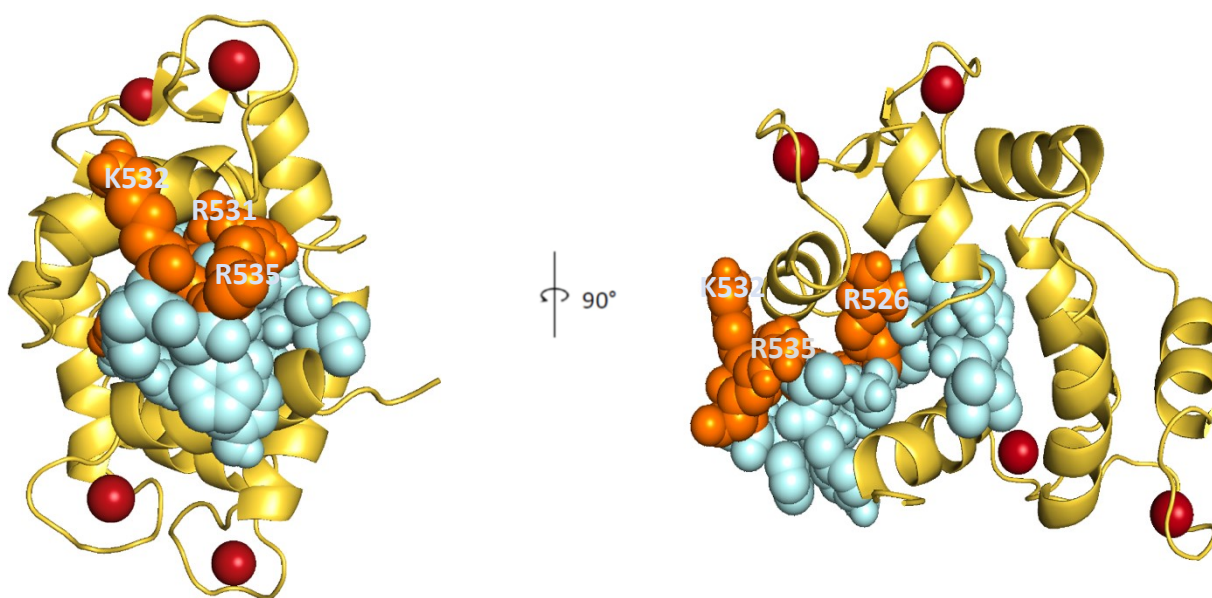
Obr. 8: Vazebný epitop TRPM6np v komplexu s CaM/Ca^{2+}. Molekulové dokování TRPM6np (modře) s vyznačenými bazickými rezidui R526, R531, K532 a R535 (oranžově) do struktury CaM (žlutě) v komplexu s ionty Ca^{2+} (červeně), PDB: 1PRW (Fallon and Quiocho, 2003). Molekulový model byl připraven v programu ChimeraX-1.3 (Pettersen et al., 2021).

4.2. Modulace vlastností CaM prostřednictvím proteinových fúzí

Molekula CaM byla kromě regulace medicínsky významných cílových proteinů podrodiny TRPM studována také s ohledem na možné vylepšení vlastností CaM v rámci fúzních proteinových konstruktů. Pro fúzi s CaM byly zvoleny vnitřně neuspořádané proteinové sekvence, jejichž vysoce dynamický charakter je předpokladem pro komunikaci mezi fúzními partnery a vzájemnou modulaci vlastností molekul.

4.2.1. Design a základní charakteristiky fúzní molekuly

CaM byl prostřednictvím flexibilního linkeru GGGGSS fúzován s vnitřně neuspořádanou proteinovou doménou AMBN-Ct a výsledný proteinový konstrukt označen jako CaM/AMBN-Ct. Flexibilní linker byl zvolen z důvodu podpory volnosti pohybu CaM a AMBN-Ct v rámci molekuly CaM/AMBN-Ct. Analytická gelová chromatografie (ASEC) směsi CaM a AMBN-Ct prokázala nezávislé chování jednotlivých fúzních partnerů mimo

konstrukt CaM/AMBN-Ct (**Obr. 9 A**). Při ASEC fúzního konstruktu CaM/AMBN-Ct byl patrný jediný pík, odpovídající vyšším molekulovým hmotnostem (Mw) (**Obr. 9 A**). Vnitřně neuspořádaný charakter (tzv. IDP charakter) AMBN-Ct je příčinou vysokého hydrodynamického poloměru AMBN-Ct i CaM/AMBN-Ct a výrazně zkresleného odečtu Mw oproti globulárním standardům pro ASEC. Lehce nadhodnocený odhad Mw samotného CaM je dán navýšením hydrodynamického poloměru v důsledku protáhlého tvaru molekuly.
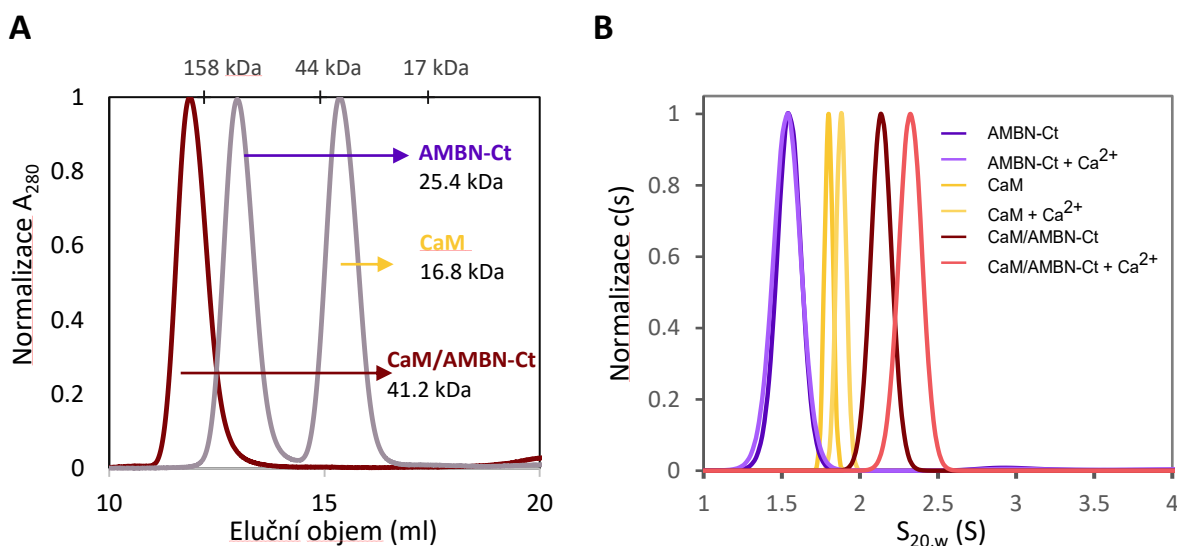
Obr. 9: Analytická gelová chromatografie a analytická ultracentrifugace vybraných proteinových konstruktů CaM/AMBN-Ct, CaM a AMBN-Ct. (**A**) Chromatografický profil CaM/AMBN-Ct a směsi CaM a AMBN-Ct získaný detekcí absorbance při vlnové délce 280 nm na koloně Superdex 200 Increase 10/300 (GE Healthcare, Chicago, IL, USA). (**B**) Analýza sedimentační rychlosti studovaných proteinů za a bez přítomnosti Ca^{2+}, kde c(s) značí kontinuální distribuci sedimentačních koeficientů.

Měření sedimentačních rychlostí studovaných proteinů potvrdilo monodisperzní populace studovaných molekul (**Obr. 9 B**). Hodnoty sedimentačních koeficientů přepočítaných na standardní podmínky (20 °C, čistá voda) ($s_{20,w}$) ve všech případech odpovídaly monomerním molekulám. V případě CaM a CaM/AMBN-Ct indukovala přítomnost iontů Ca^{2+} konformační změny molekul, vedoucí k navýšení hodnoty $s_{20,w}$, reflektující zkompaktnění molekul. Pozorovaný efekt je přitom nejvýraznější u konstruktu CaM/AMBN-Ct a zahrnuje i změny ve fúzované doméně AMBN-Ct, která sama o sobě na přítomnost Ca^{2+} nereaguje (**Obr. 9 B**).

Výsledky sedimentačních experimentů indikují vzájemnou komunikaci fúzních partnerů CaM a AMBN-Ct

4.2.2. Analýza sekundární a terciální struktury CaM/AMBN-Ct

Měřením spektra cirkulárního dichroismu (CD) ve vzdálené UV oblasti (190-260 nm) byl studován obsah sekundárních struktur molekul. V případě AMBN-Ct odpovídal průběh spektra s minimem při 199 nm IDP charakteru proteinové domény (**Obr. 10 A**). U molekuly CaM byly pozorovány dva podobně intenzivní negativní píky při 208 a 222 nm, typické pro α-helikální proteiny. Spektrum CD molekuly CaM/AMBN-Ct vykazovalo minimum při 208 a 222 nm, avšak spektrální intenzita při 208 nm byla výrazně vyšší. Průběh spektra je dán kombinací α-helikálních i IDP oblastí v molekule CaM/AMBN-Ct. Přítomnost iontů Ca^{2+} nevedla u molekuly AMBN-Ct k strukturním změnám detekovatelným spektroskopií CD. V případě CaM došlo v důsledku vazby Ca^{2+} k navýšení intenzity obou negativních píků. Lehký nárůst spektrální intenzity při 208 i 222 nm indikoval u konstruktu CaM/AMBN-Ct strukturní změny typické pro vazbu Ca^{2+} k podjednotce CaM.

Ze získaných experimentálních spekter CaM a AMBN-Ct byla vypočítána modelová spektra pro nezávislé chování CaM a AMBN-Ct v konstruktu CaM/AMBN-Ct (**Obr. 10 B**). Modelová spektra CaM/AMBN-Ct obsahovala dvě minima při 203 a 222 nm. Modelová spektra CaM/AMBN-Ct vykazovala oproti experimentálním (1) posun maxima prvního negativního píku z 208 na 203 a (2) odlišný poměr intenzit obou minim. Tyto změny indikují mírné navýšení helicity konstruktu CaM/AMBN-Ct oproti modelovému spektru pro nezávislé chování fúzních partnerů a vzájemné interakce mezi CaM a AMBN-Ct, které však zásadně nemění základní strukturní vlastnosti jednotlivých molekul.

Pomocí spektroskopie CD v blízké UV oblasti byla studována terciální struktura molekul CaM a CaM/AMBN-Ct. Ve spektru CD molekuly CaM se objevily negativní pásy při 255, 262 a 268 nm odpovídající signálu z fenylalaninů a v oblasti nad 275 nm je patrný signál tyrozinů (**Obr. 10 A**). Podobný průběh mělo i spektrum CD konstruktu CaM/AMBN-Ct. V případě CaM i CaM/AMBN-Ct indukovaly ionty Ca^{2+} nárůst spektrální intenzity pásů.
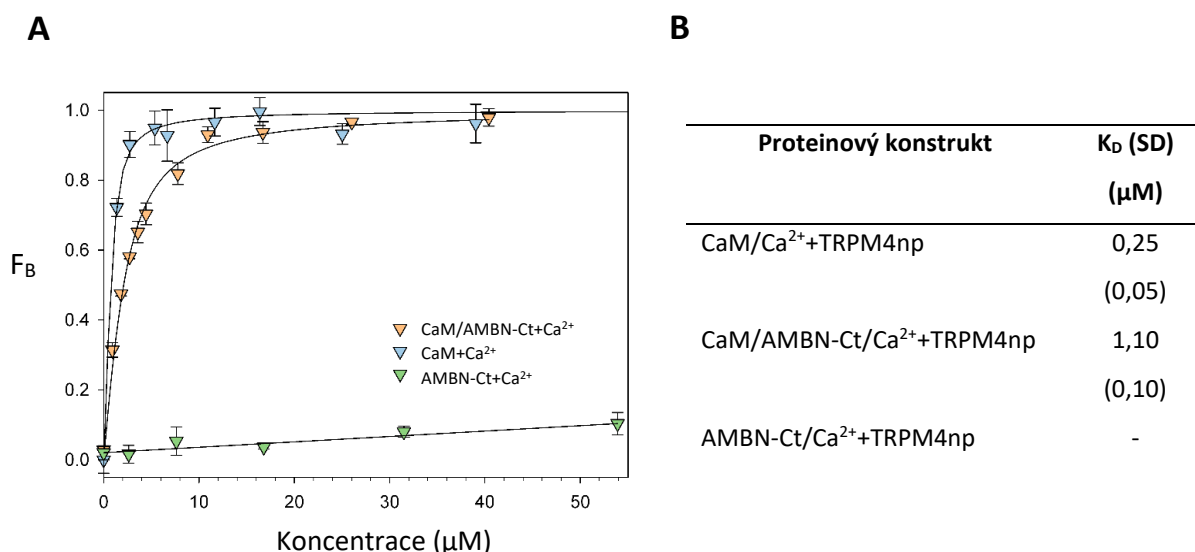
A
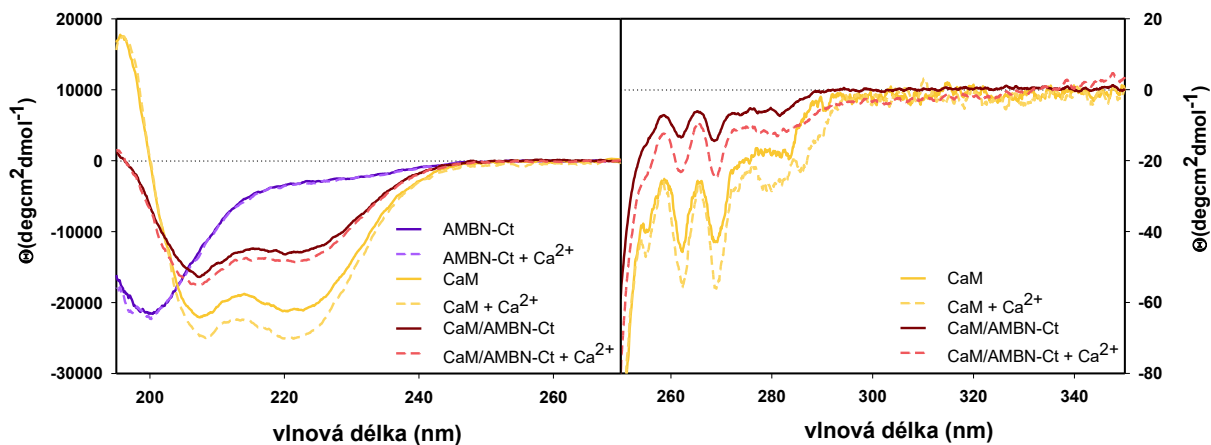
B
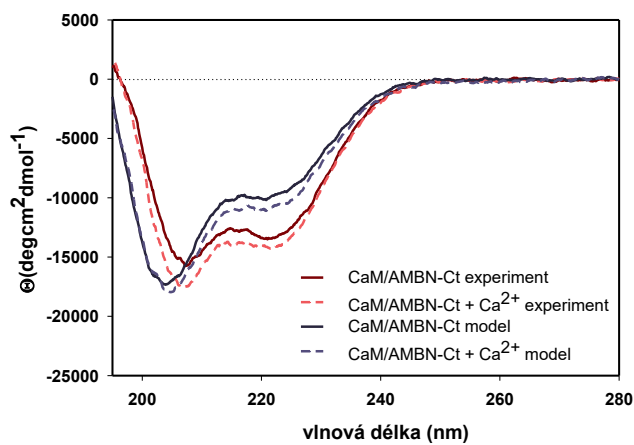
Obr. 10: Analýza spekter cirkulárního dichroismu vybraných proteinových konstruktů CaM/AMBN-Ct, CaM a AMBN-Ct za a bez přítomnosti Ca^{2+}. (**A**) Spektra CD studovaných molekul ve vzdálené (vlevo) a blízké (vpravo) spektrální oblasti. (**B**) Porovnání experimentálních spekter molekuly CaM/AMBN-Ct s modely pro nezávislé fungování fúzních podjednotek CaM a AMBN-Ct.

4.2.3. Vazebné funkce konstruktu CaM/AMBN-Ct

Zachování vazebné funkce CaM v konstruktu CaM/AMBN-Ct bylo ověřeno prostřednictvím interakce s dříve popsaným vazebným epitopem TRPM4np odvozeným z iontového kanálu TRPM4 (Bousova et al., 2018). Interakce molekul CaM/AMBN-Ct, CaM

(pozitivní kontrola) a AMBN-Ct (negativní kontrola) s TRPM4np byla studována prostřednictvím měření anizotropie při ustálené fluorescenci. Ze změn fluorescenční anizotropie během titrace fluorescenčně značených epitopů studovanými proteiny byla stanovena hodnota F_B. Závislost F_B na koncentraci ligandu byla proložena rovnicí 2 (3. Materiál a metody, 3.2. Fluorescenční spektroskopie) a určeny hodnoty K_D jednotlivých komplexů (**Obr. 11 A, B**). K_D komplexu TRPM4np s CaM dosahovala hodnoty $0,25 \pm 0,05$ μM, v případě komplexu TRPM4np s CaM/AMBN-Ct činila $1,10 \pm 0,10$ μM.

A

B

Proteinový konstrukt	K_D (SD) (μM)
CaM/Ca^{2+}+TRPM4np	0,25 (0,05)
CaM/AMBN-Ct/Ca^{2+}+TRPM4np	1,10 (0,10)
AMBN-Ct/Ca^{2+}+TRPM4np	-

Obr. 11: Fluorescenční spektroskopická analýza TRPM4np v komplexu s vybranými proteinovými konstrukty CaM/AMBN-Ct, CaM a AMBN-Ct za přítomnosti Ca^{2+}. (**A**) Podíl vazebných epitopů TRPM4np interagujících s CaM/AMBN-Ct (oranžově), CaM (modře) a AMBN-Ct (zeleně) v prostředí s ionty Ca^{2+}. (**B**) Hodnoty K_D komplexů CaM/AMBN-Ct + TRPM4np, CaM + TRPM4np a AMBN-Ct + TRPM4np v přítomnosti Ca^{2+}. Zkratkou SD je označena směrodatná odchylka.

4.2.4. Studium teplotní stability CaM/AMBN-Ct

Potenciální vliv fúzované domény AMBN-Ct na teplotní stabilitu CaM byl studován prostřednictvím spektroskopie CD. Rozpad struktury samotného CaM a CaM fúzovaného s AMBN-Ct byl monitorován prostřednictvím teplotně závislého snížení spektrální intenzity při 222 nm (**Obr. 12**). Pro vyhodnocení experimentální dat byl použit model dvoustavového přechodu. Získaná hodnota teploty tání proteinu (Tm) byla 52,0 ± 0,4 °C v případě CaM a 56,7 ± 0,5 °C u konstruktu CaM/AMBN-Ct. Teplotní stabilita CaM i CaM/AMBN-Ct byla výrazně navýšena v prostředí s ionty Ca^{2+} a hodnotu Tm zde nebylo možné stanovit.
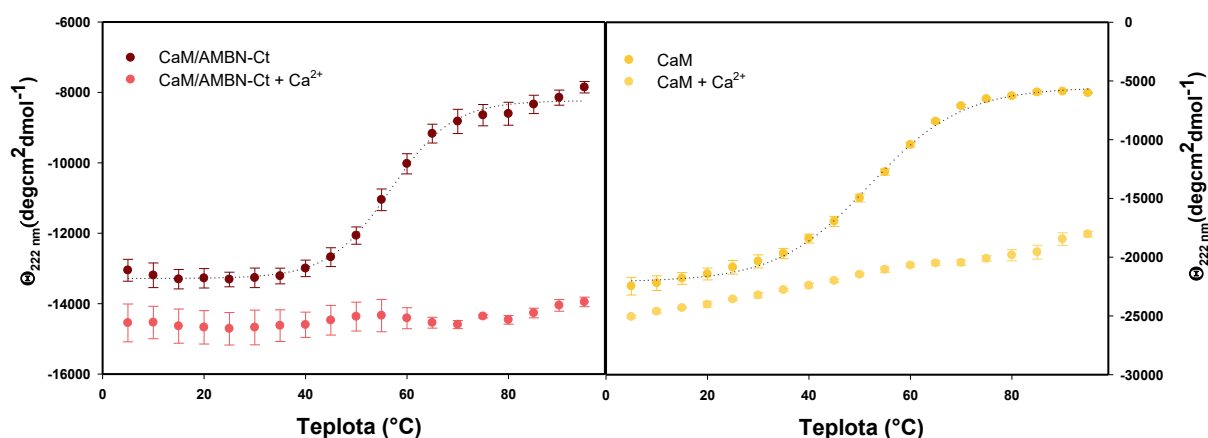

Obr. 12: Analýza teplotní stability CaM/AMBN-Ct a CaM prostřednictvím spektroskopie CD. Jednotlivé body jsou průměrem ze 3 nezávislých měření, chybové úsečky zobrazují standardní odchylku měření.

4.2.5. Analýza fúzní molekuly pomocí molekulového modelování naznačila kontakt CaM a AMBN-Ct za přítomnosti Ca^{2+}

Prostřednictvím metod molekulové dynamiky bylo simulováno chování CaM/AMBN-Ct v prostředí bez iontů Ca^{2+} a v přítomnosti Ca^{2+}. Výsledky molekulární dynamiky korelují s výstupy sedimentačních analýz i s výsledky CD spektroskopie studovaných molekul a potvrzují zachování vysoce flexibilních IDP charakteristik domény AMBN-Ct v rámci CaM/AMBN-Ct (**Obr. 13 A, B**). Experimentálně pozorované zkompaktnění CaM/AMBN-Ct indukované vazbou Ca^{2+} však nebylo zachyceno tak významně jako v případě experimentálních metod a získané modely je třeba posuzovat spíše kvalitativně. Frekvence

kontaktů mezi CaM a fúzovanou doménou AMBN-Ct se nicméně v prostředí bez a s ionty Ca^{2+} lišila a doména AMBN-Ct vykazovala v přítomnosti iontů Ca^{2+} vyšší afinitu k CaM (**Obr. 13 C**). Kontakt obou domén za přítomnosti Ca^{2+} byl dán vystavením hydrofobních reziduí na povrch CaM a umožněním transientních interakcí s hydrofobními zbytky domény AMBN-Ct.
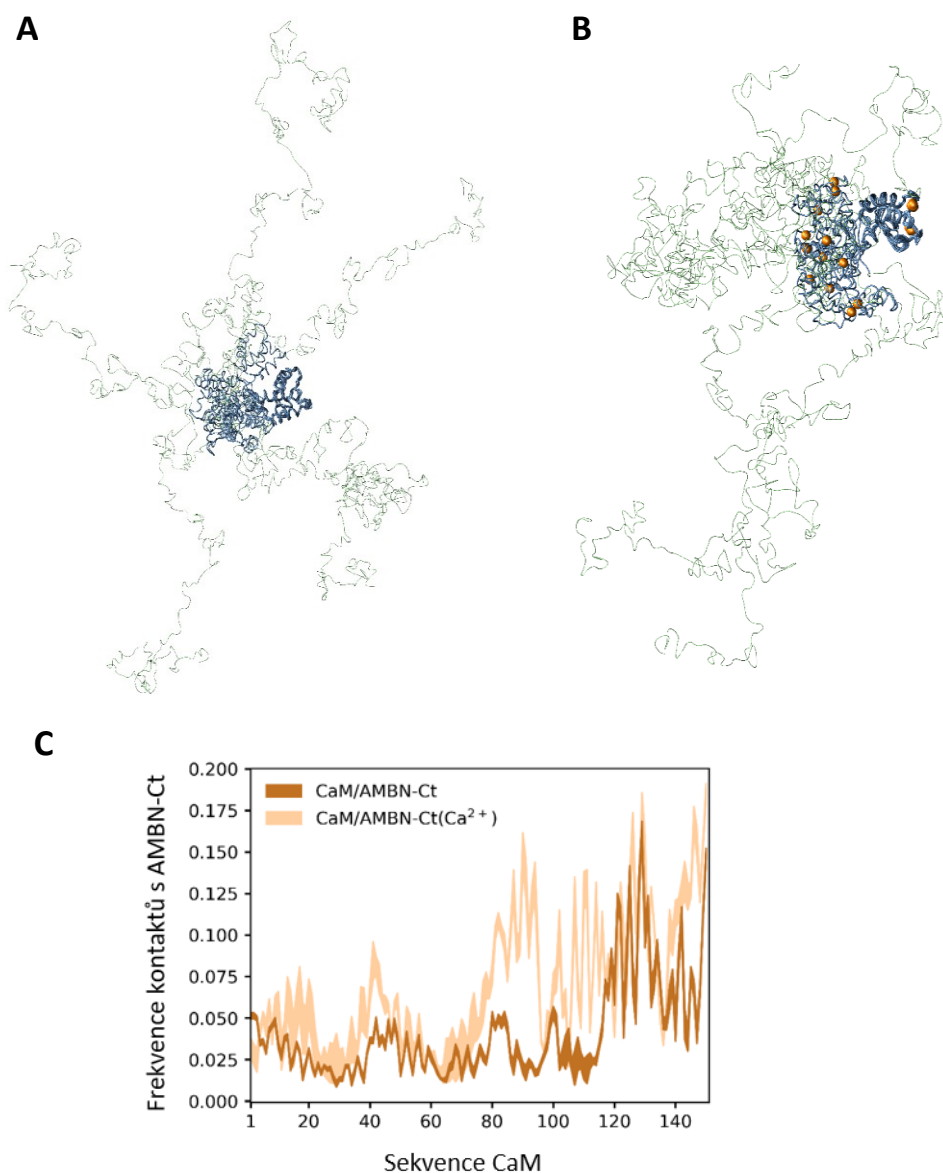
Obr. 13: Molekulová dynamika fúzního proteinu CaM/AMBN-Ct. Molekulový model (**A**) CaM/AMBN-Ct a (**B**) CaM/AMBN-Ct s Ca^{2+} (oranžově). Zobrazeno je vždy 5 molekul superponovaných na N-koncovou doménu CaM. (**C**) Frekvence kontaktů mezi CaM a fúzovanou doménou AMBN-Ct ve fúzním proteinu CaM/AMBN-Ct.

5. DISKUZE

Molekula CaM funguje jako univerzální senzor intracelulární hladiny Ca^{2+}, který v závislosti na přítomnosti iontů Ca^{2+} reguluje nespočet esenciálních buněčných procesů. Mezi cílové proteiny CaM patří všeobecně exprimované iontové kanály podrodiny TRPM. Ačkoli je pro podrodinu TRPM typická regulace rozsáhlým spektrem extracelulárních i intracelulárních stimulů, CaM pravděpodobně představuje univerzální regulační molekulu zástupců této podrodiny (Hasan and Zhang, 2018).

V rámci rodiny TRP kanálů byla regulace molekulou CaM detailně popsána na strukturní úrovni v případě TRPV6 (Singh et al., 2018a). Inhibice TRPV6 prostřednictvím CaM je komplexní proces, kdy se na vazbě jedné molekuly CaM podílí celkem šest různých oblastí TRPV6. Při vazbě CaM tak může docházet k postupným koordinovaným konformačním změnám napříč celým TRP kanálem. V rámci podrodiny TRPM poukazuje přítomnost více vazebných epitopů pro CaM u TRPM2, TRPM3 a TRPM4 na podobnou komplexitu interakce jako u CaM/TRPV6 (Gattkowski et al., 2019, Tong et al., 2006, Bousova et al., 2018, Bousova et al., 2020, Holakovska et al., 2012, Holendova et al., 2012, Przibilla et al., 2018). Informace ohledně možnosti přímé regulace prostřednictvím CaM v případě studovaných iontových kanálů TRPM5, TRPM6 a TRPM7 dosud chyběly. Ačkoli bylo u podrodiny TRPM identifikováno několik vazebných epitopů pro CaM, jejich funkční význam ve většině případů není znám. Pro detailní porozumění komplexitě interakcí mezi zástupci podrodiny TRPM a CaM je třeba lokalizovat jednotlivé vazebné epitopy pro CaM a následně ověřit jejich funkci pomocí elektrofyziologických experimentů. Předkládaná práce souhrnně popisuje lokalizaci a biofyzikální charakterizaci nových vazebných epitopů pro CaM u iontových kanálů podskupiny TRPM6/TRPM7 a TRPM4/TRPM5.

V rámci podskupiny TRPM6/TRPM7 byl detailně charakterizován nový vazebný epitop pro CaM odvozený z cytoplazmatického N-konce iontového kanálu TRPM6. Vazebný epitop TRPM6np disponuje motivem hydrofobních aminokyselin s vmezeřenými rezidui bazických aminokyselin. Pro tyto motivy je typická vazba CaM v závislosti na přítomností iontů Ca^{2+} (Rhoads and Friedberg, 1997). Z tohoto důvodu byly vazebné studie provedeny v přítomnosti 2 mM $CaCl_2$. Formování komplexů CaM/TRP je podmíněno dvěma odlišnými procesy. Dochází

ke kontaktu hydrofobních zbytků vazebných epitopů a hydrofobních zbytků CaM, které jsou exponovány na povrch molekuly v průběhu vazby iontů Ca^{2+} (Bousova et al., 2018). Dále nastává formace solných můstků mezi bazickými aminokyselinami vazebného motivu pro CaM a negativně nabitými aminokyselinovými zbytky molekuly CaM. Typické hodnoty K_D se v případě komplexů CaM/TRP pohybují v řádu jednotek mikromolů (Grycova et al., 2015, Bousova et al., 2018, Holakovska et al., 2012). Měření anizotropie při ustálené fluorescenci poskytlo hodnotu K_D odpovídající slabší vazebné afinitě mezi TRPM6np a CaM v porovnání s popsanými komplexy CaM/vazebný epitop TRP. Obecně vysoká vazebná afinita mezi CaM a vazebnými epitopy TRP kanálů je dána synergickým efektem jednotlivých interagujících aminokyselin.

Klíčová role klastru bazických aminokyselin TRPM6np při formování komplexu CaM/TRPM6np byla potvrzena vazebnými studiemi mezi CaM a mutovanými formami TRPM6np. Zatímco substituce K532A u TRPM6np vedla k mírnému poklesu vazebné afinity, vnesení další mutace R531A způsobilo výrazný pokles hodnoty K_D a potvrdilo funkční význam tandemu bazických zbytků. Pouze nepatrný pokles vazebné afinity byl výsledkem následné mutace R535A. K dalšímu výraznému poklesu vazebné afinity vedla substituce R526A. Vysoká sekvenční homologie mezi TRPM6 a TRPM7 umožnila konstrukci homologního modelu TRPM6 podle publikované struktury TRPM7 (Duan et al., 2018a). Vazebný epitop TRPM6np se nachází v blízkosti cytoplazmatické membrány a je dobře dostupný pro interakci s CaM. Molekulární dokování vizualizovalo vazebné rozhraní komplexu CaM/TRPM6np a podpořilo zapojení bazických zbytků TRPM6np při formování komplexu s CaM.

V rámci podskupiny TRPM6/TRPM7 byl dále identifikován nový vazebný epitop TRPM7np odvozený z cytoplazmatického N-konce TRPM7. Hodnota K_D komplexu CaM/TRPM7np se pohybovala v typickém řádu jednotek μM (Grycova et al., 2015, Holakovska et al., 2012, Bousova et al., 2018). Z porovnání sekvencí TRPM6np a TRPM7np je patrná vysoká sekvenční homologie a zachování vzájemné pozice klíčových aminokyselin vazebných motivů pro CaM. V rámci iontového kanálu TRPM7 je TRPM7np lokalizován v totožné oblasti jako TRPM6np u TRPM6. Z uvedených charakteristik lze předpovědět existenci podobného vazebného rozhraní jako v případě CaM/TRPM6np. Nižší hodnota K_D komplexu CaM/TRPM7np než v případě CaM/TRPM6np může být dána přítomností další bazické

aminokyseliny R532, která se u vazebného epitopu TRPM6np nevyskytuje. TRPM6np a TRPM7np představují první identifikované vazebné epitopy pro CaM v rámci podskupiny TRPM6/TRPM7 a pokládají základy pro studium potenciální CaM-dependentní regulace TRPM6 a TRPM7.

Analogicky probíhala charakterizace vazebných epitopů pro CaM u podskupiny TRPM4/TRPM5. Celkem byly popsány tři nové vazebné epitopy pro CaM: TRPM4np, TRPM4cp a TRPM5np. Hodnota K_D všech komplexů se pohybovala v typickém rozmezí pro interakci CaM/TRP a role bazických aminokyselin při formování komplexů byla potvrzena experimentálně. U iontového kanálu TRPM4 byla prokázána pozitivní regulace molekulou CaM, podmíněná pravděpodobně interakcí mezi CaM a cytoplazmatickým C-koncem TRPM4 (Nilius et al., 2005). TRPM4ct je součástí tzv. re-entrant helixu TRP domény, který v publikovaných strukturách TRPM4 vstupuje do cytoplazmatické membrány, kde je nepřístupný pro interakci s CaM (Duan et al., 2018b, Autzen et al., 2018, Winkler et al., 2017). Struktury TRPV2 kanálu ukázaly možnost přestupu re-entrant helixu z cytoplazmatické membrány do cytoplazmy (Huynh et al., 2016, Zubcevic et al., 2018). Tento mechanismus by umožnil zapojení TRPM4ct do regulace aktivity TRPM4 prostřednictvím CaM, ale i membránových fosfolipidů jako je např. PIP2. Druhý vazebný epitop TRPM4np je lokalizován v cytoplazmatické časti TRPM4, kde se může spolupodílet na vazbě molekuly CaM. Ačkoli jsou TRPM4 i TRPM5 aktivovány při nárůstu cytoplazmatické koncentrace Ca^{2+} a jedná se o blízké homology v rámci podrodiny TRPM, nebylo u TRPM5 dosud prokázáno zapojení CaM do regulace iontového kanálu. TRPM5np představuje první identifikovaný vazebný epitop pro CaM u iontového kanálu TRPM5.

U molekuly CaM byla následně studována možnost modulace vlastností prostřednictvím fúze s IDP doménou AMBN-Ct. IDP domény obecně disponují značným regulačním potenciálem, daným jejich enormní flexibilitou a konformační dynamikou. V závislosti na přítomnosti dalších molekul může docházet ke sbalování IDP domén do uspořádaných struktur nebo ke změně preferovaných konformací bez vzniku specifických 3D struktur (Grzybowska, 2018). Schopnost IDP domén zaujímat nespočet různých konformací a dynamicky reagovat na změny v prostředí z nich činí vhodné kandidáty pro modulátory svých fúzních partnerů. Během přípravy fúzních proteinů může dojít ke změnám původní 3D struktury

fúzovaných molekul, které mohou mít negativní dopad na funkčnost molekul. U nových fúzních molekul je třeba ověřit zachování požadovaných strukturních charakteristik i funkčních vlastností.

Spektroskopie CD ve vzdálené UV oblasti potvrdila u molekuly CaM/AMBN-Ct přítomnost α-helikálních i IDP oblastí. Porovnání experimentálních a modelových spekter pro nezávislé chování fúzních partnerů odhalilo u molekuly CaM/AMBN-Ct nárůst helicity, který pravděpodobně odpovídá změnám v doméně AMBN-Ct v důsledku mezi-doménové komunikace s molekulou CaM v rámci fúzního konstruktu CaM/AMBN-Ct. Jelikož u CaM/AMBN-Ct nedošlo ke ztrátě α-helikálního charakteru ani nárůstu β-struktur oproti spektrům CD jednotlivých molekul, lze předpokládat zachování sekundární struktury CaM v rámci CaM/AMBN-Ct. Charakteristiky spektra CD v blízké UV oblasti konstruktu CaM/AMBN-Ct odpovídaly spektru CaM. Terciální struktura CaM v rámci CaM/AMBN-Ct je pravděpodobně zachována a udává negativní pásy spektra. Vyloučit však nelze vznik terciálních struktur podjednotky AMBN-Ct, která sama o sobě terciální struktury netvoří. Reorientace α-helixů CaM při vazbě iontů Ca^{2+} vede k nárůstu spektrální intenzity negativních pásů ve vzdálené i blízké UV oblasti (Martin and Bayley, 1986). Stejný trend byl pozorován i v případě CaM/AMBN-Ct a indikuje vznik charakteristických strukturních změn v důsledku interakcí mezi CaM a ionty Ca^{2+}. CaM v konstruktu CaM/AMBN-Ct má tedy zachovanou nativní strukturu a pravděpodobně i schopnost interakce s ionty Ca^{2+}.

Typickou vlastností CaM je schopnost interakce s enormním množstvím cílových proteinů. Zachování vazebných vlastností CaM v molekule CaM/AMBN bylo studováno prostřednictvím interakce konstruktu CaM/AMBN-Ct s vazebným epitopem odvozeným z iontového kanálu TRPM4 (Bousova et al., 2018). Studovaný vazebný epitop měl schopnost vazby CaM i CaM/AMBN-Ct a neinteragoval se samotnou doménou AMBN-Ct. V obou případech byla interakce podmíněna aktivací CaM ionty Ca^{2+}. K_D komplexu s CaM/AMBN-Ct byla asi čtyřikrát vyšší v porovnání s komplexem samotné molekuly CaM. Ačkoli má CaM v konstruktu CaM/AMBN-Ct lehce sníženou vazebnou afinitu k vybranému vazebnému epitopu, stále se hodnota K_D tohoto komplexu pohybuje v řádu jednotek μM. CaM po fúzi s AMBN-Ct si tedy zachoval schopnost vysokoafinitní interakce s vazebným epitopem odvozeným z TRP kanálů. Vyšší hodnota K_D komplexu s CaM/AMBN-Ct je dána

mezi-doménovou komunikací mezi CaM a AMBN-Ct, kterou indikoval průběh spektra CD ve vzdálené UV oblasti i simulace molekulové dynamiky. Podjednotka AMBN-Ct může ovlivnit formování komplexu prostřednictvím alosterické modulace oblasti vazebného místa pro studovaný epitop nebo jeho přímou okluzí. Efekt mezi-doménové komunikace v konstruktu CaM/AMBN-Ct byl patrný také z výsledků sedimentačních analýz. V případě CaM i CaM/AMBN-Ct docházelo v prostředí s ionty Ca^{2+} ke konformačním změnám a zvýšení kompaktnosti molekul. Tento efekt byl nejvýraznější u molekuly CaM/AMBN-Ct a zahrnoval také změny v podjednotce AMBN-Ct, která sama o sobě na přítomnost iontů Ca^{2+} nereagovala. Konformační změny dané vazbou Ca^{2+} k podjednotce CaM tedy vedou ke změnám v mezi-doménové komunikaci, které se projeví kompaktnější molekulou CaM/AMBN-Ct.

Podjednotky CaM a AMBN-Ct v rámci CaM/AMBN-Ct nefungují zcela nezávisle. I přes efekt mezi-doménové komunikace však zůstávají zachovány základní strukturní a vazebné charakteristiky molekuly CaM. Vzhledem k vzájemné komunikaci podjednotek mohlo dojít ke změněně teplotní stability CaM v rámci CaM/AMBN-Ct. Rozvolnění struktury CaM bylo sledováno prostřednictvím spektroskopie CD a při vyhodnocení experimentálních dat byl aplikován jednoduchý model dvoustavového přechodu. Získaná hodnota Tm pro CaM/AMBN-Ct byla asi o 5 °C vyšší v porovnání se samotnou molekulou CaM. Konkrétní hodnota Tm je výrazným zjednodušením celkového průběhu teplotní denaturace CaM, jelikož se jedná o komplexní proces, spojený se vznikem přechodových mezi-stavů (Protasevich et al., 1997). Z porovnání křivek tání CaM a CaM/AMBN-Ct je patrné, že fúze s AMBN-Ct vedla ke snížení sklonu křivky v oblasti nižších teplot, a tedy k potlačení vzniku raných přechodových mezi-stavů CaM. Vazba iontů Ca^{2+} vedla u CaM i CaM/AMBN-Ct k enormní teplotní stabilizaci a znemožnění odečtu konkrétních hodnot Tm. Výrazná teplotní stabilizace v důsledku vazby iontu Ca^{2+} představuje charakteristický rys molekuly CaM (Minnes et al., 2017). Dle průběhu křivek tání je patrná vyšší teplotní stabilita opět v případě CaM/AMBN-Ct. Fúzí CaM s IDP doménou AMBN-Ct jsme získali novou molekulu CaM/AMBN-Ct se zachovanými nativními vlastnostmi a vylepšenou teplotní stabilitou podjednotky CaM.

6. ZÁVĚR

Náplní disertační práce bylo studium molekuly CaM s ohledem na potenciální zapojení do regulace vybraných zástupců medicínsky atraktivní podrodiny iontových kanálů TRPM. Vazebné epitopy pro CaM byly u iontových kanálu TRPM4, TRPM5, TRPM6 a TRPM7 vytipovány *in silico*. Navazující vazebné studie mezi odvozenými vazebnými epitopy a molekulou CaM potvrdily vazebnou afinitu pohybující se v hodnotách typických pro komplexy CaM/TRP. Formace komplexů CaM/TRP zahrnuje vzájemnou interakci mezi bazickými aminokyselinami TRP kanálů a kyselými rezidui CaM. Nové vazebné epitopy pro CaM byly syntetizovány v mutovaných formách obsahujících postupnou záměnu klíčových bazických reziduí. Vazebné studie mezi pozměněnými vazebnými epitopy a molekulou CaM prokázaly významný pokles vazebné afinity až úplné narušení tvorby komplexů. Výsledky těchto studií poukazují na specifitu interakcí mezi identifikovanými vazebnými epitopy a molekulou CaM. Modely iontových kanálů TRPM4, TRPM5, TRPM6 i TRPM7 ukázaly dobrou přístupnost studovaných vazebných epitopů pro molekulu CaM. Následné molekulové dokování struktury studovaných vazebných epitopů do molekuly CaM dále potvrzuje vazebné rozhraní typické pro interakce CaM/TRP.

Cílem druhé části disertační práce byla optimalizace funkčních vlastností studované molekuly CaM prostřednictvím metod proteinového inženýrství. Fúzí CaM a vysoce flexibilní IDP domény AMBN-Ct byla připravena nová molekula CaM/AMBN-Ct. Výsledky CD spektroskopie prokázaly zachování sekundárních i terciálních strukturních charakteristik CaM v rámci konstruktu CaM/AMBN-Ct. Navýšení helicity i teplotní stability CaM/AMBN-Ct v prostředí s ionty Ca^{2+} indikuje strukturní změny typické pro interakce CaM s ionty Ca^{2+}. Měření časově rozlišené anizotropie fluorescence ukázalo Ca^{2+}-dependentní vazebnou interakci mezi CaM/AMBN-Ct a vazebným epitopem pro CaM odvozeným z iontového kanálu TRPM4. Výsledky vazebných studií prokazují zachování klíčových vazebných vlastností CaM (Ca^{2+}-dependentní aktivace a interakce s cílovým vazebným epitopem) v molekule CaM/AMBN-Ct. CD spektroskopie i sedimentační analýzy studovaných molekul indikují mezi-doménovou komunikaci mezi CaM a AMBN-Ct v konstruktu CaM/AMBN-Ct. Studium teplotní denaturace ukázalo potlačení tvorby raných přechodových mezi-stavů CaM v rámci CaM/AMBN-Ct a navýšení celkové hodnoty Tm proteinu. Prostřednictvím fúze dvou původně

nezávislých proteinových sekvencí CaM a AMBN-Ct jsme získali novou fúzní molekulu CaM/AMBN-Ct. Ačkoli základní strukturně-funkční charakteristiky jednotlivých fúzních partnerů zůstaly zachovány, dochází k ustavení vzájemné komunikace mezi CaM a AMBN-Ct. Efekt mezi-doménové komunikace pak přináší navýšení teplotní stability molekuly CaM v rámci CaM/AMBN-Ct.

Výstup řešení disertační práce představují jednak nové vazebné epitopy pro CaM odvozené z iontových kanálů podrodiny TRPM a dále design inovativní chimérní molekuly CaM/AMBN-Ct. Nově identifikované vazebné epitopy mohou být zapojené do CaM-dependentní regulace iontových kanálů TRPM4, TRPM5, TRPM6 a TRPM7. Porozumění komplexním mechanismům regulace těchto kanálů představuje nezbytnou prerekvizitu pro vývoj terapeutik širokého spektra civilizačních onemocnění. Unikátní vlastnosti molekuly CaM navíc tvoří základ řady biotechnologicky/biomedicínsky významných fúzních molekul. Optimalizace teplotní stability CaM usnadňuje využití těchto molekul v suboptimálních podmínkách. Poznatky získané při studiu CaM/AMBN-Ct mohou nacházet uplatnění při designu teplotně stabilnějších proteinových molekul. Samotný konstrukt CaM/AMBN-Ct má navíc potenciál tvořit základ dalších inovativních molekul.

7. SOUHRN

CaM monitoruje přítomnost iontů Ca^{2+} v cytoplazmě a v závislosti na hladině Ca^{2+} reguluje stovky cílových proteinů včetně zástupců podrodiny iontových kanálů TRPM. Dysregulace TRPM je spojena s rozvojem závažných kardiovaskulárních, metabolických i nádorových onemocnění a porozumění komplexním mechanismům modulace jejich aktivity představuje klíčovou prerekvizitu vývoje nových léčiv. Informace ohledně regulace aktivity jednotlivých zástupců TRPM prostřednictvím CaM přesto zůstávají stále velmi limitované.

Cílem disertační práce bylo rozšíření spektra vazebných epitopů pro CaM u zástupců podrodiny TRPM. Celkem bylo popsáno pět nových vazebných epitopů pro CaM, přičemž dva byly odvozené z iontového kanálu TRPM4 a zbývající tři z TRPM5, TRPM6 a TRPM7. Detailní studium vazebného rozhraní komplexů odhalilo charakteristiky typické pro interakce CaM s TRP kanály, a tím potvrdilo specifitu studovaných interakcí. V případě iontového kanálu TRPM4 byla dříve potvrzena aktivace prostřednictvím CaM a nové vazebné epitopy rozšiřují spektrum popsaných vazebných míst pro CaM, které se mohou spolupodílet na tvorbě komplexu CaM/TRPM4. U TRPM5, TRPM6 a TRPM7 se jedná o první popsané vazebné epitopy pro CaM, které mohou být základem dalšího studia regulace prostřednictvím molekuly CaM.

Unikátní vlastnosti CaM, zejména jeho konformační plasticita a typické strukturní změny indukované vazbou iontů Ca^{2+}, jsou využívány při designu nových proteinových molekul pro oblast biotechnologií i biomedicíny. Vzhledem k širokému aplikačnímu potenciálu CaM je žádoucí příprava souboru modifikovaných variant CaM s optimalizovanými vlastnostmi. Univerzální využití mohou nacházet stabilnější molekuly CaM s prodlouženou životností v suboptimálních podmínkách. Prostřednictvím fúze CaM s vnitřně neuspořádanou doménou AMBN-Ct byl připraven nový proteinový konstrukt CaM/AMBN-Ct. CaM má v rámci konstruktu CaM/AMBN-Ct zachovanou sekundární i terciální strukturu a základní vazebné vlastnosti, tj. schopnost interakce s ionty Ca^{2+} nebo vazebným epitopem odvozeným z iontového kanálu rodiny TRP. Výsledkem vzájemného působení mezi CaM a AMBN-Ct je navýšení teplotní stability CaM. Fúzní konstrukt CaM/AMBN-Ct tedy může sloužit jako základ nových, teplotně stabilnějších molekul, využívajících typických strukturně-funkčních vlastností molekuly CaM.

8. SUMMARY

CaM monitors the presence of Ca^{2+} ions in the cytoplasm, and depending on Ca^{2+} levels, it regulates hundreds of target proteins including those of the TRPM ion channel subfamily. TRPM dysregulation is associated with the development of serious cardiovascular, metabolic, and cancerous diseases, and the understanding of the complex mechanisms that modulate the activity of these proteins is crucial for the development of new drugs. However, information on how the activity of individual TRPM members is regulated through CaM still remains very limited.

The aim of the thesis was to expand the spectrum of binding epitopes for CaM in TRPM members. In total, 5 new CaM-binding epitopes were described: 2 are derived from the TRPM4 and the other 3 are derived from TRPM5, TRPM6, and TRPM7. Detailed study of the binding interface of the complexes revealed characteristics typical for CaM interactions with TRP, thereby confirming the specificity of the studied interactions. Activation by CaM was previously confirmed for TRPM4, and the new binding epitopes expand the spectrum of described CaM binding sites that may be involved in the formation of the CaM/TRPM4 complex. As for TRPM5, TRPM6, and TRPM7, the CaM-binding epitopes are the first ones described and can be used as the basis for further study of TRPM5, TRPM6, and TRPM7 regulation by CaM.

The unique properties of CaM, particularly its conformational plasticity and typical structural changes induced by Ca^{2+} binding, are used in the design of novel protein molecules in the field of biotechnologies and in biomedicine. Considering the wide application potential of CaM, it is desirable to prepare a set of modified CaM variants with optimized properties. Universal applications may be offered by more stable CaM molecules with an extended lifetime in suboptimal conditions. CaM/AMBN-Ct, a novel protein construct, was prepared by fusing CaM with the intrinsically disordered domain AMBN-Ct. The secondary as well as tertiary structure of CaM is preserved in CaM/AMBN-Ct, and its essential binding properties, i.e. its ability to interact with Ca^{2+} ions, and the binding epitope derived from the TRP member are preserved, as well. Increased thermal stability of CaM is a result of mutual contacts between CaM and AMBN-Ct. Thus the fusion construct CaM/AMBN-Ct can be used for novel molecules with higher thermal stability that employ the typical structural and functional properties of CaM.

9. LITERATURA

1. ABBASI, W. A., ASIF, A., ANDLEEB, S. & MINHAS, F. 2017. CaMELS: In silico prediction of calmodulin binding proteins and their binding sites. *Proteins,* 85**,** 1724-1740. DOI: 10.1002/prot.25330.
2. ABRAHAM, M. J., MURTOLA, T., SCHULZ, R., PÁLL, S., SMITH, J. C., HESS, B. & LINDAHL, E. 2015. GROMACS: High performance molecular simulations through multi-level parallelism from laptops to supercomputers. *SoftwareX,* 1**,** 19-25. DOI: 10.1016/j.softx.2015.06.001.
3. AKBARI, B., FARAJNIA, S., AHDI KHOSROSHAHI, S., SAFARI, F., YOUSEFI, M., DARIUSHNEJAD, H. & RAHBARNIA, L. 2017. Immunotoxins in cancer therapy: Review and update. *Int Rev Immunol,* 36**,** 207-219. DOI: 10.1080/08830185.2017.1284211.
4. ANDO, T., KUDO, Y., IIZUKA, S., TSUNEMATSU, T., UMEHARA, H., SHRESTHA, M., MATSUO, T., KUBO, T., SHIMOSE, S., ARIHIRO, K., OGAWA, I., OCHI, M. & TAKATA, T. 2017. Ameloblastin induces tumor suppressive phenotype and enhances chemosensitivity to doxorubicin via Src-Stat3 inactivation in osteosarcoma. *Sci Rep,* 7**,** 40187. DOI: 10.1038/srep40187.
5. ANDRADY, C., SHARMA, S. K. & CHESTER, K. A. 2011. Antibody-enzyme fusion proteins for cancer therapy. *Immunotherapy,* 3**,** 193-211. DOI: 10.2217/imt.10.90.
6. ANDREWS, C., XU, Y., KIRBERGER, M. & YANG, J. J. 2020. Structural aspects and prediction of calmodulin-binding proteins. *International Journal of Molecular Sciences,* 22**,** 308. DOI: 10.3390/ijms22010308.
7. AUTZEN, H. E., MYASNIKOV, A. G., CAMPBELL, M. G., ASARNOW, D., JULIUS, D. & CHENG, Y. 2018. Structure of the human TRPM4 ion channel in a lipid nanodisc. *Science,* 359**,** 228-232. DOI: 10.1126/science.aar4510.
8. BAHLER, M. & RHOADS, A. 2002. Calmodulin signaling via the IQ motif. *FEBS Lett,* 513**,** 107-13. DOI: 10.1016/s0014-5793(01)03239-2.
9. BARBATO, G., IKURA, M., KAY, L. E., PASTOR, R. W. & BAX, A. 1992. Backbone dynamics of calmodulin studied by 15N relaxation using inverse detected two-dimensional NMR spectroscopy: the central helix is flexible. *Biochemistry,* 31**,** 5269-78. DOI: 10.1021/bi00138a005.
10. BARBIERO, V. S., GIAMBELLI, R., MUSAZZI, L., TIRABOSCHI, E., TARDITO, D., PEREZ, J., DRAGO, F., RACAGNI, G. & POPOLI, M. 2007. Chronic antidepressants induce redistribution and differential activation of alphaCaM kinase II between presynaptic compartments. *Neuropsychopharmacology,* 32**,** 2511-9. DOI: 10.1038/sj.npp.1301378.
11. BEN-JOHNY, M., DICK, I. E., SANG, L., LIMPITIKUL, W. B., KANG, P. W., NIU, J., BANERJEE, R., YANG, W., BABICH, J. S., ISSA, J. B., LEE, S. R., NAMKUNG, H., LI, J., ZHANG, M., YANG, P. S., BAZZAZI, H., ADAMS, P. J., JOSHI-MUKHERJEE, R., YUE, D. N. & YUE, D. T. 2015. Towards a Unified Theory of Calmodulin Regulation (Calmodulation) of Voltage-Gated Calcium and Sodium Channels. *Curr Mol Pharmacol,* 8**,** 188-205. DOI: 10.2174/1874467208666150507110359.
12. BERCHTOLD, M. W. & VILLALOBO, A. 2014. The many faces of calmodulin in cell proliferation, programmed cell death, autophagy, and cancer. *Biochim Biophys Acta,* 1843**,** 398-435. DOI: 10.1016/j.bbamcr.2013.10.021.
13. BESSAC, B. F. & FLEIG, A. 2007. TRPM7 channel is sensitive to osmotic gradients in human kidney cells. *J Physiol,* 582**,** 1073-86. DOI: 10.1113/jphysiol.2007.130534.

14. BIEKOFSKY, R. R., MARTIN, S. R., BROWNE, J. P., BAYLEY, P. M. & FEENEY, J. 1998. Ca2+ coordination to backbone carbonyl oxygen atoms in calmodulin and other EF-hand proteins: 15N chemical shifts as probes for monitoring individual-site Ca2+ coordination. *Biochemistry,* 37**,** 7617-29. DOI: 10.1021/bi9800449.

15. BOADO, R. J., HUI, E. K., LU, J. Z., ZHOU, Q. H. & PARDRIDGE, W. M. 2010. Selective targeting of a TNFR decoy receptor pharmaceutical to the primate brain as a receptor-specific IgG fusion protein. *J Biotechnol,* 146**,** 84-91. DOI: 10.1016/j.jbiotec.2010.01.011.

16. BOADO, R. J., ZHANG, Y., ZHANG, Y., XIA, C. F., WANG, Y. & PARDRIDGE, W. M. 2008. Genetic engineering of a lysosomal enzyme fusion protein for targeted delivery across the human blood-brain barrier. *Biotechnol Bioeng,* 99**,** 475-84. DOI: 10.1002/bit.21602.

17. BOOTZ, F. & NERI, D. 2016. Immunocytokines: a novel class of products for the treatment of chronic inflammation and autoimmune conditions. *Drug Discov Today,* 21**,** 180-189. DOI: 10.1016/j.drudis.2015.10.012.

18. BORGHUIS, B. G., TIAN, L., XU, Y., NIKONOV, S. S., VARDI, N., ZEMELMAN, B. V. & LOOGER, L. L. 2011. Imaging light responses of targeted neuron populations in the rodent retina. *J Neurosci,* 31**,** 2855-67. DOI: 10.1523/JNEUROSCI.6064-10.2011.

19. BORGSTROM, A., PEINELT, C. & STOKLOSA, P. 2021. TRPM4 in Cancer-A New Potential Drug Target. *Biomolecules,* 11. DOI: 10.3390/biom11020229.

20. BOUSOVA, K., BARVIK, I., HERMAN, P., HOFBAUEROVA, K., MONINCOVA, L., MAJER, P., ZOUHAROVA, M., VETYSKOVA, V., POSTULKOVA, K. & VONDRASEK, J. 2020. Mapping of CaM, S100A1 and PIP2-Binding Epitopes in the Intracellular N- and C-Termini of TRPM4. *Int J Mol Sci,* 21. DOI: 10.3390/ijms21124323.

21. BOUSOVA, K., BEDNAROVA, L., ZOUHAROVA, M., VETYSKOVA, V., POSTULKOVA, K., HOFBAUEROVA, K., PETRVALSKA, O., VANEK, O., TRIPSIANES, K. & VONDRASEK, J. 2021a. The order of PDZ3 and TrpCage in fusion chimeras determines their properties-a biophysical characterization. *Protein Sci,* 30**,** 1653-1666. DOI: 10.1002/pro.4107.

22. BOUSOVA, K., HERMAN, P., VECER, J., BEDNAROVA, L., MONINCOVA, L., MAJER, P., VYKLICKY, L., VONDRASEK, J. & TEISINGER, J. 2018. Shared CaM- and S100A1-binding epitopes in the distal TRPM4 N terminus. *FEBS J,* 285**,** 599-613. DOI: 10.1111/febs.14362.

23. BOUSOVA, K., ZOUHAROVA, M., HERMAN, P., VETYSKOVA, V., JIRASKOVA, K. & VONDRASEK, J. 2021b. TRPM7 N-terminal region forms complexes with calcium binding proteins CaM and S100A1. *Heliyon,* 7**,** e08490. DOI: 10.1016/j.heliyon.2021.e08490.

24. BOUSOVA, K., ZOUHAROVA, M., HERMAN, P., VYMETAL, J., VETYSKOVA, V., JIRASKOVA, K. & VONDRASEK, J. 2022. TRPM5 Channel Binds Calcium-Binding Proteins Calmodulin and S100A1. *Biochemistry,* 61**,** 413-423. DOI: 10.1021/acs.biochem.1c00647.

25. CEBALLOS GARZON, A., AMADO, D., ROBERT, E., PARRA GIRALDO, C. M. & LE PAPE, P. 2020. Impact of calmodulin inhibition by fluphenazine on susceptibility, biofilm formation and pathogenicity of caspofungin-resistant Candida glabrata. *J Antimicrob Chemother,* 75**,** 1187-1193. DOI: 10.1093/jac/dkz565.

26. CHEN, X., ZARO, J. L. & SHEN, W. C. 2013. Fusion protein linkers: property, design and functionality. *Adv Drug Deliv Rev,* 65**,** 1357-69. DOI: 10.1016/j.addr.2012.09.039.

27. CHOY, E. H. & PANAYI, G. S. 2001. Cytokine pathways and joint inflammation in rheumatoid arthritis. *N Engl J Med,* 344**,** 907-16. DOI: 10.1056/NEJM200103223441207.

28. CLAPHAM, D. E. 2003. TRP channels as cellular sensors. *Nature,* 426**,** 517-24. DOI: 10.1038/nature02196.

29. CLARK, K., MIDDELBEEK, J., DOROVKOV, M. V., FIGDOR, C. G., RYAZANOV, A. G., LASONDER, E. & VAN LEEUWEN, F. N. 2008a. The alpha-kinases TRPM6 and TRPM7, but not eEF-2 kinase, phosphorylate the assembly domain of myosin IIA, IIB and IIC. *FEBS Lett,* 582**,** 2993-7. DOI: 10.1016/j.febslet.2008.07.043.

30. CLARK, K., MIDDELBEEK, J., MORRICE, N. A., FIGDOR, C. G., LASONDER, E. & VAN LEEUWEN, F. N. 2008b. Massive autophosphorylation of the Ser/Thr-rich domain controls protein kinase activity of TRPM6 and TRPM7. *PLoS One,* 3**,** e1876. DOI: 10.1371/journal.pone.0001876.

31. CROTTI, L., SPAZZOLINI, C., TESTER, D. J., GHIDONI, A., BARUTEAU, A. E., BECKMANN, B. M., BEHR, E. R., BENNETT, J. S., BEZZINA, C. R., BHUIYAN, Z. A., CELIKER, A., CERRONE, M., DAGRADI, F., DE FERRARI, G. M., ETHERIDGE, S. P., FATAH, M., GARCIA-PAVIA, P., AL-GHAMDI, S., HAMILTON, R. M., AL-HASSNAN, Z. N., HORIE, M., JIMENEZ-JAIMEZ, J., KANTER, R. J., KASKI, J. P., KOTTA, M. C., LAHROUCHI, N., MAKITA, N., NORRISH, G., ODLAND, H. H., OHNO, S., PAPAGIANNIS, J., PARATI, G., SEKARSKI, N., TVETEN, K., VATTA, M., WEBSTER, G., WILDE, A. A. M., WOJCIAK, J., GEORGE, A. L., ACKERMAN, M. J. & SCHWARTZ, P. J. 2019. Calmodulin mutations and life-threatening cardiac arrhythmias: insights from the International Calmodulinopathy Registry. *Eur Heart J,* 40**,** 2964-2975. DOI: 10.1093/eurheartj/ehz311.

32. CUMMINGS, J. L., TONG, G. & BALLARD, C. 2019. Treatment Combinations for Alzheimer's Disease: Current and Future Pharmacotherapy Options. *J Alzheimers Dis,* 67**,** 779-794. DOI: 10.3233/JAD-180766.

33. DIKICI, E., DEO, S. K. & DAUNERT, S. 2003. Drug detection based on the conformational changes of calmodulin and the fluorescence of its enhanced green fluorescent protein fusion partner. *Analytica Chimica Acta,* 500**,** 237-245. DOI: 10.1016/j.aca.2003.08.027.

34. DIVER, M. M., CHENG, Y. & JULIUS, D. 2019. Structural insights into TRPM8 inhibition and desensitization. *Science,* 365**,** 1434-1440. DOI: 10.1126/science.aax6672.

35. DOMBECK, D. A., HARVEY, C. D., TIAN, L., LOOGER, L. L. & TANK, D. W. 2010. Functional imaging of hippocampal place cells at cellular resolution during virtual navigation. *Nat Neurosci,* 13**,** 1433-40. DOI: 10.1038/nn.2648.

36. DUAN, J., LI, Z., LI, J., HULSE, R. E., SANTA-CRUZ, A., VALINSKY, W. C., ABIRIA, S. A., KRAPIVINSKY, G., ZHANG, J. & CLAPHAM, D. E. 2018a. Structure of the mammalian TRPM7, a magnesium channel required during embryonic development. *Proc Natl Acad Sci U S A,* 115**,** E8201-E8210. DOI: 10.1073/pnas.1810719115.

37. DUAN, J., LI, Z., LI, J., SANTA-CRUZ, A., SANCHEZ-MARTINEZ, S., ZHANG, J. & CLAPHAM, D. E. 2018b. Structure of full-length human TRPM4. *Proc Natl Acad Sci U S A,* 115**,** 2377-2382. DOI: 10.1073/pnas.1722038115.

38. DUITAMA, M., VARGAS-LÓPEZ, V., CASAS, Z., ALBARRACIN, S. L., SUTACHAN, J.-J. & TORRES, Y. P. 2020. TRP channels role in pain associated with neurodegenerative diseases. *Frontiers in Neuroscience,* 14**,** 782. DOI: 10.3389/fnins.2020.00782.

39. DUTTA BANIK, D., MARTIN, L. E., FREICHEL, M., TORREGROSSA, A. M. & MEDLER, K. F. 2018. TRPM4 and TRPM5 are both required for normal signaling in taste receptor cells. *Proc Natl Acad Sci U S A,* 115**,** E772-E781. DOI: 10.1073/pnas.1718802115.

40. EARLEY, S., WALDRON, B. J. & BRAYDEN, J. E. 2004. Critical role for transient receptor potential channel TRPM4 in myogenic constriction of cerebral arteries. *Circ Res,* 95**,** 922-9. DOI: 10.1161/01.RES.0000147311.54833.03.

41. FALLON, J. L. & QUIOCHO, F. A. 2003. A closed compact structure of native Ca(2+)-calmodulin. *Structure,* 11**,** 1303-7. DOI: 10.1016/j.str.2003.09.004.

42. FECAROTTA, S., GASPERINI, S. & PARENTI, G. 2018. New treatments for the mucopolysaccharidoses: from pathophysiology to therapy. *Ital J Pediatr,* 44**,** 124. DOI: 10.1186/s13052-018-0564-z.

43. FISCHER, R., KOLLER, M., FLURA, M., MATHEWS, S., STREHLER-PAGE, M. A., KREBS, J., PENNISTON, J. T., CARAFOLI, E. & STREHLER, E. E. 1988. Multiple divergent mRNAs code for a single human calmodulin. *J Biol Chem,* 263**,** 17055-62. DOI: 10.1016/S0021-9258(18)37497-0.

44. FONFRIA, E., MURDOCK, P. R., CUSDIN, F. S., BENHAM, C. D., KELSELL, R. E. & MCNULTY, S. 2006. Tissue distribution profiles of the human TRPM cation channel family. *J Recept Signal Transduct Res,* 26**,** 159-78. DOI: 10.1080/10799890600637506.

45. FRIEDRICH, F. W., BAUSERO, P., SUN, Y., TRESZL, A., KRAMER, E., JUHR, D., RICHARD, P., WEGSCHEIDER, K., SCHWARTZ, K., BRITO, D., ARBUSTINI, E., WALDENSTROM, A., ISNARD, R., KOMAJDA, M., ESCHENHAGEN, T., CARRIER, L. & PROJECT, E. H. F. 2009. A new polymorphism in human calmodulin III gene promoter is a potential modifier gene for familial hypertrophic cardiomyopathy. *Eur Heart J,* 30**,** 1648-55. DOI: 10.1093/eurheartj/ehp153.

46. FUKUMOTO, S., KIBA, T., HALL, B., IEHARA, N., NAKAMURA, T., LONGENECKER, G., KREBSBACH, P. H., NANCI, A., KULKARNI, A. B. & YAMADA, Y. 2004. Ameloblastin is a cell adhesion molecule required for maintaining the differentiation state of ameloblasts. *J Cell Biol,* 167**,** 973-83. DOI: 10.1083/jcb.200409077.

47. GARCIA-SANZ, N., VALENTE, P., GOMIS, A., FERNANDEZ-CARVAJAL, A., FERNANDEZ-BALLESTER, G., VIANA, F., BELMONTE, C. & FERRER-MONTIEL, A. 2007. A role of the transient receptor potential domain of vanilloid receptor I in channel gating. *J Neurosci,* 27**,** 11641-50. DOI: 10.1523/JNEUROSCI.2457-07.2007.

48. GATTKOWSKI, E., JOHNSEN, A., BAUCHE, A., MOCKL, F., KULOW, F., GARCIA ALAI, M., RUTHERFORD, T. J., FLIEGERT, R. & TIDOW, H. 2019. Novel CaM-binding motif in its NudT9H domain contributes to temperature sensitivity of TRPM2. *Biochim Biophys Acta Mol Cell Res,* 1866**,** 1162-1170. DOI: 10.1016/j.bbamcr.2018.12.010.

49. GOFFE, B. & CATHER, J. C. 2003. Etanercept: An overview. *J Am Acad Dermatol,* 49**,** S105-11. DOI: 10.1016/mjd.2003.554.

50. GOTTLIEB, A. B. & ANTONI, C. E. 2004. Treating psoriatic arthritis: how effective are TNF antagonists? *Arthritis Res Ther,* 6 Suppl 2**,** S31-5. DOI: 10.1186/ar1016.

51. GRANT, B. M. M., ENOMOTO, M., IKURA, M. & MARSHALL, C. B. 2020. A Non-Canonical Calmodulin Target Motif Comprising a Polybasic Region and Lipidated Terminal Residue Regulates Localization. *Int J Mol Sci,* 21. DOI: 10.3390/ijms21082751.

52. GRIMM, C., KRAFT, R., SAUERBRUCH, S., SCHULTZ, G. & HARTENECK, C. 2003. Molecular and functional characterization of the melastatin-related cation channel TRPM3. *J Biol Chem,* 278**,** 21493-501. DOI: 10.1074/jbc.M300945200.

53. GRYCOVA, L., HOLENDOVA, B., LANSKY, Z., BUMBA, L., JIRKU, M., BOUSOVA, K. & TEISINGER, J. 2015. Ca(2+) binding protein S100A1 competes with calmodulin and PIP2 for binding site on the C-terminus of the TPRV1 receptor. *ACS Chem Neurosci,* 6**,** 386-92. DOI: 10.1021/cn500250r.

54. GRZYBOWSKA, E. A. 2018. Calcium-Binding Proteins with Disordered Structure and Their Role in Secretion, Storage, and Cellular Signaling. *Biomolecules,* 8. DOI: 10.3390/biom8020042.

55. GUO, X. F., ZHANG, Y. Y., KANG, J., DOU, Q. H. & ZHU, X. F. 2022. A bispecific decoy receptor VEGFR-EGFR/Fc binding EGF-like ligands and VEGF shows potent antitumor efficacy. *J Drug Target,* 30**,** 302-312. DOI: 10.1080/1061186X.2021.1961791.

56. HALLING, D. B., LIEBESKIND, B. J., HALL, A. W. & ALDRICH, R. W. 2016. Conserved properties of individual Ca2+-binding sites in calmodulin. *Proc Natl Acad Sci U S A,* 113**,** E1216-25. DOI: 10.1073/pnas.1600385113.

57. HAN, Z. & LU, Z. R. 2017. Targeting Fibronectin for Cancer Imaging and Therapy. *J Mater Chem B,* 5**,** 639-654. DOI: 10.1039/C6TB02008A.

58. HARDING, F. A., STICKLER, M. M., RAZO, J. & DUBRIDGE, R. B. 2010. The immunogenicity of humanized and fully human antibodies: residual immunogenicity resides in the CDR regions. *MAbs,* 2**,** 256-65. DOI: 10.4161/mabs.2.3.11641.

59. HARTENECK, C. 2005. Function and pharmacology of TRPM cation channels. *Naunyn Schmiedebergs Arch Pharmacol,* 371**,** 307-14. DOI: 10.1007/s00210-005-1034-x.

60. HASAN, R., LEESON-PAYNE, A. T., JAGGAR, J. H. & ZHANG, X. 2017. Calmodulin is responsible for Ca(2+)-dependent regulation of TRPA1 Channels. *Sci Rep,* 7**,** 45098. DOI: 10.1038/srep45098.

61. HASAN, R. & ZHANG, X. 2018. Ca(2+) Regulation of TRP Ion Channels. *Int J Mol Sci,* 19. DOI: 10.3390/ijms19041256.

62. HOFMANN, T., CHUBANOV, V., GUDERMANN, T. & MONTELL, C. 2003. TRPM5 is a voltage-modulated and Ca(2+)-activated monovalent selective cation channel. *Curr Biol,* 13**,** 1153-8. DOI: 10.1016/s0960-9822(03)00431-7.

63. HOLAKOVSKA, B., GRYCOVA, L., JIRKU, M., SULC, M., BUMBA, L. & TEISINGER, J. 2012. Calmodulin and S100A1 protein interact with N terminus of TRPM3 channel. *J Biol Chem,* 287**,** 16645-55. DOI: 10.1074/jbc.M112.350686.

64. HOLENDOVA, B., GRYCOVA, L., JIRKU, M. & TEISINGER, J. 2012. PtdIns(4,5)P2 interacts with CaM binding domains on TRPM3 N-terminus. *Channels (Austin),* 6**,** 479-82. DOI: 10.4161/chan.22177.

65. HORIKAWA, K., YAMADA, Y., MATSUDA, T., KOBAYASHI, K., HASHIMOTO, M., MATSU-URA, T., MIYAWAKI, A., MICHIKAWA, T., MIKOSHIBA, K. & NAGAI, T. 2010. Spontaneous network activity visualized by ultrasensitive Ca(2+) indicators, yellow Cameleon-Nano. *Nat Methods,* 7**,** 729-32. DOI: 10.1038/nmeth.1488.

66. HUANG, C. 2009. Receptor-Fc fusion therapeutics, traps, and MIMETIBODY technology. *Curr Opin Biotechnol,* 20**,** 692-9. DOI: 10.1016/j.copbio.2009.10.010.

67. HUANG, Y., FLIEGERT, R., GUSE, A. H., LU, W. & DU, J. 2020. A structural overview of the ion channels of the TRPM family. *Cell Calcium,* 85**,** 102111. DOI: 10.1016/j.ceca.2019.102111.

68. HUMPE, A. & PEIPP, M. 2017. Antibody Engineering - Tailor-Made Next Generation Antibodies by Molecular Design. *Transfus Med Hemother,* 44**,** 290-291. DOI: 10.1159/000479617.

69. HUYNH, K. W., COHEN, M. R., JIANG, J., SAMANTA, A., LODOWSKI, D. T., ZHOU, Z. H. & MOISEENKOVA-BELL, V. Y. 2016. Structure of the full-length TRPV2 channel by cryo-EM. *Nat Commun,* 7**,** 11130. DOI: 10.1038/ncomms11130.

70. IIZUKA, S., KUDO, Y., YOSHIDA, M., TSUNEMATSU, T., YOSHIKO, Y., UCHIDA, T., OGAWA, I., MIYAUCHI, M. & TAKATA, T. 2011. Ameloblastin regulates osteogenic

differentiation by inhibiting Src kinase via cross talk between integrin beta1 and CD63. *Mol Cell Biol,* 31**,** 783-92. DOI: 10.1128/MCB.00912-10.

71. INOUE, R., KURAHARA, L.-H. & HIRAISHI, K. TRP channels in cardiac and intestinal fibrosis. Seminars in Cell & Developmental Biology, 2019. Elsevier, 40-49. DOI: 10.1016/j.semcdb.2018.11.002

72. ISHIDA, H., NGUYEN, L. T., GOPAL, R., AIZAWA, T. & VOGEL, H. J. 2016. Overexpression of Antimicrobial, Anticancer, and Transmembrane Peptides in Escherichia coli through a Calmodulin-Peptide Fusion System. *J Am Chem Soc,* 138**,** 11318-26. DOI: 10.1021/jacs.6b06781.

73. JENSEN, H. H., BROHUS, M., NYEGAARD, M. & OVERGAARD, M. T. 2018. Human Calmodulin Mutations. *Front Mol Neurosci,* 11**,** 396. DOI: 10.3389/fnmol.2018.00396.

74. JIANG, J., XU, K., WANG, L., XIN, W., ZHAO, G., HUANG, M., LI, S., LUAN, X. & FANG, J. 2018. Pharmacology study of a chimeric decoy receptor trap fusion protein on retina neovascularization by dual blockage of VEGF and FGF-2. *Eur J Pharm Sci,* 121**,** 251-259. DOI: 10.1016/j.ejps.2018.04.043.

75. JIMENEZ, I., PRADO, Y., MARCHANT, F., OTERO, C., ELTIT, F., CABELLO-VERRUGIO, C., CERDA, O. & SIMON, F. 2020. TRPM Channels in Human Diseases. *Cells,* 9. DOI: 10.3390/cells9122604.

76. JOHNSON, C. N., POTET, F., THOMPSON, M. K., KRONCKE, B. M., GLAZER, A. M., VOEHLER, M. W., KNOLLMANN, B. C., GEORGE, A. L., JR. & CHAZIN, W. J. 2018. A Mechanism of Calmodulin Modulation of the Human Cardiac Sodium Channel. *Structure,* 26**,** 683-694 e3. DOI: 10.1016/j.str.2018.03.005.

77. JUNG, H. J., KIM, J. H., SHIM, J. S. & KWON, H. J. 2010. A novel Ca2+/calmodulin antagonist HBC inhibits angiogenesis and down-regulates hypoxia-inducible factor. *J Biol Chem,* 285**,** 25867-74. DOI: 10.1074/jbc.M110.135632.

78. KHALIL, M., ALLIGER, K., WEIDINGER, C., YERINDE, C., WIRTZ, S., BECKER, C. & ENGEL, M. A. 2018. Functional Role of Transient Receptor Potential Channels in Immune Cells and Epithelia. *Front Immunol,* 9**,** 174. DOI: 10.3389/fimmu.2018.00174.

79. KORENDOVYCH, I. V. & DEGRADO, W. F. 2020. De novo protein design, a retrospective. *Quarterly reviews of biophysics,* 53**,** e3. DOI: 10.1017/S0033583519000131.

80. KOZAKOV, D., HALL, D. R., XIA, B., PORTER, K. A., PADHORNY, D., YUEH, C., BEGLOV, D. & VAJDA, S. 2017. The ClusPro web server for protein-protein docking. *Nat Protoc,* 12**,** 255-278. DOI: 10.1038/nprot.2016.169.

81. KRETSINGER, R. H. & NOCKOLDS, C. E. 1973. Carp muscle calcium-binding protein. II. Structure determination and general description. *J Biol Chem,* 248**,** 3313-26. DOI: 10.1016/S0021-9258(19)44043-X.

82. KUBONIWA, H., TJANDRA, N., GRZESIEK, S., REN, H., KLEE, C. B. & BAX, A. 1995. Solution structure of calcium-free calmodulin. *Nat Struct Biol,* 2**,** 768-76. DOI: 10.1038/nsb0995-768.

83. LEE, C. G., KIM, T., HONG, S., CHU, J., KANG, J. E., PARK, H. G., CHOI, J. Y., SONG, K., RHA, S. Y., LEE, S., CHOI, J. S., KIM, S. M., JEONG, H. M. & SHIN, Y. K. 2020. Antibody-Based Targeting of Interferon-Beta-1a Mutein in HER2-Positive Cancer Enhances Antitumor Effects Through Immune Responses and Direct Cell Killing. *Front Pharmacol,* 11**,** 608774. DOI: 10.3389/fphar.2020.608774.

84. LI, Y., MALEKI, M., CARRUTHERS, N. J., STEMMER, P. M., NGOM, A. & RUEDA, L. 2018. The predictive performance of short-linear motif features in the prediction of

calmodulin-binding proteins. *BMC Bioinformatics,* 19**,** 410. DOI: 10.1186/s12859-018-2378-9.

85. LIU, D. & LIMAN, E. R. 2003. Intracellular Ca2+ and the phospholipid PIP2 regulate the taste transduction ion channel TRPM5. *Proc Natl Acad Sci U S A,* 100**,** 15160-5. DOI: 10.1073/pnas.2334159100.

86. LIU, F., CHU, X., LU, H. P. & WANG, J. 2017. Molecular mechanism of multispecific recognition of Calmodulin through conformational changes. *Proc Natl Acad Sci U S A,* 114**,** E3927-E3934. DOI: 10.1073/pnas.1615949114.

87. LIU, J. O. 2009. Calmodulin-dependent phosphatase, kinases, and transcriptional corepressors involved in T-cell activation. *Immunol Rev,* 228**,** 184-98. DOI: 10.1111/j.1600-065X.2008.00756.x.

88. LIU, Q., XUN, G. & FENG, Y. 2019a. The state-of-the-art strategies of protein engineering for enzyme stabilization. *Biotechnol Adv,* 37**,** 530-537. DOI: 10.1016/j.biotechadv.2018.10.011.

89. LIU, X. R., ZHANG, M. M., REMPEL, D. L. & GROSS, M. L. 2019b. A Single Approach Reveals the Composite Conformational Changes, Order of Binding, and Affinities for Calcium Binding to Calmodulin. *Anal Chem,* 91**,** 5508-5512. DOI: 10.1021/acs.analchem.9b01062.

90. LIU, Y., LYU, Y. & WANG, H. 2022. TRP Channels as Molecular Targets to Relieve Endocrine-Related Diseases. *Frontiers in Molecular Biosciences,* 9. DOI: 10.3389/fmolb.2022.895814.

91. LOHR, C., BEIERSDORFER, A., FISCHER, T., HIRNET, D., ROTERMUND, N., SAUER, J., SCHULZ, K. & GEE, C. E. 2021. Using Genetically Encoded Calcium Indicators to Study Astrocyte Physiology: A Field Guide. *Front Cell Neurosci,* 15**,** 690147. DOI: 10.3389/fncel.2021.690147.

92. LU, X., ITO, Y., ATSAWASUWAN, P., DANGARIA, S., YAN, X., WU, T., EVANS, C. A. & LUAN, X. 2013. Ameloblastin modulates osteoclastogenesis through the integrin/ERK pathway. *Bone,* 54**,** 157-168. DOI: 10.1016/j.bone.2013.01.041.

93. LU, X., LI, W., FUKUMOTO, S., YAMADA, Y., EVANS, C. A., DIEKWISCH, T. & LUAN, X. 2016. The ameloblastin extracellular matrix molecule enhances bone fracture resistance and promotes rapid bone fracture healing. *Matrix Biol,* 52-54**,** 113-126. DOI: 10.1016/j.matbio.2016.02.007.

94. LUTZ, S. 2010. Beyond directed evolution—semi-rational protein engineering and design. *Current opinion in biotechnology,* 21**,** 734-743. DOI: 10.1016/j.copbio.2010.08.011.

95. LUTZ, S. & IAMURRI, S. M. 2018. Protein engineering: past, present, and future. *Protein Engineering: Methods and Protocols***,** 1-12. DOI: 10.1007/978-1-4939-7366-8_1.

96. MANSUROV, A., LAUTERBACH, A., BUDINA, E., ALPAR, A. T., HUBBELL, J. A. & ISHIHARA, J. 2021. Immunoengineering approaches for cytokine therapy. *Am J Physiol Cell Physiol,* 321**,** C369-C383. DOI: 10.1152/ajpcell.00515.2020.

97. MARCHETTI, G. M., BURWELL, T. J., PETERSON, N. C., CANN, J. A., HANNA, R. N., LI, Q., ONGSTAD, E. L., BOYD, J. T., KENNEDY, M. A., ZHAO, W., RICKERT, K. W., GRIMSBY, J. S., DALL'ACQUA, W. F., WU, H., TSUI, P., BORROK, M. J. & GUPTA, R. 2019. Targeted drug delivery via caveolae-associated protein PV1 improves lung fibrosis. *Commun Biol,* 2**,** 92. DOI: 10.1038/s42003-019-0337-2.

98. MARTIN, S. R. & BAYLEY, P. M. 1986. The effects of Ca2+ and Cd2+ on the secondary and tertiary structure of bovine testis calmodulin. A circular-dichroism study. *Biochem J,* 238**,** 485-90. DOI: 10.1042/bj2380485.

99. MATHEW, M. & VERMA, R. S. 2009. Humanized immunotoxins: a new generation of immunotoxins for targeted cancer therapy. *Cancer Sci,* 100**,** 1359-65. DOI: 10.1111/j.1349-7006.2009.01192.x.

100. MAYUR, Y. C., JAGADEESH, S. & THIMMAIAH, K. N. 2006. Targeting calmodulin in reversing multi drug resistance in cancer cells. *Mini Rev Med Chem,* 6**,** 1383-9. DOI: 10.2174/138955706778993021.

101. MAZOR, R. & PASTAN, I. 2020. Immunogenicity of Immunotoxins Containing Pseudomonas Exotoxin A: Causes, Consequences, and Mitigation. *Front Immunol,* 11**,** 1261. DOI: 10.3389/fimmu.2020.01261.

102. MCKEMY, D. D., NEUHAUSSER, W. M. & JULIUS, D. 2002. Identification of a cold receptor reveals a general role for TRP channels in thermosensation. *Nature,* 416**,** 52-8. DOI: 10.1038/nature719.

103. MELKKO, S., HALIN, C., BORSI, L., ZARDI, L. & NERI, D. 2002. An antibody-calmodulin fusion protein reveals a functional dependence between macromolecular isoelectric point and tumor targeting performance. *Int J Radiat Oncol Biol Phys,* 54**,** 1485-90. DOI: 10.1016/s0360-3016(02)03927-5.

104. MILLER, B. A. & CHEUNG, J. Y. 2016. TRPM2 protects against tissue damage following oxidative stress and ischaemia-reperfusion. *J Physiol,* 594**,** 4181-91. DOI: 10.1113/JP270934.

105. MINKE, B. 1977. Drosophila mutant with a transducer defect. *Biophys Struct Mech,* 3**,** 59-64. DOI: 10.1007/BF00536455.

106. MINNES, L., SHAW, D. J., COSSINS, B. P., DONALDSON, P. M., GREETHAM, G. M., TOWRIE, M., PARKER, A. W., BAKER, M. J., HENRY, A. J., TAYLOR, R. J. & HUNT, N. T. 2017. Quantifying Secondary Structure Changes in Calmodulin Using 2D-IR Spectroscopy. *Anal Chem,* 89**,** 10898-10906. DOI: 10.1021/acs.analchem.7b02610.

107. MISHRA, A. P., CHANDRA, S., TIWARI, R., SRIVASTAVA, A. & TIWARI, G. 2018. Therapeutic Potential of Prodrugs Towards Targeted Drug Delivery. *Open Med Chem J,* 12**,** 111-123. DOI: 10.2174/1874104501812010111.

108. MIYAWAKI, A., LLOPIS, J., HEIM, R., MCCAFFERY, J. M., ADAMS, J. A., IKURA, M. & TSIEN, R. Y. 1997. Fluorescent indicators for Ca2+ based on green fluorescent proteins and calmodulin. *Nature,* 388**,** 882-7. DOI: 10.1038/42264.

109. MONTEILH-ZOLLER, M. K., HERMOSURA, M. C., NADLER, M. J., SCHARENBERG, A. M., PENNER, R. & FLEIG, A. 2003. TRPM7 provides an ion channel mechanism for cellular entry of trace metal ions. *J Gen Physiol,* 121**,** 49-60. DOI: 10.1085/jgp.20028740.

110. MORIMOTO, E., TSUBOYAMA, K. & TOMARI, Y. 2022. Fusion with heat-resistant obscure (Hero) proteins have the potential to improve the molecular property of recombinant proteins. *PLoS One,* 17**,** e0270097. DOI: 10.1371/journal.pone.0270097.

111. NADLER, M. J., HERMOSURA, M. C., INABE, K., PERRAUD, A. L., ZHU, Q., STOKES, A. J., KUROSAKI, T., KINET, J. P., PENNER, R., SCHARENBERG, A. M. & FLEIG, A. 2001. LTRPC7 is a Mg.ATP-regulated divalent cation channel required for cell viability. *Nature,* 411**,** 590-5. DOI: 10.1038/35079092.

112. NAKAI, J., OHKURA, M. & IMOTO, K. 2001. A high signal-to-noise Ca(2+) probe composed of a single green fluorescent protein. *Nat Biotechnol,* 19**,** 137-41. DOI: 10.1038/84397.

113. NEMETH-CAHALAN, K. L. & HALL, J. E. 2000. pH and calcium regulate the water permeability of aquaporin 0. *J Biol Chem,* 275**,** 6777-82. DOI: 10.1074/jbc.275.10.6777.

114. NILIUS, B. 2007. TRP channels in disease. *Biochim Biophys Acta,* 1772**,** 805-12. DOI: 10.1016/j.bbadis.2007.02.002.

115. NILIUS, B., MAHIEU, F., PRENEN, J., JANSSENS, A., OWSIANIK, G., VENNEKENS, R. & VOETS, T. 2006. The Ca2+-activated cation channel TRPM4 is regulated by phosphatidylinositol 4,5-biphosphate. *EMBO J,* 25**,** 467-78. DOI: 10.1038/sj.emboj.7600963.

116. NILIUS, B., PRENEN, J., TANG, J., WANG, C., OWSIANIK, G., JANSSENS, A., VOETS, T. & ZHU, M. X. 2005. Regulation of the Ca2+ sensitivity of the nonselective cation channel TRPM4. *J Biol Chem,* 280**,** 6423-33. DOI: 10.1074/jbc.M411089200.

117. O'CONNOR, D. H., PERON, S. P., HUBER, D. & SVOBODA, K. 2010. Neural activity in barrel cortex underlying vibrissa-based object localization in mice. *Neuron,* 67**,** 1048-61. DOI: 10.1016/j.neuron.2010.08.026.

118. O'DAY, D. H. 2020. Calmodulin Binding Proteins and Alzheimer's Disease: Biomarkers, Regulatory Enzymes and Receptors That Are Regulated by Calmodulin. *Int J Mol Sci,* 21. DOI: 10.3390/ijms21197344.

119. OLAH, Z., JOSVAY, K., PECZE, L., LETOHA, T., BABAI, N., BUDAI, D., OTVOS, F., SZALMA, S. & VIZLER, C. 2007. Anti-calmodulins and tricyclic adjuvants in pain therapy block the TRPV1 channel. *PLoS One,* 2**,** e545. DOI: 10.1371/journal.pone.0000545.

120. PALMER, A. E., GIACOMELLO, M., KORTEMME, T., HIRES, S. A., LEV-RAM, V., BAKER, D. & TSIEN, R. Y. 2006. Ca2+ indicators based on computationally redesigned calmodulin-peptide pairs. *Chem Biol,* 13**,** 521-30. DOI: 10.1016/j.chembiol.2006.03.007.

121. PALOVCAK, E., DELEMOTTE, L., KLEIN, M. L. & CARNEVALE, V. 2015. Comparative sequence analysis suggests a conserved gating mechanism for TRP channels. *J Gen Physiol,* 146**,** 37-50. DOI: 10.1085/jgp.201411329.

122. PARDRIDGE, W. M. & BOADO, R. J. 2012. Reengineering biopharmaceuticals for targeted delivery across the blood-brain barrier. *Methods Enzymol,* 503**,** 269-92. DOI: 10.1016/B978-0-12-396962-0.00011-2.

123. PATRA, M., ZARSCHLER, K., PIETZSCH, H. J., STEPHAN, H. & GASSER, G. 2016. New insights into the pretargeting approach to image and treat tumours. *Chem Soc Rev,* 45**,** 6415-6431. DOI: 10.1039/c5cs00784d.

124. PENTONY, M. M. & JONES, D. T. 2010. Modularity of intrinsic disorder in the human proteome. *Proteins,* 78**,** 212-21. DOI: 10.1002/prot.22504.

125. PERRAUD, A. L., FLEIG, A., DUNN, C. A., BAGLEY, L. A., LAUNAY, P., SCHMITZ, C., STOKES, A. J., ZHU, Q., BESSMAN, M. J., PENNER, R., KINET, J. P. & SCHARENBERG, A. M. 2001. ADP-ribose gating of the calcium-permeable LTRPC2 channel revealed by Nudix motif homology. *Nature,* 411**,** 595-9. DOI: 10.1038/35079100.

126. PERRAUD, A. L., KNOWLES, H. M. & SCHMITZ, C. 2004. Novel aspects of signaling and ion-homeostasis regulation in immunocytes. The TRPM ion channels and their potential role in modulating the immune response. *Mol Immunol,* 41**,** 657-73. DOI: 10.1016/j.molimm.2004.04.013.

127. PETTERSEN, E. F., GODDARD, T. D., HUANG, C. C., MENG, E. C., COUCH, G. S., CROLL, T. I., MORRIS, J. H. & FERRIN, T. E. 2021. UCSF ChimeraX: Structure visualization for researchers, educators, and developers. *Protein Science,* 30**,** 70-82. DOI: 10.1002/pro.3943.

128. PHILO, J. S. 2023. SEDNTERP: a calculation and database utility to aid interpretation of analytical ultracentrifugation and light scattering data. *Eur Biophys J,* 52**,** 233-266. DOI: 10.1007/s00249-023-01629-0.

129. PONGSUPASA, V., ANUWAN, P., MAENPUEN, S. & WONGNATE, T. 2022. Rational-design engineering to improve enzyme thermostability. *Enzyme Engineering: Methods and Protocols*, 159-178. DOI: 10.1007/978-1-0716-1826-4_9.

130. POULTER, J. A., MURILLO, G., BROOKES, S. J., SMITH, C. E., PARRY, D. A., SILVA, S., KIRKHAM, J., INGLEHEARN, C. F. & MIGHELL, A. J. 2014. Deletion of ameloblastin exon 6 is associated with amelogenesis imperfecta. *Hum Mol Genet,* 23, 5317-24. DOI: 10.1093/hmg/ddu247.

131. PRAWITT, D., MONTEILH-ZOLLER, M. K., BRIXEL, L., SPANGENBERG, C., ZABEL, B., FLEIG, A. & PENNER, R. 2003. TRPM5 is a transient Ca2+-activated cation channel responding to rapid changes in [Ca2+]i. *Proc Natl Acad Sci U S A,* 100, 15166-71. DOI: 10.1073/pnas.2334624100.

132. PROTASEVICH, I., RANJBAR, B., LOBACHOV, V., MAKAROV, A., GILLI, R., BRIAND, C., LAFITTE, D. & HAIECH, J. 1997. Conformation and thermal denaturation of apocalmodulin: role of electrostatic mutations. *Biochemistry,* 36, 2017-24. DOI: 10.1021/bi962538g.

133. PRZIBILLA, J., DEMBLA, S., RIZUN, O., LIS, A., JUNG, M., OBERWINKLER, J., BECK, A. & PHILIPP, S. E. 2018. Ca(2+)-dependent regulation and binding of calmodulin to multiple sites of Transient Receptor Potential Melastatin 3 (TRPM3) ion channels. *Cell Calcium,* 73, 40-52. DOI: 10.1016/j.ceca.2018.03.005.

134. PUCCI, F., SCHWERSENSKY, M. & ROOMAN, M. 2022. Artificial intelligence challenges for predicting the impact of mutations on protein stability. *Curr Opin Struct Biol,* 72, 161-168. DOI: 10.1016/j.sbi.2021.11.001.

135. PUTKEY, J. A., KLEEREKOPER, Q., GAERTNER, T. R. & WAXHAM, M. N. 2003. A new role for IQ motif proteins in regulating calmodulin function. *J Biol Chem,* 278, 49667-70. DOI: 10.1074/jbc.C300372200.

136. RAMAMOURTHY, G., ARIAS, M., NGUYEN, L. T., ISHIDA, H. & VOGEL, H. J. 2019. Expression and Purification of Chemokine MIP-3alpha (CCL20) through a Calmodulin-Fusion Protein System. *Microorganisms,* 7. DOI: 10.3390/microorganisms7010008.

137. REDDY CHICHILI, V. P., XIAO, Y., SEETHARAMAN, J., CUMMINS, T. R. & SIVARAMAN, J. 2013. Structural basis for the modulation of the neuronal voltage-gated sodium channel NaV1.6 by calmodulin. *Sci Rep,* 3, 2435. DOI: 10.1038/srep02435.

138. RHOADS, A. R. & FRIEDBERG, F. 1997. Sequence motifs for calmodulin recognition. *FASEB J,* 11, 331-40. DOI: 10.1096/fasebj.11.5.9141499.

139. ROHACS, T., LOPES, C. M., MICHAILIDIS, I. & LOGOTHETIS, D. E. 2005. PI(4,5)P2 regulates the activation and desensitization of TRPM8 channels through the TRP domain. *Nat Neurosci,* 8, 626-34. DOI: 10.1038/nn1451.

140. RUNNELS, L. W., YUE, L. & CLAPHAM, D. E. 2002. The TRPM7 channel is inactivated by PIP(2) hydrolysis. *Nat Cell Biol,* 4, 329-36. DOI: 10.1038/ncb781.

141. RYAZANOVA, L. V., PAVUR, K. S., PETROV, A. N., DOROVKOV, M. V. & RYAZANOV, A. G. 2001. [Novel type of signaling molecules: protein kinases covalently linked to ion channels]. *Mol Biol (Mosk),* 35, 321-32. DOI: 10.1023/A:1010499720185.

142. SAMANTA, A., HUGHES, T. E. T. & MOISEENKOVA-BELL, V. Y. 2018. Transient Receptor Potential (TRP) Channels. *Subcell Biochem,* 87, 141-165. DOI: 10.1007/978-981-10-7757-9_6.

143. SARRIA, I., LING, J., ZHU, M. X. & GU, J. G. 2011. TRPM8 acute desensitization is mediated by calmodulin and requires PIP(2): distinction from tachyphylaxis. *J Neurophysiol,* 106, 3056-66. DOI: 10.1152/jn.00544.2011.

144. SCHATTLING, B., STEINBACH, K., THIES, E., KRUSE, M., MENIGOZ, A., UFER, F., FLOCKERZI, V., BRUCK, W., PONGS, O., VENNEKENS, R., KNEUSSEL, M., FREICHEL, M., MERKLER, D. & FRIESE, M. A. 2012. TRPM4 cation channel mediates axonal and neuronal degeneration in experimental autoimmune encephalomyelitis and multiple sclerosis. *Nat Med,* 18**,** 1805-11. DOI: 10.1038/nm.3015.

145. SCHUCK, P. 2000. Size-distribution analysis of macromolecules by sedimentation velocity ultracentrifugation and lamm equation modeling. *Biophys J,* 78**,** 1606-19. DOI: 10.1016/S0006-3495(00)76713-0.

146. SHINDO, A., HARA, Y., YAMAMOTO, T. S., OHKURA, M., NAKAI, J. & UENO, N. 2010. Tissue-tissue interaction-triggered calcium elevation is required for cell polarization during Xenopus gastrulation. *PLoS One,* 5**,** e8897. DOI: 10.1371/journal.pone.0008897.

147. SHIVAROV, V., IVANOVA, M. & TIU, R. V. 2014. Mutated calreticulin retains structurally disordered C terminus that cannot bind Ca(2+): some mechanistic and therapeutic implications. *Blood Cancer J,* 4**,** e185. DOI: 10.1038/bcj.2014.7.

148. SINGH, A. K., MCGOLDRICK, L. L., TWOMEY, E. C. & SOBOLEVSKY, A. I. 2018a. Mechanism of calmodulin inactivation of the calcium-selective TRP channel TRPV6. *Sci Adv,* 4**,** eaau6088. DOI: 10.1126/sciadv.aau6088.

149. SINGH, R. K., LEE, J. K., SELVARAJ, C., SINGH, R., LI, J., KIM, S. Y. & KALIA, V. C. 2018b. Protein Engineering Approaches in the Post-Genomic Era. *Curr Protein Pept Sci,* 19**,** 5-15. DOI: 10.2174/1389203718666161117114243.

150. SINHA, R. & SHUKLA, P. 2019. Current trends in protein engineering: updates and progress. *Current Protein and Peptide Science,* 20**,** 398-407. DOI: 10.2174/1389203720666181119120120.

151. SISCO, N. J., HELSELL, C. V. M. & VAN HORN, W. D. 2019. Competitive Interactions between PIRT, the Cold Sensing Ion Channel TRPM8, and PIP(2) Suggest a Mechanism for Regulation. *Sci Rep,* 9**,** 14128. DOI: 10.1038/s41598-019-49912-5.

152. SISCO, N. J., LUU, D. D., KIM, M. & VAN HORN, W. D. 2020. PIRT the TRP Channel Regulating Protein Binds Calmodulin and Cholesterol-Like Ligands. *Biomolecules,* 10. DOI: 10.3390/biom10030478.

153. SORENSEN, A. B., SONDERGAARD, M. T. & OVERGAARD, M. T. 2013. Calmodulin in a heartbeat. *FEBS J,* 280**,** 5511-32. DOI: 10.1111/febs.12337.

154. SPIESS, K., JAKOBSEN, M. H., KLEDAL, T. N. & ROSENKILDE, M. M. 2016. The future of antiviral immunotoxins. *J Leukoc Biol,* 99**,** 911-25. DOI: 10.1189/jlb.2MR1015-468R.

155. STAKKESTAD, O., LYNGSTADAAS, S. P., THIEDE, B., VONDRASEK, J., SKALHEGG, B. S. & RESELAND, J. E. 2017. Phosphorylation Modulates Ameloblastin Self-assembly and Ca (2+) Binding. *Front Physiol,* 8**,** 531. DOI: 10.3389/fphys.2017.00531.

156. STOERGER, C. & FLOCKERZI, V. 2014. The transient receptor potential cation channel subfamily V member 6 (TRPV6): Genetics, biochemical properties, and functions of exceptional calcium channel proteins. *Biochemistry and Cell Biology,* 92**,** 441-448. DOI: 10.1139/bcb-2014-0063.

157. STROHL, W. R. 2015. Fusion Proteins for Half-Life Extension of Biologics as a Strategy to Make Biobetters. *BioDrugs,* 29**,** 215-39. DOI: 10.1007/s40259-015-0133-6.

158. SUMBRIA, R. K., BOADO, R. J. & PARDRIDGE, W. M. 2012. Brain protection from stroke with intravenous TNFalpha decoy receptor-Trojan horse fusion protein. *J Cereb Blood Flow Metab,* 32**,** 1933-8. DOI: 10.1038/jcbfm.2012.97.

159. SUMBRIA, R. K., HUI, E. K., LU, J. Z., BOADO, R. J. & PARDRIDGE, W. M. 2013. Disaggregation of amyloid plaque in brain of Alzheimer's disease transgenic mice with daily subcutaneous administration of a tetravalent bispecific antibody that targets the transferrin receptor and the Abeta amyloid peptide. *Mol Pharm,* 10**,** 3507-13. DOI: 10.1021/mp400348n.

160. TALLINI, Y. N., OHKURA, M., CHOI, B. R., JI, G., IMOTO, K., DORAN, R., LEE, J., PLAN, P., WILSON, J., XIN, H. B., SANBE, A., GULICK, J., MATHAI, J., ROBBINS, J., SALAMA, G., NAKAI, J. & KOTLIKOFF, M. I. 2006. Imaging cellular signals in the heart in vivo: Cardiac expression of the high-signal Ca2+ indicator GCaMP2. *Proc Natl Acad Sci U S A,* 103**,** 4753-8. DOI: 10.1073/pnas.0509378103.

161. TAN, H. L., KUPERSHMIDT, S., ZHANG, R., STEPANOVIC, S., RODEN, D. M., WILDE, A. A., ANDERSON, M. E. & BALSER, J. R. 2002. A calcium sensor in the sodium channel modulates cardiac excitability. *Nature,* 415**,** 442-7. DOI: 10.1038/415442a.

162. THIEL, G., RUBIL, S., LESCH, A., GUETHLEIN, L. A. & ROSSLER, O. G. 2017. Transient receptor potential TRPM3 channels: Pharmacology, signaling, and biological functions. *Pharmacol Res,* 124**,** 92-99. DOI: 10.1016/j.phrs.2017.07.014.

163. TIAN, L., HIRES, S. A., MAO, T., HUBER, D., CHIAPPE, M. E., CHALASANI, S. H., PETREANU, L., AKERBOOM, J., MCKINNEY, S. A., SCHREITER, E. R., BARGMANN, C. I., JAYARAMAN, V., SVOBODA, K. & LOOGER, L. L. 2009. Imaging neural activity in worms, flies and mice with improved GCaMP calcium indicators. *Nat Methods,* 6**,** 875-81. DOI: 10.1038/nmeth.1398.

164. TONG, Q., ZHANG, W., CONRAD, K., MOSTOLLER, K., CHEUNG, J. Y., PETERSON, B. Z. & MILLER, B. A. 2006. Regulation of the transient receptor potential channel TRPM2 by the Ca2+ sensor calmodulin. *J Biol Chem,* 281**,** 9076-85. DOI: 10.1074/jbc.M510422200.

165. TOTH, B. I., KONRAD, M., GHOSH, D., MOHR, F., HALASZOVICH, C. R., LEITNER, M. G., VRIENS, J., OBERWINKLER, J. & VOETS, T. 2015. Regulation of the transient receptor potential channel TRPM3 by phosphoinositides. *J Gen Physiol,* 146**,** 51-63. DOI: 10.1085/jgp.201411339.

166. TSURUDA, P. R., JULIUS, D. & MINOR, D. L., JR. 2006. Coiled coils direct assembly of a cold-activated TRP channel. *Neuron,* 51**,** 201-12. DOI: 10.1016/j.neuron.2006.06.023.

167. UVERSKY, V. N. & DUNKER, A. K. 2010. Understanding protein non-folding. *Biochim Biophys Acta,* 1804**,** 1231-64. DOI: 10.1016/j.bbapap.2010.01.017.

168. VAN DER LEE, R., BULJAN, M., LANG, B., WEATHERITT, R. J., DAUGHDRILL, G. W., DUNKER, A. K., FUXREITER, M., GOUGH, J., GSPONER, J., JONES, D. T., KIM, P. M., KRIWACKI, R. W., OLDFIELD, C. J., PAPPU, R. V., TOMPA, P., UVERSKY, V. N., WRIGHT, P. E. & BABU, M. M. 2014. Classification of intrinsically disordered regions and proteins. *Chem Rev,* 114**,** 6589-631. DOI: 10.1021/cr400525m.

169. VANGEEL, L. & VOETS, T. 2019. Transient Receptor Potential Channels and Calcium Signaling. *Cold Spring Harb Perspect Biol,* 11. DOI: 10.1101/cshperspect.a035048.

170. VENNEKENS, R., MESUERE, M. & PHILIPPAERT, K. 2018. TRPM5 in the battle against diabetes and obesity. *Acta Physiol (Oxf),* 222. DOI: 10.1111/apha.12949.

171. VERTESSY, B. G., HARMAT, V., BOCSKEI, Z., NARAY-SZABO, G., OROSZ, F. & OVADI, J. 1998. Simultaneous binding of drugs with different chemical structures to Ca2+-calmodulin: crystallographic and spectroscopic studies. *Biochemistry,* 37**,** 15300-10. DOI: 10.1021/bi980795a.

172. VETYSKOVA, V., ZOUHAROVA, M., BEDNAROVA, L., VANEK, O., SAZELOVA, P., KASICKA, V., VYMETAL, J., SRP, J., RUMLOVA, M., CHARNAVETS, T.,

POSTULKOVA, K., RESELAND, J. E., BOUSOVA, K. & VONDRASEK, J. 2020. Characterization of AMBN I and II Isoforms and Study of Their Ca(2+)-Binding Properties. *Int J Mol Sci,* 21. DOI: 10.3390/ijms21239293.

173. VOETS, T., NILIUS, B., HOEFS, S., VAN DER KEMP, A. W., DROOGMANS, G., BINDELS, R. J. & HOENDEROP, J. G. 2004. TRPM6 forms the Mg2+ influx channel involved in intestinal and renal Mg2+ absorption. *J Biol Chem,* 279**,** 19-25. DOI: 10.1074/jbc.M311201200.

174. WAGNER, T. F., LOCH, S., LAMBERT, S., STRAUB, I., MANNEBACH, S., MATHAR, I., DUFER, M., LIS, A., FLOCKERZI, V., PHILIPP, S. E. & OBERWINKLER, J. 2008. Transient receptor potential M3 channels are ionotropic steroid receptors in pancreatic beta cells. *Nat Cell Biol,* 10**,** 1421-30. DOI: 10.1038/ncb1801.

175. WALD, T., BEDNAROVA, L., OSICKA, R., PACHL, P., SULC, M., LYNGSTADAAS, S. P., SLABY, I. & VONDRASEK, J. 2011. Biophysical characterization of recombinant human ameloblastin. *Eur J Oral Sci,* 119 Suppl 1**,** 261-9. DOI: 10.1111/j.1600-0722.2011.00913.x.

176. WALD, T., OSICKOVA, A., SULC, M., BENADA, O., SEMERADTOVA, A., REZABKOVA, L., VEVERKA, V., BEDNAROVA, L., MALY, J., MACEK, P., SEBO, P., SLABY, I., VONDRASEK, J. & OSICKA, R. 2013. Intrinsically disordered enamel matrix protein ameloblastin forms ribbon-like supramolecular structures via an N-terminal segment encoded by exon 5. *J Biol Chem,* 288**,** 22333-45. DOI: 10.1074/jbc.M113.456012.

177. WALD, T., SPOUTIL, F., OSICKOVA, A., PROCHAZKOVA, M., BENADA, O., KASPAREK, P., BUMBA, L., KLEIN, O. D., SEDLACEK, R., SEBO, P., PROCHAZKA, J. & OSICKA, R. 2017. Intrinsically disordered proteins drive enamel formation via an evolutionarily conserved self-assembly motif. *Proc Natl Acad Sci U S A,* 114**,** E1641-E1650. DOI: 10.1073/pnas.1615334114.

178. WALSH, G. 2014. Biopharmaceutical benchmarks 2014. *Nat Biotechnol,* 32**,** 992-1000. DOI: 10.1038/nbt.3040.

179. WANG, C., NARUSE, K. & TAKAHASHI, K. 2018. Role of the TRPM4 Channel in Cardiovascular Physiology and Pathophysiology. *Cells,* 7. DOI: 10.3390/cells7060062.

180. WATANABE, H., MURAKAMI, M., OHBA, T., TAKAHASHI, Y. & ITO, H. 2008. TRP channel and cardiovascular disease. *Pharmacology & therapeutics,* 118**,** 337-351. DOI: 10.1016/j.pharmthera.2008.03.008.

181. WINKLER, P. A., HUANG, Y., SUN, W., DU, J. & LU, W. 2017. Electron cryo-microscopy structure of a human TRPM4 channel. *Nature,* 552**,** 200-204. DOI: 10.1038/nature24674.

182. WOJTAS, M., HOLUBOWICZ, R., POZNAR, M., MACIEJEWSKA, M., OZYHAR, A. & DOBRYSZYCKI, P. 2015. Calcium ion binding properties and the effect of phosphorylation on the intrinsically disordered Starmaker protein. *Biochemistry,* 54**,** 6525-34. DOI: 10.1021/acs.biochem.5b00933.

183. WRIGHT, P. E. & DYSON, H. J. 2015. Intrinsically disordered proteins in cellular signalling and regulation. *Nat Rev Mol Cell Biol,* 16**,** 18-29. DOI: 10.1038/nrm3920.

184. XIE, J., SUN, B., DU, J., YANG, W., CHEN, H. C., OVERTON, J. D., RUNNELS, L. W. & YUE, L. 2011. Phosphatidylinositol 4,5-bisphosphate (PIP(2)) controls magnesium gatekeeper TRPM6 activity. *Sci Rep,* 1**,** 146. DOI: 10.1038/srep00146.

185. YAMAKOSHI, Y., TANABE, T., OIDA, S., HU, C. C., SIMMER, J. P. & FUKAE, M. 2001. Calcium binding of enamel proteins and their derivatives with emphasis on the

calcium-binding domain of porcine sheathlin. *Arch Oral Biol,* 46**,** 1005-14. DOI: 10.1016/s0003-9969(01)00070-x.

186. YANG, K. K., WU, Z. & ARNOLD, F. H. 2019. Machine-learning-guided directed evolution for protein engineering. *Nature methods,* 16**,** 687-694. DOI: 10.1038/s41592-019-0496-6.

187. YANG, Y., LIU, N., HE, Y., LIU, Y., GE, L., ZOU, L., SONG, S., XIONG, W. & LIU, X. 2018. Improved calcium sensor GCaMP-X overcomes the calcium channel perturbations induced by the calmodulin in GCaMP. *Nat Commun,* 9**,** 1504. DOI: 10.1038/s41467-018-03719-6.

188. YAP, K. L., KIM, J., TRUONG, K., SHERMAN, M., YUAN, T. & IKURA, M. 2000. Calmodulin target database. *J Struct Funct Genomics,* 1**,** 8-14. DOI: 10.1023/a:1011320027914.

189. YI, H., SUN, T., ARMSTRONG, D., BORNEMAN, S., YANG, C., AUSTIN, S., KISHNANI, P. S. & SUN, B. 2017. Antibody-mediated enzyme replacement therapy targeting both lysosomal and cytoplasmic glycogen in Pompe disease. *J Mol Med (Berl),* 95**,** 513-521. DOI: 10.1007/s00109-017-1505-9.

190. ZALK, R., LEHNART, S. E. & MARKS, A. R. 2007. Modulation of the ryanodine receptor and intracellular calcium. *Annu Rev Biochem,* 76**,** 367-85. DOI: 10.1146/annurev.biochem.76.053105.094237.

191. ZHENG, J. 2013. Molecular mechanism of TRP channels. *Compr Physiol,* 3**,** 221-42. DOI: 10.1002/cphy.c120001.

192. ZHOU, Q. H., BOADO, R. J., HUI, E. K., LU, J. Z. & PARDRIDGE, W. M. 2011a. Brain-penetrating tumor necrosis factor decoy receptor in the mouse. *Drug Metab Dispos,* 39**,** 71-6. DOI: 10.1124/dmd.110.036012.

193. ZHOU, Q. H., BOADO, R. J., LU, J. Z., HUI, E. K. & PARDRIDGE, W. M. 2010. Monoclonal antibody-glial-derived neurotrophic factor fusion protein penetrates the blood-brain barrier in the mouse. *Drug Metab Dispos,* 38**,** 566-72. DOI: 10.1124/dmd.109.031534.

194. ZHOU, Q. H., SUMBRIA, R., HUI, E. K., LU, J. Z., BOADO, R. J. & PARDRIDGE, W. M. 2011b. Neuroprotection with a brain-penetrating biologic tumor necrosis factor inhibitor. *J Pharmacol Exp Ther,* 339**,** 618-23. DOI: 10.1124/jpet.111.185876.

195. ZHU, M. X. 2005. Multiple roles of calmodulin and other Ca(2+)-binding proteins in the functional regulation of TRP channels. *Pflugers Arch,* 451**,** 105-15. DOI: 10.1007/s00424-005-1427-1.

196. ZOU, Z. G., RIOS, F. J., MONTEZANO, A. C. & TOUYZ, R. M. 2019. TRPM7, Magnesium, and Signaling. *Int J Mol Sci,* 20. DOI: 10.3390/ijms20081877.

197. ZOUHAROVA, M., HERMAN, P., HOFBAUEROVA, K., VONDRASEK, J. & BOUSOVA, K. 2019. TRPM6 N-Terminal CaM- and S100A1-Binding Domains. *Int J Mol Sci,* 20. DOI: 10.3390/ijms20184430.

198. ZOUHAROVA, M., VYMETAL, J., BEDNAROVA, L., VANEK, O., HERMAN, P., VETYSKOVA, V., POSTULKOVA, K., LINGSTAADAS, P. S., VONDRASEK, J. & BOUSOVA, K. 2021. Intrinsically disordered protein domain of human ameloblastin in synthetic fusion with calmodulin increases calmodulin stability and modulates its function. *Int J Biol Macromol,* 168**,** 1-12. DOI: 10.1016/j.ijbiomac.2020.11.216.

199. ZUBCEVIC, L., LE, S., YANG, H. & LEE, S. Y. 2018. Conformational plasticity in the selectivity filter of the TRPV2 ion channel. *Nat Struct Mol Biol,* 25**,** 405-415. DOI: 10.1038/s41594-018-0059-z.

10. SEZNAM PUBLIKACÍ A PŘÍLOH

Vědecké publikace, které jsou podkladem disertační práce:

Příloha 1

ZOUHAROVA, M., HERMAN, P., HOFBAUEROVA, K., VONDRASEK, J. & BOUSOVA, K. 2019. TRPM6 N-Terminal CaM- and S100A1-Binding Domains. *Int J Mol Sci,* 20.

Příloha 2

ZOUHAROVA, M., VYMETAL, J., BEDNAROVA, L., VANEK, O., HERMAN, P., VETYSKOVA, V., POSTULKOVA, K., LINGSTAADAS, P. S., VONDRASEK, J. & BOUSOVA, K. 2021. Intrinsically disordered protein domain of human ameloblastin in synthetic fusion with calmodulin increases calmodulin stability and modulates its function. *Int J Biol Macromol,* 168**,** 1-12.

Příloha 3

BOUSOVA, K., **ZOUHAROVA, M.**, HERMAN, P., VYMETAL, J., VETYSKOVA, V., JIRASKOVA, K. & VONDRASEK, J. 2022. TRPM5 Channel Binds Calcium-Binding Proteins Calmodulin and S100A1. *Biochemistry,* 61**,** 413-423.

Příloha 4

BOUSOVA, K., **ZOUHAROVA, M.**, HERMAN, P., VETYSKOVA, V., JIRASKOVA, K. & VONDRASEK, J. 2021b. TRPM7 N-terminal region forms complexes with calcium binding proteins CaM and S100A1. *Heliyon,* 7**,** e08490.

Příloha 5

BOUSOVA, K., BARVIK, I., HERMAN, P., HOFBAUEROVA, K., MONINCOVA, L., MAJER, P., **ZOUHAROVA, M.**, VETYSKOVA, V., POSTULKOVA, K. & VONDRASEK, J. 2020. Mapping of CaM, S100A1 and PIP2-Binding Epitopes in the Intracellular N- and C-Termini of TRPM4. *Int J Mol Sci,* 21.

Vědecké publikace, která nejsou podkladem disertační práce:

BOUSOVA, K., BEDNAROVA, L., **ZOUHAROVA, M.**, VETYSKOVA, V., POSTULKOVA, K., HOFBAUEROVA, K., PETRVALSKA, O., VANEK, O., TRIPSIANES, K. & VONDRASEK, J. 2021a. The order of PDZ3 and TrpCage in fusion chimeras determines their properties-a biophysical characterization. *Protein Sci,* 30**,** 1653-1666.

VETYSKOVA, V., **ZOUHAROVA, M.**, BEDNAROVA, L., VANEK, O., SAZELOVA, P., KASICKA, V., VYMETAL, J., SRP, J., RUMLOVA, M., CHARNAVETS, T., POSTULKOVA, K., RESELAND, J. E., BOUSOVA, K. & VONDRASEK, J. 2020. Characterization of AMBN I and II Isoforms and Study of Their Ca(2+)-Binding Properties. *Int J Mol Sci,* 21.

VETYSKOVA, V., **ZOUHAROVA, M.** & BOUSOVA, K. 2022. Production of recombinant human ameloblastin by a fully native purification pathway. *Protein Expr Purif,* 198**,** 106133.

Příloha 1

ZOUHAROVA, M., HERMAN, P., HOFBAUEROVA, K., VONDRASEK, J. & BOUSOVA, K. 2019. TRPM6 N-Terminal CaM- and S100A1-Binding Domains. *Int J Mol Sci,* 20.

Article

TRPM6 N-Terminal CaM- and S100A1-Binding Domains

Monika Zouharova [1,2], Petr Herman [3], Kateřina Hofbauerová [3,4], Jiri Vondrasek [1,*] and Kristyna Bousova [1,*]

[1] Institute of Organic Chemistry and Biochemistry, Czech Academy of Sciences, Flemingovo namesti 2, 160 00 Prague 6, Czech Republic

[2] Second Faculty of Medicine, Charles University, V Uvalu 84, 150 06 Prague 5, Czech Republic

[3] Faculty of Mathematics and Physics, Charles University, Ke Karlovu 5, 121 16 Prague 2, Czech Republic

[4] Institute of Microbiology of the Czech Academy of Sciences, Videnska 1083, 142 20 Prague 4, Czech Republic

* Correspondence: jiri.vondrasek@uochb.cas.cz (J.V.); kristyna.bousova@uochb.cas.cz (K.B.)

check for updates

Abstract: Transient receptor potential (TRPs) channels are crucial downstream targets of calcium signalling cascades. They can be modulated either by calcium itself and/or by calcium-binding proteins (CBPs). Intracellular messengers usually interact with binding domains present at the most variable TRP regions—N- and C-cytoplasmic termini. Calmodulin (CaM) is a calcium-dependent cytosolic protein serving as a modulator of most transmembrane receptors. Although CaM-binding domains are widespread within intracellular parts of TRPs, no such binding domain has been characterised at the TRP melastatin member—the transient receptor potential melastatin 6 (TRPM6) channel. Another CBP, the S100 calcium-binding protein A1 (S100A1), is also known for its modulatory activities towards receptors. S100A1 commonly shares a CaM-binding domain. Here, we present the first identified CaM and S100A1 binding sites at the N-terminal of TRPM6. We have confirmed the L520-R535 N-terminal TRPM6 domain as a shared binding site for CaM and S100A1 using biophysical and molecular modelling methods. A specific domain of basic amino acid residues (R526/R531/K532/R535) present at this TRPM6 domain has been identified as crucial to maintain non-covalent interactions with the ligands. Our data unambiguously confirm that CaM and S100A1 share the same binding domain at the TRPM6 N-terminus although the ligand-binding mechanism is different.

Keywords: TRPM6; calmodulin binding motif; binding domain; CaM and S100A1; fluorescence anisotropy; molecular modelling

---

1. Introduction

Transient receptor potential melastatin (TRPM) channels are an eight-member subfamily of the cation-permeable transient receptor potential (TRP) superfamily, which exhibits heterogeneous functions and expression patterns [1]. The TRPM6 channel acts as a voltage-independent divalent cation channel with a 5-fold higher permeability for Mg^{2+} than for Ca^{2+} [2]. This channel is a tissue-specific receptor predominantly expressed in the intestinal and renal epithelium, where it provides absorption and reabsorption of Mg^{2+} [2–4]. TRPM6 is also rarely expressed in smooth tissue muscles [5] where the calcium-binding proteins (CBPs) studied in this research are also expressed here, although in lower expression levels [6–8]. The mutations of TRPM6 have been associated with hypomagnesemia and secondary hypocalcemia leading to developmental delays and to affected adults may be having seizures and tetany [9–11].

The whole TRP family forms large, mostly homotetramer functional complexes [12]. It is predicted that TRPM6 forms homotetramers [13,14], though it has been found that TRPM6, with its closest

homologue TRPM7, co-assembles into heterotetramers [2,15]. A TRP monomer subunit contains six α-helical transmembrane segments (S1–S6) with selective pores between S5 and S6 along with intracellular N- and C-termini [16–20]. TRP cytoplasmic tails substantially differ between members and contain multiple binding motifs and domains [21,22] affecting channel function [23]. The structural information on TRPM7 has recently been obtained by Cryogenic Electron Microscopy (Cryo-EM) methods [22] which has indirectly provided more information on TRPM6 function of which the structural information is not yet available. TRP modulation is affected by many intracellular and extracellular binding agents; they commonly stimulate the activity of the channel or inhibit it [24]. Most of the TRP members (primarily canonical, vaniloid, and melastatin) can be regulated by Ca^{2+} in Ca^{2+} or CaM—dependent environment [25–27]. CBPs like CaM and Calcium-binding protein 1 (CaBP-1) are known as calcium-dependent TRP modulators with specific binding motifs within the TRP intracellular tails [28]. Although the binding sites of CBPs have been reported in various TRPM channels, such in vitro and in vivo, data are completely lacking for TRPM6 [29–32]. The modulation of TRPM6 has been studied by electrophysiology approaches and has revealed the control of TRPM6 activation and Mg^{2+} influx by phosphatidylinositol 4, 5-bisphosphate (PIP2) [33]. The hydrolysis of PIP2 by phospholipase C in the presence of other agonists can lead to TRPM6 gating. Otherwise, TRPM6 activity is suppressed by free intracellular Mg^{2+} [14,34,35]; channel regulation by Ca^{2+} has not been proved [34–36].

Transient receptor potential (TRPs) channels are well-known integrators of Ca^{2+} signalling cascades exhibiting different modes of Ca^{2+}-dependent modulation. The widespread Ca^{2+}-dependent mechanism of TRP-channel modulation is based on the interaction with CBPs [37]. One of the most important eukaryotic CBPs is CaM. It is a monomeric protein composed of N- and C-terminus domains linked by a flexible linker [38–40]. Each of the domains contains two helix-loop-helix conformations known as "EF-hand" motifs. Upon Ca^{2+} binding, the helices creating EF-hands reorient, which leads to the more hydrophobic extended conformation of CaM [41]. As a result, the CaM hydrophobic patch is exposed to the CaM surface and becomes accessible for interaction with the target receptor (examples of many identified receptor hydrophobic motifs: 1–5–10, 1–8–14, or isoleucine-glutamine "IQ" motif) [42] Since CaM EF-hand domains differ in Ca^{2+}-binding affinities, CaM can act as an activator or inhibitor depending on the Ca^{2+} occupancy of each EF-hand [43,44]. The other CBP modulator of membrane receptors is S100A1 [45]. This homodimer protein forms a canonical EF-hand domain at the C-terminus and a pseudo-EF-arm at the N-terminus [46]. Upon S100A1/Ca^{2+} complex formation, canonically oriented EF-hand spirals are transferred, which results in exposure of the hydrophobic patch on the S100A1 surface. This S100A1 patch causes similar changes in the target receptor-binding domain to CaM. The first described structure of the whole TRP channel in the interaction with CaM was solved by Cryo-EM on the transient receptor potential vanilloid 6 channel (TRPV6) [42]. In this case, the TRPV6 is inactivated by binding to CaM. The structure revealed six separate TRPV6 surface areas, ensuring the binding of only one CaM molecule. Despite the abundant characterized shared CaM- and S100A1-binding domains at membrane receptors [30,31,47], the only structural analysis of the S100A1-binding mechanism was solved at ryanodine receptor 1 (RyR1) [45]. The modulating function of the S100A1 protein has not yet been demonstrated at any TRP receptor.

This paper provides the characterisation of new binding domains for CaM and S100A1 present at the TRPM6 N-terminus. In order to investigate the role of specific basic amino acids at the TRPM6 domain potentially involved in CaM and S100A1 complex formations, we have designed alanine-scanning mutations of the TRPM6 domain in the specific amino acid positions. We have found that, although the CaM- and S100A-binding domains overlap, the TRPM6/CaM and TRPM6/S100A1 complex interfaces differ.

2. Results

2.1. The Identification of TRPM6np Binding Domains for CaM and S100A1

It is known that the CaM-binding domains on TRPs exhibit two important characteristics: the hydrophobic motifs (1–4/5, 1–10, 1–14, 1–5–10, 1–7–10, 1–8–14, and IQ motif) and a cluster of at least 2 positively charged amino acids [45,47,48]. The TRPs binding domains hydrophobic motifs participate in formations of first contacts with the hydrophobic patch of the CaM/ Ca^{2+} complex (the detail mechanism of CaM and S100A1 interactions is described in the Introduction). The hydrophobic contacts between the TRP binding domain and CaM or S100A1 can often induce structural changes of the TRP binding domain which help to prepare it for specific (predominantly non-covalent) interactions with the ligands [30,31].

The search for potential CaM-binding motifs at TRPM6 was performed using the Calmodulin Target Database [49]. We have identified a potential CaM-binding motif at the proximal TRPM6 N-terminus (specified as TRPM6np; see the Methods section, first caption). TRPM6np contains several hydrophobic motifs with high propensity to form interactions with CaM (Y525-F534 (1–10 motifs), L520-A524-Y529 (1–5–10 motifs), and I521-F534 (1–14 motifs)—Figure 1A). TRPM6np also involves a cluster of five basic residues: R523, R526, R531, K532, and R535. We have predicted R526, R531, K532, and R535 as essential for specific interactions with CaM. Due to a known overlap of CaM and S100A1 binding sites [30,31,45], we anticipated similar binding principles in the formation of the TRPM6np/S100A1 complex. The TRPM6npWT peptide and its mutants were prepared as described in the Methods section, Section 4.1 (Figure 1B), and they were used for in vitro and in silico experiments to confirm and characterize the predicted CaM- and S100A1-binding domains.

2.2. CaM- and S100A1-Binding Domains of the TRPM6 N-Termini Overlap

The binding affinity of TRPM6np to CaM and S100A1 was quantified by steady-state fluorescence anisotropy experiments. Fluorescein-5-isothiocyanate (FITC)-labelled TRPM6npWT was titrated with increasing aliquots of CaM or S100A1, and the fluorescence anisotropy value was recorded for each CaM or S100A1 addition. Due to the Ca^{2+} dependence of TRPs/CBPs interactions, all measurements were carried out in the presence of 2 mM CaCl$_2$ [30]. Upon both TRPM6npWT/CaM and TRPM6npWT/S100A1 complex formation, an increase in fluorescence anisotropy resulting from decreased rotational diffusion of TRPM6npWT was observed. Fluorescence lifetimes of the free TRPM6npWT and TRPM6npWT/CaM or TRPM6npWT/S100A1 complexes were measured and utilised to determine the quantum yield ratio (Q) of the bound to the free TRPM6npWT peptide. Subsequently, the fraction of bound TRPM6npWT peptide was plotted as a function of ligand concentration to define the equilibrium dissociation constants of TRPM6npWT/ligand complexes (Figure 1C–E). The dissociation constant (K$_D$) values were determined to be 14.87 μM for TRPM6npWT/CaM and 17.80 μM for TRPM6npWT/S100A1. Our data indicate that TRPM6npWT/CaM-binding affinity is in the similar range as for the TRPM6npWT/S100A1 complex.

2.3. Characterisation of the TRPM6np/CaM Complex

The role of specific TRPM6np amino acid residues in the interactions with CaM was determined by alanine-scanning mutagenesis using a steady-state fluorescence anisotropy binding assay (Figure 2A,B). The alanine-scanning mutagenesis was performed at chosen basic residues of TRPM6np because only these amino acid residues were predicted to ensure a specific TRPM6np interaction with the ligands. We have designed the alanine-replacement mutants of single (K532A), double (K532A/R531A), triple (K532A/R531A/R535A), and tetra (K532A/R531A/R535A/R526A) basic amino acids in the TRPM6npWT peptide.
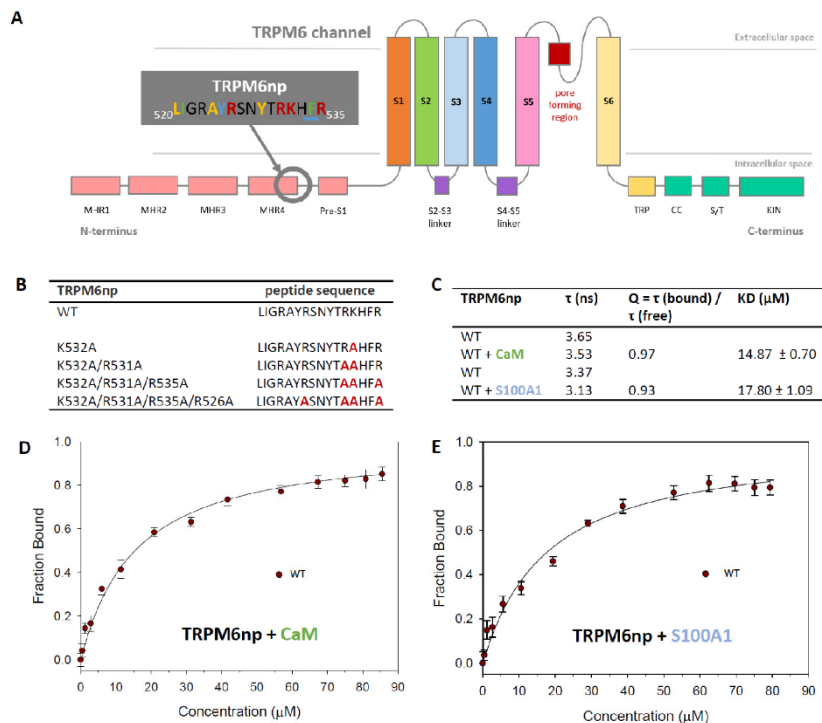
A

TRPM6 channel

TRPM6np
520 LIGRAYRSNYTRKHFR 535

B

TRPM6np	peptide sequence
WT	LIGRAYRSNYTRKHFR
K532A	LIGRAYRSNYTRAHFR
K532A/R531A	LIGRAYRSNYTAAHFR
K532A/R531A/R535A	LIGRAYRSNYTAAHFA
K532A/R531A/R535A/R526A	LIGRAYASNYTAAHFA

C

TRPM6np	τ (ns)	Q = τ (bound) / τ (free)	KD (μM)
WT	3.65		
WT + CaM	3.53	0.97	14.87 ± 0.70
WT	3.37		
WT + S100A1	3.13	0.93	17.80 ± 1.09

D TRPM6np + CaM

E TRPM6np + S100A1

Figure 1. TRPM6np binding domains for CaM and S100A1: (**A**) Schematic representation of the TRPM6 channel. TRPM6 is composed of six transmembrane domains (S1–S6), a pore region between S5 and S6 with a pore helix, and intracellular N- and C-termini. The individual domains are labelled by different colours. The TRPM6 scheme (according to TRPM7 structure) presents the N-terminal tail with four melastatin homology regions (MHR 1–4) and pre-S1 domain. The TRPM6 C-terminus is composed of TRP, coiled-coil (CC), Ser/Thr (S/T), and kinase (KIN) domains. Predicted CaM and S100A1 binding domain in the grey box shows the TRPM6np sequence (L520-R535) containing several CaM recognition hydrophobic motifs (Y525-F534 (1–10 motifs) highlighted in blue, L520-A524-Y529 (1–5–10 motifs) highlighted in yellow, and I521-F534 (1–14 motifs) highlighted in green). TRPM6np basic amino acids (highlighted in red) represent a cluster of amino acids potentially involved in the interactions with CaM and S100A1. (**B**) TRPM6np amino acid sequences of wild type (WT) and mutated analogues used for the investigation of CaM and 100A1 binding site (substitutions of R/K for Figure 1A highlighted in red). The TRPM6np binding affinity to CaM and S100A1 was investigated by the steady-state fluorescence anisotropy method. This technique is based on measurement of the changing orientation of a molecule in space with respect to the time between the absorption and emission events. (**C**) The table represents a summary of the fluorescence lifetimes of fluorescein-5-isothiocyanate (FITC)-labelled TRPM6npWT (free and bound), the corresponding correction factors, and the resultant equilibrium dissociation constants of the TRPM6npWT/CaM and TRPM6npWT/S100A1 complexes obtained by steady-state fluorescence anisotropy measurements. The bound fractions of FITC-labelled TRPM6np as a function of CaM (**D**) and S100A1 (**E**) concentrations were obtained by steady-state fluorescence anisotropy measurement. The fraction bound (F_B) of TRPM6npWT calculated according to Equation (1) was plotted against particular CaM or S100A1 concentrations, and the best fit obtained using Equation (2) gave the binding isotherms (solid lines; see the Methods section). The error bars represent the standard deviation obtained from at least five measurements.
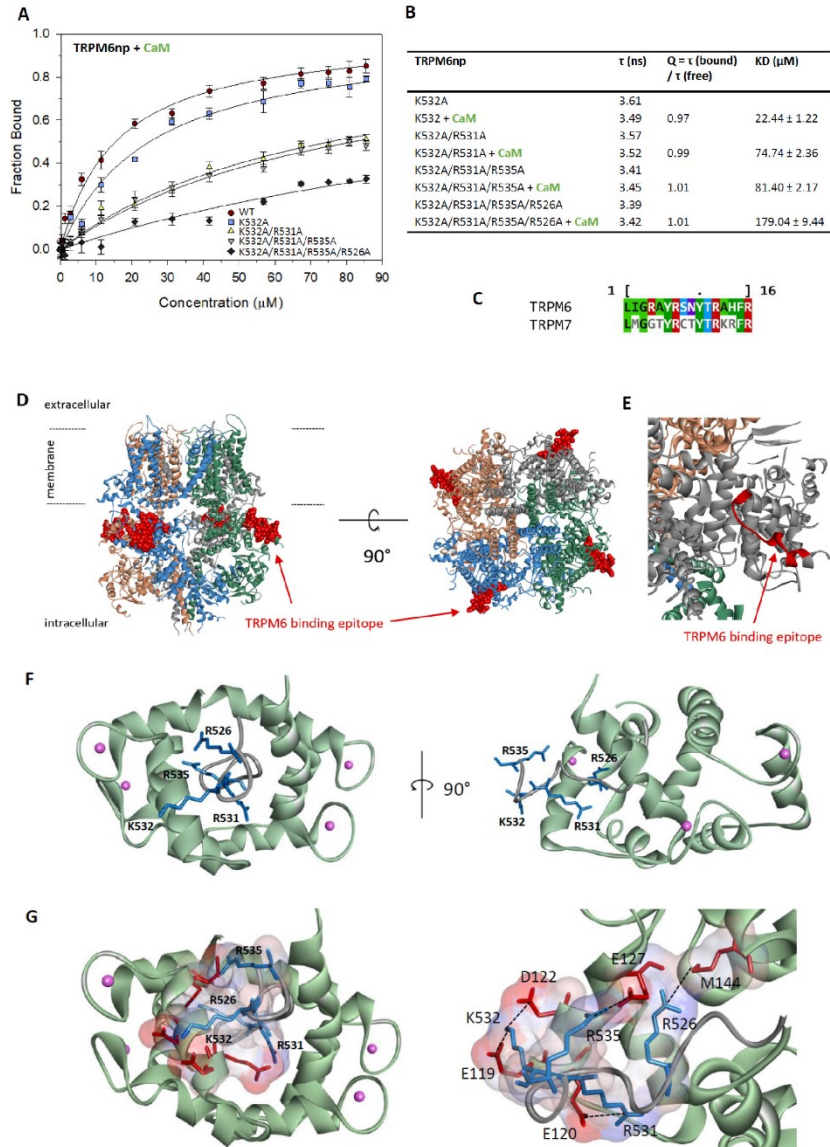
B

TRPM6np	τ (ns)	Q = τ (bound) / τ (free)	KD (µM)
K532A	3.61		
K532 + CaM	3.49	0.97	22.44 ± 1.22
K532A/R531A	3.57		
K532A/R531A + CaM	3.52	0.99	74.74 ± 2.36
K532A/R531A/R535A	3.41		
K532A/R531A/R535A + CaM	3.45	1.01	81.40 ± 2.17
K532A/R531A/R535A/R526A	3.39		
K532A/R531A/R535A/R526A + CaM	3.42	1.01	179.04 ± 9.44

Figure 2. The TRPM6np/CaM complex characterisation: (**A**) The bound fractions of FITC-labelled TRPM6np as a function of CaM concentration obtained by steady-state fluorescence anisotropy measurement. The F_B of FITC-labelled TRPM6np (WT and K532A, K532A/R531A, K532A/R531A/R535A, and K532A/R531A/R535A/R526A mutants) calculated according to Equation (1) was plotted against particular CaM concentrations, and the best fit obtained using Equation (2) gave the binding isotherms (WT and mutants appropriate solid lines; see the Methods section). The error bars represent the standard deviation obtained from at least five measurements. (**B**) A summary of fluorescence lifetimes of FITC-labelled

TRPM6np-derived mutants K532A, K532A/R531A, K532A/R531A/R535A, and K532A/R531A/R535A/R526A (free and bound); corresponding correction factors; and resultant equilibrium dissociation constants of the TRPM6np/CaM complex obtained by steady-state fluorescence anisotropy measurements. (**C**) The TRPM6np and its homology TRPM7 binding motif amino acid sequences alignment: The TRPM7 motif corresponds to a part of the CryoEM assigned structure (PDB: 5ZX5). (**D**) Schematic side and top views of TRPM6 in the membrane modelled according to homologous TRPM7 structural data (5ZX5): Each TRPM6 homomeric subunit is coloured differently. TRPM6np (red ball representation) displays the CaM and S100A1 binding domain locations in the whole TRPM6. (**E**) Detail of the TRPM6np binding domain location based on the TRPM7 channel homology model: The binding domain does not contain a secondary structure element. (**F**) Top and side view of TRPM6np/CaM complex representation: TRPM6np (backbone in grey) and CaM (backbone in light green) composing the binding interface. The basic residues (R526, R531, K532, and R535) of TRPM6np involved in the interactions are shown in blue. Calcium ions are shown in pink as scaled ball representations. (**G**) Full and detailed TRPM6np/CaM complex binding interface with surface representation of positively (R526, R531, K532, and R535 from TRPM6np, coloured in blue) and negatively (E119, E120, D122, E127, and M144 from CaM, coloured in red) charged residues involved in the non-covalent interactions. The colour convention has been used as in the Figure 2F representation.

The fluorescence anisotropy data revealed only a small decrease in CaM-binding affinity of a single mutant (K532A, K_D = 24.44 µM) in comparison to TRPM6npWT (14.87 µM). Additional mutation of the neighbouring arginine residue generated a double-mutated peptide (K532A/R531A) with significantly lower binding to CaM (K_D = 74.74 µM). These results indicate the importance of tandem basic residues (K532A/R531A) for strong TRPM6npWT/CaM binding. In contrast to R531A substitution, the additional mutation of arginine residue (triple-mutated peptide (K532A/R531A/R535A)) did not cause a significant decrease of CaM binding (K_D = 81.40 µM) compared to double mutant K532A/R531A. The affinity of TRPM6np to CaM was reduced in tetra-mutated peptide (K532A/R531A/R535A/R526A), where the additional substitution of R526A caused an increase of K_D to 179.04 µM. Our results have confirmed the specificity of TRPM6np/CaM complex formation due to non-covalent interactions.

2.4. Characterisation of the TRPM6np/S100A1 Complex

To assess the impact of TRPM6np basic residues on the interaction with S100A1, we have performed steady-state fluorescence anisotropy measurements using a set of previously designed (the same mutants as used for binding assay with CaM.; see the section above) alanine-replacement mutants in the TRPM6np region (Figure 3A,B). The single- (K532A), double- (K532A/R531A), triple- (K532A/R531A/R535A), and tetra- (K532A/R531A/R535A/R526A) mutated peptides were used for the measurements.

The K_D value for the complex of single-mutated peptide (K532A) with S100A1 remained similar (K_D = 24.79 µM) to that for TRPM6npWT/S100A1 (K_D = 17.80 µM). A decrease of TRPM6npWT binding affinity to S100A1 was achieved by additional substitution of R531 to alanine (K532A/R531A, K_D = 50.17 µM). Our data indicate the significance of this residue in TRPM6npWT/S100A1 complex formation, but its contribution to binding is not as significant as in the case of the TRPM6npWT/CaM complex, where K532A/R531A mutations led to a more than 2-fold decrease of binding affinity. The placement of three simultaneous mutations (K532A/R531A/R535A) in the TRPM6np region caused further reduction of binding affinity to S100A1 (K_D = 81.79 µM), and finally, in tetra-mutated peptide (K532A/R531A/R535A/R526A), the K_D value increased to 130.16 µM. These data confirmed the pivotal role of predicted basic amino acid residues in both complexes. It can be concluded that the basic TRPM6np residues involved in the CaM interactions are also involved in S100A1 interactions.
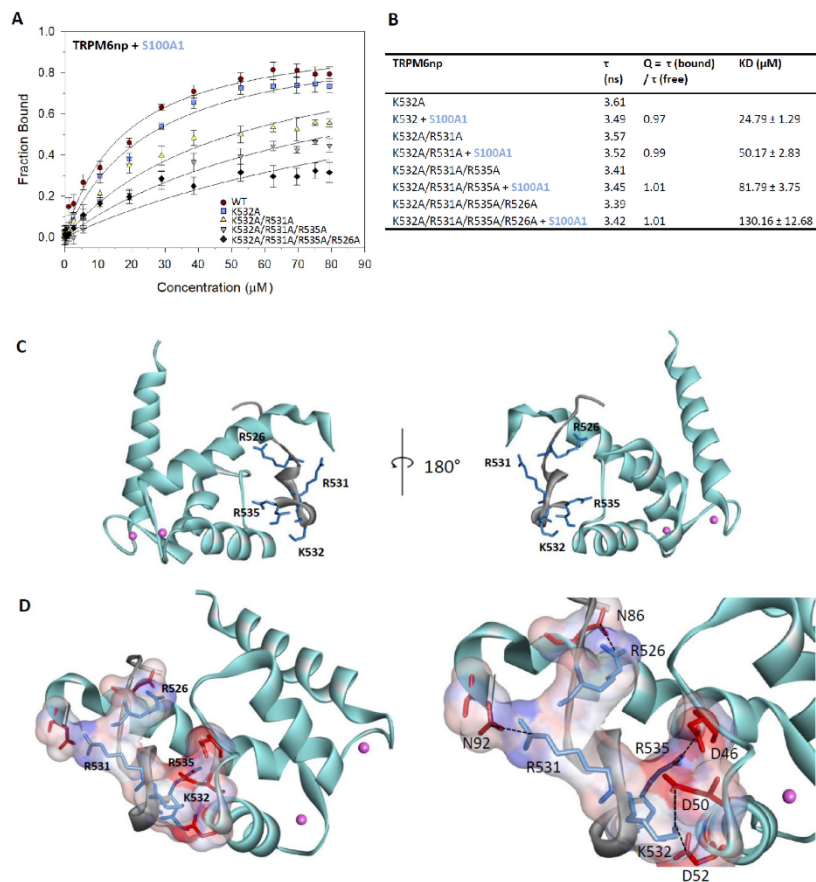
TRPM6np	τ (ns)	Q = τ (bound) / τ (free)	KD (µM)
K532A	3.61		
K532 + S100A1	3.49	0.97	24.79 ± 1.29
K532A/R531A	3.57		
K532A/R531A + S100A1	3.52	0.99	50.17 ± 2.83
K532A/R531A/R535A	3.41		
K532A/R531A/R535A + S100A1	3.45	1.01	81.79 ± 3.75
K532A/R531A/R535A/R526A	3.39		
K532A/R531A/R535A/R526A + S100A1	3.42	1.01	130.16 ± 12.68

Figure 3. The TRPM6np/S100A1 complex characterisation: (**A**) The bound fractions of FITC-labelled TRPM6np as a function of S100A1 concentration obtained by steady-state fluorescence anisotropy measurement. The F_B of FITC-labelled TRPM6np (WT and K532A, K532A/R531A, K532A/R531A/R535A, and K532A/R531A/R535A/R526A mutants) calculated according to Equation (1) was plotted against particular S100A1 concentrations, and the best fit obtained using Equation (2) gave the binding isotherms (WT and mutants appropriate solid lines; see the Methods section). The error bars represent the standard deviation obtained from at least five measurements. (**B**) A summary of fluorescence lifetimes of FITC-labelled TRPM6np-derived mutants K532A, K532A/R531A, K532A/R531A/R535A, and K532A/R531A/R535A/R526A (free and bound); corresponding correction factors; and resultant equilibrium dissociation constants of the TRPM6np/S100A1 complex obtained by steady-state fluorescence anisotropy measurements. (**C**) Top and side view of TRPM6np/S100A1 complex representation: TRPM6np (backbone in grey) and S100A1 (backbone in light blue) composing the binding interface. The basic residues (R526, R531, K532, and R535) of TRPM6np involved in the interactions are shown in blue. Calcium ions are shown in pink as scaled balls representations. (**D**) Full and detailed TRPM6np/ S100A1 complex binding interface with surface representation of positively (R526, R531, K532, and R535 from TRPM6np, coloured in blue) and negatively (D46, D50, D52, N86, and N92 from S100A1, coloured in red) charged residues involved in the non-covalent interactions: The colour convention has been used as in the Figure 3C representation.

2.5. TRPM6np Molecular Modelling and CaM and S100A1 Docking

Homology modelling methods were used to build a molecular model of TRPM6, taking into account that the structure of the TRPM6 channel is still unknown. The structure of the mouse TRPM7 channel (PDB: 5ZX5) [22] with a 61.74% sequence identity to TRPM6 (Figure S1) was used as a template to build the TRPM6 model by SWISS-MODEL [50]. Specifically, according to the sequence of TRPM6np, the homology region of TRPM7 was selected (UniProt: Q96QT4.1; sequence: LMGGTYRCTYTRKRFRL) (Figure 2C) [51]. The high sequence-homology degree of the TRPM6 and TRPM7 regions made it possible to select the TRPM6 model built by the SWISS-MODEL. The TRPM6np structure from this homology model was separated and optimised by energy minimisation using Molecular Operating Environment software [52].

TRPM6np was consequently docked into CaM and S100A1 by the ClusPro2.0 method and server [53] (see the Methods section, Section 4.6). The TRPM6np/CaM complex (Figure 2F,G) was adjusted according to its similarity with the CaM binding domain of TRPV1 containing 1–10 hydrophobic motifs. The TRPV1p/CaM complex was solved by X-ray crystallography (PDB: 3SUI) [48]. The TRPM6np/S100A1 complex (Figure 3C,D) was adjusted based on its similarity with the crystal structure of the complex RyR1P12 peptide with S100A1 (PDB: 2K2F) [45]. The TRPM6np/CaM and TRPM6np/S100A1 complexes were compared with structural information derived from the analysis of TRPV1/CaM and RyR1P12/S100A1 complexes [45,48]. The hydrophobic motifs present in three different positions of TRPM6np (Y525-F534 (1–10 motifs), L520-A524-Y529 (1–5–10 motifs), and I521-F534 (1–14 motifs) indicate strong hydrophobic interactions with CaM and S100A1. Ligand docking has confirmed that R526, R531, K532, and R535 of TRPM6np are crucial for the interactions with negatively charged residues of CaM and S100A1 (E119, E120, D122, E127, and Met144 in CaM and D46, D50, D52, N86, and N92 in S100A1; Figures 2G and 3D). The molecular modelling of TRPM6np/CaM and TRPM6np/S100A1 binding interfaces thus supports data from the binding assay.

3. Discussion

We decided to investigate the binding of two known CBPs, CaM and S100A1, to the TRPM6 N-terminus. CaM is a very well-known modulator of the activity of many receptors as well as for TRPs [37,41,54]. Actually, the detailed structural analysis of CaM in the complex with the TRPV6 receptor leading to channel inhibition has been described recently [42]. The modulation of receptors by S100A1 is also well described, e.g., for RyR1 [55], the authors described that RyR1 shared the CaM and S100A1 binding sites and the activating effect of these bindings on the channel function. Therefore, we decided to investigate if CaM and S100A1 can also share the binding site at TRPM6np. The TRPM6np capability of separately binding CaM and S100A1 by has been confirmed by steady-state fluorescence anisotropy. The binding affinity is almost the same for both of the ligands, and the obtained K_D values are in a range of micromolar concentrations and is around 5–10 times lower than for the K_D values of other in vitro investigated complexes of TRP channels (TRPM1, TRPM3, TRPM4, TRPC6, and TRPV1) with CaM and/or S100A1 [29–31,47,56]. The strong binding affinity of the complex is dependent on complementarity of interacting amino acids in the binding site. Molecular modelling predicted potential binding interfaces with typical CaM and S100A1 binding characteristics [45,48]. The formation of these complexes is a sequential process where CaM or S100A1 nonspecifically interacts with hydrophobic residues of the TRP binding domain. Based on this TRP adaptation, basic amino acids become more accessible for the interaction with negative amino acids of CaM or S100A1 [30,31]. Clusters of mutated basic amino acids K532A/R531A/R535A/R526A in specific peptide analogues have been showed a substantial decrease of CaM or S100A1-binding affinities and has determined participation of these residues on the interactions. The different binding affinities of the mutants have indicated that the structural parameters of ligand binding are different, which has been supported by results of molecular modelling. The fifth R523 N-terminal residue of TRPM6np certainly contributes to the positive character of the basic amino acid cluster, which is important for binding to TRPM6np. The molecular models of TRPM6np/CaM and TRPM6np/S100A1 which were developed confirmed

that R526A, R531A, K532A, and R535A form salt bridges directly with negatively charged amino acids CaM or S100A. The R523 is not involved in such strong interactions as apparent at the molecular models; therefore, we primarily targeted electrostatic compatibility at the binding site that includes four residues R526A, R531A, K532A, and R535A. Mutual competitions of CaM and S100A1 for overlapping binding sites of TRPs on N- and C-termini and RyR1 have already been characterised many times previously [30,45,55–57]; therefore, we anticipate mutual competition of CaM and S100A1 for TRPM6np as well. We have not investigated the specific role of the hydrophobic residues in the TRPM6np binding domain because the hydrophobic patch of the receptor mostly forms nonspecific interactions with the ligands. The main specificity of the complex is always led through basic residues of the receptor and acidic residues of CaM or S100A1 [29,31,42,47,56]. The in vitro Ca^{2+} dependency interactions of the TRP channel protein/peptide segments (specifically: TRPM3, TRPC6, and TRPV1) with CaM and/or S100A1 has been validated in vitro by spectroscopy methods in our previous experiments [30,47,56], which allowed us now the use of experimental buffers with the same Ca^{2+} concentrations (2 mM). Therefore, it was supposed that the CaM/TRPM6np and S100A1/TRPM6np complexes were formed by ligands with bound Ca^{2+}. Since the modulation activity of CaM and S100A1 at TRPM6 is still not known, this should be investigated by electrophysiology measurements.

The molecular modelling of the TRPM6np/CaM and TRPM6np/S100A1 complexes was performed to visualise the specific character of the binding interfaces for both complexes. High sequence similarity of TRPM6 with TRPM7 made it possible to use homology modelling for this purpose [22]. We have identified the TRPM7 region in the Cryo-EM structure that corresponds to the TRPM6np sequence and that exhibits a structural form with no secondary structure element. Given the character of this region, we can assume that TRPM6np can behave in a rather adaptive way, depending on its binding partner. The binding interface of TRPM6np/CaM corresponds to previously published structures of receptor-fragment/CaM complexes [44,48,54,58]. As we published earlier, the amino acids of TRP in the CaM-binding domain cooperate as a cluster via ligand interaction [30,31,47]. The binding role of CaM amino acids at the position around 130 has been confirmed in the TRPV6/CaM and TRPV5/CaM structures, and the amino acids have been identified as critical positions for the interactions. In the presented molecular model, we have confirmed the same CaM amino acids involved in interactions with TRPM6np (specifically: E120 and M144) [36]. The interpretation of the TRPM6np/CaM and TRPM6np/S100A1 models is strongly supported by data from fluorescence anisotropy experiments, indicating the synergy of the basic residues in individual clusters. The TRPV6/CaM and TRPV5/CaM structures confirmed the presence of mutual binding sites for one CaM molecule by different TRP tails or subunits [36,42]. This can drive a coordinated conformational changes ongoing across the whole channel, leading to its functional modulation [36,59]. This complex process can be used to multiply the ligand signal into a channel structure to transfer structural changes more rapidly to the target location of the channel via its allostery. The ligand multi-binding character of TRPs has been discussed in previous publications [29,60].

The TRPM6 N-terminus is a universal binding domain for CaM and S100A1 in the presence of Ca^{2+}. The binding affinities of the TRPM6np/CaM-Ca^{2+} and TRPM6np/S100A1-Ca^{2+} complexes have been investigated in vitro by the fluorescence spectroscopy method, which has revealed the micromolar range of the interactions. Homology modelling using the TRPM7 Cryo-EM structure as a template has provided TRPM6np structurally adaptive character through the binding process. Intracellular parts of all TRPs have a common feature—their mostly disordered character, which allows their binding domains to be implicated in a wide range of modulatory molecules. Although TRPM6 has been studied quite well, information about its N-terminal function is not yet well understood. This study provides a new in vitro insight at the role of CBP as potential TRPM6 modulators and reveals new information on the channel signalling pathways. While no functional TRPM6 data (i.e., physiological consequences) is presented, the interactions with CaM and S100A1 are likely to provide stimulatory follow-up studies in this field. Therefore, the discovered new TRPM6 binding domains and interaction plasticity information could serve to develop new drugs.

4. Methods

4.1. TRPM6-Binding Domain Design and Synthesis

The DNA sequence of human TRPM6 has been searched for a potential CaM and S100A1-binding motifs using the Calmodulin Target Database [49]. To verify a new CaM- and S100A1-binding domain at TRPM6, we have selected a potential binding domain from the N-terminus TRPM6. The selected binding domain is referred to here as TRPM6np (UniProt: Q9BX84–2; sequence: 520-LIGRAYRSNYTRKHFR-535). TRPM6np wild type (TRPM6npWT) and its alanine scan analogues have been synthesised into the variants: K532A, R531A/K532A, R526A/R531A/K532A, and R526A/R531A/K532A/R535A as peptides (GenicBio Limited, Shanghai, China). All of these peptides were N-terminally labelled with fluorescein-5-isothiocyanate (FITC). The peptide probes were dissolved in a 50 mM Tris-HCl buffer (pH 7.5) containing 500 mM NaCl and 1 mM $CaCl_2$.

4.2. Expression and Purification of CaM and S100A1

CaM and S100A1 were expressed from pET3a and pET28b expression vectors in *E. coli* BL21 cells, respectively. The cultures were incubated at 37 °C in Lysogeny Broth medium with ampicillin or kanamycin until the OD_{600} reached 0.9. The cell suspension was cooled at 25 °C, and protein expression was induced by 0.5 mM IPTG for 12 h. The cells were resuspended in 50 mM Tris-HCl buffer (pH 7.5) containing 2 mM ethylenediaminetetraacetic (EDTA), 2 mM β-mercaptoethanol, and 0.2 mM phenylmethylsulphonyl fluoride (PMSF) and disrupted by sonication, and 5 mM $CaCl_2$ was added to the supernatant. CBPs were purified using affinity chromatography on Phenyl Sepharose CL-4B (GE Healthcare, Brondby, Denmark), where 50 mM Tris-HCl buffer (pH 7.5) containing 100 mM NaCl and 1.5 mM EDTA was used for elution. Size-exclusion chromatography on a Superdex 75 10/300 GL column (GE Healthcare, Brondby, Denmark) was used as the final purification step. The proteins were eluted by 50 mM Tris-HCl buffer (pH 7.5) containing 500 mM NaCl and 1 mM $CaCl_2$, and their purity was verified by SDS-PAGE. The identity of proteins was confirmed by mass spectrometry.

4.3. Steady-State Fluorescence Anisotropy Measurements

Steady-state fluorescence anisotropy experiments were performed at room temperature on a photon counting spectrometer PC1 (ISS Inc., Champaign, Illinois, USA). TRPM6npWT and its mutants were dissolved in a buffer containing 50 mM Tris-HCl (pH 7.5), 150 mM NaCl, and 2 mM $CaCl_2$ for a final concentration of 1 μM. The samples were titrated in a 2-mm path cuvette with increasing aliquots of 100 μM CaM or S100A1. Fluorescence was excited at 495 nm; the intensity of emission in parallel (I_{II}) and perpendicular ($I_{\perp}$) orientations to the direction of the polarised excitation was obtained at 520 nm by switching the emission polariser. The steady-state fluorescence anisotropy value (r) was calculated from the equation $r = (I_{II} - I_{\perp}) / (I_{II} + 2I_{\perp})$. Further analysis was based on the mean anisotropy value acquired from five independent measurements at each CaM or S100A1 addition. The fractions of bound CaM or S100A1 were given by fraction bound (F_B)

$$F_B = (r_{obs} - r_{min})/[(r_{max} - r_{obs}) Q + (r_{obs} - r_{min})] \tag{1}$$

where r_{max} is the anisotropy of a saturated binding complex, r_{min} stands for the anisotropy of a peptide probe without a ligand, and r_{obs} is the anisotropy at a particular CaM or S100A1 concentration. Q represents the quantum yield ratio of the bound to the free peptide, calculated from fluorescence lifetimes (τ) according to equation $Q = \tau_{bound}/\tau_{free}$.

To determine the equilibrium dissociation constant (K_D), F_B was plotted as a function of CaM or S100A1 concentration and fitted by as follows [24]:

$$F_B = \frac{K_D + [P1] + [P2] - \sqrt{(K_D + [P1] + [P2])^2 - 4[P1][P2]}}{2[P1]}, \tag{2}$$

where (*P1*) is the TRPM4np concentration and (*P2*) is the CaM or S100A1 concentration. Nonlinear data fitting was performed using SigmaPlot 11.0 (Systat software Inc., San Jose, CA, USA).

4.4. Lifetime Experiments

Lifetimes were evaluated at room temperature in a drop placed on a coverslip and inserted into an inverted confocal microscope IX83 (Olympus, Tokyo, Japan) equipped with time-correlated single photon counting electronics and cooled GaAsP hybrid detectors (all PicoQuant, Berlin, Germany). TRPM4np fluorescence was excited at 485 nm by an LDH-485 picosecond laser (PicoQuant, Berlin, Germany). Emission decays were collected in the epi-fluorescence mode using a combination of a 488-nm dichroic long-pass filter (Olympus, Tokyo, Japan) and a 520/35 bandpass filter (Semrock, Rochester, NY, USA) in the detection path. The intensity-weighted mean fluorescence lifetimes used in the calculation of the Q correction factor were evaluated as follows:

$$\tau_{\text{mean}} = \sum_i \alpha_i \tau_i^2 / \sum_i \alpha_i \tau_i, \tag{3}$$

where τ_i stands for fluorescence lifetimes and α_i are the corresponding amplitudes.

4.5. Model Building

The TRPM6np (Uniprot: Q9BX84–2) molecular model was generated via homology modelling methods using SWISS-MODEL [49]. The structure of the mouse TRPM7 channel (PDB: 5ZX5) [22] with the highest sequence similarity to TRPM6 has been used as a template to build the TRPM6np molecular model. The TRPM6np models were built, and one representative model was carefully chosen based on the positions of the basic and hydrophobic residues to be exposed to the solvent. Additional criteria were applied on the geometric parameters of the potential CaM- and S100A1-binding sites. The TRPM6np molecular model was then optimised by energy minimisation using MOE software [51] and checked for errors in the three-dimensional protein structure. The quality of the resulting structure was further assessed using STING Millenium [61] and ProSA-web [62].

4.6. Ligand Docking

The docking of CaM and S100A1 into the TRPM6np homology model was performed using the ClusPro program [53,63,64]. CaM and S100A1 templates were selected from the structures of complexes TRPV1 with CaM/Ca^{2+} (PDB: 3SUI) and RyR1 with S100A1/Ca^{2+} (PDB: 2K2F). The molecular models of both TRPM6np/CaM and TRPM6np/S100A1 were optimised by energy minimisation using MOE software [53] and checked to identify errors in the three-dimensional protein structure. The schematic representations of the TRPM6npWT/CaM and TRPM6npWT/S100A1 complexes were generated using Discovery Studio Visualizer [65]

Abbreviations

ATP	adenosine trisphosphate
CaM	calmodulin
CBPs	calcium-binding proteins
Cryo-EM	Cryogenic Electron Microscopy
IDPs	intrinsically disordered proteins
PIP2	phosphatidylinositol 4, 5- bisphosphate
RyR	rhyanodine receptor
S100A1	S100 calcium-binding protein A1
TRP	transient receptor potential channel
TRPM	transient receptor potential channel melastatin
TRPM6np	transient receptor potential channel melastatin 6 N-terminal peptide
TRPs	transient receptor potential channels
TRPV	transient receptor potential channels
WT	wild type

References

1. Kraft, R.; Harteneck, C. The mammalian melastatin-related transient receptor potential cation channels: An overview. *Pflug. Arch.* **2005**, *451*, 204–211. [CrossRef] [PubMed]

2. Voets, T.; Nilius, B.; Hoefs, S.; van der Kemp, A.W.; Droogmans, G.; Bindels, R.J.; Hoenderop, J.G. TRPM6 forms the Mg^{2+} influx channel involved in intestinal and renal Mg^{2+} absorption. *J. Biol. Chem.* **2004**, *279*, 19–25. [CrossRef] [PubMed]

3. Fonfria, E.; Murdock, P.R.; Cusdin, F.S.; Benham, C.D.; Kelsell, R.E.; McNulty, S. Tissue distribution profiles of the human TRPM cation channel family. *J. Recept Signal Transduct Res.* **2006**, *26*, 159–178. [CrossRef] [PubMed]

4. Groenestege, W.M.; Hoenderop, J.G.; van den Heuvel, L.; Knoers, N.; Bindels, R.J. The epithelial Mg^{2+} channel transient receptor potential melastatin 6 is regulated by dietary Mg^{2+} content and estrogens. *J. Am. Soc. Nephrol.* **2006**, *17*, 1035–1043. [CrossRef] [PubMed]

5. Yang, X.R.; Lin, M.J.; McIntosh, L.S.; Sham, J.S. Functional expression of transient receptor potential melastatin-and vanilloid-related channels in pulmonary arterial and aortic smooth muscle. *Am. J. Physiol. Lung. Cell. Mol. Physiol.* **2006**, L1267–L1276. [CrossRef] [PubMed]

6. Mandinova, A.; Atar, D.; Schafer, B.; Spiess, M.; Aebi, U.; Heizmann, C.W. Distinct subcellular localization of calcium binding S100 proteins in human smooth muscle cells and their relocation in response to rises in intracellular calcium. *J. Cell Sci.* **1998**, *111*, 2043–2054. [PubMed]

7. Bagchi, I.C.; Huang, Q.; Means, A.R. Identification of amino acids essential for calmodulin binding and activation of smooth muscle myosin light chain kinase. *J. Biol. Chem.* **1992**, *267*, 3024–3029. [PubMed]

8. Marston, S.B.; Fraser, I.; Huber, P.; Pritchard, K.; Gusev, N.B.; Torok, K. Location of two contact sites between human smooth muscle caldesmon and Ca (2+)-calmodulin. *J. Biol. Chem.* **1994**, *269*, 8134–8139. [PubMed]

9. Paunier, L.; Radde, I.C.; Kooh, S.W.; Conen, P.E.; Fraser, D.D.D. Primary hypomagnesemia with secondary hypocalcemia in an infant. *Pediatrics* **1968**, *41*, 385–402.

10. Schlingmann, K.P.; Weber, S.; Peters, M.; Niemann Nejsum, L.; Vitzthum, H.; Klingel, K.; Kratz, M.; Haddad, E.; Ristoff, E.; Dinour, D.; et al. Hypomagnesemia with secondary hypocalcemia is caused by mutations in TRPM6, a new member of the TRPM gene family. *Nat. Genet.* **2002**, *31*, 166–170. [CrossRef]

11. Walder, R.Y.; Landau, D.; Meyer, P.; Shalev, H.; Tsolia, M.; Borochowitz, Z.; Boettger, M.B.; Beck, G.E.; Englehardt, R.K.; Carmi, R.; et al. Mutation of TRPM6 causes familial hypomagnesemia with secondary hypocalcemia. *Nat. Genet.* **2002**, *31*, 171–174. [CrossRef] [PubMed]

12. Garcia-Sanz, N.; Fernandez-Carvajal, A.; Morenilla-Palao, C.; Planells-Cases, R.; Fajardo-Sanchez, E.; Fernandez-Ballester, G.; Ferrer-Montiel, A. Identification of a tetramerization domain in the C terminus of the vanilloid receptor. *J. Neurosci.* **2004**, *24*, 5307–5314. [CrossRef] [PubMed]

13. Li, M.; Jiang, J.; Yue, L. Functional characterization of homo- and heteromeric channel kinases TRPM6 and TRPM7. *J. Gen. Physiol.* **2006**, *127*, 525–537. [CrossRef] [PubMed]

14. Zhang, Z.; Yu, H.; Huang, J.; Faouzi, M.; Schmitz, C.; Penner, R.; Fleig, A. The TRPM6 kinase domain determines the Mg.ATP sensitivity of TRPM7/M6 heteromeric ion channels. *J. Biol. Chem.* **2014**, *289*, 5217–5227. [CrossRef] [PubMed]

15. Chubanov, V.; Waldegger, S.; Mederos y Schnitzler, M.; Vitzthum, H.; Sassen, M.C.; Seyberth, H.W.; Konrad, M.; Gudermann, T. Disruption of TRPM6/TRPM7 complex formation by a mutation in the TRPM6 gene causes hypomagnesemia with secondary hypocalcemia. *Proc. Natl. Acad. Sci. USA* **2004**, *101*, 2894–2899. [CrossRef] [PubMed]

16. Liao, M.; Cao, E.; Julius, D.; Cheng, Y. Structure of the TRPV1 ion channel determined by electron cryo-microscopy. *Nature* **2013**, *504*, 107–112. [CrossRef]

17. Moiseenkova-Bell, V.Y.; Stanciu, L.A.; Serysheva, I.; Tobe, B.J.; Wensel, T.G. Structure of TRPV1 channel revealed by electron cryomicroscopy. *Proc. Natl. Acad. Sci. USA* **2008**, *105*, 7451–7455. [CrossRef] [PubMed]

18. Gao, Y.; Cao, E.; Julius, D.; Cheng, Y. TRPV1 structures in nanodiscs reveal mechanisms of ligand and lipid action. *Nature* **2016**, *534*, 347–351. [CrossRef] [PubMed]

19. Autzen, H.E.; Myasnikov, A.G.; Campbell, M.G.; Asarnow, D.; Julius, D.; Cheng, Y. Structure of the human TRPM4 ion channel in a lipid nanodisc. *Science* **2018**, *359*, 228–232. [CrossRef]

20. Winkler, P.A.; Huang, Y.; Sun, W.; Du, J.; Lu, W. Electron cryo-microscopy structure of a human TRPM4 channel. *Nature* **2017**, *552*, 200–204. [CrossRef]

21. Chubanov, V.; Mittermeier, L.; Gudermann, T. TRPM7 reflected in Cryo-EMirror. *Cell Calcium* **2018**, *76*, 129–131. [CrossRef] [PubMed]

22. Duan, J.; Li, Z.; Li, J.; Hulse, R.E.; Santa-Cruz, A.; Valinsky, W.C.; Abiria, S.A.; Krapivinsky, G.; Zhang, J.; Clapham, D.E. Structure of the mammalian TRPM7, a magnesium channel required during embryonic development. *Proc. Natl. Acad. Sci. USA* **2018**, *115*, E8201–E8210. [CrossRef] [PubMed]

23. Owsianik, G.; D'Hoedt, D.; Voets, T.; Nilius, B. Structure-function relationship of the TRP channel superfamily. *Rev. Physiol. Biochem. Pharmacol.* **2006**, *156*, 61–90. [PubMed]

24. Clapham, D.E. TRP channels as cellular sensors. *Nature* **2003**, *426*, 517–524. [CrossRef] [PubMed]

25. Harteneck, C. Proteins modulating TRP channel function. *Cell Calcium* **2003**, *33*, 303–310. [CrossRef]

26. Obukhov, A.; Schultz, G.; Lückhoff, A. Regulation of heterologously expressed transient receptor potential-like channels by calcium ions. *Neuroscience* **1998**, *85*, 487–495. [CrossRef]

27. Zhu, M.X. Multiple roles of calmodulin and other Ca^{2+}-binding proteins in the functional regulation of TRP channels. *Pflügers Arch.* **2005**, *451*, 105–115. [CrossRef]

28. Kinoshita-Kawada, M.; Tang, J.; Xiao, R.; Kaneko, S.; Foskett, J.K.; Zhu, M.X. Inhibition of TRPC5 channels by Ca 2+-binding protein 1 in Xenopus oocytes. *Pflügers Arch.* **2005**, *450*, 345–354. [CrossRef]

29. Jirku, M.; Lansky, Z.; Bednarova, L.; Sulc, M.; Monincova, L.; Majer, P.; Vyklicky, L.; Vondrasek, J.; Teisinger, J.; Bousova, K. The characterization of a novel S100A1 binding site in the N-terminus of TRPM1. *Int. J. Biochem. Cell Biol.* **2016**, *78*, 186–193. [CrossRef]

30. Holakovska, B.; Grycova, L.; Jirku, M.; Sulc, M.; Bumba, L.; Teisinger, J. Calmodulin and S100A1 protein interact with N terminus of TRPM3 channel. *J. Biol. Chem.* **2012**, *287*, 16645–16655. [CrossRef]

31. Bousova, K.; Herman, P.; Vecer, J.; Bednarova, L.; Monincova, L.; Majer, P.; Vyklicky, L.; Vondrasek, J.; Teisinger, J. Shared CaM- and S100A1-binding epitopes in the distal TRPM4 N terminus. *FEBS J.* **2018**, *285*, 599–613. [CrossRef] [PubMed]

32. Tong, Q.; Zhang, W.; Conrad, K.; Mostoller, K.; Cheung, J.Y.; Peterson, B.Z.; Miller, B.A. Regulation of the transient receptor potential channel TRPM2 by the Ca2+ sensor calmodulin. *J. Biol. Chem.* **2006**, *281*, 9076–9085. [CrossRef] [PubMed]

33. Xie, J.; Sun, B.; Du, J.; Yang, W.; Chen, H.C.; Overton, J.D.; Runnels, L.W.; Yue, L. Phosphatidylinositol 4,5-bisphosphate (PIP(2)) controls magnesium gatekeeper TRPM6 activity. *Sci. Rep.* **2011**, *1*, 146. [CrossRef] [PubMed]

34. Park, E.Y.J.; Baik, J.Y.; Kwak, M.; So, I. The role of calmodulin in regulating calcium-permeable PKD2L1 channel activity. *Korean J. Physiol. Pharmacol.* **2019**, *23*, 219–224. [CrossRef] [PubMed]

35. Emery, E.C.; Diakogiannaki, E.; Gentry, C.; Psichas, A.; Habib, A.M.; Bevan, S.; Fischer, M.J.; Reimann, F.; Gribble, F.M. Stimulation of GLP-1 secretion downstream of the ligand-gated ion channel TRPA1. *Diabetes* **2015**, *64*, 1202–1210. [CrossRef] [PubMed]

36. Dang, S.; van Goor, M.K.; Asarnow, D.; Wang, Y.; Julius, D.; Cheng, Y.; van der Wijst, J. Structural insight into TRPV5 channel function and modulation. *Proc. Natl. Acad. Sci. USA* **2019**, *116*, 8869–8878. [CrossRef]

37.   Hasan, R.; Zhang, X. Ca(2+) Regulation of TRP Ion Channels. *Int. J. Mol. Sci.* **2018**, *19*, 1256. [CrossRef]
38.   Babu, Y.S.; Sack, J.S.; Greenhough, T.J.; Bugg, C.E.; Means, A.R.; Cook, W.J.J.J. Three-dimensional structure of calmodulin. *Nature* **1985**, *315*, 37–40. [CrossRef]
39.   Barbato, G.; Ikura, M.; Kay, L.E.; Pastor, R.W.; Bax, A.A. Backbone dynamics of calmodulin studied by 15N relaxation using inverse detected two-dimensional NMR spectroscopy: The central helix is flexible. *Biochemistry* **1992**, *31*, 5269–5278. [CrossRef]
40.   Babu, Y.S.; Bugg, C.E.; Cook, W.J.J. Structure of calmodulin refined at 2.2 A resolution. *J. Mol. Biol.* **1988**, *204*, 191–204. [CrossRef]
41.   Chin, D.; Means, A.R.R. Calmodulin: A prototypical calcium sensor. *Trends Cell Biol.* **2000**, *10*, 322–328. [CrossRef]
42.   Singh, A.K.; McGoldrick, L.L.; Twomey, E.C.; Sobolevsky, A.I.I. Mechanism of calmodulin inactivation of the calcium-selective TRP channel TRPV6. *Sci. Adv.* **2018**, *4*. [CrossRef] [PubMed]
43.   Hasan, R.; Leeson-Payne, A.T.; Jaggar, J.H.; Zhang, X. Calmodulin is responsible for Ca(2+)-dependent regulation of TRPA1 Channels. *Sci. Rep.* **2017**, *7*, 45098. [CrossRef]
44.   Bate, N.; Caves, R.E.; Skinner, S.P.; Goult, B.T.; Basran, J.; Mitcheson, J.S.; Vuister, G.W. A novel mechanism for calmodulin-dependent inactivation of transient receptor potential vanilloid 6. *Biochemistry* **2018**, *57*, 2611–2622. [CrossRef] [PubMed]
45.   Prosser, B.L.; Wright, N.T.; Hernandez-Ochoa, E.O.; Varney, K.M.; Liu, Y.; Olojo, R.O.; Zimmer, D.B.; Weber, D.J.; Schneider, M.F. S100A1 binds to the calmodulin-binding site of ryanodine receptor and modulates skeletal muscle excitation-contraction coupling. *J. Biol. Chem.* **2008**, *283*, 5046–5057. [CrossRef] [PubMed]
46.   Wright, N.T.; Varney, K.M.; Ellis, K.C.; Markowitz, J.; Gitti, R.K.; Zimmer, D.B.; Weber, D.J. The three-dimensional solution structure of Ca(2+)-bound S100A1 as determined by NMR spectroscopy. *J. Mol. Biol.* **2005**, *353*, 410–426. [CrossRef]
47.   Bily, J.; Grycova, L.; Holendova, B.; Jirku, M.; Janouskova, H.; Bousova, K.; Teisinger, J. Characterization of the S100A1 protein binding site on TRPC6 C-terminus. *PLoS ONE* **2013**, *8*, e62677. [CrossRef] [PubMed]
48.   Lau, S.-Y.; Procko, E.; Gaudet, R. Distinct properties of Ca^{2+}–calmodulin binding to N-and C-terminal regulatory regions of the TRPV1 channel. *J. Gen. Physiol.* **2012**, *140*, 541–555. [CrossRef]
49.   Yap, K.L.; Kim, J.; Truong, K.; Sherman, M.; Yuan, T.; Ikura, M. Calmodulin target database. *J. Struct. Funct. Genom.* **2000**, *1*, 8–14. [CrossRef]
50.   Waterhouse, A.; Bertoni, M.; Bienert, S.; Studer, G.; Tauriello, G.; Gumienny, R.; Heer, F.T.; de Beer, T.A.P.; Rempfer, C.; Bordoli, L. SWISS-MODEL: Homology modelling of protein structures and complexes. *Nucleic Acids Res.* **2018**, *46*, W296–W303. [CrossRef]
51.   Brown, N.P.; Leroy, C.; Sander, C. MView: A web-compatible database search or multiple alignment viewer. *Bioinformatics* **1998**, *14*, 380–381. [CrossRef] [PubMed]
52.   Vilar, S.; Cozza, G.; Moro, S. Medicinal chemistry and the molecular operating environment (MOE): Application of QSAR and molecular docking to drug discovery. *Curr. Top. Med. Chem.* **2008**, *8*, 1555–1572. [CrossRef] [PubMed]
53.   Kozakov, D.; Hall, D.R.; Xia, B.; Porter, K.A.; Padhorny, D.; Yueh, C.; Beglov, D.; Vajda, S. The ClusPro web server for protein–protein docking. *Nat. Protoc.* **2017**, *12*, 255. [CrossRef] [PubMed]
54.   Fallon, J.L.; Halling, D.B.; Hamilton, S.L.; Quiocho, F.A. Structure of calmodulin bound to the hydrophobic IQ domain of the cardiac Cav1. 2 calcium channel. *Structure* **2005**, *13*, 1881–1886. [CrossRef] [PubMed]
55.   Wright, N.T.; Prosser, B.L.; Varney, K.M.; Zimmer, D.B.; Schneider, M.F.; Weber, D.J. S100A1 and calmodulin compete for the same binding site on ryanodine receptor. *J. Biol. Chem.* **2008**, *283*, 26676–26683. [CrossRef] [PubMed]
56.   Grycova, L.; Holendova, B.; Lansky, Z.; Bumba, L.; Jirku, M.; Bousova, K.; Teisinger, J. Ca^{2+} Binding protein S100A1 competes with calmodulin and PIP2 for binding site on the C-terminus of the TPRV1 receptor. *ACS Chem. Neurosci.* **2014**, *6*, 386–392. [CrossRef]
57.   Prosser, B.L.; Hernández-Ochoa, E.O.; Schneider, M.F. S100A1 and calmodulin regulation of ryanodine receptor in striated muscle. *Cell Calcium* **2011**, *50*, 323–331. [CrossRef]
58.   Whicher, J.R.; MacKinnon, R. Structure of the voltage-gated K^{+} channel Eag1 reveals an alternative voltage sensing mechanism. *Science* **2016**, *353*, 664–669. [CrossRef]

59. López-Romero, A.E.; Hernández-Araiza, I.; Torres-Quiroz, F.; Tovar-Y-Romo, L.B.; Islas, L.D.; Rosenbaum, T. TRP ion channels: Proteins with conformational flexibility. *Channels* **2019**, *13*, 207–226. [CrossRef]

60. Jirku, M.; Bumba, L.; Bednarova, L.; Kubala, M.; Sulc, M.; Franek, M.; Vyklicky, L.; Vondrasek, J.; Teisinger, J.; Bousova, K. Characterization of the part of N-terminal PIP2 binding site of the TRPM1 channel. *Biophys. Chem.* **2015**, *207*, 135–142. [CrossRef]

61. Neshich, G.; Togawa, R.C.; Mancini, A.L.; Kuser, P.R.; Yamagishi, M.E.; Pappas, G.; Torres, W.V.; e Campos, T.F.; Ferreira, L.L.; Luna, F.M. STING Millennium: A web-based suite of programs for comprehensive and simultaneous analysis of protein structure and sequence. *Nucleic Acids Res.* **2003**, *31*, 3386–3392. [CrossRef] [PubMed]

62. Wiederstein, M.; Sippl, M.J. ProSA-web: Interactive web service for the recognition of errors in three-dimensional structures of proteins. *Nucleic Acids Res.* **2007**, *35*, W407–W410. [CrossRef] [PubMed]

63. Kozakov, D.; Beglov, D.; Bohnuud, T.; Mottarella, S.E.; Xia, B.; Hall, D.R.; Vajda, S. How good is automated protein docking? *Proteins: Struct. Funct. Bioinform.* **2013**, *81*, 2159–2166. [CrossRef] [PubMed]

64. Vajda, S.; Yueh, C.; Beglov, D.; Bohnuud, T.; Mottarella, S.E.; Xia, B.; Hall, D.R.; Kozakov, D. New additions to the C lus P ro server motivated by CAPRI. *Proteins: Struct. Funct. Bioinform.* **2017**, *85*, 435–444. [CrossRef] [PubMed]

65. Biovia, D.S. *Discovery Studio Modeling Environment. Release: 2017*; Dassault Systèmes: San Diego, CA, USA, 2016.

Příloha 2

ZOUHAROVA, M., VYMETAL, J., BEDNAROVA, L., VANEK, O., HERMAN, P., VETYSKOVA, V., POSTULKOVA, K., LINGSTAADAS, P. S., VONDRASEK, J. & BOUSOVA, K. 2021. Intrinsically disordered protein domain of human ameloblastin in synthetic fusion with calmodulin increases calmodulin stability and modulates its function. *Int J Biol Macromol,* 168**,** 1-12.

Contents lists available at ScienceDirect

International Journal of Biological Macromolecules

Intrinsically disordered protein domain of human ameloblastin in synthetic fusion with calmodulin increases calmodulin stability and modulates its function

Monika Zouharova [a,b], Jiri Vymetal [a], Lucie Bednarova [a], Ondrej Vanek [c], Petr Herman [d], Veronika Vetyskova [a,e], Klara Postulkova [a,b], Petter S. Lingstaadas [f], Jiri Vondrasek [a], Kristyna Bousova [a,*]

[a] Institute of Organic Chemistry and Biochemistry of the Czech Academy of Sciences, 160 00 Prague, Czech Republic
[b] Second Faculty of Medicine, Charles University, 150 06 Prague, Czech Republic
[c] Department of Biochemistry, Faculty of Science, Charles University, 128 40 Prague, Czech Republic
[d] Faculty of Mathematics and Physics, Charles University, 121 16 Prague, Czech Republic
[e] Department of Biochemistry and Microbiology, University of Chemistry and Technology, Prague, 166 28 Prague, Czech Republic
[f] Institute of Clinical Dentistry, University of Oslo, 0317 Oslo, Norway

ARTICLE INFO

ABSTRACT

Constantly increasing attention to bioengineered proteins has led to the rapid development of new functional targets. Here we present the biophysical and functional characteristics of the newly designed CaM/AMBN-Ct fusion protein. The two-domain artificial target consists of calmodulin (CaM) and ameloblastin C-terminus (AMBN-Ct). CaM as a well-characterized calcium ions (Ca^{2+}) binding protein offers plenty of options in terms of Ca^{2+} detection in biomedicine and biotechnologies. Highly negatively charged AMBN-Ct belongs to intrinsically disordered proteins (IDPs). CaM/AMBN-Ct was designed to open new ways of communication synergies between the domains with potential functional improvement. The character and function of CaM/AMBN-Ct were explored by biophysical and molecular modelling methods. Experimental studies have revealed increased stability and preserved CaM/AMBN-Ct function. The results of molecular dynamic simulations (MDs) outlined different interface patterns between the domains with potential allosteric communication within the fusion.

© 2020 Elsevier B.V. All rights reserved.

1. Introduction

Most prokaryotic and eukaryotic proteins are multidomain proteins that have evolved by duplication and recombination of a limited pool of protein domains [1]. A domain is a functional protein unit considered to be a building block in the modular evolution of proteins [2]. Widespread approaches in protein engineering mimic the natural phenomena of domain rearrangements and generate proteins for biomedicine or biotechnology purposes. However, the synthetic fusion of protein domains may also lead to new intramolecular allosteric patterns [3]. Recent studies

have revealed intramolecular allosteric modulations as a fine-tuning tool to generate conformation plasticity of e.g. *PSD-95/Dlg/ZO-1* (PDZ) domains resulting in diversified ligand recognition patterns [4,5]. Engineering of allostery has been widely used in biosensors where ligand-induced conformation changes in one domain were propagated to the other domain with positive modulation of its own activity [6,7]. Some of the biosensors based on the fusion of domains can propagate conformational changes triggered upon calcium ions (Ca^{2+}) binding [8–10]. It is well known that Ca^{2+} regulates countless cellular processes, from fertilization to cell death. Various extra- and intra-cellular stimuli trigger the elevation of cytoplasmic Ca^{2+} from 100 to 1000 nM, resulting in its interactions with various Ca^{2+} signaling sensors or buffers, e.g. Ca^{2+}-binding proteins (CBPs) [11].

The prototypical ubiquitously expressed Ca^{2+} sensor calmodulin (CaM) mediates a regulation of receptors, transporters, enzymatic activities (CaM kinases, adenyl cyclases) or gene transcription [12–15]. CaM senses Ca^{2+} concentration through four canonical EF-hand motifs composed of two α-helices bridged by a loop coordinating bond of Ca^{2+} ion [16,17]. The EF-hand motifs mostly occur in pairs (as the EF-domain) and cooperate to bind Ca^{2+} with a high affinity [18]. The CaM molecule consists of N- and C-terminal globular EF-hand domains connected by a

flexible linker [19–21]. Antiparallel EF-hand helices reorient to be nearly perpendicular upon Ca^{2+} binding, so the CaM molecule adopts a more helical conformation and expose its hydrophobic patches immediately [22]. The CaM interactions with target proteins further change CaM conformation to various degrees which can lead to an additional increase of its affinity for Ca^{2+} [23]. The differences in Ca^{2+} binding affinities and conformational promiscuity make CaM a very dynamic and versatile protein sensor regulating the target proteins in a wide range of Ca^{2+} levels. The plasticity of CaM conformations reflected by changes of Ca^{2+} concentration has been employed in biosensors revealing Ca^{2+} oscillations in the context of single cells and even in the whole organism [24,25].

A small subset of CBPs belong to intrinsically disordered proteins (IDPs) interacting with Ca^{2+} through disordered motifs [26]. The binding of ligand/ion or posttranslational modifications can induce IDPs folding and it consequently serves as a regulatory switch mechanism [27,28]. Some IDPs remain unfolded even after ligand/ion binding which indicates the necessity of an intrinsic disorder for biological functions [29]. Despite being widespread in human proteome (44% of proteins), only a minority of IDPs binds Ca^{2+} and these include Ca^{2+} storage proteins in sarco- and endo-plasmatic reticulum (calsequesterin, calreticulin) and especially proteins necessary in biomineralization processes e.g. ameloblastin (AMBN) or amelogenin (AMEL) [30,32–34].

AMBN is involved in the formation of the hardest mineralized tissue in humans - tooth enamel. Together with AMEL, it assembles into supramolecular structures and regulates the growth of hydroxyapatite prisms [35]. Furthermore, AMBN was associated with bone development and even with the prevention and healing of bone fractures [36]. AMBN is oligomeric Ca^{2+} binding IDP, although a detailed biochemical and functional characterization of AMBN is still lacking [37]. Originally, AMBN was characterized by bioinformatic analysis as a two-domain protein with highly IDP character [38]. The N-terminal domain contains a specific segment encoded by exon 5 that provides an AMBN oligomeric character [39]. The C-terminal domain (AMBN-Ct) is highly acidic and was suggested to mediate the interaction with Ca^{2+} [38]. Interestingly, the phosphorylation of AMBN was shown to suppress supramolecular assembly and Ca^{2+} binding, and can serve as a regulator of AMBN functions [37].

In the present study, we proposed and designed a synthetic fusion a two-domain CaM/AMBN-Ct protein composed of CaM and AMBN-Ct. Flexible IDPs like AMBN-Ct tend to occupy various conformational states which make them perfect candidates for direct or allosteric modulations of their fusion partners. The CaM/AMBN-Ct was constructed to study potential modulations of CaM by disordered AMBN-Ct. With respect to the high negative charge of the CaM, we hypothesized on non-specific interplay between CaM and the AMBN-Ct within the fusion construct. The fusion protein was characterized with respect to molecular size and shape, thermal stability and its binding of peptide derived from the CaM native binding partner transient receptor potential melastatin-4 (TRPM4) channel.

2. Materials and methods

2.1. Design of CaM/AMBN-Ct fusion construct

The cDNA sequence coding the CaM/AMBN-Ct was designed in silico using SnapGene (GSL Biotech, San Diego, California, USA). The CaM (UniProtKB P0DP29-1) located at N-terminus of the fusion was linked by a flexible linker (GGGGSS) with AMBN-Ct (UniProtKB Q9NP70-1, positions L223-P447) placed on its C-terminus and TEV cleavage site was added to N-terminus of the construct. The cDNA sequence coding for CaM/AMBN-Ct was cloned in silico into pET28b vector by extensions containing recognition sites for *Nde*I and *Xho*I restriction endonucleases and checked for in-frame translation with upstream 6xHis expressed

from pET28b. Designed cDNA sequence was synthetized and cloned by GenScript (Piscataway, New Jersey, USA) as described.

2.2. Expression and purification of CaM, AMBN-Ct and CaM/AMBN-Ct

CaM was expressed by pET3a vector in *E. coli* BL21 by induction with 0.5 mM IPTG at 25 °C for 12 h. The cells were harvested in 50 mM Tris-HCl (pH 7.5), 2 mM EDTA, 2 mM 2-mercaptoethanol, 0.2 mM phenylmethylsulphonyl fluoride, sonicated and 5 mM $CaCl_2$ was added to the soluble fraction. CaM was purified using hydrophobic interaction chromatography on Phenyl Sepharose CL-4B (GE Healthcare, Chicago, IL, USA) and eluted by 50 mM Tris-HCl (pH 7.5), 100 mM NaCl, 1.5 mM EDTA. CaM was finally purified on Superdex 200 Increase 10/300 GL (GE Healthcare, Chicago, IL, USA) equilibrated with 10 mM Tris (pH 7.5), 100 mM NaCl.

AMBN-Ct [40] and CaM/AMBN-Ct were expressed in *E. coli* Bl-21 by 0.5 mM IPTG induction with 15 °C. The cells were harvested after 18 h and resuspended in 50 mM Na_2HPO_4 (pH 8.0), 50 mM NaCl, 0.1% 2-mercaptoethanol (AMBN-Ct) or 50 mM Tris-HCl (pH 8.0), 50 mM NaCl, 2 mM 2-mercaptoethanol, 2 mM EDTA (CaM/AMBN-Ct). Cells with expressed AMBN-Ct were disrupted by sonication, a soluble fraction was supplemented with 8 M urea and loaded on Chelating Sepharose Fast Flow (GE Healthcare, Chicago, IL, USA) charged with Ni^{2+} ions. AMBN-Ct was eluted with 50 mM Tris-HCl (pH 7.5), 600 mM NaCl, 8 M urea, 600 mM imidazole, renatured in 50 mM Tris-HCl (pH 7.5), 500 mM NaCl and processed by TEV protease. The protein mixture was loaded on Chelating Sepharose Fast Flow (GE Healthcare, Chicago, IL, USA) charged with Ni^{2+} ions and weakly-bounded AMBN-Ct was eluted with 10 mM Tris-HCl (pH 7.5), 100 mM NaCl, 100 mM imidazole. Ca^{2+} contamination was chelated by the addition of 10 mM EGTA for 20 min. Finally, AMBN-Ct was subjected to size-exclusion chromatography on Superdex 200 Increase 10/300 GL (GE Healthcare, Chicago, IL, USA) equilibrated with 10 mM Tris (pH 7.5), 100 mM NaCl.

CaM/AMBN-Ct was purified on Phenyl Sepharose CL-4B (GE Healthcare, Chicago, IL, USA) as described for standardly purified isolated CaM [41]. The eluted protein was dialyzed into 50 mM Tris-HCl (pH 7.5), 500 mM NaCl and processed by TEV protease. The Ca^{2+} contamination was removed by incubation with 10 mM EGTA for 20 min. Cleaved 6xHis and TEV protease were separated from CaM/AMBN-Ct using size-exclusion chromatography on Superdex 200 Increase 10/300 GL (GE Healthcare, Chicago, IL, USA) equilibrated with 10 mM Tris pH (7.5), 100 mM NaCl.

2.3. Peptide synthesis

The TRPM4np peptide (UniProtKB Q8TD43, positions V129-Q147) derived from CaM-binding domain in TRPM4 was synthesized by a solid-phase peptide synthesis using a standardized N^{α}-Fmoc protocol [42].The purity and identity of the TRPM4np was determined by an Agilent 1260 HPLC (Agilent Technologies, Santa Clara, CA, USA) coupled to an ESI-TOF Agilent 6530 (Agilent Technologies, Santa Clara, CA, USA) with Agilent Jet Stream technology.

2.4. Dynamic light scattering

Dynamic light scattering experiments were performed at 18 °C on the RiNA Laser Spectroscatter 201 (RiNA, Berlin, Germany). Protein samples (1.0 $mg \cdot ml^{-1}$) were centrifuged and supernatant was equilibrated at 18 °C for 10 min. The scattered light was detected at a scattering angle of 90° with an acquisition time of 15 s. For each sample, at least 50 measurements were recorded. The measured raw $G^{(2)}$ autocorrelation functions were recorded and thoroughly examined for artifacts. Samples with a residual baseline or an anomalous photocurrent count rate were discarded. Individual autocorrelograms were fitted by second-order cumulant analysis providing the z-averaged size and polydispersity index (PDI). Hydrodynamic radii (R_h) were estimated

using Stokes-Einstein relation. The reported values of R_h and PDI were calculated as an arithmetic average over 50–75 analyzed autocorrelation curves. Their uncertainty was estimated as the standard errors of the mean (SEM). The obtained R_h values were compared with predicted R_h values for a folded globular, disordered and denatured protein of the same length [43].

2.5. Analytical ultracentrifugation

Sedimentation velocity measurements were performed four times for each sample using an analytical ultracentrifuge ProteomeLab XL-I (Beckman Coulter, Indianapolis, IN, USA). The protein samples were analyzed in a 10 mM Tris-HCl (pH 7.5), 100 mM NaCl buffer with or without 10 mM $CaCl_2$ added prior to the analysis. Sedimentation velocity experiments were conducted at 48000 rpm and 20 °C using double sector cells and An50-Ti rotor at 2.8 (CaM), 1.1 (AMBN-Ct), and 1.3 (CaM/AMBN-Ct) mg·ml^{-1} protein concentration. In total, 200 absorbance scans were recorded at 280 nm at 3–6 min intervals. Buffer density, protein partial specific volume, sedimentation coefficient values corrected to standard conditions, and particle dimensions were calculated in Sednterp [44]. Data were analyzed in Sedfit [45] using a continuous sedimentation coefficient distribution c(s) model. The figure was prepared in GUSSI [46].

2.6. Circular dichroism spectroscopy

The circular dichroism (CD) measurements were performed on a Jasco-1500 spectropolarimeter equipped with a Peltier thermostated holder PTC-517 (JASCO, Easton, MD, USA). The spectra were recorded in a temperature range from 10 °C to 90 °C in far-UV (195 nm - 280 nm) and near-UV spectral region (240 nm - 350 nm) using the following experimental setup: far-UV region: 0.5 mm rectangular quartz cell, standard instrument sensitivity, 1 nm bandwidth, a scanning speed of 10 nm/min, a response time of 8 s, one accumulation, with a temperature increment of 5 °C; near-UV region: 1 mm rectangular quartz cell, standard instrument sensitivity, 1 nm bandwidth, a scanning speed of 5 nm/min, a response time of 16 s, one accumulation, with a temperature increment of 10 °C. The temperature reversibility was checked by measurement of the cooled sample back to the starting temperature. After baseline subtraction, the final data was expressed as molar ellipticities Θ (deg·cm^2·dmol^{-1}) per residue.

All samples were in a buffer containing a 10 mM Tris (pH 7.5), 100 mM NaCl and with or without 10 mM $CaCl_2$. The concentration used for CD measurements was 160 μM (CaM), 65 μM (CaM/AMBN-Ct) and 47 μM (AMBN-Ct) for the near-UV spectral region and 10× diluted for measurements in the far-UV spectral region. The numerical analysis of secondary structures was performed using the CDPro software package [47–49]. Melting temperatures were calculated using temperature dependence of the molar ellipticities at 222 nm using the program Sigmaplot 12.5 (Systat software, San Jose, CA, USA) when sigmoid fitting was applied.

2.7. Fluorescence measurements

Steady-state fluorescence anisotropy measurements were performed on a photon counting spectrometer K2 (ISS Inc., Champaign, IL, USA). Fluorescein-labelled peptide TRPM4np was diluted in a buffer containing 50 mM Tris-HCl (pH 7.5) and 100 mM NaCl to a final concentration of 1 μM. For Ca^{2+}-dependent experiments, the buffer was supplemented by 2 mM $CaCl_2$. Small aliquots from a 150 μM stock solution of CaM, CaM/AMBN-Ct or AMBN-Ct (with or without 2 mM $CaCl_2$) were added into a 2-mm pathlength cuvette with 1 μM TRPM4np. Fluorescence was excited at 490 nm and the steady-state fluorescence anisotropy value (r) was recorded at 530 nm. The scattered light was suppressed by a dielectric 520 nm long-pass filter placed in

front of the input slit of the emission monochromator. Emission anisotropy was calculated as [50]:

$$r = (I_{\parallel} - GI_{\perp})/(I_{\parallel} + 2GI_{\perp}) \tag{1}$$

where $I_{\parallel}$ and $I_{\perp}$ is the emission intensity polarized parallel and perpendicular to the direction of the polarized excitation, respectively, and G is a factor normalizing sensitivity of the detection channel for the different polarizations [50]. Five measurements were performed at each titration point and the mean r value was used for the calculation of the bound fraction (F_B) of CaM, CaM/AMBN-Ct or AMBN-Ct according to [51].

$$F_B = (r_{obs} - r_{min})/[(r_{max} - r_{obs})\,Q + (r_{obs} - r_{min})] \tag{2}$$

Quantity r_{obs} represents the measured anisotropy at a particular ligand concentration, r_{min} is the anisotropy of free TRPM4np and r_{max} stands for the anisotropy at saturation. Since the ligand binding is generally accompanied by a change in fluorescence intensity, proper weighting of the free and bound state in the measured signal is introduced by a correction factor Q that represents the quantum yield ratio of the bound to the free form. Because the quantum yield is proportional to the emission lifetime τ [50], the correction Q can be calculated as $Q = \tau_{bound}/\tau_{free}$ where τ_{free} and τ_{bound} is a fluorescence lifetime of the free and bound peptide, respectively. The equilibrium dissociation constants (K_D) of studied complexes were obtained by plotting F_B against ligand concentration and fitting the data by a simple single-binding-site model [52].

$$F_B = \frac{K_D + [P1] + [P2] - \sqrt{(K_D + [P1] + [P2])^2 - 4[P1][P2]}}{2[P1]} \tag{3}$$

where [P1] stands for the concentration of TRPM4np and [P2] represents ligand concentration. Nonlinear data fitting was performed using SIGMAPLOT 11.0 (Systat software, Inc., San Jose, CA, USA). Fluorescence lifetimes were measured as described elsewhere [42]. Briefly, a drop of sample was placed on a coverslip and inserted into an inverted confocal microscope IX83 (Olympus, Tokyo, Japan) equipped with TimeHarp 260 PICO time-correlated single photon counting electronics (PicoQuant, Berlin, Germany). Fluorescence was excited at 485 nm by LDH-485 ps laser (PicoQuant, Berlin, Germany). Emission decays were collected using a 520/35 bandpass filter in the detection path and the lifetimes were evaluated by a SymPhoTime 64 software (PicoQuant, Berlin, Germany).

2.8. Microscale thermophoresis

The Ca^{2+} affinity to AMBN and AMBN-Ct was measured using Monolith NT.LabelFree instrument (NanoTemper Technologies GmbH, Munich, Germany) and LabelFree Premium capillaries (NanoTemper Technologies GmbH, Munich, Germany). A constant concentration of AMBN (1.3 μM) and AMBN-Ct (3.2 μM) was titrated by a serial dilution of $CaCl_2$ (500–0.015 mM) at 25 °C. All the experiments were carried out in 10 mM Tris-HCl (pH 7.5), 100 mM NaCl and 0.05% Tween 20 with LED power of 30% and MST power of 40%.

The intrinsic fluorescence signal from CaM/AMBN-Ct is affected by Ca^{2+}-binding to CaM subunit. Therefore, Ca^{2+}-binding to CaM/AMBN-Ct was studied using fluorescently labelled CaM/AMBN-Ct generating a constant initial fluorescence intensity throughout the Ca^{2+} titration series. CaM/AMBN-Ct was dialyzed into 50 mM HEPES pH 7.5, 150 mM NaCl and labelled using Monolith™ NT.115 Protein Labeling Kit RED-NHS (NanoTemper Technologies GmbH, Munich, Germany). The microscale thermophoresis (MST) experiments were performed on Monolith NT.115 (NanoTemper Technologies GmbH, Munich, Germany) in NT.115 Standard Treated Capillaries (NanoTemper Technologies GmbH, Munich, Germany) at 25 °C. The CaM/AMBN-Ct at a constant concentration of 50 nM was titrated by a 2-fold serial dilution

of $CaCl_2$ (500–0.03 μM). All the experiments were carried out in 50 mM HEPES (pH 7.5),150 mM NaCl and 0.05% tween with LED power of 20% and MST power of 80%. Data from two independent measurements were used to determine the equilibrium dissociation constant (K_D) using equation

$$\frac{[BL]}{[B_0]} = \frac{([L_0] + [B_0] + K_D) - \sqrt{([L_0] + [B_0] + K_D)^2 - 4 \times [L_0] \times [B_0]}}{2 \times [B_0]},$$

where $[B_0]$ stands for the concentration of binding sites, $[L_0]$ for the concentration of ligand and $[BL]$ for the concentration of complex between ligand and binding sites.

2.9. Coarse grain model for molecular dynamic simulations (MDs)

The coarse grain model utilized in this study was based on a modified bead-necklace model for intrinsically disordered proteins [53,54], which we adapted for molecular dynamics simulations. Each amino-acid residue was represented by a single bead with a uniform mass of 50 amu (amu). Beads corresponding to the neighboring residues were linked via harmonic bonded potential with an equilibrium length of 0.41 nm and a force constant of 240 $kJ·mol^{-1}·nm^{-2}$. Beads interacted with Lennard-Jones potential U_{LJ}

$$U_{LJ}(r_{ij}) = \frac{C^{(12)}}{r_{ij}^{12}} - \frac{C^{(6)}}{r_{ij}^6},$$

where r_{ij} stands for the distance between beads, the attractive $C^{(6)}$ coefficient has the value of $6·10^{-3}$ $kJ·mol·nm^6$ and repulsive $C^{(12)}$ coefficient $2.8·10^{-5}$ $kJ·mol·nm^{12}$. In order to capture hydrophobic interactions between beads, the Lennard-Jones potential was strengthened selectively between particular hydrophobic residues (leucine, isoleucine, valine, phenylalanine, tyrosine and tryptophan). Both $C^{(6)}$ and $C^{(12)}$ coefficients of these interactions were increased to 10-times higher values ($6·10^{-2}$ $kJ·mol·nm^6$ and $2.8·10^{-4}$ $kJ·mol·nm^{12}$). This particular value was decided as a compromise between performance of the unmodified model and strength of newly introduced effects (Figs. S1, S2).

Additionally, interactions between charged residues were modeled by Debye-Hückel potential that accounts for the electrostatic screening in solutions of electrolytes:

$$U_{EL}(r_{ij}) = \frac{Z_i Z_j e}{4\epsilon_0 \epsilon_r} \frac{exp(-\kappa(r_{ij} - (R_i + R_j)))}{(1 + \kappa R_i)(1 + \kappa R_j)} \frac{1}{r_{ij}}.$$

Charge Z of the bead particle was assigned to 1 for positively (R, K) and − 1 for negatively charged residues (D, E). The elemental charge is represented by e, ϵ_0 stands for vacuum permittivity, ϵ_r for the dielectric constant of the medium, κ for the inverse Debye screening length of the particular buffer (1.040 nm^{-1} for 0.1 M NaCl) and R for the hard sphere radius of the beads (0.2 nm). The ions in the buffer were modeled implicitly by means of their screening effect on electrostatic interactions. The effects of additional $CaCl_2$ on the Debye screening length were neglected and the same value of κ (1.040 nm^{-1}) were used in all simulations.

2.10. Model building

The structure of Ca^{2+}-free CaM was adopted from a NMR model (PDBID: 1CFD) [55]. The three-dimensional structure of Ca^{2+}-bound CaM was modeled according to the closed compact X-ray model (PDBID: 1PRW) [56]. The Cα atoms of individual residues were translated into centers of the beads. Bound Ca^{2+} in the EF hand motif were modeled explicitly by beads with a charge of 2+. The fold of the CaM N-terminal and C-terminal domains were stabilized by distance-restraining potential extracted from experimental models. The respective distances of all beads within a 1.2 nm range were restrained by a

harmonic potential with a force constant of 240 $kJ·mol^{-1}·nm^{-2}$. The N-terminal domain (A5-T79) and C-terminal domain (S81-K148) were treated independently, therefore their mutual orientation remained unrestrained. In order to model a fusion construct, the flexible linker (GGGGSS) and the C-terminal domain of AMBN (L223-P447, numbered according to the AMBN sequence) were appended in an extended conformation to both Ca^{2+}-free and Ca^{2+}-bound conformation. The charged N- and C- termini were represented by extra beads with ± 1 charge, respectively. The generated structures were relaxed by energy minimization by means of a steep descent algorithm performed in GROMACS [57].

2.11. Simulation details

Simulations were conducted in GROMACS molecular dynamics package (v. 5.1.1) [57] using stochastic dynamics integrator with a time step of 20 fs and an inverse friction constant of 20 ps at 300 K. All nonbonded interactions were truncated at 1.9 nm by a potential-shift modifier. Debye-Hückel potential was implemented as tabulated potential. Molecular dynamics were propagated for 100 million steps. Each system was simulated in 5 independent replicas in order to estimate the convergence of the sampling and confidence intervals.

2.12. Analysis of the MDs

Analysis of the hydrodynamic properties (hydrodynamic radius R_h and sedimentation coefficient $s_{20,w}$) were conducted by the HYDROPRO (v.10) program [58]. The calculation was performed in mode 2, using the recommended radius of primary elements 4.80 Å, temperature 20 °C, viscosity 0.01 P, solvent density 1.0 $g·cm^{-3}$ and the partial specific volume 0.72 $g·cm^{-3}$. The molecular weight of AMBN-Ct was estimated as 23.95 kDa and the fusion construct CaM/AMBN-Ct as 41.23 kDa. Due to performance reasons, HYDROPRO calculations were conducted on subsampled trajectories that consisted of 2000 frames each. Analysis of contacts was performed by the *gmx mindist* tool from GROMACS suite. Contacts were considered productive if the distance between beads was closer than 0.8 nm.

3. Results and discussion

3.1. The design and characterization of CaM/AMBN-Ct

The CaM/AMBN-Ct construct was designed to study the macromolecular properties of the fusion protein and the effect of the disordered AMBN C-terminal domain (assigned as AMBN-Ct) on the function of CaM [40]. The order of components in the designed fusion was CaM on the N-terminus, AMBN-Ct on the C-terminus and a GGGGSS flexible linker joining the CaM and AMBN-Ct domains (Fig. 1A). The flexible linker was chosen to allow CaM and AMBN-Ct maximum flexibility. From the amino acid sequence, the molecular weight of the CaM/AMBN-Ct is expected to be 41.2 kDa. While CaM is a negatively charged (−23) α-helical protein with Mw of 16.8 M_W kDa (when saturated by Ca^{2+} the CaM charge decrease to −15), the AMBN-Ct has Mw of 25.4 kDa with an overall charge of −19 [59]. The purified proteins were obtained by size-exclusion chromatography (SEC) in the last purification step (Fig. 1B). The overestimated Mw of AMBN-Ct and CaM calculated from SEC chromatogram using globular markers is caused by the effect of the elongated shape of CaM [60] and the IDP character of AMBN-Ct [38,39] (Fig. 1B). The SEC of a mixture of isolated AMBN-Ct and CaM domains showed two independent proteins and excluded the possible formation of a complex between separated AMBN-Ct and CaM. The CaM/AMBN-Ct showed higher apparent Mw in comparison with the isolated AMBN-Ct domain, clearly indicating the conservation of the IDP character of the AMBN-Ct subunit. To reveal the changes in CaM induced by fusion with AMBN-Ct, we characterized CaM/AMBN-
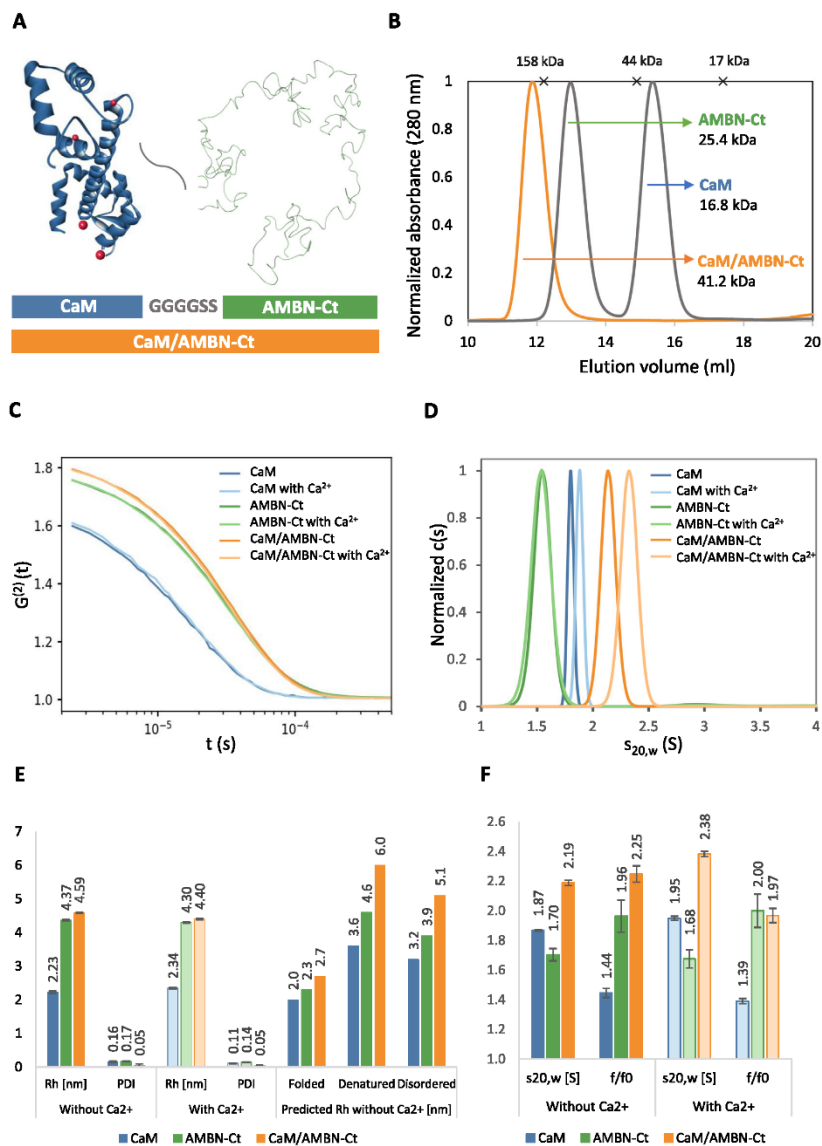
Fig. 1. (A) Schematic view of the CaM/AMBN-Ct protein chimera. CaM (blue) was fused with AMBN-Ct (green) by flexible linker (GGGGSS). The models of CaM and AMBN-Ct are represented as a fusion CaM/AMBN-Ct with Ca^{2+} (pink balls representation), models in ribbon representation. (B) Chromatogram profile of CaM/AMBN-Ct and CaM together with AMBN-Ct eluted from Superdex 200 column. SEC excluded complex formation between individual domains of the fusion protein. (C) DLS averaged $G^{(2)}(t)$ autocorrelation functions for CaM, AMBN-Ct and CaM/AMBN-Ct in the presence and absence of Ca^{2+}. (D) Sedimentation velocity analyses of AMBN-Ct, CaM and CaM/AMBN-Ct in the presence or absence of Ca^{2+} ions shown as continuous size distribution c(s) of the sedimenting species. (E) Comparison of DLS estimated hydrodynamic radii (R_h) and polydispersity indexes (PDI) of CaM, AMBN-Ct and CaM/AMBN-Ct together with the predicted R_h values of Ca^{2+}-free constructs. Light color shades represent proteins saturated with Ca^{2+}. The error bars represent the standard deviation. (F) Summary of sedimentation coefficients ($s_{20,w}$) and frictional ratios (f/f₀) derived from sedimentation velocity profiles of CaM, AMBN-Ct and CaM/AMBN-Ct. Light color shades represent Ca^{2+}-bound proteins. Results are mean values of four experiments, error bars represent standard deviation.

Ct and its isolated protein / domain in detail. We described the molecular size, shape, secondary/tertiary structure content and thermostability of CaM, AMBN-Ct and CaM/AMBN-Ct separately. Because CaM is an important calcium-signaling target in cells, we used the calcium-binding function to investigate how the ability of CaM calcium binding could change the CaM folding caused by AMBN-Ct influence in the fusion [61]. Therefore, all methods and measurements were also performed in the presence of Ca^{2+}.

3.2. The CaM/AMBN-Ct suggested monomeric extended character

Dynamic light scattering (DLS) experiments provided data to estimate the hydrodynamic radius (Rh) and potential polydispersity of the studied proteins (Fig. 1C, E). The polydispersity index (PDI) indicated monodisperse solutions of all proteins with the highest value of 0.17, which is usual for monomeric protein samples. This justifies the application of cumulant analysis, which was performed for the interpretation of measured autocorrelation functions (Fig. 1C). Importantly, the estimated Rh of CaM (2.23 nm) is close to the predicted [43] value for a folded globular protein of the same length (2.0 nm) (Fig. 1E). The Rh of AMBN-Ct (4.37 nm) lies between values for IDP of the same length (3.9 nm) and the denatured protein chain (4.6 nm), suggesting the highly IDP character of the AMBN-Ct. The CaM/AMBN-Ct manifests Rh (4.59 nm) between a folded (2.7 nm) and IDP (5.1 nm) state, closer to the latter. Such behavior signalizes conserved IDP properties of the unstructured part with a compact or folded region. DLS measurements of Ca^{2+} saturated constructs confirmed the preservation of the monodispersed population at a monomeric state (Fig. 1C). However, no extensive changes in particle diameter were observed upon incubation with 10 mM $CaCl_2$. To gain a more accurate estimate of Ca^{2+}-induced changes of molecular shape, we performed sedimentation analysis in an analytical ultracentrifuge (AUC).

AUC measurements confirmed monodisperse populations of all studied proteins with corrected sedimentation coefficients ($s_{20,w}$) corresponding to monomeric states (Fig. 1D, F). The $s_{20,w}$ value reflects the molecular weight and shape of the molecule. The molecular shape is estimated from the ratio of frictional coefficients of the observed particle (f) that is fitted in data analysis, and of a sphere of the same weight (f_0). The CaM sedimented at 1.87 S with an f/f_0 ratio of 1.4 which corresponds to the particle dimensions of $2–3 \times 6–8$ nm for a prolate ellipsoid or cylindrical particle, thus indicating a globular, well-folded protein with a moderately elongated shape, perfectly in line with the dimensions of the CaM published crystal structure ($2–4 \times 6–7$ nm) [20]. In contrast, AMBN-Ct sedimented at 1.7 S with an f/f_0 ratio of 2.0, suggesting a highly asymmetric molecule, a result typical for IDPs [40]. The CaM/AMBN-Ct fusion protein exhibited the $s_{20,w}$ value of 2.19 S and f/f_0 ratio of 2.3, as expected for a combination of an elongated CaM and IDP AMBN-Ct molecules. Upon the addition of Ca^{2+} ions, no significant change of AMBN-Ct $s_{20,w}$ and f/f_0 ratio values was observed. This is consistent with our model for Ca^{2+} binding to AMBN, where AMBN-Ct provides interactions with Ca^{2+} ions only in supramolecular assemblies of AMBN, whose formation is driven by a specific sequence motif present in the N-terminal domain of AMBN [37–39,62]. However, in the presence of Ca^{2+} a significant increase of the $s_{20,w}$ and simultaneous decrease of the f/f_0 values was observed for both CaM and CaM/AMBN-Ct proteins in the presence of Ca^{2+}, suggesting their compaction (Fig. 1D). Interestingly, the increase of the $s_{20,w}$ value observed in the case of CaM/AMBN-Ct fusion protein is considerably larger than for the isolated CaM subunit, reaching the value of 2.38 S with a concomitant decrease of the f/f_0 ratio to 2.0. This means that while both CaM and CaM/AMBN-Ct undergo Ca^{2+}-induced conformational changes and become more compact, these changes also very probably affect the AMBN-Ct part of the CaM/AMBN-Ct fusion protein. We propose that Ca^{2+}-binding to CaM/AMBN-Ct causes conformational changes which enable closer contact between CaM and AMBN-Ct parts, most probably through interactions of exposed hydrophobic CaM residues with its AMBN-Ct counterparts or decreased electrostatic repulsion.

3.3. Secondary/tertiary structural analysis and thermal stability of CaM/AMBN-Ct

The CD spectrum in the far-UV spectral region (190 nm - 260 nm) of AMBN-Ct at 5 °C revealed a negative spectral band at ~199 nm (Fig. 2A). With increased temperature, a decrease in this signal intensity was observed, accompanied by its spectral shift (to 204 nm). Simultaneously,

the broad negative spectral band at ~220 nm gained intensity with an isosbestic point at ~209 nm (Fig. S3). These spectral characteristics are caused by heat-induced folding changes typical for IDPs and can be interpreted as i) the formation of α-helical structures, ii) as an unfolding of extended PPII structures, iii) as a combination of both structural changes [40,63]. The structural changes caused the protein to become more compact [64]. Thus, CD spectroscopy confirmed the IDP character of AMBN-Ct [40,63]. Measurements revealed no difference in curve shape or spectral intensity after incubation of AMBN-Ct with 10 mM $CaCl_2$ (Figs. 2A, S3). Therefore, we conclude that the presence of Ca^{2+} does not induce structural changes of AMBN-Ct detectable by CD.

The CD spectra of CaM in far-UV have typical properties of α-helical proteins with two negative peaks at 208 and 222 nm with comparable intensities (Fig. 2A) [65]. The Ca^{2+} interaction increased the intensity of both negative spectral bands as a result of the reorientation/distortion of the existing α-helices (Fig. 2A, Table S4) [66]. The near-UV CD spectrum obtained from the isolated CaM subunit revealed negative spectral bands at 255, 262 and 268 nm which can be attributed to phenylalanine residues and a negative signal with a lower intensity above 275 nm, corresponding to two tyrosine residues (Fig. 2A). The increase in spectral intensity observed for the Ca^{2+}/CaM complex reflects the conformational changes induced by the Ca^{2+} binding, which affect the environment of both residues with aromatic side chains [65]. In case of CaM thermal stability studies, the decreasing intensity at 222 nm was characteristic for CaM unfolding (Fig. S5). The melting temperature (T_m) of CaM without Ca^{2+} was determined to be 52.0 °C (Fig. 2B), which is consistent with published data (T_m of 55 °C) [65]. The T_m of CaM/Ca^{2+} saturated complex was not achieved due to the extreme structural stability of the complex. The only a two-state model was used to calculate the thermal unfolding, assuming that this rough simplification would be sufficient to distinguish the thermal stability of CaM and CaM/AMBN-Ct.

The far-UV spectrum of CaM/AMBN-Ct was characterized by negative peaks at 208 and 222 nm (Fig. 2A). The higher intensity spectral band at 208 nm indicated a portion of the IDP character, and the lower overall spectral intensity compared to CaM revealed presence of β-structures. Numerical analysis discovered a significant fraction of α-helical structures (~39%), which was complemented with a portion of β-structures (β-sheets ~6% and β-turns ~23%) and IDP character (~32%) (Table S4). The CaM/AMBN-Ct complex with Ca^{2+} revealed a slight increase in intensity for negative peaks at 208 and 222 nm, similar to the spectral changes observed for CaM (Fig. 2A). In the near-UV spectral region, the CD spectrum revealed negative maxima at 262 nm, 268 nm and above 275 nm. We hypothesize that CaM, as part of the CaM/AMBN-Ct fusion protein, preserves its original tertiary structure and determines the CaM/AMBN-Ct near-UV CD spectra. However, the formation of the tertiary structure of the AMBN-Ct subunit as a part of the CaM/AMBN-Ct fusion protein cannot be excluded, although no tertiary structure was observed for AMBN-Ct alone (data not shown). Furthermore, an increase in the spectral intensity and thermostability of CaM/AMBN-Ct and CaM in Ca^{2+} environment was observed (Figs. 2A, S6).

The percentage of overall secondary structure of all studied proteins is represented as the number of amino acids forming a specific secondary structure in the absence and presence of Ca^{2+} (Table S4). The number of amino acids that have the α-helical structural motif of CaM/AMBN-Ct was estimated to be 150 in the absence of Ca^{2+} and 158 in the presence of Ca^{2+}, which means higher content of amino acids in the α-helical conformation for CaM/AMBN-Ct compared to CaM. To get a closer insight into structural changes resulting from the fusion of CaM and AMBN-Ct, we calculated the model spectra of CaM/AMBN-Ct with and without Ca^{2+}. Model spectra of CaM/AMBN-Ct in the presence and absence of Ca^{2+} (Fig. 2C) were obtained as a simple sum of CD spectra of CaM and AMBN-Ct at the same concentrations, finally expressed as molar ellipticities Θ (deg·cm^2·$dmol^{-1}$) per residue. The model spectra of CaM/AMBN-Ct with and without Ca^{2+} were characterized by negative minima at 203 nm and 222 nm. The above-mentioned model
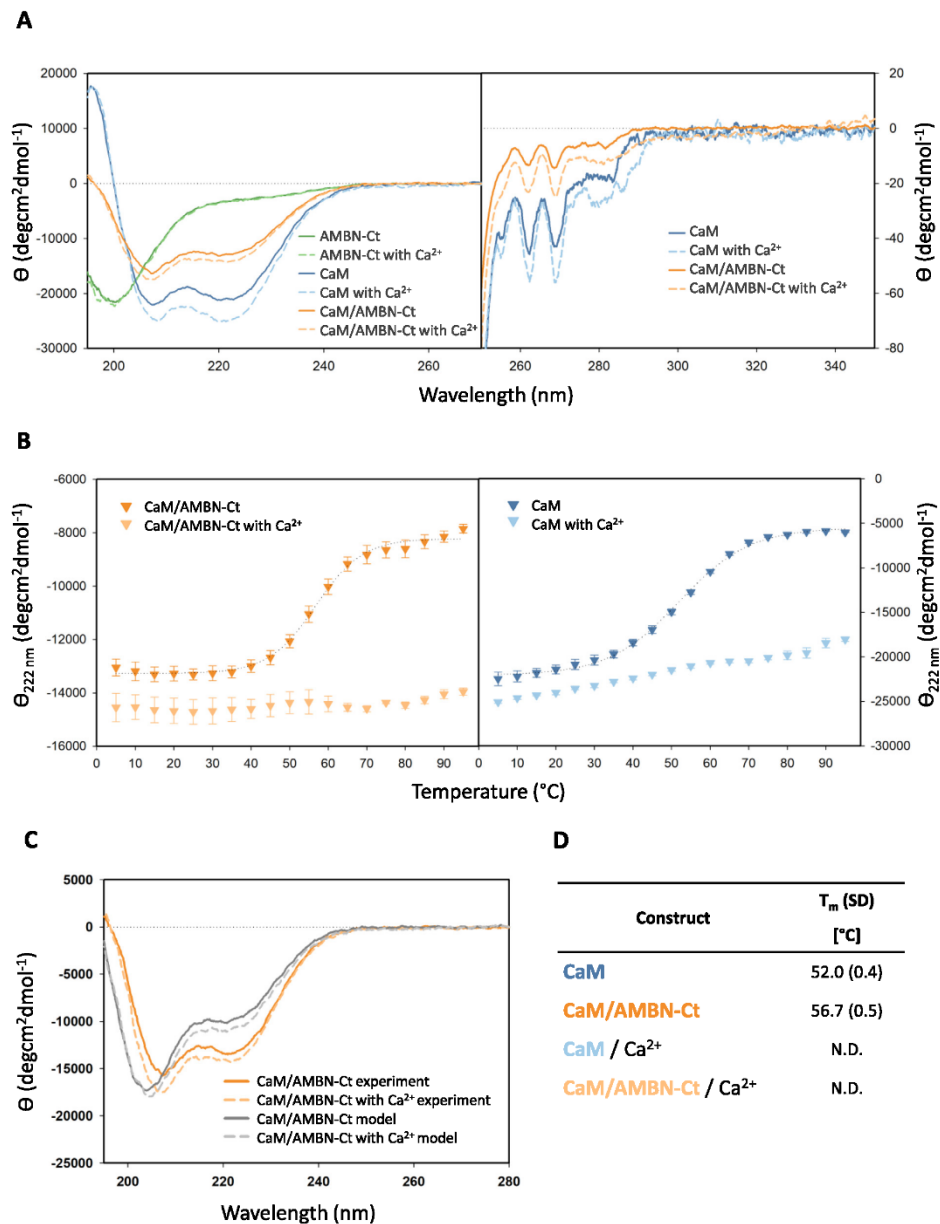
A

B

C

D

Construct	T_m (SD) [°C]
CaM	52.0 (0.4)
CaM/AMBN-Ct	56.7 (0.5)
CaM / Ca^{2+}	N.D.
CaM/AMBN-Ct / Ca^{2+}	N.D.

Fig. 2. (A) CD spectra of AMBN-Ct, CaM and CaM/AMBN-Ct without and in the presence of Ca^{2+} in the far-UV (left) and near-UV (right) spectral region. (B) Temperature stability of CaM/AMBN-Ct and CaM without and with Ca^{2+} determined at 222 nm. Results are mean values of three experiments, error bars represent standard deviation. (C) Comparison of the experimental far-UV spectra of CaM/AMBN-Ct with model spectra calculated for the independent behavior of fusion domains. (D) Summarization of T_m values calculated for Ca^{2+}-free and Ca^{2+}-bound CaM and CaM/AMBN-Ct. N.D. stands for not determined. Results are mean values of three experiments with standard deviation.

spectra revealed a shift of the low wavelength negative maximum (from 208 for experimental one to 203 nm) together with the different intensity ratio between negative maxima of the model and experimental CD spectra indicates higher α-helical portion in CaM/AMBN-Ct than expected. The increase of α-helical content is compensated by the decrease in the β-sheet structure content (Fig. 2C, Table S4). Upon the spectral changes observed for CaM/AMBN-Ct and CaM we can assume that the CaM structure is preserved in the fusion protein. The AMBN-Ct structure probably form segments with higher helicity content, suggesting a communication between the fusion subunits.

Thermal unfolding of CaM/AMBN-Ct indicated changes of the CD signal at 222 nm (Figs. 2B, S5). Using a fit for two-state unfolding process, the T_m for CaM/AMBN-Ct was calculated as 56.7 °C. The T_m should be taken only as a rough estimate of the overall thermal properties of studied proteins, because the folding of CaM goes through two transition states [66]. Moreover, the folding process of the CaM/AMBN-Ct is expected to be even more complex. Despite this simplification, a comparison of the thermal unfolding of CaM and CaM/AMBN-Ct revealed a different overall shape the unfolding curves. The decrease in the slope of the CaM/AMBN-Ct unfolding curve observed at lower temperatures could indicate stabilization of early developing CaM unfolding intermediates as an effect of macromolecular crowding [67]. Significant structural stabilization for CaM/AMBN-Ct with Ca^{2+} was observed. However, due to the high temperature stability of CaM/AMBN-Ct (similar to CaM) caused by Ca^{2+} binding, the T_m of the fusion protein was not determined. We can speculate that IDP domain of AMBN-Ct can potentially increase the stability of the fusion protein by a similar mechanism as described in [67], because of more stable trend of the CaM/AMBN-Ct curve in the complex with Ca^{2+} (Fig. 2B).

3.4. The functional modulations of CaM in CaM/AMBN-Ct induced by IDP domain AMBN-Ct

CaM is a known regulator of many receptors in the cell, and one of the most important of these is TRP channel [68–73]. Numerous peptides mimicking CaM-binding epitopes at different TRPs subfamilies have been identified [41,42,74,75]. To study the nature of the AMBN-Ct effect on CaM function, we performed a binding assay in which CaM interacted with the TRPM4np peptide derived from intracellular N-terminus of TRPM4 [42]. The identification of TRPM4np binding affinity, in complex with studied proteins, was carried out using steady-state fluorescence-anisotropy assay. The carboxyfluorescein-labelled TRPM4np was titrated with CaM/AMBN-Ct, CaM (positive control) and AMBN-Ct (negative control). The fluorescence anisotropy value of the peptide was recorded at each titration point. To asses Ca^{2+}-dependency of CaM/TRP-derived peptide interaction [75,76], we performed all measurements in a buffer supplemented with 10 mM $CaCl_2$ and without $CaCl_2$ (10 mM EDTA added). The fluorescence lifetime of the carboxyfluorescein-labelled TRPM4np (~4 ns) was found to be nearly independent of the peptide binding. The fractions of bound (F_B) TRPM4np were calculated for each measurement and plotted against the TRPM4np concentration to determine the equilibrium dissociation constants (K_D) of all studied complexes.

The complex formation of CaM with TRPM4np was shown to be Ca^{2+}-dependent (Figs. 3A, S7). The K_D values were calculated to be 0.25 µM for CaM and 1.1 µM for CaM/AMBN-Ct fusion construct. No complex formation was observed for AMBN-Ct as a negative control. Our results revealed an approximately four-fold decrease of CaM binding to TRPM4np in comparison to CaM/AMBN-Ct. The possible engagement of the isolated AMBN-Ct subunit in complex between TRPM4np and CaM was excluded by SEC in the presence of 2 mM $CaCl_2$ revealing two independent peaks (Fig. 3B). The first peak represents the intact AMBN-Ct subunit, and the latter stands for CaM in a complex with TRPM4np. None of CaM, CaM/AMBN-Ct and AMBN-Ct interacted with TRPM4np in the absence of Ca^{2+} (Fig. S7). The fluorescence anisotropy experiments proved the modulation of CaM by AMBN-Ct in CaM/

AMBN-Ct fusion as indicated by CD spectroscopy and AUC, and revealed communication between CaM and AMBN-Ct domains. The AMBN-Ct can interfere with the CaM/TRPM4np complex formation through (1) direct occlusion of the binding site for TRPM4np in the CaM subunit or (2) allosteric modulation of the CaM binding cavity for TRPM4np, resulting in changes of its structural-functional properties. To explain a potential mechanism of how AMBN-Ct modulates a CaM peptide-binding site in CaM/AMBN-Ct, we built a fusion molecular model and studied a mutual domains influence by MDs.

3.5. Investigation of CaM/AMBN-Ct Ca^{2+} binding properties

To verify that CaM is the only Ca^{2+} binding domain within the fusion protein, we examined the Ca^{2+} binding affinity of CaM/AMBN-Ct using MST (Fig. 3D). K_D was determined as 7.4 (SD 0.8) µM. The CaM/AMBN-Ct complex with Ca^{2+} had a K_D in the same range as for discrete CaM (3 µM) previously measured by MST [77]. These results suggest that Ca^{2+} in the CaM/AMBN-Ct is still bound to CaM only. Therefore, we decided to directly verify the binding affinity of Ca^{2+} to the AMBN-Ct domain also using MST. We confirmed no Ca^{2+} binding affinity of intact AMBN-Ct and excluded the potential Ca^{2+} binding in the isolated domain (Fig. S8). The MST data showed that the AMBN-Ct domain does not impair CaM sensitivity to Ca^{2+}. MST data for CaM/AMBN-Ct and AMBN-Ct domain cannot be directly compared because of different way of proteins labeling (see 2.8 Microscale Thermophoresis).

3.6. CaM/AMBN-Ct in presence of Ca^{2+} indicated communication between the domains

MDs of AMBN-Ct, CaM/AMBN-Ct and CaM/AMBN-Ct saturated with Ca^{2+} confirmed an expanded character of the AMBN-Ct domain in all constructs (Fig. 4A, B). The MDs predicted values of $s_{20,w}$ and Rh match reasonably well with the experimentally determined values $s_{20,w}$ and Rh for AMBN-Ct and CaM/AMBN-Ct (Fig. 4C) and justify general application of the model. However, experimentally observed compaction of CaM/AMBN-Ct induced by Ca^{2+}-binding was not captured by the utilized coarse grain model as significantly as by the experimental methods. The changes in the apparent size of AMBN-Ct and CaM/AMBN-Ct chains detected by AUC and DLS did not imply any substantial changes in the interpretation of the IDP character of the AMBN-Ct domain. Therefore, the predictions of the model should be considered rather qualitatively. Some deficiencies of the coarse grain model can be likely attributed to its low resolution and its simplicity in the treatment of local and long-range interactions, as well as Ca^{2+} in the buffer.

The effects of Ca^{2+}-binding were modeled implicitly by different conformations of the CaM domain, which are switched allosterically by interactions with Ca^{2+}. Fusion constructs with both conformation of the CaM domain provided very similar average estimates of hydrodynamic parameters (Fig. 4C), as well as their distribution (Fig. 4D). Both $s_{20,w}$ and Rh manifested broad distributions that reflect the flexible and heterogeneous character of all constructs (Fig. 4C). The width of these distributions is similar to the distributions observed by AUC experiments (Fig. 1D), indicating that simulations correctly captured the degree of IDP character. The size analysis of individual domains revealed that size and shape of the AMBN-Ct domains in fusion was only slightly affected in comparison with AMBN-Ct domain simulated as individual molecule as demonstrated by distribution of principal radii of gyration (Fig. S9) and distribution of end-to-end distances (Fig. S10). Both analyses indicate slightly more expanded character of AMBN-Ct chain in fusion if compared to behavior of the separated domain. We speculate that this effect can be caused by excluded volume of the fusion partner (CaM domain). No significant differences were found between fusion constructs with Ca^{2+}-bound and -free CaM domain. On the other hand, internal degrees of freedom of the AMBN-Ct chain did not manifest any significant deviation in a response on the fusion partner and its variant (Figs. S11–S13). The analogous analyses were also performed
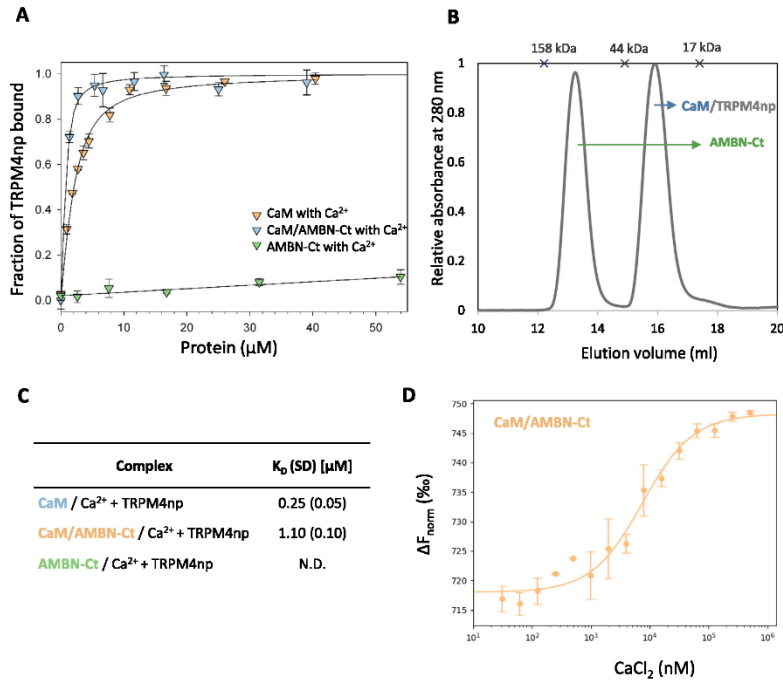
Fig. 3. (A) The fraction of the TRPM4np bound (F_B) as a function of CaM, CaM/AMBN-Ct and AMBN-Ct concentrations obtained from steady-state fluorescence anisotropy titrations. The F_B values were obtained from Eq. 2 (Methods) and plotted against ligand concentrations. The best fit by the binding isotherm according to Eq. 3 is shown as a solid line. Error bars represent the standard deviation of the mean with five independent measurements. (B) Chromatographic profile obtained after SEC was performed using a mixture of isolated CaM, AMBN-Ct domain and TRPM4np at 1:1:1 ratio on a Superdex 200 Increase 10/300 GL column in a buffer with 10 mM CaCl$_2$ (see Methods). SEC excluded complex formation between CaM/TRPM4np and the individual AMBN-Ct. (C) Summary of the equilibrium dissociation constants (K_D) of the CaM/TRPM4np, CaM/AMBN-Ct/TRPM4np and AMBN-Ct/TRPM4np complexes determined in the presence of Ca^{2+}. (D) Binding of Ca^{2+} to fluorescently labelled CaM/AMBN-Ct measured using MST. The normalized fluorescence change (ΔF_{norm}) between the unbound and bound states of CaM/AMBN-Ct was plotted against CaCl$_2$ concentrations. Error bars represent the standard deviation of the mean from two independent measurements. The binding isotherm is shown as a solid line.

for Ca^{2+}-bound and free CaM domain. Both variants sample distinct distribution of principal radii of gyration as well as total radius of gyration, but no changes were detected upon fusion with AMBN-Ct domain (Figs. S14, S15). These observations indicate that no artifacts were introduced in the model by fusion of an IDP and a folded domain, and the model provides consistent description of both parts.

Although simulations predicted no significant difference in hydrodynamic parameters in the presence of Ca^{2+}, structural details of the simulated ensembles of CaM/AMBN-Ct and CaM/AMBN-Ct with Ca^{2+} differed in some characteristics. The AMBN-Ct domain, in the presence of Ca^{2+}-bound CaM, showed a higher affinity to the latter domain, mostly to the C-terminal lobe. This is illustrated by the contact analysis (Fig. 4E). Indeed, this difference was caused by exposed hydrophobic residues in the CaM domain upon Ca^{2+}-binding, which were enabled to transiently interact with stretches of hydrophobic residues in the sequence of AMBN-Ct. These transient inter-domain interactions might interfere with the proper ligand-binding function of CaM and reduce its binding affinity due to the steric occlusion of the binding pocket.

On the other hand, other mechanisms of the allosteric modulation of the CaM domain are possible. For example, the adjacent IDP domain might modify the population of binding-competent states of the CaM domain or change the conformational dynamics of the binding pocket. These mechanisms could not have been addressed by the utilized coarse grain model. To explore these hypotheses, a more detailed, full atomistic model is necessary. However, such simulations of the same conclusive

sampling extent as the coarse grain model would be prohibitively computationally demanding and beyond the current state of the art in the field.

Similarly, the effects on thermal stability could not have been investigated directly by the current coarse grain model. Nevertheless, we speculate that the predicted transient interactions might contribute to the higher thermal stability of CaM/AMBN-Ct fusion by various mechanisms such as stabilization of binding the interface, partial induction of the structure in the IDP AMBN/Ct domain, protection against aggregation or an increase of the solubility. The actual mechanism of stabilization could arise from a combination of different effects and their importance remains to be elucidated.

4. Conclusions

We designed, prepared, and characterized a unique artificial fusion molecule to study how the IDP domain can affect the size, stability, and function of other protein region domain - represented here by a well-folded CaM. It is well known that the highly dynamic flexibility of IDPs enable them to occupy an ensemble of multiple conformations in solution. The highly dynamic character makes IDPs attractive candidates for effective direct or allosteric modulation of the attached domain. In the present work, we report the characterization of the CaM/AMBN-Ct fusion protein formed by IDP AMBN-Ct fused to highly α-helical CaM.
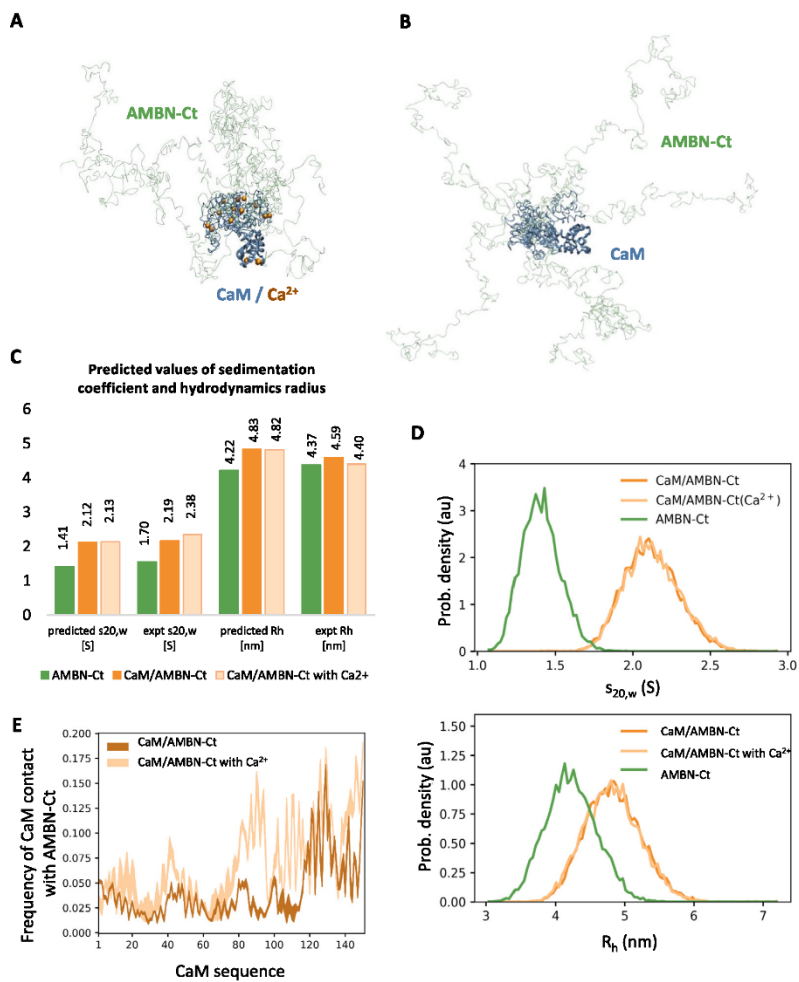
Fig. 4. The representative structures of (A) CaM/AMBN-Ct with Ca^{2+} and (B) CaM/AMBN-Ct conformations sampled in MDs. Both panels show 5 molecules superimposed on the N-terminal lobe of CaM. (C) The predicted values of sedimentation coefficient and hydrodynamics radius of AMBN-Ct, CaM/AMBN-Ct and CaM/AMBN-Ct with Ca^{2+}. (D) Distribution of sedimentation coefficient ($s_{20,w}$) and hydrodynamic radius (Rh) predicted by simulations. (E) Frequency of contacts between CaM and the adjacent AMBN-Ct domain as observed in simulation. Width of lines express variance across 5 simulations.

The biophysical methods provided results confirming that there could be an increased stability of CaM in the CaM/AMBN-Ct. This stability significantly increases in the presence of Ca^{2+} as we can conclude from the trend of the temperature dependence for CaM/AMBN-Ct/Ca^{2+} complex in Fig. 2B. We verified that CaM in CaM/AMBN-Ct is able to preserve its function even with a 4-fold drop of the TRPM4np binding affinity in the fusion compared to the CaM alone.

The in silico approach demonstrated by coarse-grain MDs provided results suggesting a different pattern of interdomain interactions in the CaM/AMBN-Ct construct between CaM and AMBN-Ct depending on the presence of Ca^{2+}. AMBN-Ct can modulate CaM binding properties via two different mechanisms of their synergy: i) Transient hydrophobic inter-domain interactions of AMBN-Ct might interfere with the proper ligand-binding function of CaM and they can reduce its binding affinity due to the steric occlusion of the binding pocket. ii) The adjacent

IDP domain might modify the population of binding-competent states of the CaM domain or it can alter the conformational dynamics (by allosteric modulations) of the CaM binding pocket.

Author contributions

KB and JV designed the research. MZ, J Vym, LB, PH, OV, VV, KP performed the experiments. MZ, J Vym, LB, PH, OV, PL, JV and KB analyzed the data. MZ, JV and KB wrote the manuscript.

Funding

VaVpICZ.1.05/4.1.00/16.0340] and the Czech Science Foundation [GACR 19–04099S].

Declaration of competing interest

Acknowledgments

Appendix A. Supplementary data

Supplementary data to this article can be found online at https://doi.org/10.1016/j.ijbiomac.2020.11.216.

References

[1] G. Apic, W. Huber, S.A. Teichmann, Multi-domain protein families and domain pairs: comparison with known structures and a random model of domain recombination, J. Struct. Funct. Genom. 4 (2–3) (2003) 67–78.

[2] M. Long, A new function evolved from gene fusion, Genome Res. 10 (11) (2000) 1655–1657.

[3] P. Kirubakaran, et al., Artificial proteins as allosteric modulators of PDZ3 and SH3 in two-domain constructs: a computational characterization of novel chimeric proteins, Proteins 84 (10) (2016) 1358–1374.

[4] A.S. Raman, K.I. White, R. Ranganathan, Origins of Allostery and Evolvability in proteins: a case study, Cell 166 (2) (2016) 468–480.

[5] R.N. McLaughlin Jr., et al., The spatial architecture of protein function and adaptation, Nature 491 (7422) (2012) 138–142.

[6] G.E. Meister, N.S. Joshi, An engineered calmodulin-based allosteric switch for peptide biosensing, Chembiochem 14 (12) (2013) 1460–1467.

[7] A. Tanimura, et al., Fluorescent biosensor for quantitative real-time measurements of inositol 1,4,5-trisphosphate in single living cells, J. Biol. Chem. 279 (37) (2004) 38095–38098.

[8] A. Miyawaki, et al., Fluorescent indicators for Ca2+ based on green fluorescent proteins and calmodulin, Nature 388 (6645) (1997) 882–887.

[9] Z. Guo, et al., Engineering PQQ-glucose dehydrogenase into an allosteric electrochemical Ca2+ sensor, Chem. Commun. 52 (3) (2016) 485–488.

[10] N. Heim, O. Griesbeck, Genetically encoded indicators of cellular calcium dynamics based on troponin C and green fluorescent protein, J. Biol. Chem. 279 (14) (2004) 14280–14286.

[11] M.J. Berridge, P. Lipp, M.D. Bootman, The versatility and universality of calcium signalling, Nat. Rev. Mol. Cell Biol. 1 (1) (2000) 11–21.

[12] K. Deisseroth, E.K. Heist, R.W. Tsien, Translocation of calmodulin to the nucleus supports CREB phosphorylation in hippocampal neurons, Nature 392 (6672) (1998) 198–202.

[13] Y. Saimi, C. Kung, Calmodulin as an ion channel subunit, Annu. Rev. Physiol. 64 (2002) 289–311.

[14] S. MacNeil, T. Lakey, S. Tomlinson, Calmodulin regulation of adenylate cyclase activity, Cell Calcium 6 (3) (1985) 213–216.

[15] M.T. Swulius, M.N. Waxham, Ca(2+)/calmodulin-dependent protein kinases, Cell. Mol. Life Sci. 65 (17) (2008) 2637–2657.

[16] N.C. Strynadka, M.N. James, Crystal structures of the helix-loop-helix calcium-binding proteins, Annu. Rev. Biochem. 58 (1989) 951–998.

[17] R.H. Kretsinger, C.E. Nockolds, Carp muscle calcium-binding protein. II. Structure determination and general description, J. Biol. Chem. 248 (9) (1973) 3313–3326.

[18] S. Linse, S. Forsen, Determinants that govern high-affinity calcium-binding, Calcium Regul. Cell. Func. 30 (1995) 89–151.

[19] Y.S. Babu, et al., Three-dimensional structure of calmodulin, Nature 315 (6014) (1985) 37–40.

[20] Y.S. Babu, C.E. Bugg, W.J. Cook, Structure of calmodulin refined at 2.2 a resolution, J. Mol. Biol. 204 (1) (1988) 191–204.

[21] G. Barbato, et al., Backbone dynamics of calmodulin studied by 15N relaxation using inverse detected two-dimensional NMR spectroscopy: the central helix is flexible, Biochemistry 31 (23) (1992) 5269–5278.

[22] M.R. Nelson, W.J. Chazin, An interaction-based analysis of calcium-induced conformational changes in Ca2+ sensor proteins, Protein Sci. 7 (2) (1998) 270–282.

[23] M. Zhang, et al., Structural basis for Calmodulin as a dynamic calcium sensor, Structure 20 (5) (2012) 911–923.

[24] T.W. Chen, et al., Ultrasensitive fluorescent proteins for imaging neuronal activity, Nature 499 (7458) (2013) 295–300.

[25] J. Nakai, M. Ohkura, K. Imoto, A high signal-to-noise Ca2+ probe composed of a single green fluorescent protein, Nat. Biotechnol. 19 (2) (2001) 137–141.

[26] E.A. Grzybowska, Calcium-binding proteins with disordered structure and their role in secretion, storage, and cellular signaling, Biomolecules 8 (2) (2018).

[27] A. Bah, et al., Folding of an intrinsically disordered protein by phosphorylation as a regulatory switch, Nature 519 (7541) (2015) 106–109.

[28] V.N. Uversky, et al., Rigidity of human alpha-fetoprotein tertiary structure is under ligand control, Biochemistry 36 (44) (1997) 13638–13645.

[29] P. Tompa, M. Fuxreiter, Fuzzy complexes: polymorphism and structural disorder in protein-protein interactions, Trends Biochem. Sci. 33 (1) (2008) 2–8.

[30] M.M. Pentony, D.T. Jones, Modularity of intrinsic disorder in the human proteome, Proteins Struct. Funct. Bioinforma. 78 (1) (2010) 212–221.

[32] H.J. Park, et al., Comparing skeletal and cardiac calsequestrin structures and their calcium binding - a proposed mechanism for coupled calcium binding and protein polymerization, J. Biol. Chem. 279 (17) (2004) 18026–18033.

[33] V. Shivarov, M. Ivanova, R.V. Tiu, Mutated calreticulin retains structurally disordered C terminus that cannot bind Ca2+: some mechanistic and therapeutic implications, Blood Cancer J. 4 (2014).

[34] A.L. Boskey, E. Villarreal-Ramirez, Intrinsically disordered proteins and biomineralization, Matrix Biol. 52-54 (2016) 43–59.

[35] M.L. Paine, et al., Functional domains for amelogenin revealed by compound genetic defects, J. Bone Miner. Res. 18 (3) (2003) 466–472.

[36] X. Lu, et al., The ameloblastin extracellular matrix molecule enhances bone fracture resistance and promotes rapid bone fracture healing, Matrix Biol. 52-54 (2016) 113–126.

[37] O. Stakkestad, et al., Phosphorylation modulates Ameloblastin self-assembly and Ca (2+) binding, Front. Physiol. 8 (2017) 531.

[38] J. Vymetal, et al., Bioinformatic analysis and molecular modelling of human ameloblastin suggest a two-domain intrinsically unstructured calcium-binding protein, Eur. J. Oral Sci. 116 (2) (2008) 124–134.

[39] T. Wald, et al., Intrinsically disordered enamel matrix protein ameloblastin forms ribbon-like supramolecular structures via an N-terminal segment encoded by exon 5, J. Biol. Chem. 288 (31) (2013) 22333–22345.

[40] T. Wald, et al., Biophysical characterization of recombinant human ameloblastin, Eur. J. Oral Sci. 119 Suppl 1 (2011) 261–269.

[41] B. Holakovska, et al., Characterization of calmodulin binding domains in TRPV2 and TRPV5 C-tails, Amino Acids 40 (2) (2011) 741–748.

[42] K. Bousova, et al., Shared CaM- and S100A1-binding epitopes in the distal TRPM4 N terminus, FEBS J. 285 (3) (2018) 599–613.

[43] J.A. Marsh, J.D. Forman-Kay, Sequence determinants of compaction in intrinsically disordered proteins, Biophys. J. 98 (10) (2010) 2383–2390.

[44] D. Hayes, T. Laue, J. Philo, Program Sednterp: sedimentation interpretation program, Alliance Protein Laboratories, Thousand Oaks, CA, 1995.

[45] P. Schuck, Size-distribution analysis of macromolecules by sedimentation velocity ultracentrifugation and lamm equation modeling, Biophys. J. 78 (3) (2000) 1606–1619.

[46] C.A. Brautigam, Calculations and publication-quality illustrations for analytical ultracentrifugation data, Methods Enzymol. 562 (2015) 109–133.

[47] N. Sreerama, R.W. Woody, On the analysis of membrane protein circular dichroism spectra, Protein Sci. 13 (1) (2004) 100–112.

[48] N. Sreerama, R.W. Woody, Computation and analysis of protein circular dichroism spectra, Methods Enzymol. 383 (2004) 318–351.

[49] N. Sreerama, R.W. Woody, Estimation of protein secondary structure from circular dichroism spectra: comparison of CONTIN, SELCON, and CDSSTR methods with an expanded reference set, Anal. Biochem. 287 (2) (2000) 252–260.

[50] J.R. Lakowicz, Principles of Fluorescence Spectroscopy, Springer, New York, 2006.

[51] C.C. Harper, J.M. Berg, S.J. Gould, PEX5 binds the PTS1 independently of Hsp70 and the peroxin PEX12, J. Biol. Chem. 278 (10) (2003) 7897–7901.

[52] K.A. Lacourciere, J.T. Stivers, J.P. Marino, Mechanism of neomycin and rev peptide binding to the rev responsive element of HIV-1 as determined by fluorescence and NMR spectroscopy, Biochemistry 39 (19) (2000) 5630–5641.

[53] C. Cragnell, E. Rieloff, M. Skepo, Utilizing coarse-grained modeling and Monte Carlo simulations to evaluate the conformational Ensemble of Intrinsically Disordered Proteins and Regions, J. Mol. Biol. 430 (16) (2018) 2478–2492.

[54] E. Fagerberg, S. Lenton, M. Skepo, Evaluating models of varying complexity of crowded intrinsically disordered protein solutions against SAXS, J. Chem. Theory Comput. 15 (12) (2019) 6968–6983.

[55] H. Kuboniwa, et al., Solution structure of calcium-free calmodulin, Nat. Struct. Biol. 2 (9) (1995) 768–776.

[56] J.L. Fallon, F.A. Quiocho, A closed compact structure of native Ca(2+)-calmodulin, Structure 11 (10) (2003) 1303–1307.

[57] M.J. Abraham, et al., GROMACS: high performance molecular simulations through multi-level parallelism from laptops to supercomputers, SoftwareX 1 (2015) 19–25.

[58] A. Ortega, D. Amoros, J.G. de la Torre, Prediction of hydrodynamic and other solution properties of rigid proteins from atomic- and residue-level models, Biophys. J. 101 (4) (2011) 892–898.

[59] E. Hellstrand, et al., Forster resonance energy transfer studies of calmodulin produced by native protein ligation reveal inter-domain electrostatic repulsion, FEBS J. 280 (11) (2013) 2675–2687.

[60] B.R. Sorensen, M.A. Shea, Calcium binding decreases the stokes radius of calmodulin and mutants R74A, R90A, and R90G, Biophys. J. 71 (6) (1996) 3407–3420.

[61] A. Crivici, M. Ikura, Molecular and structural basis of target recognition by calmodulin, Annu. Rev. Biophys. Biomol. Struct. 24 (1995) 85–116.

[62] J. Evans, "Liquid-like" biomineralization protein assemblies: a key to the regulation of non-classical nucleation, CrystEngComm 15 (2013) 8388.

[63] V.N. Uversky, Intrinsically disordered proteins and their environment: effects of strong denaturants, temperature, pH, counter ions, membranes, binding partners, Osmolytes, and macromolecular crowding, Protein J. 28 (7–8) (2009) 305–325.

[64] M. Kjaergaard, et al., Temperature-dependent structural changes in intrinsically disordered proteins: formation of alpha-helices or loss of polyproline II? Protein Sci. 19 (8) (2010) 1555–1564.

[65] S.R. Martin, P.M. Bayley, The effects of Ca2+ and Cd2+ on the secondary and tertiary structure of bovine testis calmodulin. A circular-dichroism study, Biochem. J. 238 (2) (1986) 485–490.

[66] I. Protasevich, et al., Conformation and thermal denaturation of apocalmodulin: role of electrostatic mutations, Biochemistry 36 (8) (1997) 2017–2024.

[67] Q. Wang, et al., The effect of macromolecular crowding, ionic strength and calcium binding on calmodulin dynamics, PLoS Comput. Biol. 7 (7) (2011), e1002114, .

[68] Q. Tong, et al., Regulation of the transient receptor potential channel TRPM2 by the Ca2+ sensor calmodulin, J. Biol. Chem. 281 (14) (2006) 9076–9085.

[69] B. Nilius, et al., Regulation of the Ca2+ sensitivity of the nonselective cation channel TRPM4, J. Biol. Chem. 280 (8) (2005) 6423–6433.

[70] R. Strotmann, G. Schultz, T.D. Plant, Ca2+-dependent potentiation of the nonselective cation channel TRPV4 is mediated by a C-terminal calmodulin binding site, J. Biol. Chem. 278 (29) (2003) 26541–26549.

[71] M. Numazaki, et al., Structural determinant of TRPV1 desensitization interacts with calmodulin, Proc. Natl. Acad. Sci. U. S. A. 100 (13) (2003) 8002–8006.

[72] R. Xiao, et al., Calcium plays a central role in the sensitization of TRPV3 channel to repetitive stimulations, J. Biol. Chem. 283 (10) (2008) 6162–6174.

[73] T. de Groot, et al., Molecular mechanisms of calmodulin action on TRPV5 and modulation by parathyroid hormone, Mol. Cell. Biol. 31 (14) (2011) 2845–2853.

[74] M. Zouharova, et al., TRPM6 N-terminal CaM- and S100A1-binding domains, Int. J. Mol. Sci. 20 (18) (2019).

[75] B. Holakovska, et al., Calmodulin and S100A1 protein interact with N terminus of TRPM3 channel, J. Biol. Chem. 287 (20) (2012) 16645–16655.

[76] L. Grycova, et al., Ca(2+) binding protein S100A1 competes with calmodulin and PIP2 for binding site on the C-terminus of the TPRV1 receptor, ACS Chem. Neurosci. 6 (3) (2015) 386–392.

[77] C. Seeger, V.O. Talibov, U.H. Danielson, Biophysical analysis of the dynamics of calmodulin interactions with neurogranin and Ca(2+)/calmodulin-dependent kinase II, J. Mol. Recognit. 30 (8) (2017).

Příloha 3

BOUSOVA, K., **ZOUHAROVA, M.**, HERMAN, P., VYMETAL, J., VETYSKOVA, V., JIRASKOVA, K. & VONDRASEK, J. 2022. TRPM5 Channel Binds Calcium-Binding Proteins Calmodulin and S100A1. *Biochemistry,* 61**,** 413-423.

Biochemistry

Article

TRPM5 Channel Binds Calcium-Binding Proteins Calmodulin and S100A1

Kristyna Bousova,* Monika Zouharova, Petr Herman, Jiri Vymetal, Veronika Vetyskova, Katerina Jiraskova, and Jiri Vondrasek

Cite This: https://doi.org/10.1021/acs.biochem.1c00647

Read Online

ACCESS | Metrics & More | Article Recommendations | Supporting Information

ABSTRACT: Melastatin transient receptor potential (TRPM) channels belong to one of the most significant subgroups of the transient receptor potential (TRP) channel family. Here, we studied the TRPM5 member, the receptor exposed to calcium-mediated activation, resulting in taste transduction. It is known that most TRP channels are highly modulated through interactions with extracellular and intracellular agents. The binding sites for these ligands are usually located at the intracellular N- and C-termini of the TRP channels, and they can demonstrate the character of an intrinsically disordered protein (IDP), which allows such a region to bind various types of molecules. We explored the N-termini of TRPM5 and found the intracellular regions for calcium-binding proteins (CBPs) the calmodulin (CaM) and calcium-binding protein S1 (S100A1) by in vitro binding assays. Furthermore, molecular docking and molecular dynamics simulations (MDs) of the discovered complexes confirmed their known common binding interface patterns and the uniqueness of the basic residues present in the TRPM binding regions for CaM/S100A1.
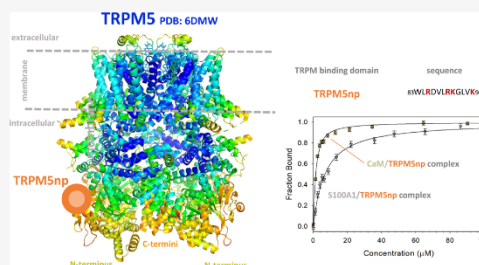
INTRODUCTION

Transient receptor potential (TRP) channels are ubiquitous integrators of calcium (Ca^{2+}) signaling with a common tetrameric architecture.[1] All four TRP channel subunits comprise six membrane-spanning regions and cytoplasmic N- and C-termini mediating interactions with intracellular signaling molecules.[1−8] TRP channels are categorized into seven subfamilies according to amino acid sequence homology. The melastatin transient receptor potential (TRPM) subfamily is composed of a diverse selectivity to cations and specific activation and inhibition mechanisms.[9] The TRPM plays a critical role in reaction to all major classes of physicochemical stimuli, including light, sound, chemical agents, temperature, touch, and so forth. TRPM5 is mostly confined to taste buds, with additional expression in the intestinal tract, pancreas, and brain stem.[10] TRPM5 and its closest homolog TRPM4 transport only monovalent cations in contrast to other members of the TRPM subfamily that are highly permeable for divalent cations.[11] TRPM5 activates in response to an increase in cytoplasmic Ca^{2+}, which acts directly on TRPM5 and desensitizes upon prolonged Ca^{2+} exposure.[12] TRPM5 desensitization was shown to be partially reversed by phosphatidylinositol 4,5-bisphosphat (PIP2).[12,13] The modulation by calcium-binding proteins (CBPs) has been described in many TRP channels, including members of TRPM;[14] still

there are no available studies focused on a possible role of CBPs in the Ca^{2+}-dependent regulation of TRPM5.

Ca^{2+} ions represent the second messenger involved in a myriad of crucial physiological processes from proliferation and apoptosis to bone formation and fertilization.[15,16] A specific family of CBPs with a high potential to bind Ca^{2+} are important multifunctional messengers dependent on Ca^{2+} with expression in a wide range of eukaryotic cells.[17] For example, calmodulin (CaM) as a monomeric protein forms two significant N- and C-terminal regions linked by a flexible linker, with each of the regions containing two Ca^{2+}-binding helix−loop−helix structural domain (EF)-hand motifs).[18] Another CBP protein that acts as a symmetric, antiparallel homodimer is S100 CBPA1 (S100A1).[19] S100A1 is distinguished from other EF-hand proteins in a unique manner in which they bind Ca^{2+} in their N-terminal noncanonical and C-terminal canonical orders of each monomer.[20]

The Ca^{2+} binding motifs or binding sites of Ca^{2+} signal intermediators have been identified at a large number of ion
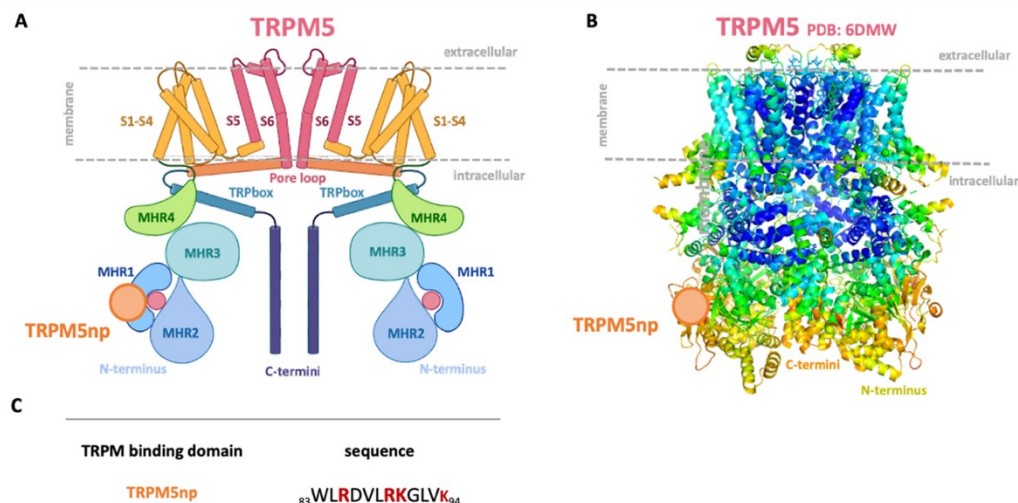
Figure 1. TRPM5 binding region for CaM and S100A1. (A) Common membrane topology of TRPMs, together with the depicted location of the TRPM5np (orange circle) binding epitope. TRPMs commonly consist of six transmembrane helices (pink and orange parts anchored in the membrane) with a transport loop buried in the 5th and 6th helices. The TRPM N-terminal cytoplasmic tail commonly contains melastatin homology regions (MHR, pink, orange, purple, and blue) and a pre-S1 region (green).[1] Cytosolic N- and C-termini-specific regulatory ligand-binding regions. The orange circle frame localizes the TRPM5np binding site. Created with BioRender.com. (B) TRPM5 side view of the whole structure upon Ca^{2+} binding (PDB: 6DMW).[32] The orange circle locates the TRPM5np potential ligand-binding site. (C) Sequence of the TRPM5np (W83-K94) potential binding region with labeled basic residues (red) used to investigate novel CaM and S100A1 binding regions.
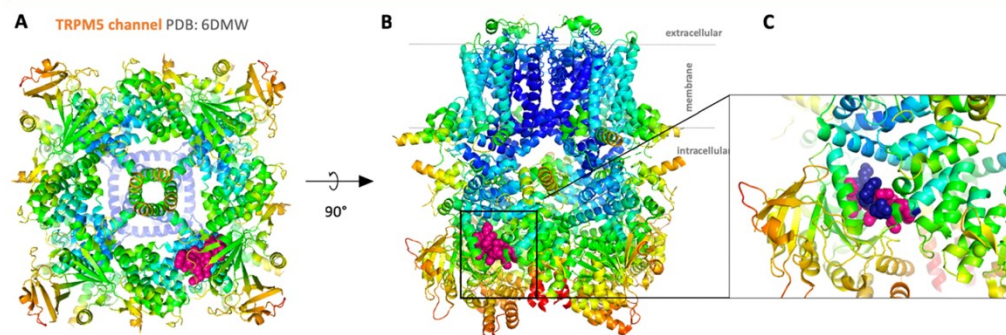
Figure 2. TRPM5np position in the TRPM5 channel. (A) TRPM5 bottom view of the whole structure (PDB: 6DMW)[32] displays the TRPM5np potential binding region (ball representation, magenta). (B) TRPM5 side view displays TRPM5np (ball representation, magenta). (C) Details of TRPM5np showing the amino acids approachable for cytosolic ligand binding; potentially significant basic amino acids for the ligand interaction labeled in ball representation, dark blue; hydrophobic amino acids labeled in magenta.

channels.[21−23] The rapid influx of Ca^{2+} into the cell commonly initiates a negative signaling mechanism inactivating Ca^{2+}-permeable ion channels to prevent the cell from Ca^{2+} overload. In many cases, the Ca^{2+}-induced inactivation is directly performed through binding of intracellular CaM or S100A1 on transmembrane transporters like TRP channels, ryanodine receptors (RyR).[22,24] Dysregulation of Ca^{2+} homeostasis through mutations affects the function of membrane receptors, which can result in a variety of serious diseases, including cancer or heart attacks.[25]

CaM-dependent Ca^{2+}-induced modulation of TRP vaniloid (TRPV) 5 and 6 members provided one of the first deep insights into the modulatory mechanisms of CaM in CaM/TRP channel complexes,[26,27] which we implemented in our TRP investigative approach. In this study, we present an identification method for new CaM/S100A1 binding epitopes at the TRPM5 N-terminus. We specifically characterized the TRPM5 binding motifs that play a significant role in the interactions with the ligands by in vitro binding assay fluorescence spectroscopy and microscale thermophoresis. The experiments were accompanied by an atomistic explan-
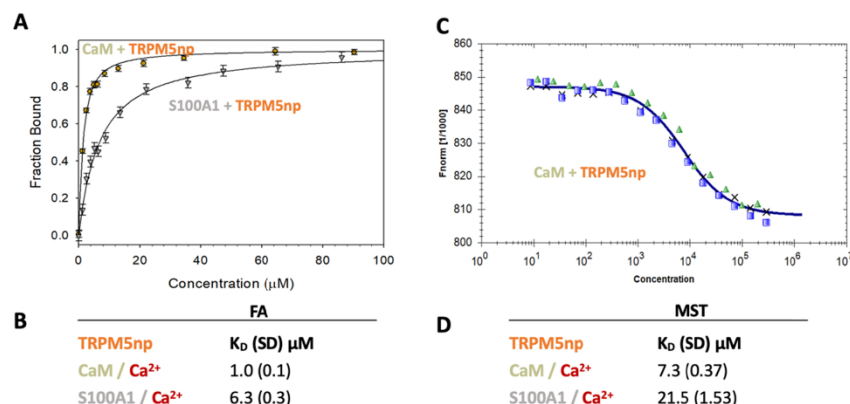
Figure 3. Interactions of TRPM5np with CaM and S100A1. (A) TRPM5np/CaM and TRPM5np/S100A1 complexes presented in the graph by F_B as a function of CaM/S100A1 concentrations; data obtained by FA. Five independent measurements represented by error bars were performed. (B) TRPM5 and CaM/S100A1 equilibrium K_D with corresponding SD calculated from FA data. (C) MST dose−response curve of CaM binding to TRPM5np. The difference in normalized fluorescence was plotted against increasing concentrations of CaM; the blue, green and black marks represent three independent measurements. (D) TRPM5 and CaM/S100A1 equilibrium K_D with corresponding SD calculated from MST data.

ation of the complex binding interface addressed by molecular modeling and molecular dynamic (MDs) simulations. To confirm the importance of the CaM/S100A1 ligand-binding amino acids, in silico mutations of the identified residues in TRPM5 N-terminal binding motifs into alanine were performed, and the evaluation of the changes in the binding energy was quantified based on empirical force field models. Here, we present the common character of the amino acid sequence of TRPM termini binding epitopes for CaM/S100A1, accompanied by a detailed description of the binding interfaces of the TRPM-CaM/S100A1 complexes. These descriptions lead to an understanding of the general mechanism of the formation of these complexes.

RESULTS

Identification of the TRPM5 N-Terminal Binding Epitope. The human TRPM5 sequence was analyzed for the presence of a CaM-binding region using the Calmodulin Target Database.[28] The TRPM5 putative CaM-binding site was identified in the distal part of the TRPM5 N-terminus, position W83 to K94, hereinafter referred to as TRPM5np (Figure 1). The structure of the TRPM5 channel (PDB: 6DMW) with labeled TRPM5np (UniProtKB/SwissProt: Q9NZQ8, positions W83-K94) binding site confirmed the accessibility to bind both suggested ligands (Figure 2). The TRPM5np binding region contains hydrophobic amino acids that form two possible CaM-binding motifs W83-V87-L92 [1-5-10 motif] and L84-L88-V93 [1-5-10 motif] with four embedded basic amino acids (R85, R89, K90, and K94) (Figure 1C). The TRPM5npR85A/R89A/K90A/K94A mutant was designed to investigate the role of the basic amino acid residue cluster in the CaM interaction. Given the known shared CaM /S100A1 binding epitopes on membrane receptors, such as TRP channels (RyR),[22,23,29−31] we also examined the S100A1 binding region on TRPM5np. TRPM5np wild type (wt) and TRPM5npR85A/R89A/K90A/K94A were synthesized as peptides, and their

propensity to bind CaM/S100A1 was examined by in silico and in vitro setups.

TRPM5np Binds CaM. The interaction of TRPM5np and CaM was measured by in vitro binding assay steady-state fluorescence anisotropy (FA) (Figure 3A). The FA of the FITC-labeled TRPM5np wt peptide was recorded during titration with CaM. The incubation of TRPM5np with CaM (1 min) served the stabilization of rotation diffusion that resulted in a clearly apparent increase in FA. The quantum yield ratio (Q) of the bound CaM to the TRPM5np was calculated from the corresponding fluorescence lifetimes. The CaM-bound fractions (F_B) of TRPM5np at each titration point of the ligand were determined by Q. F_B values plotted against CaM concentrations led to the determination of the equilibrium dissociation constant (K_D) of the TRPM5np/CaM complex. The binding affinity of the complex fell in the micromolar range: K_D = 1.0 (SD 0.1) μM (Figure 3B). The addition of 10 mM EDTA to the complex did not cause any complex formation (Figure S1A). The binding affinity trend of the TRPM5np/CaM complex was verified by another in vitro binding assay: the microscale thermophoresis (MST). The method was used to trace the CaM/TRPM5np thermophoresis (Figure 3C) and provided the signal decrease without any signs of aggregation. Similar to FA data, the complex showed the micromolar range of the binding affinity: K_D = 7.3 (SD 0.37) μM (Figure 3D). We have also studied the potential competition of S100A1 with the TRPM5np/CaM complex by the titration of the complex with a competitor (S100A1) that showed the significant sign of fluorescence signal decrease by MST, suggesting the ligand competition (Figure S2A).

TRPM5np Binds S100A1. S100A1 recognizes similar binding motifs on TRP channels as CaM. In the past, we identified many overlapping S100A1 and CaM-binding regions, so we decided to explore TRPM5np as well. (Figure 3A). The interaction of S100A1 with TRPM5np was characterized by FA and MST binding assays in the same manner, as described for the CaM interaction above. The K_D of the TRPM5np/S100A1 complex assessed by FA was 6.3 (SD

0.3) μM (Figure 3B). The addition of 10 mM EDTA to the complex did not cause any complex formation (Figure S1B). The binding of TRPM5np to S100A1 suggested a moderately higher K_D than that for CaM. The MST measurements confirmed a weaker interaction between S100A1 and TRPM5np (K_D = 21.5, SD 1.53 μM) (Figure 3C, D) compared to the CaM/TRPM5np complex, which corresponds to FA data. The difference in the K_D values of TRPM5np and CaM/S100A1 indicated distinct binding modes of the complexes. We have also studied the potential competition of CaM with the TRPM5np/S100A1 complex by the titration of the complex with the competitor (CaM) that showed the significant sign of fluorescence signal decrease by MST, suggesting the ligand competition (Figure S2B).

TRPM5np Binding Specificity Prediction. The interactions of TRP channels with CaM or S100A1 are profoundly maintained by TRP channels positively charged amino acid residues that form noncovalent interactions with CaM/S100A1 negatively charged amino acid residues. The clusters of positively charged residues at TRP channel binding epitopes commonly bear specific patterns in their positions.[23,30,33,34] To predict the basic residues of TRPM5np involved in the CaM/S100A1complex interface, we analyzed the other TRPM binding region sequences for CaM (S100A1), which we had experimentally confirmed in our previous in vitro studies[23,29,30,35] (Figure 4A, C). The selection of TRPM5np positively charged residues was performed by the sequence alignment of TRPM N-termini binding regions (Figure 4B). This multiple sequence alignment performed by CLUSTAL 1.2.4[36] revealed consensus basic residues sequences (RxxxxR/K, where x represents any amino acid) in all analyzed TRPM binding epitopes.

The identical hydrophobic binding motif was found for TRPM5np and TRPM4np1 (TRPM4 channel, UniProtKB/SwissProt: Q8TD43, V129-Q147). The 1-5-10 hydrophobic motif is localized in positions L84-L88-V93 (TRPM5np) and L134-L138-V143 (TRPM4np1). The alignment confirmed a strong consensus of TRPM5np R89 and K94 in all TRPM basic residues. The TRPM5np K90 shows the character of basic residue identity with TRPM4np1 and TRPM1np. The TRPM5np R85 does not fit into consensus with any TRPM binding epitopes. We expected that the TRPM5np R89, K90, and K94 clusters participated in the interactions with CaM/S100A1. Figure 4C represents the TRPM/CaM and TRPM/S100A1 complexes with the previously investigated K_D values ranging at a micromolar level.[23,29,31,34]

TRPM5np Basic Amino Acids Involved in the Formation of Complexes with CaM and S100A1. The role of basic amino acids of TRPM5np in the interaction with CaM/S100A1 was investigated by scanning alanine analogue TRPM5np_R85A/R89A/K90A/K94A mutant. FA and MST data (Figures 5A, B and 6A, B) revealed a decrease in K_D with a similar difference between the wild type and mutant for CaM (FA: K_D = 13.6, SD 0.5 μM; MST: K_D = 91.3, SD 1.32 μM) complexes (Figure 5C). An even more pronounced decrease in binding affinities was observed for TRPM5np_R85A/R89A/K90A/K94A with S100A using both FA and MST methods (FA: K_D = 134, SD 4 μM; MST: K_D = N.D.) (Figure 6C). These results confirmed the participation of TRPM5np basic residues in the interaction with both CaM and S100A1 and highlighted the different binding modes of these ligands.

TRPM5np/CaM and TRPM5np/S100A1 Models. The TRPM5np peptide derived from a TRPM5 homology model

A

binding epitope	sequence
TRPM1np	$_{270}$VKLRRQLEKHI$_{280}$
TRPM4np1	$_{129}$VLQTWLQDLLRRGLVRAAQ$_{147}$
TRPM5np	$_{83}$WLRDVLRKGLVK$_{94}$
TRPM4np2	$_{627}$FGECYRSSEVRAARLLLRRCP$_{647}$
TRPM6np	$_{520}$LIGRAYRSNYTRKHFR$_{535}$

B

TRPM	peptide sequence	AA
TRPM1np	--------VKLRRQLEKHI--------	11
TRPM4np1	VLQTWLQDLLRRGLVRAAQ-------	19
TRPM5np	----WLRDVLRKGLVK---------	12
TRPM4np2	-----FGECYRSSEVRAARLLLRRCP	21
TRPM6np	----LIGRAYRSNYTRKHFR------	16
	* :	

C

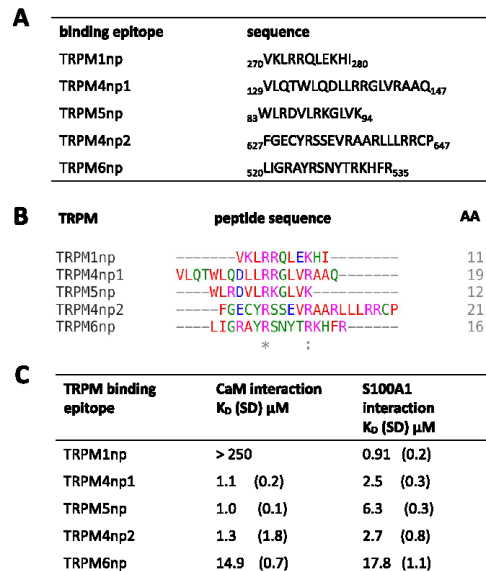| TRPM binding epitope	CaM interaction K_D (SD) μM		S100A1 interaction K_D (SD) μM	
TRPM1np	> 250		0.91	(0.2)
TRPM4np1	1.1	(0.2)	2.5	(0.3)
TRPM5np	1.0	(0.1)	6.3	(0.3)
TRPM4np2	1.3	(1.8)	2.7	(0.8)
TRPM6np	14.9	(0.7)	17.8	(1.1)

Figure 4. Selected TRPM N-termini binding epitopes sequence alignment. (A) The amino acid sequences of determined CaM/S100A1 binding epitopes placed at cytoplasmic TRPMs N-termini. Numbers denote the location of the binding epitope in the context of the whole specific channel. (B) Multiple alignments of TRPM sequences of CaM/S100A1 binding epitopes. The perfect match (marked with asterisk) of arginine residue and the most accurate match (marked with dots) with TRPM basic residues at the latest TRPM5np position suggested potential the significant role of these residues within the complex formations. Hydrophobic amino acids are represented in red, basic in pink, acidic in blue, and all other amino acids in green. The numbers display TRPM amino acid lengths. (C) TRPM/CaM and TRPM/S100A1 complexes with the previously investigated K_D values ranging in the micromolar level.

was docked by CaM/S100A1 ligands with ClusPro2.0 tool.[37] The TRPM5np/CaM-Ca^{2+} complex was built using ClusPro based on its similarity with the TRPV1p/CaM complex (PDB: 3SUI),[38] as well as based on our previous docking TRPM/CaM strategy (Figure 5D, E).[23,29,31] The TRPM5np/S100A1-Ca^{2+} complex was built using ClusPro based on the closest known S100A1/receptor-peptide structure of the RyR1P12/S100A1 (PDB: 2K2F) (Figure 6D, E).[39] The resulted complexes were compared with the TRPV1p/CaM and RyR1P12/S100A1 structures.[38,39] Consequently, we optimized the selected binding modes, as described by Bousova et al.[35] The final TRPM5np/CaM and TRPM5np/S100A1 complexes confirmed the interactions of TRPM5np R85, R89, K90, and K94 with negatively charged residues of the ligands. TRPM5np interacted with these specific CaM negatively charged residues E11, E119, E123, and E127. These amino acid residues unambiguously correspond to CaM residues that participated in the interactions with TRPV6.[27] The S100A1 negatively charged residues D50, D52, and N92 involved in the TRPM5np complex formation correspond to the S100A1 cluster of negatively charged residues involved in the TRPM6np/S100A1 complex formation.[29] The CaM and
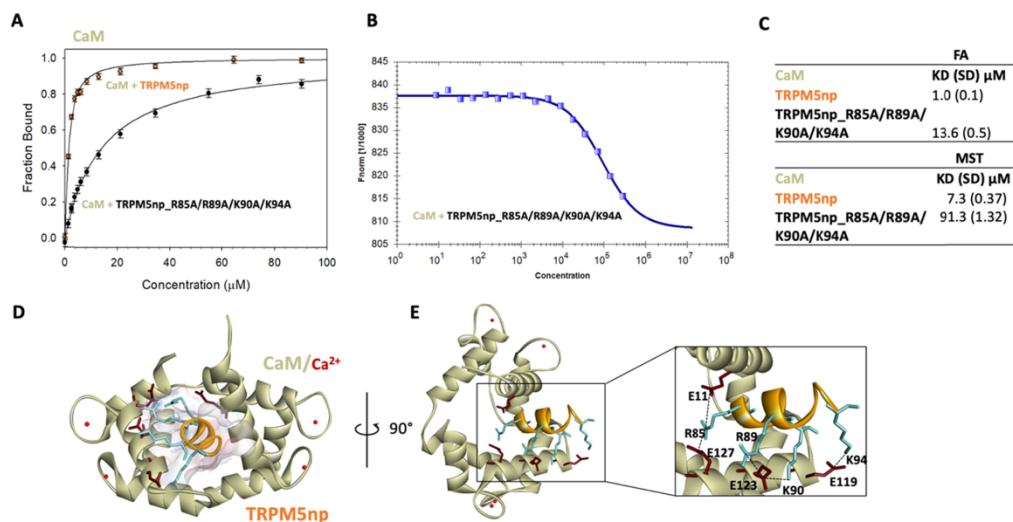
Figure 5. TRPM5np basic amino acids participate in the interactions with CaM. (A) TRPM5np/CaM and TRPM5np_R85A/R89A/K90A/K94A/ CaM complexes presented in the graph by F_B as a function of CaM concentrations, data obtained by FA. Five independent measurements were performed; represented by error bars. (B) MST trace from a serial dilution of CaM titrated against FITC-labeled TRPM5npR85A/R89A/K90A/ K94A. The difference in normalized fluorescence was plotted against the increasing concentration of CaM, the blue marks represent the measurement for CaM/TRPM5npR85A/R89A/K90A/K94A (CaM/TRPM5np MST data are shown in Figure 3C). (C) Equilibrium K_D of TRPM5np/CaM and TRPM5npR85A/R89A/K90A/K94A/CaM with the corresponding SD calculated from FA and MST data. (D) Top view of the TRPM5np/CaM molecular model. TRPM5np (backbone in orange) and CaM (backbone in green) composed of the binding interface. The TRPM5np basic residues involved in the interactions with CaM are displayed in blue. The negatively charged residues of CaM involved in the interactions with TRP5Mnp are displayed in red. Ca^{2+} are shown by red-scaled balls. (E) Full and detailed TRPM5np/CaM complex binding interface with the surface representation of positively charged residues R85, R89, K90, and K94 from TRPM5np (colored in blue) and negatively charged residues E11, E119, E123, and E127 of CaM (colored in red) involved in the noncovalent bonding.

S100A1 docking confirmed the high participation of basic TRPM5np residues in the formation of the complexes, as predicted by the TRPM sequence alignment.

MD Simulations of TRPM5np and CaM/S100A1 Complexes. As an alternative to homology modeling of the ligand and its docking into the structures of CaM/S100A1, we decided to build another model. In this round, we used homology modeling for the complex from the very beginning. Approximately 80 templates were found for the CaM complexes and two for S100A1 protein to properly set up geometries for MD runs. PDB templates suitable for model building were identified by the condition that sequence matches needed to be present in the binding region. The PDB entries chosen as templates for homology modeling were 2LGF for TRPM5np/CaM and 2K2F for TRPM5np/S100A1. The selected models built by the MODELLER suite were refined by 200 ns of MDs. For each complex, at least one model preserved the RMSD of backbone atoms between the initial and final states between 1−3 Å. These models were selected for other analyses and simulations. Following long-scale MD simulations, we further tested the stability of the complexes. No dissociation events were observed, and the ligands kept their binding poses. However, the RMSD from the refined structures indicated some gradual and cumulative conformation changes (Figure 7A). The most notable deviations were observed for the TRPM5np-CaM complex, which underwent a slight reorientation of two calmodulin lobes and shift of a peptide ligand in the course of the 1000 ns

simulation (Figure 7B). This figure also compares the initial and final states of other complexes that manifested less dynamic behavior. The simulation of the mutated ligands started from the conformation of bound complexes with all basic amino acids in peptides replaced with alanine. Similarly, as in the case of wild-type sequences, no dissociation events and dramatic changes of binding poses were observed at the time scale of 1000 ns.

In order to quantify the strength of the interaction between the CaM, the S100A1 protein, and the bound peptide and to prove the role of basic amino acids, interaction matrices were evaluated through the trajectories. The total interaction energy between molecules was calculated as the sum of all amino acid contributions. Figure 7C shows the calculated distributions of interaction energies and their comparison for the wild type and the mutated sequences of the peptide, where all the basic residues were replaced with alanine (TRPM5np: $_{83}$WLADV-LAAGLVA$_{94}$). In the mutated peptide, no significant changes in the peptide conformations were observed. The mutated sequences provided distributions that shifted toward more positive values, indicating weaker interactions. Nevertheless, the interaction energies cannot be used here as straightforward proxies for the free energy of binding because they are missing important entropic contributions to the binding and interaction with the solvent. A broad range of calculated values also indicates significant compensation of interaction energies by unconsidered terms, which should together result in realistic estimates of the free energy of binding (∼25
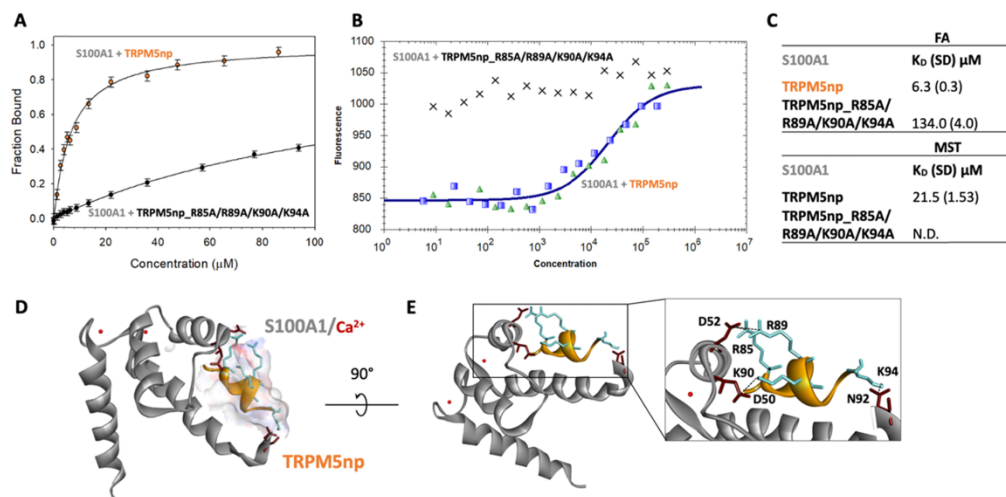
Figure 6. TRPM5np basic amino acids participate in the interactions with S100A1. (A) TRPM5np/S100A1 and TRPM5np_R85A/R89A/K90A/K94A/S100A1 complexes presented in the graph by F_B as a function of S100A1 concentrations; data obtained by FA. Five independent measurements were performed represented by error bars. (B) MST trace from the serial dilution of S100A1 titrated against FITC-labeled TRPM5np_and TRPM5npR85A/R89A/K90A/K94A. The difference in fluorescence was plotted against the increasing concentration of S100A1, and the black marks represent the measurement for CaM/TRPM5npR85A/R89A/K90A/K94A; blue and green marks represent the CaM/TRPM5np complex. (C) Equilibrium K_D of TRPM5np/S100A1 and TRPM5npR85A/R89A/K90A/K94A/S100A1 with corresponding SD calculated from FA and MST data. (D) Side view of the TRPM5np/S100A1 molecular model (1:1). TRPM5np (backbone in orange) and S100A1 (backbone in gray) composed of the binding interface. The color convention is the same as that in the previous representation. (E) Full and detailed TRPM5np/S100A1 complex binding interface with the surface representation of positively charged residues R85, R89, K90, and K94 from TRPM5np (colored in blue) and negatively charged residues D50, D52, and N92 of S100A1 (colored in red) involved in the noncovalent bonding. The color convention is the same as that in the previous representation.

kJ.mol^{-1}). Indeed, the difference in interaction energies between wild-type and mutated sequences is definitely caused by missing basic amino acids.

◼ DISCUSSION

The presented results provide a deeper understanding of the potential mechanism of TRPM interactions with intracellular regulatory molecules. The various intracellular signaling agents (e.g., CBPs, phosphoinositide, inorganic ions, and so forth) were found to be recognized by exceptionally extensive intracellular TRPM termini and to modulate the function of these channels.[40−42] By a combination of in vitro and in silico approaches, we identified the most probable CaM-binding region of TRPM5 cytoplasmic N-terminus, and we determined the role of the identified residues in the binding event. Moreover, the newly identified CaM-binding motif overlaps with the interaction site for another CBP−S100A1. Experimentally determined dissociation constants for the TRPM5/S100A1-Ca^{2+} complex are slightly higher than those for the complex with CaM-Ca^{2+}. Still, the range of the complexes is within micromolar levels, which is typical for these types of TRP channels strictly Ca^{2+}-dependent interactions.[23,29,30] Both complexes are formed in the presence of Ca^{2+};[23,29,30] on the other hand, with the presence of 10 mM EDTA, the complexes are not formed (Figure S1). The atomistic details of the intermolecular interactions between CaM, S100A1, and the peptides differ at CaM/S100A1 binding interfaces, which also correspond, to some extent, to the differences in the

dissociation constants. Based on the available literature, we suppose that shared CaM/S100A1 binding epitopes are a common phenomenon observed among the TRP channel members.[22,23,29] The negative binding control of TRPM5np with bovine serum albumin (BSA) confirmed the specific selectivity of CaM and S100A1 to the TRPM5np binding site (Figure S3).

The multiple sequence alignment of the TRPM5np binding epitope for CaM/S100A1 with other TRPM binding region sequences for CaM (S100A1) revealed the significant sequence consensus of the basic amino acid residues ($Rxxxx[K/R]$) present within the TRPM binding sites (Figure 4B). The analysis of the longer amino acid sequences (100 aa) of the respective TRPM members binding CaM/S100A1 also confirmed the conservation of the TRPM binding sites throughout the members (Figure S4). These basic residues are generally responsible for the interaction with the negative residues of CaM and S100A1.[27] TRPM5 and TRPM4 are the closest homologs in the TRPM subfamily, both being activated through interactions of the conserved Ca^{2+}-binding motif with Ca^{2+} ions.[43] Furthermore, CaM binding was found to potentiate currents in TRPM4.[42] The TRPM4np1 and TRPM5np binding epitopes (Figure 4A, B) share the same conserved hydrophobic binding motif positions 1-5-10, which is very often necessary for the CaM/S100A1 initiation for complex formation.[23] Because of the high homogeneous sequence similarity of the TRPM4 and TRPM5 channels, we expect that the effect of CaM on TRPM5 regulation will be similar to that of TRPM4, so the positive modulation is
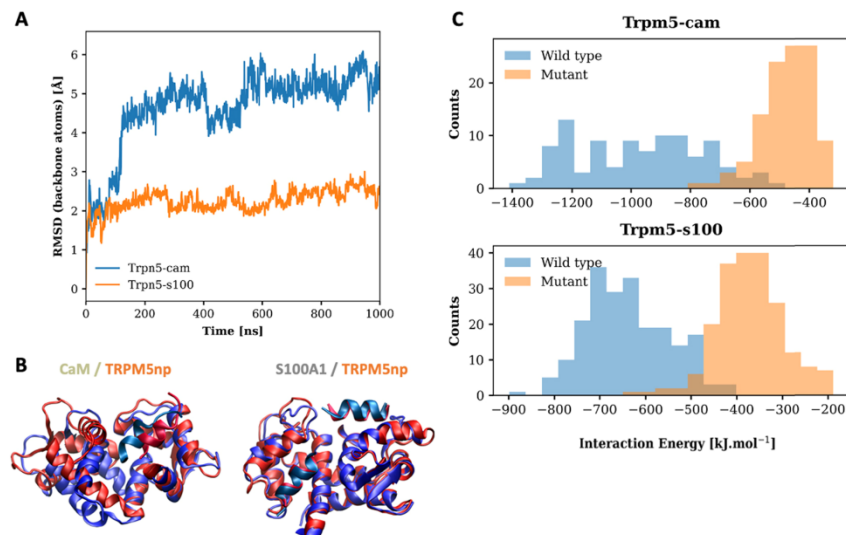
Figure 7. MDs of TRPM5 and CaM/S100A1 complexes. (A) RMSD of backbone atoms from the refined TRPM5/CaM and TRPM5/S100A1 models as a function of simulation time. (B) Comparison of the TRPM5/CaM and TRPM5/S100A1 refined models (red) and final states after 1000 ns MD simulations (in blue). Bound peptides of TRPM5 are colored for clarity in distinct shades of red and blue. (C) Distribution of interaction energies between TRPM5np wild type and its alanine mutant (TRPM5np: $_{83}$WLADVLAAGLVA$_{94}$) with CaM/S100A1 ligands. Histograms for S100A1 complexes merge distributions for both binding sites in protein dimers.

expected, resulting in increased TRPM5 permeability for the cell. However, this assumption must be confirmed by the electrophysiological measurements of receptor activities directly on the cell membrane.

The outcome of the TRPM N-termini sequence alignment identifying key residues for interactions was confirmed by molecular modeling, which allowed a deeper understanding of the role of the individual basic residues participating in the interactions. Indeed, results obtained by applying two different molecular modeling approaches captured the atomistic details of the binding and the role of the basic residues in the event. Our models not only confirmed their stabilizing contribution mapping established salt bridges but, using long MDs, also explored and confirmed the dynamical character of the noncovalent interactions within the complexes. Finally, yet importantly, in silico mutations of arginines and lysines into alanines in the identified TRPM5np epitope and the consequent evaluation of their interaction energy profiles unambiguously support the major stabilizing effect of basic residues in the binding (Figure 7C).

To conclude, a new TRPM5 binding site for CaM/S100A1 at the N-terminus has been experimentally and theoretically characterized. The binding affinities of all these complexes fit into the typical micromolar range for TRP channels/CaM and TRP channels/S100A1 complexes.[23,29,31,34] The alignment of TRPMs N-termini epitopes revealed conserved TRPM5np basic residues potentially participated in the formation of the complexes (CaM, S100A1). Moreover, the specific hydrophobic amino acid clusters that potentially serve as anchors to the hydrophobic pockets of the CaM/S100A1 surfaces were also identified. Our data provide new information about TRPM5 termini as a multiple binding target for both Ca^{2+}-

binding proteins—CaM/S100A1. These ligands are potentially expected to be involved in the modulation of TRPM5, which is mainly expressed in tissues mediating taste transduction.[44,45] An insight based on atomistic resolution, which provided molecular docking, could better elucidate the potential triggers of channel disorders that could lead to the worst-case scenarios of serious diseases. Therefore, we anticipate that the information provided in the current study and in our previous TRPM projects[23,29−31,34] could lead to a better understanding of the function of TRPM channels in general and might further help address TRPM-related disease issues in the future.

■ MATERIALS AND METHODS

Design of the TRPM5 N-Terminal Region. The cDNA of human TRPM5 was scanned to search for a CaM/ 100A1 binding motif by the Calmodulin Target Database.[28] To confirm the presence of CaM and S100A1 binding parts at the N-terminus of TRPM5, we chose the following binding region as UniProtKB/SwissProt: Q9NZQ8, positions W83-K94, hereinafter referred to as TRPM5np. To confirm the basic amino acid residues of TRPM5np involved in the CaM/ S100A1 interactions, we designed the alanine mutant of TRPM5np, hereinafter referred to as TRPM5npR85A/R89A/ K90A/K94A. The designed sequences were synthesized as peptides, and the interactions to CaM/S100A1 were characterized by in vitro and in silico setup.

TRPM5np Peptide Synthesis. TRPM5np and its alanine scan analogue (TRPM5np_R85A/R89A/K90A/K94A) were synthesized as peptides (IOCB CAS, Prague, Czech Republic). The peptides were C-termini-probed with fluorescein-5-isothiocyanate (FITC, PubChem CID: 18730). The purity of all peptides was >95% and checked by high-performance liquid

chromatography (HPLC) (IOCB CAS, Prague, Czech Republic). The peptides were dissolved in a 50 mM Tris–HCl buffer (pH 7.5) with 150 mM NaCl and 1 mM $CaCl_2$.

CaM and S100A1 Protein Production. The cDNAs of CaM and S100A1 in the pET28b expression vector were used to express the proteins. The CaM and S100A1 were purified according to our standard purification protocol.[23]

Steady-State Fluorescence Anisotropy Measurements. Steady-state FA experiments were performed on a K2 spectrometer (ISS Inc., Champaign, Illinois, USA) at RT according to our previously described in-house FA protocol.[35]

Lifetime Measurements. Fluorescence lifetimes were evaluated at RT using a confocal microscope IX83 (Olympus, Tokyo, Japan) according to our previously described in-house lifetime measurement protocol.[35]

Microscale Thermophoresis. The CaM/S100A1 binding affinity to TRPM5np and TRPM5np_R85A/R89A/K90A/K94A was characterized by MST using Monolith NT.115 (NanoTemper Technologies GmbH, Munich, Germany). FITC-labeled TRPM5np and TRPM5np_R85A/R89A/K90A/K94A at a constant concentration of 50 nM were titrated by a twofold serial dilution of CaM (284 × 103−8.667 nM) and S100A1 (289 × 103−8.8196 nM). The MST experiments were performed in Monolith NT.115 Capillaries (NanoTemper Technologies GmbH, Munich, Germany) in 50 mM Tris–HCl (pH 7.5), 150 mM NaCl, 0.05% Tween 20, with an LED power of 50% and an MST power of 40%. The MST data were analyzed using NT Analysis software version 1.5.4 (NanoTemper Technologies GmbH, Munich, Germany).

TRPM5 Channel and the TRPM5np Structural Model. The structure of the TRPM5 channel (PDB: 6DMW) provided recently with full structural analysis by Cryo-EM[32] was built using PyMOL[46] software by the selection of an appropriate TRPM5np region with sequence position W83-K94. The representative TRPM5np structural model was processed, as described previously[35,39,47] in the MOE software. The final structure quality was evaluated using STING Millennium[48] and ProSA-web.[49]

TRPM5np Docking into CaM/S100A1. The TRPM5np structural model was run by ligand docking analysis with CaM/S100A1 structural models using the ClusPro tool.[37,50,51] The CaM and S100A1 templates were selected from the TRPV1-CaM/Ca^{2+} (PDB: 3SUI) and RyR1-S100A1/Ca^{2+} (PDB: 2K2F) structures. The TRPM5np/CaM and TRPM5np/S100A1 molecular model complexes were selected based on the predicted binding interfaces and processed, as described previously.[47] The model representations of the complexes were prepared using Discovery Studio Visualizer.[52]

Homology Models of TRPM5np Complexes with CaM/S100A1. An alternative approach for modeling the interaction of CaM/S100A1 with the TRPM5np peptide was also explored. Structures of CaM/S100A1 proteins in complex with the peptide ligand were obtained in one homology modeling step, completely replacing the docking procedure. Templates for homology modeling were carefully selected from the PDB database, based on the sequence of the bounded peptide ligand. First, a list of peptide sequences bound to the CaM/S100A1 protein was compiled, together with the corresponding PDB IDs. The suitable templates were identified by the sequence alignment of peptide sequences performed using a ClustalW[53] algorithm with default parameters. The complexes with the best matches in the sequence of the ligands were checked manually to verify if the

aligned sequences corresponded to the binding regions. The deposited PDB models fulfilling these criteria were then chosen as templates for homology modeling. The automodel procedure of the MODELLER[54] program (version 9.19) was used for the construction of homology models employing the elaborated sequence alignments. The S100 protein was always modeled as a dimer with two ligands. For each complex, 100 models were generated, and the three with the lowest value of the MODELLER objective function were selected for the refinement by MD simulations. The refinement involved the preparation of a fully solvated model, and its geometry optimization and equilibration were followed by 200 ns of MD. Afterward, the final framework of the simulation, which was the least different from the initial structure in terms of the deviation of the square root of the atomic positions, was marked as a refined model. The in silico mutation of positively charged residues in peptide ligands (K, L) was performed manually by deleting extra side-chain atoms and then renaming the corresponding residues. Afterward, the same short geometry optimization and equilibration of the models were conducted.

Details of MD Simulations. Models of CaM/S100A1 protein with bound peptide ligands were placed in adequately sized dodecahedron simulation boxes (430 and 560 nm3, respectively) and solvated by TIP3P explicit water molecules.[55] The net charge of the protein molecules was compensated by sodium and chloride ions in amounts providing 100 mM ionic strength of the buffer. The Ca^{2+} ions in EF hands of the CaM/S100A1 protein were modeled explicitly. Interactions of simulated particles were described by AMBER parm14SB force field.[56]

All MD simulations and analysis were performed with the GROMACS2019 simulation toolkit.[57,58] First, short energy minimization (1000 steps of the steepest descent integrator) was conducted for the elimination of close interatomic contacts. Subsequently, 1 ns long equilibration in the NpT thermodynamic ensemble was performed with temperature maintained by v-rescale algorithm[59] and pressure-controlled using a Berendsen barostat.[60] MD simulations were performed with a time step of 2 fs, which required constraining of hydrogen-associated chemical bonds with the LINCS algorithm.[61] Lennard-Jones interactions were truncated at 12 Å distance, and the electrostatic interactions were treated using the particle mesh Ewald method.[62] The final MD simulations were run for 1000 ns.

Analysis of Trajectories. The produced trajectories were analyzed by means of a dedicated GROMACS tool (e.g., gmx rms). Salt bridges were reported by VMD.[63] Calculations of interaction energies were performed by the backend of the amino acid interaction (INTAA) web server.[64] The reported interaction energies include all noncovalent terms between protein chains, including screened pairwise electrostatic interaction. The screening was calculated using a generalized born solvation model in OBC II parametrization.[65] Self-polarization (desolvation) and solvent-accessible-surface-area-dependent terms were not considered.

■ ASSOCIATED CONTENT

ⓢ Supporting Information

The Supporting Information is available free of charge at https://pubs.acs.org/doi/10.1021/acs.biochem.1c00647.

Ca2+-dependent binding of CaM and S100A1 to TRPM5np; competition assays of CaM and S100A1 with TRPM5np complexes; negative control binding assay of TRPM5np with BSA; and multiple sequence alignment of TRPM binding sites for CaM / S100A1 (PDF)

Accession Codes

TRPM5 channel, UniProtKB/SwissProt: Q9NZQ8; PDB: 6DMW, TRPV1-CaM/Ca^{2+} (PDB: 3SUI), RyR1-S100A1/Ca^{2+} (PDB: 2K2F).

■ AUTHOR INFORMATION

Corresponding Author

Kristyna Bousova − *Institute of Organic Chemistry and Biochemistry of the Czech Academy of Sciences, 16000 Prague, Czech Republic;* ⊙ orcid.org/0000-0001-9030-3811; Phone: 420-220-183-131; Email: kristyna.bousova@uochb.cas.cz

Authors

Monika Zouharova − *Institute of Organic Chemistry and Biochemistry of the Czech Academy of Sciences, 16000 Prague, Czech Republic; Second Faculty of Medicine, Charles University, 150 06 Prague 5, Czech Republic;* ⊙ orcid.org/0000-0002-2254-6480

Petr Herman − *Faculty of Mathematics and Physics, Charles University, 12116 Prague, Czech Republic*

Jiri Vymetal − *Institute of Organic Chemistry and Biochemistry of the Czech Academy of Sciences, 16000 Prague, Czech Republic;* ⊙ orcid.org/0000-0002-0165-8707

Veronika Vetyskova − *Institute of Organic Chemistry and Biochemistry of the Czech Academy of Sciences, 16000 Prague, Czech Republic; Department of Biochemistry and Microbiology, University of Chemistry and Technology Prague, 166 28 Prague, Czech Republic*

Katerina Jiraskova − *Institute of Organic Chemistry and Biochemistry of the Czech Academy of Sciences, 16000 Prague, Czech Republic*

Jiri Vondrasek − *Institute of Organic Chemistry and Biochemistry of the Czech Academy of Sciences, 16000 Prague, Czech Republic;* ⊙ orcid.org/0000-0002-6066-973X

Complete contact information is available at:
https://pubs.acs.org/10.1021/acs.biochem.1c00647

Author Contributions

K.B. designed research. K.B., M.Z., P.H., J.Vym, V.V., and K.J. performed the experiments. K.B., M.Z., P.H., J.Vym, and J.Vond analyzed the data. K.B., M.Z., J.Vym, and J.Vond wrote the manuscript.

Notes

The authors declare no competing financial interest.

■ ABBREVIATIONS

BSA	bovine serum albumin
CaM	calmodulin
CBP	calcium-binding protein
EM	electron microscopy
FA	steady-state fluorescence anisotropy
IDP	intrinsically disordered protein
MDs	molecular dynamics simulations
MHR	melastatin homology regions
MST	microscale electrophoresis
PIP2	phosphatidylinositol 4, 5-bisphosphate
RT	room temperature
RyR	ryanodine receptor
S100A1	S100 calcium-binding protein A1
TRP	transient receptor potential
TRPC	TRP canonical
TRPV	TRP vaniloid
TRPM5	TRP cation channel subfamily melastatin member 5

■ REFERENCES

(1) Autzen, H. E.; Myasnikov, A. G.; Campbell, M. G.; Asarnow, D.; Julius, D.; Cheng, Y. Structure of the human TRPM4 ion channel in a lipid nanodisc. *Science* **2018**, *359*, 228−232.

(2) Liao, M.; Cao, E.; Julius, D.; Cheng, Y. Structure of the TRPV1 ion channel determined by electron cryo-microscopy. *Nature* **2013**, *504*, 107−112.

(3) Moiseenkova-Bell, V. Y.; Stanciu, L. A.; Serysheva, I. I.; Tobe, B. J.; Wensel, T. G. Structure of TRPV1 channel revealed by electron cryomicroscopy. *Proc. Natl. Acad. Sci. U. S. A.* **2008**, *105*, 7451−7455.

(4) Gao, Y.; Cao, E.; Julius, D.; Cheng, Y. TRPV1 structures in nanodiscs reveal mechanisms of ligand and lipid action. *Nature* **2016**, *534*, 347−351.

(5) Winkler, P. A.; Huang, Y.; Sun, W.; du, J.; Lü, W. Electron cryo-microscopy structure of a human TRPM4 channel. *Nature* **2017**, *552*, 200−204.

(6) Chubanov, V.; Mittermeier, L.; Gudermann, T. TRPM7 reflected in Cryo-EMirror. *Cell Calcium* **2018**, *76*, 129−131.

(7) Owsianik, G.; D'hoedt, D.; Voets, T.; Nilius, B. Structure-function relationship of the TRP channel superfamily. *Rev. Physiol., Biochem. Pharmacol.* **2006**, *156*, 61−90.

(8) Duan, J.; Li, Z.; Li, J.; Hulse, R. E.; Santa-Cruz, A.; Valinsky, W. C.; Abiria, S. A.; Krapivinsky, G.; Zhang, J.; Clapham, D. E. Structure of the mammalian TRPM7, a magnesium channel required during embryonic development. *Proc. Natl. Acad. Sci. U. S. A.* **2018**, *115*, E8201−E8210.

(9) Harteneck, C. Function and pharmacology of TRPM cation channels. *Naunyn-Schmiedeberg's Arch. Pharmacol.* **2005**, *371*, 307−314.

(10) Pérez, C. A.; Huang, L.; Rong, M.; Kozak, J. A.; Preuss, A. K.; Zhang, H.; Max, M.; Margolskee, R. F. A transient receptor potential channel expressed in taste receptor cells. *Nat. Neurosci.* **2002**, *5*, 1169−1176.

(11) Prawitt, D.; Monteilh-Zoller, M. K.; Brixel, L.; Spangenberg, C.; Zabel, B.; Fleig, A.; Penner, R. TRPM5 is a transient Ca2+−activated cation channel responding to rapid changes in [Ca2+]i. *Proc. Natl. Acad. Sci. U. S. A.* **2003**, *100*, 15166−15171.

(12) Liu, D.; Liman, E. R. Intracellular Ca2+ and the phospholipid PIP2 regulate the taste transduction ion channel TRPM5. *Proc. Natl. Acad. Sci. U. S. A.* **2003**, *100*, 15160−15165.

(13) Zhang, Z.; Zhao, Z.; Margolskee, R.; Liman, E. The transduction channel TRPM5 is gated by intracellular calcium in taste cells. *J. Neurosci.* **2007**, *27*, 5777−5786.

(14) Hasan, R.; Zhang, X. Ca(2+) Regulation of TRP Ion Channels. *Int. J. Mol. Sci.* **2018**, *19*, 1256.

(15) Clapham, D. E. Calcium signaling. *Cell* **2007**, *131*, 1047−1058.

(16) Bagur, R.; Hajnóczky, G. Intracellular Ca(2+) Sensing: Its Role in Calcium Homeostasis and Signaling. *Mol. Cell* **2017**, *66*, 780−788.

(17) Stevens, F. C. Calmodulin: an introduction. *Can. J. Biochem. Cell Biol.* **1983**, *61*, 906−910.

(18) Babu, Y. S.; Sack, J. S.; Greenhough, T. J.; Bugg, C. E.; Means, A. R.; Cook, W. J. Three-dimensional structure of calmodulin. *Nature* **1985**, *315*, 37.

(19) Melville, Z.; Aligholizadeh, E.; McKnight, L. E.; Weber, D. J.; Pozharski, E.; Weber, D. J. X-ray crystal structure of human calcium-bound S100A1. *Acta Crystallogr. F Struct. Biol. Commun.* **2017**, *73*, 215−221.

(20) Ritterhoff, J.; Most, P. Targeting S100A1 in heart failure. *Gene Ther.* **2012**, *19*, 613−621.

(21) Marston, S. B.; Fraser, I.; Huber, P.; Pritchard, K.; Gusev, N. B.; Torok, K. Location of two contact sites between human smooth muscle caldesmon and Ca (2+)-calmodulin. *J. Biol. Chem.* **1994**, *269*, 8134−8139.

(22) Wright, N. T.; Prosser, B. L.; Varney, K. M.; Zimmer, D. B.; Schneider, M. F.; Weber, D. J. S100A1 and calmodulin compete for the same binding site on ryanodine receptor. *J. Biol. Chem.* **2008**, *283*, 26676−26683.

(23) Bousova, K.; Herman, P.; Vecer, J.; Bednarova, L.; Monincova, L.; Majer, P.; Vyklicky, L.; Vondrasek, J.; Teisinger, J. Shared CaM- and S100A1-binding epitopes in the distal TRPM 4 N terminus. *FEBS J.* **2018**, *285*, 599−613.

(24) Rebbeck, R. T.; Nitu, F. R.; Rohde, D.; Most, P.; Bers, D. M.; Thomas, D. D.; Cornea, R. L. S100A1 protein does not compete with calmodulin for ryanodine receptor binding but structurally alters the ryanodine receptor· calmodulin complex. *J. Biol. Chem.* **2016**, *291*, 15896−15907.

(25) Saimi, Y.; Kung, C. Calmodulin as an ion channel subunit. *Annu. Rev. Physiol.* **2002**, *64*, 289−311.

(26) Dang, S.; van Goor, M. K.; Asarnow, D.; Wang, Y.; Julius, D.; Cheng, Y.; van der Wijst, J. Structural insight into TRPV5 channel function and modulation. *Proc. Natl. Acad. Sci. U. S. A.* **2019**, *116*, 8869−8878.

(27) Singh, A. K.; McGoldrick, L. L.; Twomey, E. C.; Sobolevsky, A. I. Mechanism of calmodulin inactivation of the calcium-selective TRP channel TRPV6. *Sci. Adv.* **2018**, *4*, No. eaau6088.

(28) Yap, K. L.; Kim, J.; Truong, K.; Sherman, M.; Yuan, T.; Ikura, M. Calmodulin target database. *J. Struct. Funct. Genomics* **2000**, *1*, 8−14.

(29) Zouharova, M.; Herman, P.; Hofbauerová, K.; Vondrasek, J.; Bousova, K. TRPM6 N-Terminal CaM- and S100A1-Binding Domains. *Int. J. Mol. Sci.* **2019**, *20*, 4430.

(30) Holakovska, B.; Grycova, L.; Jirku, M.; Sulc, M.; Bumba, L.; Teisinger, J. Calmodulin and S100A1 protein interact with N terminus of TRPM3 channel. *J. Biol. Chem.* **2012**, *287*, 16645−16655.

(31) Bousova, K.; Barvik, I.; Herman, P.; Hofbauerová, K.; Monincova, L.; Majer, P.; Zouharova, M.; Vetyskova, V.; Postulkova, K.; Vondrasek, J. Mapping of CaM, S100A1 and PIP2-Binding Epitopes in the Intracellular N-and C-Termini of TRPM4. *Int. J. Mol. Sci.* **2020**, *21*, 4323.

(32) Lu, W.; Du, J.; Ruan, Z.; Haley, E.; Orozco, I.; Roth, R.; Sabat, M.; Myers, R. Structures of TRPM5 channel elucidate mechanism of activation and inhibition. *bioRxiv* **2021**.

(33) Bily, J.; Grycova, L.; Holendova, B.; Jirku, M.; Janouskova, H.; Bousova, K.; Teisinger, J. Characterization of the S100A1 protein binding site on TRPC6 C-terminus. *PLoS One* **2013**, *8*, No. e62677.

(34) Jirku, M.; Lansky, Z.; Bednarova, L.; Sulc, M.; Monincova, L.; Majer, P.; Vyklicky, L.; Vondrasek, J.; Teisinger, J.; Bousova, K. The characterization of a novel S100A1 binding site in the N-terminus of TRPM1. *Int. J. Biochem. Cell Biol.* **2016**, *78*, 186−193.

(35) Bousova, K.; Zouharova, M.; Herman, P.; Vetyskova, V.; Jiraskova, K.; Vondrasek, J. TRPM7 N-terminal region forms complexes with calcium binding proteins CaM and S100A1. *Heliyon* **2021**, *7*, No. e08490.

(36) Sievers, F.; Wilm, A.; Dineen, D.; Gibson, T. J.; Karplus, K.; Li, W.; Lopez, R.; McWilliam, H.; Remmert, M.; Söding, J.; Thompson, J. D.; Higgins, D. G. Fast, scalable generation of high-quality protein multiple sequence alignments using Clustal Omega. *Mol. Syst. Biol.* **2011**, *7*, 539.

(37) Kozakov, D.; Hall, D. R.; Xia, B.; Porter, K. A.; Padhorny, D.; Yueh, C.; Beglov, D.; Vajda, S. The ClusPro web server for protein−protein docking. *Nat. Protoc.* **2017**, *12*, 255.

(38) Lau, S.-Y.; Procko, E.; Gaudet, R. Distinct properties of Ca2+−calmodulin binding to N-and C-terminal regulatory regions of the TRPV1 channel. *J. General Physiol.* **2012**, *140*, 541−555.

(39) Prosser, B. L.; Wright, N. T.; Hernández-Ochoa, E. O.; Varney, K. M.; Liu, Y.; Olojo, R. O.; Zimmer, D. B.; Weber, D. J.; Schneider, M. F. S100A1 binds to the calmodulin-binding site of ryanodine receptor and modulates skeletal muscle excitation-contraction coupling. *J. Biol. Chem.* **2008**, *283*, 5046−5057.

(40) Liu, B.; Qin, F. Functional control of cold- and menthol-sensitive TRPM8 ion channels by phosphatidylinositol 4,5-bi-sphosphate. *J. Neurosci.* **2005**, *25*, 1674−1681.

(41) Rohács, T.; Lopes, C. M. B.; Michailidis, I.; Logothetis, D. E. PI(4,5)P-2 regulates the activation and desensitization of TRPM8 channels through the TRP domain. *Nat. Neurosci.* **2005**, *8*, 626−634.

(42) Nilius, B.; Prenen, J.; Tang, J.; Wang, C.; Owsianik, G.; Janssens, A.; Voets, T.; Zhu, M. X. Regulation of the Ca2+ sensitivity of the nonselective cation channel TRPM4. *J. Biol. Chem.* **2005**, *280*, 6423−6433.

(43) Yamaguchi, S.; Tanimoto, A.; Iwasa, S.; Otsuguro, K. I. TRPM4 and TRPM5 Channels Share Crucial Amino Acid Residues for Ca(2+) Sensitivity but Not Significance of PI(4,5)P2. *Int. J. Mol. Sci.* **2019**, *20*, 2012.

(44) Zimmer, D. B.; Cornwall, E. H.; Landar, A.; Song, W. The S100 protein family: history, function, and expression. *Brain Res. Bull.* **1995**, *37*, 417−429.

(45) Rasmussen, C. D.; Means, A. R. Calmodulin, cell growth and gene expression. *Trends Neurosci.* **1989**, *12*, 433−438.

(46) DeLano, W. L. Pymol: An open-source molecular graphics tool. *CCP4 Newslett. Protein Crystallogr.* **2002**, *40*, 82−92.

(47) Vilar, S.; Cozza, G.; Moro, S. Medicinal chemistry and the molecular operating environment (MOE): application of QSAR and molecular docking to drug discovery. *Curr. Top. Med. Chem.* **2008**, *8*, 1555−1572.

(48) Neshich, G.; Togawa, R. C.; Mancini, A. L.; Kuser, P. R.; Yamagishi, M. E.; Pappas G Jr; Torres, W. V.; Fonseca e Campos, T.; Ferreira, L. L.; Luna, F. M.; Oliveira, A. G.; Miura, R. T.; Inoue, M. K.; Horita, L. G.; de Souza, D. F.; Dominiquini, F.; Alvaro, A.; Lima, C. S.; Ogawa, F. O.; Gomes, G. B.; Palandrani, J. F.; dos Santos, G. F.; de Freitas, E. M.; Mattiuz, A. R.; Costa, I. C.; de Almeida, C. L.; Souza, S.; Baudet, C.; Higa, R. H. STING Millennium: A web-based suite of programs for comprehensive and simultaneous analysis of protein structure and sequence. *Nucleic Acids Res.* **2003**, *31*, 3386−3392.

(49) Wiederstein, M.; Sippl, M. J. ProSA-web: interactive web service for the recognition of errors in three-dimensional structures of proteins. *Nucleic Acids Res.* **2007**, *35*, W407−W410.

(50) Kozakov, D.; Beglov, D.; Bohnuud, T.; Mottarella, S. E.; Xia, B.; Hall, D. R.; Vajda, S. How good is automated protein docking? *Proteins: Struct., Funct., Bioinf.* **2013**, *81*, 2159−2166.

(51) Vajda, S.; Yueh, C.; Beglov, D.; Bohnuud, T.; Mottarella, S. E.; Xia, B.; Hall, D. R.; Kozakov, D. New additions to the C plus P to server motivated by CAPRI. *Proteins: Struct., Funct., Bioinf.* **2017**, *85*, 435−444.

(52) Biovia, D. S. Discovery studio modeling environment. Release 2017.

(53) Higgins, D. G.; Sharp, P. M. CLUSTAL: a package for performing multiple sequence alignment on a microcomputer. *Gene* **1988**, *73*, 237−244.

J

(54) Eswar, N.; Webb, B.; Marti-Renom, M. A.; Madhusudhan, M.; Eramian, D.; Shen, M. y.; Pieper, U.; Sali, A. Comparative protein structure modeling using Modeller. *Curr. Protoc. Bioinf.* **2006**, *15*, 5.6.1–5.6.30.

(55) Jorgensen, W. L.; Chandrasekhar, J.; Madura, J. D.; Impey, R. W.; Klein, M. L. Comparison of simple potential functions for simulating liquid water. *J. Chem. Phys.* **1983**, *79*, 926–935.

(56) Maier, J. A.; Martinez, C.; Kasavajhala, K.; Wickstrom, L.; Hauser, K. E.; Simmerling, C. ff14SB: improving the accuracy of protein side chain and backbone parameters from ff99SB. *J. Chem. Theory Comput.* **2015**, *11*, 3696–3713.

(57) Abraham, M. J.; Murtola, T.; Schulz, R.; Páll, S.; Smith, J. C.; Hess, B.; Lindahl, E. GROMACS: High performance molecular simulations through multi-level parallelism from laptops to super-computers. *SoftwareX* **2015**, *1*, 19–25.

(58) Páll, S.; Abraham, M. J.; Kutzner, C.; Hess, B.; Lindahl, E. Tackling exascale software challenges in molecular dynamics simulations with GROMACS. In *International conference on exascale applications and software*; Springer: 2014; pp. 3–27.

(59) Bussi, G.; Donadio, D.; Parrinello, M. Canonical sampling through velocity rescaling. *J. Chem. Phys.* **2007**, *126*, No. 014101.

(60) Berendsen, H. J.; Postma, J. v.; van Gunsteren, W. F.; DiNola, A.; Haak, J. R. Molecular dynamics with coupling to an external bath. *J. Chem. Phys.* **1984**, *81*, 3684–3690.

(61) Hess, B.; Bekker, H.; Berendsen, H. J.; Fraaije, J. G. LINCS: a linear constraint solver for molecular simulations. *J. Comput. Chem.* **1997**, *18*, 1463–1472.

(62) Darden, T.; York, D.; Pedersen, L. Particle mesh Ewald: An N·log (N) method for Ewald sums in large systems. *J. Chem. Phys.* **1993**, *98*, 10089–10092.

(63) Humphrey, W.; Dalke, A.; Schulten, K. VMD: visual molecular dynamics. *J. Mol. Graph.* **1996**, *14*, 33–38.

(64) Galgonek, J.; Vymětal, J.; Jakubec, D.; Vondrášek, J. Amino acid interaction (INTAA) web server. *Nucleic Acids Res.* **2017**, *45*, W388–W392.

(65) Onufriev, A.; Bashford, D.; Case, D. A. Exploring protein native states and large-scale conformational changes with a modified generalized born model. *Proteins: Struct., Funct., Bioinf.* **2004**, *55*, 383–394.

Příloha 4

BOUSOVA, K., **ZOUHAROVA, M.**, HERMAN, P., VETYSKOVA, V., JIRASKOVA, K. & VONDRASEK, J. 2021b. TRPM7 N-terminal region forms complexes with calcium binding proteins CaM and S100A1. *Heliyon,* 7**,** e08490.

Research article

TRPM7 N-terminal region forms complexes with calcium binding proteins CaM and S100A1

Kristyna Bousova [a,*], Monika Zouharova [a,b], Petr Herman [c], Veronika Vetyskova [a,d], Katerina Jiraskova [a], Jiri Vondrasek [a]

[a] Department of Bioinformatics, Institute of Organic Chemistry and Biochemistry of the Czech Academy of Sciences, Flemingovo namesti 2, 16000 Prague, Czech Republic
[b] Department of Biochemistry and Patobiochemistry, Second Faculty of Medicine, Charles University, 150 06 Prague 5, V Uvalu 84, Czech Republic
[c] Department Faculty of Mathematics and Physics, Charles University, Ke Karlovu 5, 12116 Prague, Czech Republic
[d] Department of Biochemistry and Microbiology, University of Chemistry and Technology Prague, Technicka 5, 166 28 Prague, Czech Republic

GRAPHICAL ABSTRACT
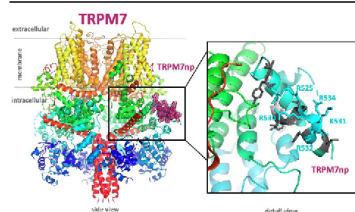
ARTICLE INFO

ABSTRACT

Transient receptor potential melastatin 7 (TRPM7) represents melastatin TRP channel with two significant functions, cation permeability and kinase activity. TRPM7 is widely expressed among tissues and is therefore involved in a variety of cellular functions representing mainly Mg^{2+} homeostasis, cellular Ca^{2+} flickering, and the regulation of DNA transcription by a cleaved kinase domain translocated to the nucleus. TRPM7 participates in several important biological processes in the nervous and cardiovascular systems. Together with the necessary function of the TRPM7 in these tissues and its recently analyzed overall structure, this channel requires further studies leading to the development of potential therapeutic targets. Here we present the first study investigating the N-termini of TRPM7 with binding regions for important intracellular modulators calmodulin (CaM) and calcium-binding protein S1 (S100A1) using in vitro and in silico approaches. Molecular simulations of the discovered complexes reveal their potential binding interfaces with common interaction patterns and the important role of basic residues present in the N-terminal binding region of TRPM.

1. Introduction

The transient receptor potential melastatin subfamily member 7 (TRPM7) is ubiquitously expressed chanzyme mediating divalent cations

Ca^{2+}, Mg^{2+}, Zn^{2+} transport. TRPM7 is involved in a number of cellular functions and is critically associated with cell proliferation, growth, apoptosis, Mg^{2+} homeostasis, Ca^{2+} signalling, including receptor tyrosine kinase mediated pathways [1, 2]. TRPM7 kinase requires Mn^{2+} or

---

Mg^{2+} for its activity and mainly uses Mg-ATP for phosphorylation [3]. Abundant auto-phosphorylation of TRPM7 increases kinase activity and substrates recognition [4, 5]. Tissue specific deletion of TRPM7 in thymocytes or macrophages, as well as inactivation of kinase activity, emphasized the importance of this channel in immune system function [6]. TRPM7 α-kinase can also be cleaved and translocated to the nucleus to modulate gene expression [7, 8]. Despite the many similarities shared by TRPM6 and TRPM7, they still modulate cell functions differently and their responses cannot be compensated by each other [9].

The cryo-EM structure of TRPM7 (lacking the α-kinase domain) revealed a similar overall architecture as the other TRPM members [10]. However, the conformation of the N-terminal cytosolic melastatin homology regions (MHR) differ between TRPM7 and another structurally characterized melastatin TRP member, TRPM4 channel. In both TRPM7 and TRPM4, the C-terminal stretcher helix penetrates through the MHR regions to the TRP box domain which could lead to signal transfer from the N-terminal MHR domains to the S6 pore gating helix. Such structural information suggests more complex modulation mechanisms in TRPM channels. It has been discovered by electrophysiology methods that TRPM7 activity is inhibited by increasing cytosolic Mg^{2+}/Mg-ATP and PIP2 hydrolysis [11, 12]. Negative modulation of TRPM7 by Ca^{2+} is at least partially mediated by Ca^{2+}/CaM-dependent kinase II [13, 14]. Possible direct or indirect and more complex regulation of TRPM7 by CaM/Ca^{2+} still needs to be explored. The closest member to TRPM7, the TRPM6 member has already revealed overlapping binding epitopes for CaM and S100A1 at the N-termini [15].

Calcium as a universal second messenger involved in fundamental physiological processes including fertilization, proliferation, neurotransmission, muscle contraction, bone formation, apoptosis, etc. [16, 17] can also act through protein mediators. Calcium-binding proteins (CBPs) represent family that is part of important multifunctional Ca^{2+} dependent messengers expressed in most of eukaryotic cells [18]. Representatives of the CBPs family are the well-described monomeric calmodulin (CaM) [19] and the dimeric protein S100 calcium-binding A1 (S100A1) [20, 21]. In many regulatory pathways of ion channels, Ca^{2+}-induced modulation is controlled by the interaction of these intracellular CBPs to the channel binding regions exposed to the intracellular environment [22, 23]. These types of interactions are often created by multicomplex machineries and can lead to many variations of activation, inhibition or non-trivial interplay activities in the channel regulation.

We identified novel CaM and S100A1 binding regions present at the N-terminus of TRPM7. The binding regions of TRPM7 involved in the interactions with the ligands was investigated using fluorescent spectroscopy method accompanied by an atomistic explanation of the binding interfaces addressed by molecular modelling. To support the evidence for significant amino acids of the TRPM7 binding regions participating on TRPM7/CaM and TRPM7/S100A1 complex formations, we characterized these amino acids using multiple sequence analysis of TRPM binding regions. This analysis was supported by molecular models of the identified complexes built on the TRPM7 structure [10]. The common mechanisms of interaction of CaM and S100A1 with the TRP binding region have been validated and may help to design potential therapeutic targets.

2. Materials and methods

2.1. Design of TRPM7 N-termini binding regions

The human TRPM7 cDNA sequence was analyzed to detect a potential CaM/S100A1 binding motif using the Calmodulin Target Database [24]. To demonstrate the presence of CaM and S100A1 binding region at the N-terminal of TRPM7, we selected the TRPM7np UniProtKB/SwissProt: Q96QT4, position T523-L535. TRPM7np was synthesized as a peptide and interactions to CaM and S100A1 were investigated by *in vitro* fluorescence anisotropy and *in silico* molecular modelling approaches.

2.2. TRPM7np peptide synthesis

Wild-type TRPM7np sequence was synthesized as a peptide by GenicBio Limited (Shanghai, China) and supplied in lyophilized powder. The peptide was C-terminally labelled with fluorescein-5-isothiocyanate (FITC, PubChem CID: 18730). The purity of the peptide was >90%, checked by HPLC (GenicBio Limited, Shanghai, China). Peptide probes were dissolved in 50 mM Tris-HCl buffer (pH 7.5) containing 500 mM NaCl and 1 mM $CaCl_2$.

2.3. CaM and S100A1 expression and purification

CaM and S100A1 cDNAs were subcloned into the expression vector pET28b and were expressed and purified according to our standard purification protocol [25].

2.4. Steady-state fluorescence anisotropy measurements

Steady-state fluorescence anisotropy measurements were performed using PC1 photon counting spectrometer (ISS Inc., Champaign, Illinois, USA) at RT. The samples were titrated in a 2-mm cuvette with increasing aliquots of 100 μM protein. Fluorescence was excited at 495 nm; the emission in parallel ($I_\parallel$) and perpendicular ($I_\perp$) orientations to the direction of the polarised excitation was gained at 520 nm by switching the emission polariser. The steady-state fluorescence anisotropy value (r) was calculated from the equation $r = (I_\parallel - I_\perp)/(I_\parallel + 2I_\perp)$. Further analysis was based on the mean anisotropy value calculated from five independent measurements for each protein addition. The fractions of bound (FB) CaM/S100A1 were expressed as [26]:

$$FB = (r_{obs} - r_{min}) \: / \: [(r_{max} - r_{obs}) \: Q + (r_{obs} - r_{min})], \qquad (1)$$

where r_{max} is the anisotropy of a saturated binding complex, r_{min} stands for the anisotropy of a peptide probe without a ligand and r_{obs} is the anisotropy at a particular protein concentration. Q represents the quantum yield ratio of the bound to the free peptide, calculated from fluorescence lifetimes (τ) according to equation

$$Q = Q_{bound}/Q_{free} = \tau_{bound}/\tau_{free}. \qquad (2)$$

To determine the equilibrium dissociation constant (KD), FB was plotted as a function of protein concentration and fitted by a single-binding-site model [27]:

$$FB = \frac{KD + [P1] + [P2] - \sqrt{(KD + [P1] + [P2])^2 - 4[P1][P2]}}{2[P1]}, \qquad (3)$$

where [P1] is the peptide concentration and [P2] is the protein concentration. Nonlinear data fitting was performed using SigmaPlot 11.0 (Systat Software Inc., San Jose, USA).

2.5. TRPM7np molecular model built from TRPM7 structure

The TRPM7np molecular model was built from the original Cryo-EM structure (3.28 Å) of mouse TRPM7 (PDB: 5ZX5) [28]. The initial structure of TRPM7np (UniProtKB/SwissProt: Q96QT4, positions: T523-L535) was completely defined by positions T523-L535 extracted in PDB coordinates from TRPM7 structure (PDB: 5ZX5) [10]. The additional criteria for TRPM7np structure were applied according to geometry requirements of the potential CaM- and S100A1-binding regions for TRPM7np based on known experimental structures of CaM and S100A1 with receptor derived peptide complexes (PDB: 3SUI, 2K2F). The specific attention was paid to the positions of the basic and hydrophobic residues in TRPM7np which should be exposed to the solvent. Consequently the TRPM7np model was optimised keeping coordinates of backbone atoms constrained by MOE optimization algorithm [29]. The final structure was assessed by STING Millennium [30] and ProSA-web [31].

2.6. TRPM binding regions analysis

To predict the basic amino acid residues of TRPM7np involved in the interactions with CaM/S100A1, we performed multiple sequence alignment of already *in vitro* characterized TRPM binding regions for CaM and S100A1 using CLUSTAL 1.2.4. software [32].

2.7. Models of TRPM7np complexes with CaM and S100A1

Docking of CaM and S100A1 into the TRPM7np structural model was performed using the ClusPro platform [33, 34, 35]. The CaM and S100A1 templates were selected from the structures of the TRPV1 complexes with CaM/Ca^{2+} (PDB: 3SUI) and RyR1 with S100A1/Ca^{2+} (PDB: 2K2F). Molecular models of the TRPM7np/CaM and TRPM7np/S100A1 complexes were built with respect to predicted binding interfaces [29]. Schematic representations of all four complexes were generated using Discovery Studio Visualizer [36].

3. Results

3.1. Characterization of the N-terminal binding region of TRPM7

The human TRPM7 sequence was analyzed in silico for potential CaM-binding region using the Calmodulin Target Database [24]. The TRPM7 binding region was identified in the proximal N-terminus of the channel between position T523 and L535 (Figure 1A–B). TRPM7np (see Material and Methods) contains aromatic and hydrophobic amino acids (Y524–Y528–F533) arranged in 1-5-10 CaM-binding motif, and five interspaced basic amino acids (R525, R530, K531, R532 and R534). Due to the known shared binding epitopes of CaM and S100A1 at e.g., ryanodine (RyR) or TRP receptors [22, 25, 37, 37, 38], we also decided to investigate binding site of S100A1 at TRPM7np. The position of TRPM7np in the TRPM7 structure (PDB: 5ZXZ) proves the accessibility of

the binding region to intracellular environment and the basic amino acid residues of TRPM7np are exposed out of the TRPM7 structure backbone which suggest suitable condition for complex formation with the ligands (Figure 2A–C).

3.2. TRPM7np forms a complex with CaM

Evaluation of CaM binding to TRPM7np was performed by measuring steady state fluorescence anisotropy with FITC-labelled TRPM7np (Figure 3A). Fluorescence anisotropy of the TRPM7np peptide was measured during CaM titration. TRPM7np about c = 1μM concentration was incubated (1 min) with a gradually increasing volume of CaM about stock solution c = 118 μM led to a reduction in its rotational diffusion, which led to an apparent increase in fluorescence anisotropy. The ratio of the quantum yield (Q) of CaM bound to the free peptide was calculated from the corresponding fluorescence lifetimes. The Q value was used to determine the CaM-bounded fraction (FB) of TRPM7np at each CaM titration point. Finally, FB was plotted against a specific concentration of CaM and the equilibrium dissociation constant (KD) for the TRPM7np/ CaM complex was determined. The CaM-binding affinity of TRPM7np is within the micromolar range and the KD was calculated to be 6.1 (SD 0.4) μM (Figure 3B).

3.3. TRPM7np forms a complex with S100A1

S100A1 recognizes transient receptor potential (TRP) channels binding motifs in a manner similar to CaM. The S100A1 and CaM binding regions often overlap, and S100A1/CaM can compete for the same binding site on the target protein [22, 39]. Based on our previous experience of shared CaM binding regions with S100A1 [25, 37, 37, 38, 39] we also investigated the possible binding of S100A1 to the identified CaM-binding epitope to TRPM7np (Figure 3A). The interaction of S100A1 with TRPM7np was confirmed by steady state fluorescence
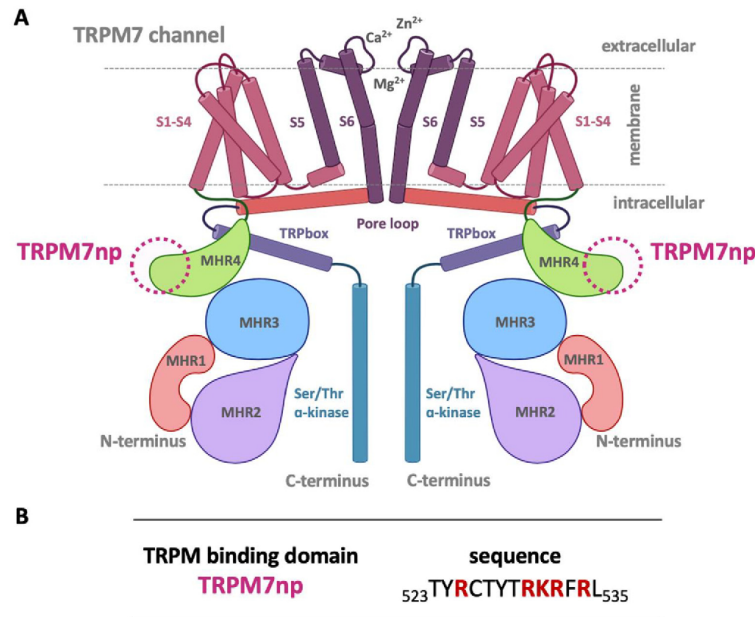

Figure 1. Shared CaM and S100A1 binding region on TRPM7. (A) Common membrane topology of the TRPM7 (homodimer in scheme) with the location of the TRPM7np binding epitope (purple dashed circle) shown in both monomeric units; the biological formation of TRPM7 channel appears commonly in homo-tetramer formation. TRP channels consist of six transmembrane helices (S1–S6) with a pore loop and a pore helix between S5 and S6. The long cytoplasmic N-terminus contains melastatin homology regions (MHR 1–4), the C-terminus contains TRP box, Ser/Thr and alpha-kinase regions. The cytosolic regions often contain specific binding regions for modulatory molecules. (B) Amino acid sequence of the TRPM7np (UniProtKB/SwissProt: Q96QT4, position T523-L535) binding epitope with red highlighted basic residues investigated as novel CaM/S100A1 binding sites.
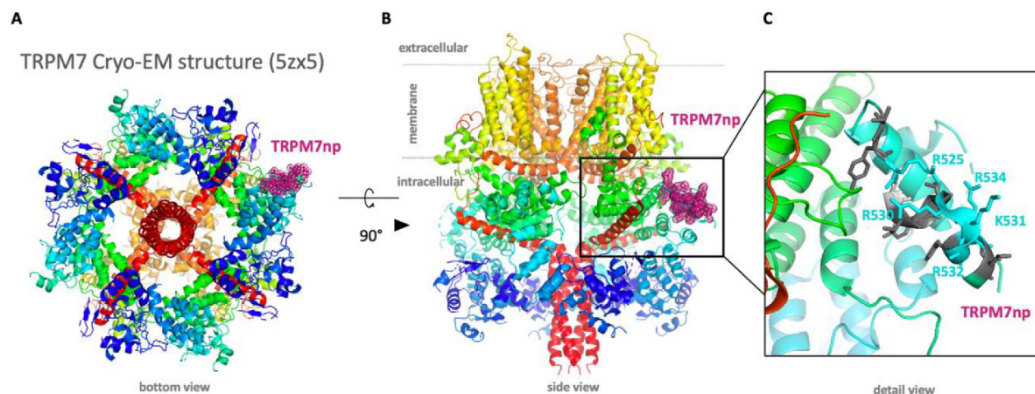
Figure 2. TRPM7np localization in the TRPM7 channel (PDB: 5ZX5). (A) Bottom view of the whole TRPM7 structure with the purple TRPM7np localization on the right. (B) Side view of the whole TRPM7 structure. The frame localizes TRPM7np binding site. (C) The corresponding region of TRPM7 known to bind CBDs in TRPM6. Detail of the TRPM7np potential binding site for CaM and S100A1 displaying the accessible amino acid side chains of TRPM7np potentially significant for the interactions. Grey sticks indicate the hydrophobic amino acids and blue sticks indicate the basic amino acids R525, R530, K531, R532, R534 predicted to be responsible for the interactions with ligands.

anisotropy similar to that described above for CaM binding experiments. TRPM7np about $c = 1\mu M$ concentration was incubated (1 min) with a gradually increasing volume of S100A1 about stock solution $c = 112\ \mu M$ led to a reduction in its rotational diffusion, which led to an apparent increase in fluorescence anisotropy. FB TRPM7np as a function of

S100A1 concentration according to equation (Equation 2) provided the expected binding isotherm. The KD value evaluated by steady state fluorescence anisotropy experiments was 38.0 (SD 2.0) μM for the TRPM7np/S100A1 complex (Figure 3B). The binding of TRPM7np to S100A1 indicated a slightly weaker affinity than for CaM. Differences in binding affinities between CaM and S100A1 could suggest the mechanism of ligands with different binding modes of interaction.

3.4. Analysis of TRPM7np binding specificity by multiple sequence alignment
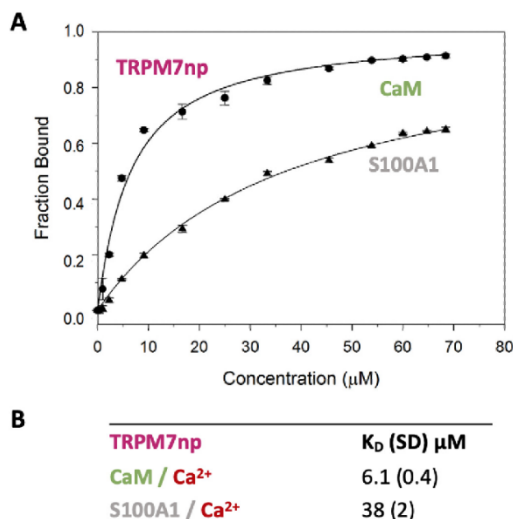
Figure 3. TRPM7np interacts with CaM and S100A1. The bound fractions (F_B) of (A) TRPM7np as a function of CaM and S100A1 concentration were obtained from steady-state fluorescence anisotropy experiments. Binding isotherms (solid lines) were generated from the best fit using Eq. (2) (Materials and Methods). Five independent measurements were performed for each gradually increasing CaM/S100A1 concentrations (stock solutions c (CaM)   118 μM, c (S100A) 112 μM) and the calculated SD is represented by error bars. (B) The equilibrium dissociation constants (KD) of CaM/S100A1 interactions with TRPM7np together with corresponding standard deviations (SD).

TRP interactions with CaM or S100A1 are maintained by hydrophobic and basic amino acid residues. Alanine scanning mutagenesis of basic residues in the TRP binding region prevented the complex formation in many studied complexes [25, 37, 40, 41]. Therefore, it has been concluded that non-covalent interactions play the most significant role in these complex formations. TRP binding regions carry typical clusters of positively charged residues [25, 37]. The multiple sequence alignment analysis of TRPM binding regions revealed consensus sequences of basic amino acid residues (RxxxxR/K, where x is any amino acid) in analysed regions (Figure 4) suggested the importance of R525, R530, K531, R532 and R534 in TRPM7np. This analysis of multiple TRPM sequences was

Figure 4. Multiple alignment of selected CaM binding regions in TRPM channels. CLUSTAL 1.2.4 multiple sequence alignment of CaM/S100A1 binding regions of TRPMs N-termini [15, 25, 37, 38, 40, 41]. The sequence alignment shows a first perfect match (indicated by an asterisk) of arginine residues and second almost accurate match (indicated by dots) of basic residues across the TRPM sequences. Red colour stands for hydrophobic, pink for basic, blue for acidic amino acids; all others amino acids stand for green. The number on the right side of the sequence marks its amino acid length.
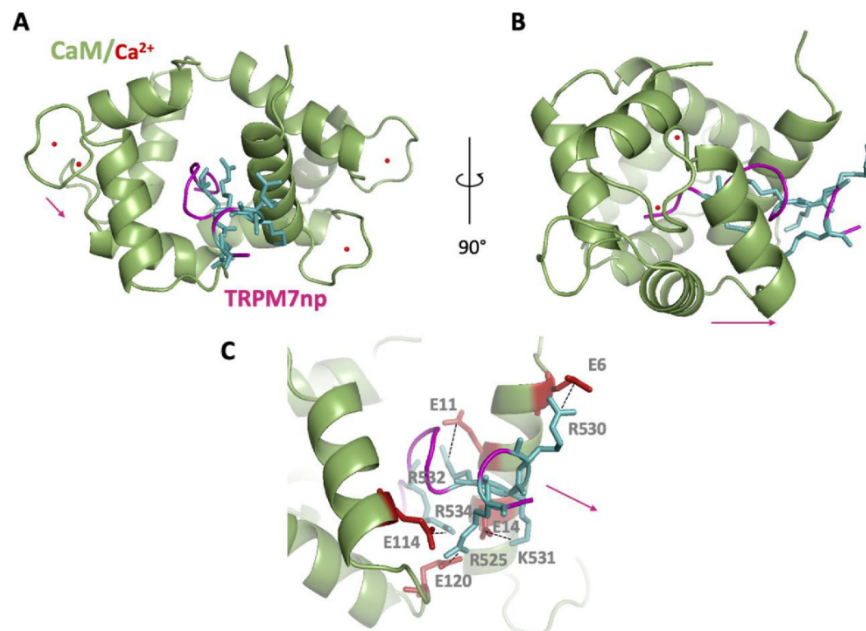
Figure 5. In silico analysis of the TRPM7np/CaM complex interface. (A) Top view of the TRPM7np/CaM-Ca^{2+} complex representation 1:1. TRPM7np (backbone in violet) and CaM (backbone in green, red balls represent calcium ions) composing the binding interface, the blue side chains represent basic amino acids of TRPM7np interacting with CaM. (B) Side view of TRPM7np/CaM complex ribbon representation with the same binding interface. (C) Detailed representation of TRPM7np positively charged residues R525, R530, K531, R532 and R534 (blue sticks) with negatively charged residues of CaM E6, E11, E14, E114 and E120 (red sticks) predicted to be involved in the non-covalent bonding. The colour convention was used same as in the A representation. The violet arrow symbolizes the direction of the helix (pseudo-helix) for a clear visualization of the orientation of the TRPM7np in the complex.

performed from *in vitro* experimentally characterized TRPM binding regions for CaM and S100A1 [25, 37, 38, 40, 41].

The highest sequence similarity was identified for TRPM7np and TRPM6np. The binding regions share an identical 1-5-10 hydrophobic binding motif at positions Y524–Y528–F533 (TRPM7np) and Y525–Y529–F534 (TRPM6np). TRPM7np and TRPM6np contain four basic residues R525-R530-K531-R534 in TRPM7 and R526-R531-K532-R535 in TRPM6 in the same position with respect to the hydrophobic motif. Alignment revealed a strong agreement for TRPM7np R525 and R530 with all TRPM binding epitopes. In addition, TRPM7np K531 and R534 are consistent with the basic residues of TRPM6np, as expected, due to their closest TRP member. Only TRPM7np R532 did not correspond to consensus with other TRPM-binding epitopes. Therefore, we assume that the TRPM7np cluster R525, R530, K531 and R534 has the highest tendency to engage in the interactions with CaM/S100A1.

3.5. TRPM7np/CaM and TRPM7np/S100A1 complexes in silico analysis

The general strategy was to use ClusPro2.0 as the ligand docking procedure for CaM and S100A1 [34]. The final TRPM7np/CaM-Ca^{2+} complex (Figure 5A, B) was chosen from results of ClusPro docking using the highest compliance with the previously published structure of the TRPV1p/CaM complex (PDB: 3SUI) [25, 37, 38, 42]. The TRPM7np/S100A1- Ca^{2+} complex (Figure 6A, B) was built by same approach using crystal structure of the RyR1P12/S100A1 complex (PDB: 2K2F) [43]. Finally, we optimised the identified binding modes by conjugate gradient energy minimisation implemented by MOE software constraining all backbone atoms of CaM/S100A1 with full relaxation of the peptide and side chains of CaM/S100A1 [29].

Further, the ligand docking analysis of TRPM7np/CaM and TRPM7np/S100A1 complexes predicted that R525, R530, K531, R532 and R534 of TRPM7np are involved in the interactions with negatively charged residues of CaM and S100A1. Specifically, the negatively charged residues of CaM involved in TRPM7np interactions were identified as: E6, E11, E14, E114 and E120 which correspond to CaM negative residues involved in the interactions in TRPV6/CaM complex [44]. The S100A1 residues D46, D52, N86 involved in TRPM7np interactions correspond to the negative cluster of S100A1 involved at TRPM6np/S100A1 complex formation [15]. The ligand docking supported the proposal of high participation of TRPM7np R525, R530, K531, R532 and R534 basic residues in the complex formations with CaM and S100A1 as predicted by multiple sequence alignment of TRPM binding regions.

4. Discussion

TRP channels are commonly known to be modulated by many intracellular and extracellular modulators [45, 46, 47, 48, 49]. CaM belongs to a significant game player in overall cellular metabolism and signalling with a dominant function in regulations in calcium homeostasis [17]. While countless CaM binding regions in TRP channels have been characterized [42, 50, 51], the regulatory or signalling functions of CaM in such ion transports remains still under necessary investigation. We are currently beginning to understand how protein machines, such as transmembrane receptors, are regulated, and it is necessary to discover every piece of the puzzle to understand the complexity involved in these processes. In recent years, number of publications mentioning more binding sites and more complex processes of interactions in
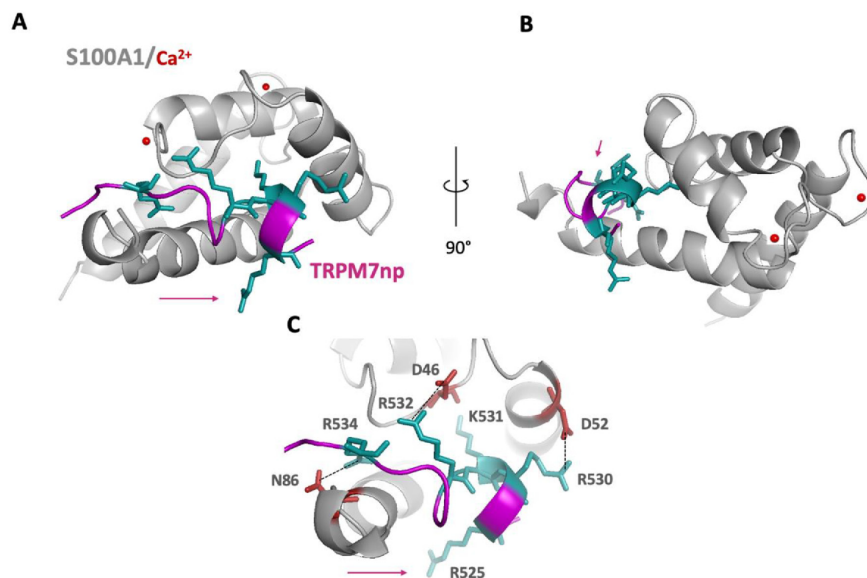
Figure 6. In silico analysis of the TRPM7np/S100A1 complex interface. (A) Top view of the TRPM7np/S100A1-Ca^{2+} complex 1:1. TRPM7np (backbone in violet) and S100A1 (backbone in grey, red balls represent calcium ions) composing the binding interface, the blue side chains represent basic amino acids of the TRPM7np interacting with S100A1. (B) Side view of TRPM7np/CaM complex ribbon representation with the same binding interface. (C) Detailed representation of TRPM7np positively charged residues R525, R530, K531, R532 and R534 (blue sticks) with negatively charged residues of S100A1 D46, D52 and N86 (red sticks) predicted to be involved in the non-covalent bonding. The colour convention was used as in the A representation. The violet arrow symbolizes the direction of the helix (pseudo-helix) for a clear visualization of the orientation of the TRPM7np in the complex.

ligands/receptors complexes have begun to rise [50]. The whole mechanism of modulation of membrane receptors has been expected to be much more complex than protein functions and interactions explained in the past.

In this work, we contribute by identification and characterization new CaM and S100A1 binding sites at the N-terminal intracellular tail of the TRPM7 channel. The provided insight into the understanding of the mechanisms of TRPM7 interactions with intracellular potential modulatory CBPs [51, 52, 53] was investigated based on our theoretical and experimental experience with the identification and characterization of similar interactions of TRPM members with CaM and S100A1 [25, 37, 38, 41]. Based on current knowledge, we hypothesize that shared CaM/S100A1 binding epitopes are a common phenomenon across all members of TRPs [22, 25, 37]. We identified a new TRPM7np T523-L535 binding region revealing the ability to bind CaM and S100A1. Our biophysical and computational characterization of TRPM7np complexes with modulatory ligands CaM and S100A1 may help to elucidate the mechanism of TRPM7 channel function [54]. The structural resolution from CryoEM analysis revealed an accessible TRPM7np binding region located throughout the TRPM7 channel. The dissociation constants of both identified complexes TRPM7np/CaM and TRPM7np/S100A1 range in typical micromolar levels for these TRP interactions. Both complexes are formed upon Ca^{2+} presence [25, 37]. Multiple sequence alignment of TRPM binding regions indicated the importance of basic residues in TRPM7np. The interface formation of the TRPM7np/CaM and TRPM7np/S100A1 complexes based on non-covalent interactions was also supported by *in silico* ligand docking analysis. Insight into the interface of the complexes provided by molecular docking with atomistic resolution can also help us understand the potential initiation of channel dysfunctions associated with severe disorders [1, 2, 14]. Therefore, we expect the information provided in the current study and in our previous

TRPM projects [25, 37, 37, 38, 41] may help to clarify a deeper understanding of TRPM channel function in general and may further assist in the design of new therapeutics for ion channel modulation.

Declarations

Author contribution statement

Kristyna Bousova: Conceived and designed the experiments; Performed the experiments; Analyzed and interpreted the data; Contributed reagents, materials, analysis tools or data; Wrote the paper.

Monika Zouharova: Performed the experiments; Analyzed and interpreted the data; Wrote the paper.

Petr Herman: Performed the experiments; Analyzed and interpreted the data.

Veronika Vetyskova: Performed the experiments.

Katerina Jiraskova: Analyzed and interpreted the data.

Jiri Vondrasek: Analyzed and interpreted the data; Contributed reagents, materials, analysis tools or data.

Funding statement

Data availability statement

Data included in article/supplementary material/referenced in article.

Declaration of interests statement

The authors declare no conflict of interest.

Additional information

No additional information is available for this paper.

References

[1] Z.G. Zou, F.J. Rios, A.C. Montezano, R.M. Touyz, TRPM7, magnesium, and signaling, Int. J. Mol. Sci. 20 (8) (2019).

[2] N. Abumaria, W. Li, A.N. Clarkson, Role of the chanzyme TRPM7 in the nervous system in health and disease, Cell. Mol. Life Sci. 76 (17) (2019) 3301 3310.

[3] L.V. Ryazanova, M.V. Dorovkov, A. Ansari, A.G. Ryazanov, Characterization of the protein kinase activity of TRPM7/ChaK1, a protein kinase fused to the transient receptor potential ion channel, J. Biol. Chem. 279 (5) (2004) 3708 3716.

[4] T.Y. Kim, S.K. Shin, M.-Y. Song, J.E. Lee, K.-S. Park, Identification of the phosphorylation sites on intact TRPM7 channels from mammalian cells, Biochem. Biophys. Res. Commun. 417 (3) (2012) 1030 1034.

[5] K. Clark, J. Middelbeek, N.A. Morrice, C.G. Figdor, E. Lasonder, F.N. van Leeuwen, Massive autophosphorylation of the Ser/Thr-rich domain controls protein kinase activity of TRPM6 and TRPM7, PLoS One 3 (3) (2008), e1876.

[6] A. Romagnani, V. Vettore, T. Rezzonico-Jost, S. Hampe, E. Rottoli, W. Nadolni, et al., TRPM7 kinase activity is essential for T cell colonization and alloreactivity in the gut, Nat. Commun. 8 (1) (2017) 1 14.

[7] G. Krapivinsky, L. Krapivinsky, Y. Manasian, D.E. Clapham, The TRPM7 chanzyme is cleaved to release a chromatin-modifying kinase, Cell 157 (5) (2014) 1061 1072.

[8] G. Krapivinsky, L. Krapivinsky, N.E. Renthal, A. Santa-Cruz, Y. Manasian, D.E. Clapham, Histone phosphorylation by TRPM6's cleaved kinase attenuates adjacent arginine methylation to regulate gene expression, Proc. Natl. Acad. Sci. U. S. A. 114 (34) (2017) E7092 E7100.

[9] S. Ferioli, S. Zierler, J. Zaißerer, J. Schredelseker, T. Gudermann, V. Chubanov, TRPM6 and TRPM7 differentially contribute to the relief of heteromeric TRPM6/7 channels from inhibition by cytosolic Mg 2+ and Mg· ATP, Sci. Rep. 7 (1) (2017) 1 19.

[10] J. Duan, Z. Li, J. Li, R.E. Hulse, A. Santa-Cruz, W.C. Valinsky, et al., Structure of the mammalian TRPM7, a magnesium channel required during embryonic development, Proc. Natl. Acad. Sci. U. S. A. 115 (35) (2018) E8201 E8210.

[11] L.W. Runnels, L. Yue, D.E. Clapham, The TRPM7 channel is inactivated by PIP(2) hydrolysis, Nat. Cell Biol. 4 (5) (2002) 329 336.

[12] M.J. Nadler, M.C. Hermosura, K. Inabe, A.L. Perraud, Q. Zhu, A.J. Stokes, et al., LTRPC7 is a Mg.ATP-regulated divalent cation channel required for cell viability, Nature 411 (6837) (2001) 590 595.

[13] R. Mishra, V. Rao, R. Ta, N. Shobeiri, C.E. Hill, Mg2+- and MgATP-inhibited and Ca2+/calmodulin-sensitive TRPM7-like current in hepatoma and hepatocytes, Am. J. Physiol. Gastrointest. Liver Physiol. 297 (4) (2009) G687 G694.

[14] E. Turlova, R. Wong, B. Xu, F. Li, L. Du, S. Habbous, et al., TRPM7 mediates neuronal cell death upstream of calcium/calmodulin-dependent protein kinase II and calcineurin mechanism in neonatal hypoxic-Ischemic brain injury, Transl. Stroke Res. 12 (1) (2021) 164 184.

[15] M. Zouharova, P. Herman, K. Hofbauerova, J. Vondrasek, K. Bousova, TRPM6 N-terminal CaM- and S100A1-binding domains, Int. J. Mol. Sci. 20 (18) (2019).

[16] D.E. Clapham, Calcium signaling, Cell 131 (6) (2007) 1047 1058.

[17] R. Bagur, G. Hajnoczky, Intracellular Ca(2+) sensing: its role in calcium homeostasis and signaling, Mol. Cell 66 (6) (2017) 780 788.

[18] F.C. Stevens, Calmodulin: an introduction, Can. J. Biochem. Cell Biol. 61 (8) (1983) 906 910.

[19] Y.S. Babu, J.S. Sack, T.J. Greenhough, C.E. Bugg, A.R. Means, W.J. Cook, Three-dimensional structure of calmodulin, Nature 315 (6014) (1985) 37.

[20] Z. Melville, E. Aligholizadeh, L.E. McKnight, D.J. Weber, E. Pozharski, D.J. Weber, X-ray crystal structure of human calcium-bound S100A1, Acta Crystallogr. F Struct. Biol. Commun. 73 (Pt 4) (2017) 215 221.

[21] J. Ritterhoff, P. Most, Targeting S100A1 in heart failure, Gene Ther. 19 (6) (2012) 613 621.

[22] N.T. Wright, B.L. Prosser, K.M. Varney, D.B. Zimmer, M.F. Schneider, D.J. Weber, S100A1 and calmodulin compete for the same binding site on ryanodine receptor, J. Biol. Chem. 283 (39) (2008) 26676 26683.

[23] R.T. Rebbeck, F.R. Nitu, D. Rohde, P. Most, D.M. Bers, D.D. Thomas, et al., S100A1 protein does not compete with calmodulin for ryanodine receptor binding but structurally alters the ryanodine receptor· calmodulin complex, J. Biol. Chem. 291 (30) (2016) 15896 15907.

[24] K.L. Yap, J. Kim, K. Truong, M. Sherman, T. Yuan, M. Ikura, Calmodulin target database, J. Struct. Funct. Genom. 1 (1) (2000) 8 14.

[25] K. Bousova, P. Herman, J. Vecer, L. Bednarova, L. Monincova, P. Majer, et al., Shared CaM-and S100A1-binding epitopes in the distal TRPM 4 N terminus, FEBS J. 285 (3) (2018) 599 613.

[26] C.C. Harper, J.M. Berg, S.J. Gould, PEX5 binds the PTS1 independently of Hsp70 and the peroxin PEX12, J. Biol. Chem. 278 (10) (2003) 7897 7901.

[27] K.A. Lacourciere, J.T. Stivers, J.P. Marino, Mechanism of neomycin and Rev peptide binding to the Rev responsive element of HIV-1 as determined by fluorescence and NMR spectroscopy, Biochemistry 39 (19) (2000) 5630 5641.

[28] V. Chubanov, L. Mittermeier, T. Gudermann, TRPM7 reflected in Cryo-EMirror, Cell Calcium 76 (2018) 129 131.

[29] S. Vilar, G. Cozza, S. Moro, Medicinal chemistry and the molecular operating environment (MOE): application of QSAR and molecular docking to drug discovery, Curr. Top. Med. Chem. 8 (18) (2008) 1555 1572.

[30] G. Neshich, R.C. Togawa, A.L. Mancini, P.R. Kuser, M.E. Yamagishi, G. Pappas Jr., et al., STING Millennium: a web-based suite of programs for comprehensive and simultaneous analysis of protein structure and sequence, Nucleic Acids Res. 31 (13) (2003) 3386 3392.

[31] M. Wiederstein, M.J. Sippl, ProSA-web: interactive web service for the recognition of errors in three-dimensional structures of proteins, Nucleic Acids Res. 35 (Web Server issue) (2007) W407 W410.

[32] F. Sievers, A. Wilm, D. Dineen, T.J. Gibson, K. Karplus, W. Li, et al., Fast, scalable generation of high-quality protein multiple sequence alignments using Clustal Omega, Mol. Syst. Biol. 7 (1) (2011).

[33] D. Kozakov, D. Beglov, T. Bohnuud, S.E. Mottarella, B. Xia, D.R. Hall, et al., How good is automated protein docking? Proteins: Struct. Funct. Bioinformat. 81 (12) (2013) 2159 2166.

[34] D. Kozakov, D.R. Hall, B. Xia, K.A. Porter, D. Padhorny, C. Yueh, et al., The ClusPro web server for protein protein docking, Nat. Protoc. 12 (2) (2017) 255.

[35] S. Vajda, C. Yueh, D. Beglov, T. Bohnuud, S.E. Mottarella, B. Xia, et al., New additions to the C lus P ro server motivated by CAPRI, Proteins: Struct. Funct. Bioinformat. 85 (3) (2017) 435 444.

[36] D.S. Biovia, Discovery Studio Modeling Environment, 2017. Release.

[37] B. Holakovska, L. Grycova, M. Jirku, M. Sulc, L. Bumba, J. Teisinger, Calmodulin and S100A1 protein interact with N terminus of TRPM3 channel, J. Biol. Chem. 287 (20) (2012) 16645 16655.

[38] K. Bousova, I. Barvik, P. Herman, K. Hofbauerová, L. Monincova, P. Majer, et al., Mapping of CaM, S100A1 and PIP2-binding epitopes in the intracellular N-and C-termini of TRPM4, Int. J. Mol. Sci. 21 (12) (2020) 4323.

[39] L. Grycova, B. Holendova, L. Bumba, J. Bily, M. Jirku, Z. Lansky, et al., Integrative binding sites within intracellular termini of TRPV1 receptor, PLoS One 7 (10) (2012), e48437.

[40] J. Bily, L. Grycova, B. Holendova, M. Jirku, H. Janouskova, K. Bousova, et al., Characterization of the S100A1 protein binding site on TRPC6 C-terminus, PLoS One 8 (5) (2013), e62677.

[41] M. Jirku, Z. Lansky, L. Bednarova, M. Sulc, L. Monincova, P. Majer, et al., The characterization of a novel S100A1 binding site in the N-terminus of TRPM1, Int. J. Biochem. Cell Biol. 78 (2016) 186 193.

[42] S.-Y. Lau, E. Procko, R. Gaudet, Distinct properties of Ca2+ calmodulin binding to N-and C-terminal regulatory regions of the TRPV1 channel, J. Gen. Physiol. 140 (5) (2012) 541 555.

[43] B.L. Prosser, N.T. Wright, E.O. Hernandez-Ochoa, K.M. Varney, Y. Liu, R.O. Olojo, et al., S100A1 binds to the calmodulin-binding site of ryanodine receptor and modulates skeletal muscle excitation-contraction coupling, J. Biol. Chem. 283 (8) (2008) 5046 5057.

[44] A.K. Singh, L.L. McGoldrick, E.C. Twomey, A.I. Sobolevsky, Mechanism of calmodulin inactivation of the calcium-selective TRP channel TRPV6, Sci. Adv. 4 (8) (2018), eaau6088.

[45] S. Dang, M.K. van Goor, D. Asarnow, Y. Wang, D. Julius, Y. Cheng, et al., Structural insight into TRPV5 channel function and modulation, Proc. Natl. Acad. Sci. Unit. States Am. 116 (18) (2019) 8869 8878.

[46] P. Demeuse, R. Penner, A. Fleig, TRPM7 channel is regulated by magnesium nucleotides via its kinase domain, J. Gen. Physiol. 127 (4) (2006) 421 434.

[47] R. Hasan, X. Zhang, Ca(2+) regulation of TRP ion channels, Int. J. Mol. Sci. 19 (4) (2018).

[48] D. Liu, E.R. Liman, Intracellular Ca2+ and the phospholipid PIP2 regulate the taste transduction ion channel TRPM5, Proc. Natl. Acad. Sci. U. S. A. 100 (25) (2003) 15160 15165.

[49] G. Owsianik, D. D'hoedt, T. Voets, B. Nilius, Structure-function relationship of the TRP channel superfamily, Rev. Physiol. Biochem. Pharmacol. 156 (2006) 61 90.

[50] W. Chen, Z. Shen, S. Asteriti, Z. Chen, F. Ye, Z. Sun, et al., Calmodulin binds to Drosophila TRP with an unexpected mode, Structure 29 (4) (2021) 330 344, e4.

[51] B. Nilius, J. Prenen, J. Tang, C. Wang, G. Owsianik, A. Janssens, et al., Regulation of the Ca2+ sensitivity of the nonselective cation channel TRPM4, J. Biol. Chem. 280 (8) (2005) 6423 6433.

[52] B. Liu, F. Qin, Functional control of cold- and menthol-sensitive TRPM8 ion channels by phosphatidylinositol 4,5-bisphosphate, J. Neurosci. 25 (7) (2005) 1674 1681.

[53] T. Rohacs, C.M.B. Lopes, I. Michailidis, D.E. Logothetis, PI(4,5)P-2 regulates the activation and desensitization of TRPM8 channels through the TRP domain, Nat. Neurosci. 8 (5) (2005) 626 634.

[54] Y. Hu, Q. Li, L.-H. Kurahara, N. Shioi, K. Hiraishi, T. Fujita, et al., An Arrhythmic mutation E7K facilitates TRPM4 channel activation via enhanced PIP2 interaction, Cells 10 (5) (2021) 983.

Příloha 5

BOUSOVA, K., BARVIK, I., HERMAN, P., HOFBAUEROVA, K., MONINCOVA, L., MAJER, P., **ZOUHAROVA, M.**, VETYSKOVA, V., POSTULKOVA, K. & VONDRASEK, J. 2020. Mapping of CaM, S100A1 and PIP2-Binding Epitopes in the Intracellular N- and C-Termini of TRPM4. *Int J Mol Sci,* 21.

Mapping of CaM, S100A1 and PIP2-Binding Epitopes in the Intracellular N- and C-Termini of TRPM4

Kristyna Bousova [1,*], Ivan Barvik [2], Petr Herman [2], Kateřina Hofbauerová [2,3],
Lenka Monincova [1], Pavel Majer [1], Monika Zouharova [1,4], Veronika Vetyskova [1],
Klara Postulkova [1] and Jiri Vondrasek [1]

[1]   Institute of Organic Chemistry and Biochemistry of the Czech Academy of Sciences, Flemingovo namesti 2,
       16000 Prague, Czech Republic; lenka.monincova@uochb.cas.cz (L.M.); pavel.majer@uochb.cas.cz (P.M.);
       monika.vargova@uochb.cas.cz (M.Z.); veronika.vetyskova@uochb.cas.cz (V.V.);
       klara.postulkova@uochb.cas.cz (K.P.); jiri.vondrasek@uochb.cas.cz (J.V.)
[2]   Faculty of Mathematics and Physics, Charles University, Ke Karlovu 5, 12116 Prague, Czech Republic;
       ibarvik@karlov.mff.cuni.cz (I.B.); herman@karlov.mff.cuni.cz (P.H.); hofbauer@karlov.mff.cuni.cz (K.H.)
[3]   Institute of Microbiology of the Czech Academy of Sciences, Videnska 1083, 14220 Prague, Czech Republic
[4]   Second Faculty of Medicine, Charles University, V Uvalu 84, 150 06 Prague, Czech Republic
[*]   Correspondence: kristyna.bousova@uochb.cas.cz; Tel.: +420-220-183-131

Abstract: Molecular determinants of the binding of various endogenous modulators to transient receptor potential (TRP) channels are crucial for the understanding of necessary cellular pathways, as well as new paths for rational drug designs. The aim of this study was to characterise interactions between the TRP cation channel subfamily melastatin member 4 (TRPM4) and endogenous intracellular modulators—calcium-binding proteins (calmodulin (CaM) and S100A1) and phosphatidylinositol 4, 5-bisphosphate (PIP_2). We have found binding epitopes at the N- and C-termini of TRPM4 shared by CaM, S100A1 and PIP_2. The binding affinities of short peptides representing the binding epitopes of N- and C-termini were measured by means of fluorescence anisotropy (FA). The importance of representative basic amino acids and their combinations from both peptides for the binding of endogenous TRPM4 modulators was proved using point alanine-scanning mutagenesis. In silico protein–protein docking of both peptides to CaM and S100A1 and extensive molecular dynamics (MD) simulations enabled the description of key stabilising interactions at the atomic level. Recently solved cryo-Electron Microscopy (EM) structures made it possible to put our findings into the context of the entire TRPM4 channel and to deduce how the binding of these endogenous modulators could allosterically affect the gating of TRPM4. Moreover, both identified binding epitopes seem to be ideally positioned to mediate the involvement of TRPM4 in higher-order hetero-multimeric complexes with important physiological functions.

Keywords: TRPM4 channel; binding epitope; PIP_2; CaM; S100A1; fluorescence anisotropy; docking; molecular dynamics simulations

1. Introduction

Transient receptor potential cation channel subfamily melastatin member 4 (TRPM4) is a nonselective monovalent cation channel that is activated and subsequently blocked by intracellular calcium (Ca^{2+}) [1] at negative plasma membrane potentials [2–4]. TRPM4 contains many regulatory motifs that modulate its Ca^{2+} responsiveness and voltage dependence [1,5–7]. Specific mutations in the TRPM4 gene lead to the inhibition of the channel function that directly causes familial cases of heart block disease [5]. Eight structures of the TRPM4 channel have been solved using single-particle

cryo-Electron Microscopy (EM) at an overall resolution ranging from 2.9 to 3.8 Å [8–11]. The TRPM4 structural topology represents a crown-like tetrameric transmembrane core with a domain-swapped architecture [9]. The cytoplasmic N- and C-termini are separated by six transmembrane helices (S1–S6) with a loop between S5 and S6, which works as a selectivity filter [9]. A cluster of hydrophobic amino acids from all four S6 helices forms a lower gate. The channel-gating can be allosterically influenced by endogenous modulators that bind to the intracellular tails of TRPM4. Similarly, the ultimate Ca^{2+} sensitivity is strongly regulated by several intracellular factors, including calmodulin (CaM), phosphatidylinositol 4, 5-bisphosphate (PIP_2), protein kinase C, ATP, etc. [1,12–14].

The cytosolic calcium-binding proteins CaM and S100A1 essentially participate in Ca^{2+} homeostasis in the cell. They are involved in many important cellular pathways due to their interactions with target messengers/receptors. The interactions of CaM or S100A1 with target-binding epitopes have been deeply analysed in the past [15–17]. Initially, these interactions are mediated through nonspecific long-range electrostatic interactions of negatively charged residues of CaM or S100A1 and positively charged residues from the binding epitopes of target receptors. Specific contacts are then formed between the so-called hydrophobic anchors from binding epitopes and dedicated hydrophobic cavities of CaM or S100A1. The specific positions of hydrophobic amino acids (either 1-5-10 and/or 1-8-14 [13,17–19]) are used for the bioinformatic identification of potential CaM-binding sites [17]. Indeed, several such binding sites have been proposed in the proximal C-terminal region of TRPM4 [12,20,21]. These binding sites seem to be interconnected to each other in a continuous sequence, because a deletion of any region has severely reduced the Ca^{2+} sensitivity of the TRPM4 channel [1].

The PIP_2 is one of the most abundant intracellular phospholipids [12]; it is also known as an extensive modulator of transient receptor potential channels (TRPs) [22]. Under physiological conditions, PIP_2 is negatively charged and interacts with positively charged binding epitopes in target proteins. They are often ordered into the so-called Pleckstrin homology (PH) domains with characteristic positions of basic residues [23]. Electrophysiology measurements have proved that the Ca^{2+} sensitivity of desensitised TRPM4 can be recovered by physiological concentrations of PIP_2 [24]. The proximal TRPM4 N-terminal binding sites for PIP_2 and PIP_3 with a modulatory function have recently been confirmed [24,25]. Moreover, the cytosolic C-terminal region proximal to the S1–S4 sensor domain involves a polybasic region that could constitute the PIP_2-binding site conserved among the TRPC, TRPV and TRPM channels [26]. Based on the cryo-EM structure of TRPM4, it has been proposed that the C-terminal re-entrant segment (protruding into the S1–S4 sensor) of TRPM4 harbours three positively charged arginine residues (R1072, R1086 and R1090) that provide an ideal binding site for membrane-bound PIP_2 [10]. The binding of PIP_2 around the S1–S4 sensor domains of different TRPs has been observed in recent cryo-EM structures [27–29]. Overall, the region near the S1–S4 sensor domain of TRPM4 appears to be a potential hotspot targeted by competing endogenous modulators (including CaM and PIP_2) that can affect TRPM4 gating.

Moreover, these endogenous compounds may function as a glue that mediates the incorporation of TRPM4 into hetero-multimeric complexes with unexpected physiological functions. The TRPM4-SUR1-AQP4 complex, involved in brain swelling, has recently been identified [30]. The CaM and PIP_2 are able to interact with all individual components of the TRPM4-SUR1-AQP4 complex [1,12,31–33]. Moreover, the potential binding sites for PIP_2 and CaM seem to be indiscriminately localised near the cytoplasmic membrane–water interface [34]. Thus, the bi-lobal CaM can potentially bridge and keep together all members of the TRPM4-SUR1-AQP4 complex [35]. In fact, the affinity of TRPM4 to CaM and its sensitivity to intracellular calcium are doubled after TRPM4 co-assembly with SUR1 [31]. Apparently, the TRPM4 antagonists or molecules that somehow disturb the TRPM4-SUR1-AQP4 complex can be used to modulate AQP4 indirectly [30]. Therefore, it is highly needed to decipher the TRPM4-SUR1-AQP4-CaM/PIP_2 structure at the atomic level.

Here, we have used in vitro and in silico approaches to identify potential CaM-binding epitopes at the intracellular N- and C-termini of TRPM4, which are both proximal to the functionally important

S1–S4 sensor domain. Short peptides representing these TRPM4-binding epitopes have been characterised by a fluorescence anisotropy (FA)-binding assay for their ability to anchor various endogenous ligands (CaM, S100A1 and PIP_2). The importance of representative basic amino acids and their combinations from both TRPM4 peptides for the recognition of the above-mentioned endogenous ligands has been determined by means of site-directed mutagenesis. Computer models of all complexes have been studied using extensive molecular dynamics (MD) simulations. Overall, six shared binding sites for CaM, S100A1 and PIP_2 at the N- and C-termini of TRPM4 have been identified and characterised. This indicates considerable promiscuity of the potential binding epitopes within the intracellular tails of TRPM4.

2. Results

2.1. The Design of Peptides Representing Potential TRPM4-Binding Epitopes for CaM, S100A1 and PIP_2

Two potential binding epitopes at the intracellular N- and C- termini of TRPM4 (Figure 1A) were proposed using the Calmodulin Target Database [34]. The N-terminal-binding epitope (positions F627–L648) was represented by the FGECYRSSEVRAARLLLRRCPL peptide (hereinafter termed "M4nt_WT"). The TRPM4 C-terminal-binding epitope (positions P1078–S1098) was represented by the PFIVISHLRLLLRQLCRRPRS peptide (hereinafter termed "M4ct_WT"). The M4nt_WT and M4ct_WT peptides (and their mutants) were used to study their ability to bind CaM, S100A1 and PIP_2. In vitro FA experiments and in silico molecular modelling (protein–protein docking and MD simulations) were used for this purpose, as described in subsequent paragraphs.

2.2. CaM and S100A1 Form Complexes with M4nt_WT and M4ct_WT

First, we studied whether M4nt_WT and M4ct_WT are able to bind CaM and S100A1 at all. The carboxyfluorescein-labelled M4nt_WT and M4ct_WT peptides were titrated with increasing amounts of CaM or S100A1, and FA was measured for each point of titration. The FA increased due to a slower rotational diffusion of the formed complexes, and the fraction bound (F_b) of M4nt_WT and M4ct_WT could be calculated (Figures 2A–5A). Since the specific interactions of M4nt_WT and M4ct_WT with CaM/S100A1 were calcium-dependent [36–40], all samples were measured in the presence of 200-μM $CaCl_2$. The fluorescence lifetimes τ_i of all peptides and their complexes (and all the following characterised peptides/complexes) were constant during all the experiments, with the values close to 3 ns. All complexes were characterised using their dissociation constants (K_D): M4nt_WT/CaM with K_D = 1.3 (SD 1.8) μM, M4nt_WT/S100A1 with K_D = 2.7 (SD 0.5) μM, M4ct_WT/CaM with K_D = 2.6 (SD 0.5) μM and M4ct_WT/S100A1 with K_D = 12 (SD 3.0) μM (Figures 2B–5B). Overall, the FA results indicated the high affinity of M4nt_WT and M4ct_WT peptides to CaM and S100A1. Both M4nt_WT and M4ct_WT peptides thus seemed to represent potential binding epitopes on TRPM4.
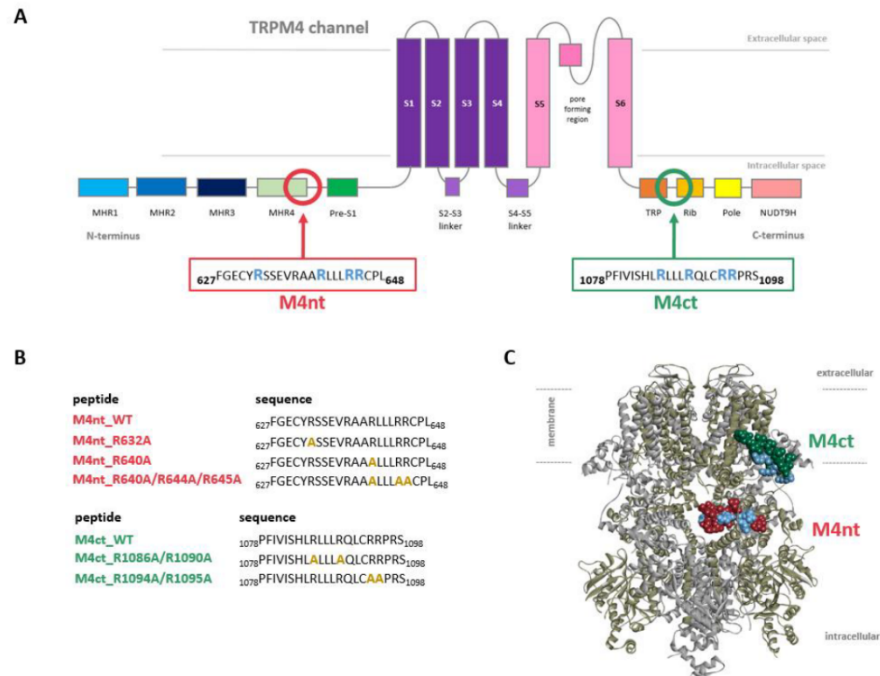
Figure 1. Localisation of transient receptor potential cation channel subfamily melastatin member 4 (TRPM4)-binding epitopes. (**A**) A scheme of the transmembrane topology and domain organisation of the TRPM4. The receptor is composed of six transmembrane helices (S1–S6, violet and pink), with a pore region between the 5th and 6th servers for the transport of monovalent ions (K^+ and Na^+). The MHR1–4 and pres-S1 (blue and green) show N-terminal modulatory domains. The Trp, Rib, Pole and NUDT9H (orange, yellow and pink) display the C-terminal modulatory domains. The predicted modulatory binding epitopes—N-terminal (M4nt and F627–L648, deep-pink frame) and C-terminal (M4ct and P1078–S1098, green frame)—display putative calmodulin (CaM), S100A1 and phosphatidylinositol 4, 5-bisphosphate (PIP_2)-binding epitopes. (**B**) The peptide M4nt and M4ct wild types and their mutant forms synthesised from the designed TRPM4-binding epitopes. The gold alanine residues in the peptide sequences show the mutated positions of the original blue arginine residues. (C) The TRPM4 structure side view (6BQV) with M4nt (deep-pink ball representation) and M4ct (green ball representation)-binding epitopes; the blue highlighted (ball representation) arginines display the potential critical basic residues involved in ligand (CaM, S100A1 and PIP2) interactions. The opposite TRPM4 homomeric subunits are shown in the cartoon representation by grey and army colours.
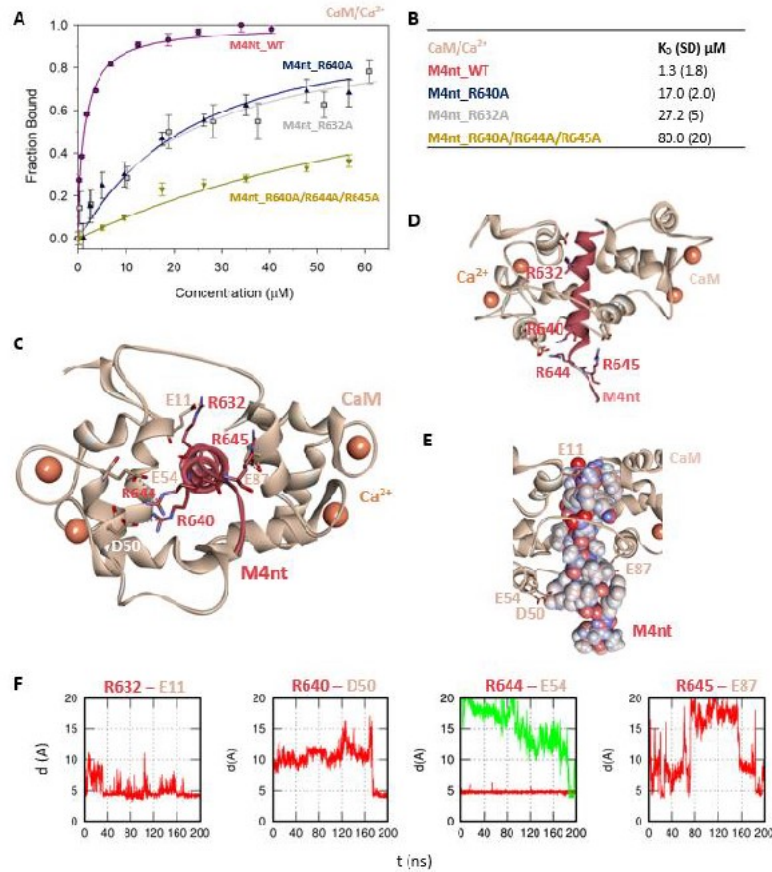
Figure 2. The M4nt/CaM complex. (**A**) The F_B of fluorescently labelled M4nt_WT (wild type) (circles), M4nt_R632A (squares), M4nt_R640A (up-triangles) and M4nt_R640A/R644A/R645 (down-triangles) as a function of CaM (beige) concentrations. M4nt peptides were titrated by CaM, and F_B was calculated according to Equation (1); the solid lines represent the best fit to the binding isotherm from Equation (2) (Methods). (**B**) The equilibrium K_D of the M4nt-binding epitope in complexes with CaM obtained by steady-state fluorescence anisotropy (FA). (**C**) M4nt/CaM in the context of the whole CaM in the presence of Ca^{2+} as a result of molecular dynamics (MDs). The side chains of M4nt (ribbon representation, deep-pink colour) amino acids involved in salt bridges with their binding counterparts from CaM (ribbon representation, beige colour) in atomic detail displayed as sticks: R632-E11, R640-D50, R644-E54 and R645-E87. (**D**) The M4nt/CaM complex from the upper view; M4nt and CaM are shown in the same representation as in Figure 2C, with displayed R632, R640, R644 and R645 basic residues (stick representation, deep-pink colour) involved in the interactions with CaM. (**E**) The M4nt/CaM complex from the upper view; M4nt is shown in CPK representation (partial charge colouring), CaM displayed with E11, D50, E54 and E87 negatively charged residues (stick representation, beige colour) involved in the interactions with M4nt. Ca^{2+} displayed in a ball representation, orange colour. (**F**) Time-dependent geometry characteristics of the studied salt bridges R632-E11, R640-D50, R644-E54 and R645-E87 from MD simulations. A stable salt bridge is expected to have a distance of about 5Å between the termini of oppositely charged amino acids. K_D: equilibrium dissociation constant.
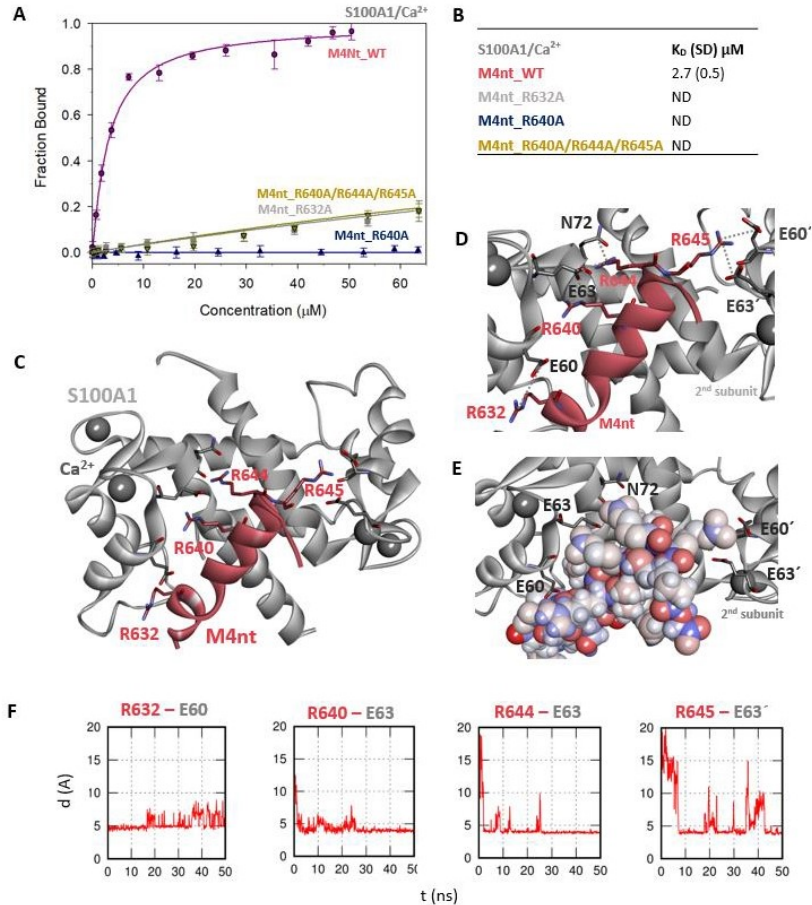
Figure 3. The M4nt/S100A1 complex. (**A**) The F_B of fluorescently labelled M4nt_WT (circles), M4nt_R632A (squares), M4nt_R640A (up-triangles) and M4nt_R640A/R644A/R645 (down-triangles) as a function of S100A1 (grey) concentrations. M4nt peptides were titrated by S100A1, and F_B was calculated according to Equation 1; the solid lines represent the best fit to the binding isotherm from Equation 2 (Methods). (**B**) The equilibrium K_D of the M4nt-binding epitope in complexes with S100A1 obtained by steady-state FA. (**C**) M4nt/S100A1 in the context of the whole S100A1 in the presence of Ca^{2+} as a result of MDs. The side chains of M4nt (ribbon representation, deep-pink colour), with displayed R632, R640, R644 and R645 basic residues involved in the interaction with S100A1 (ribbon representation, grey colour). (**D**) The M4nt/S100A1 complex in detailed view; the binding partners are shown in the same representation as in Figure 3C, with salt bridges in atomic detail displayed as sticks: R632-E60, R640-E63, R644-E63, N72 and R645-E60′ and E63′ of the 2nd monomer. (**E**) The M4nt/S100A1 complex in detailed view; M4nt is shown in CPK (partial charge colouring) representation, S100A1 displayed with E60, E63 and N72 of the 1st monomer and E60′ and E63′ of the 2nd S100A1 monomer with negatively charged residues (stick representation, grey colour) involved in the interactions with M4nt. Ca^{2+} displayed in a ball representation, grey colour. (**F**) Time-dependent geometry characteristics of the studied salt bridges R632-E60, R640-E63, R644-E63 and R645-E63′ from the MD simulations. A stable salt bridge is expected to have a distance of about 5 Å between the termini of oppositely charged amino acids. ND: not determined.
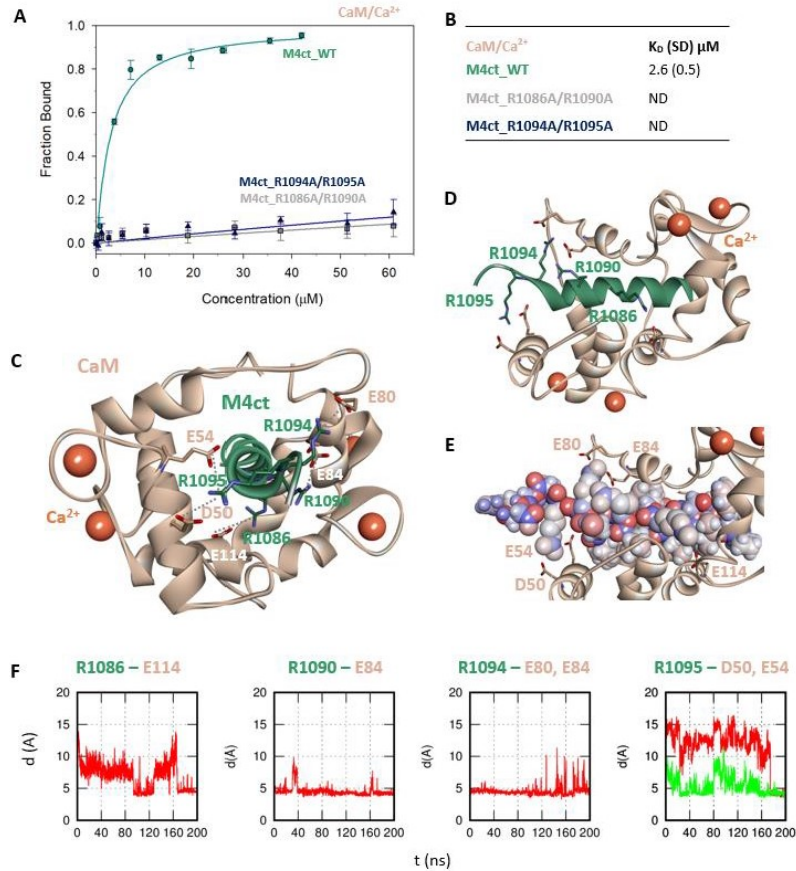
Figure 4. The M4ct/CaM complex. (**A**) The F_B of fluorescently labelled M4ct_WT (circles), M4ct_R1086A/R1090A (squares) and M4ct_R1094A/R1095A (up-triangles) as a function of CaM (beige) concentrations. M4ct peptides were titrated by CaM, and F_B was calculated according to Equation (1); the solid lines represent the best fit to the binding isotherm from Equation (2) (Methods). (**B**) The equilibrium K_D of the M4ct-binding epitope in complexes with CaM obtained by steady-state FA. (**C**) M4ct/CaM in the context of the whole CaM in the presence of Ca^{2+} as a result of MDs. The side chains of the M4ct (ribbon representation, green colour) amino acids involved in salt bridges with their binding counterparts from CaM (ribbon representation, beige colour) in atomic detail displayed as sticks: R1086-E114, R1090-E84, R1094-E80, E84 and R1095-D50 and E54. (**D**) The M4ct/CaM complex from the upper view; M4ct and CaM are shown in the same representation as Figure 4C, with displayed R1086, R1090, R1094 and R1095 basic residues (stick representation, green color) involved in the interactions with CaM. (**E**) The M4ct/CaM complex from a detailed upper view; M4ct is shown in CPK representation (partial charge colouring), CaM displayed with D50, E54, E80, E84 and E114 negatively charged residues (stick representation, beige colour) involved in the interactions with M4ct. Ca^{2+} displayed in a ball representation, orange colour. (**F**) Time-dependent geometry characteristics of the studied salt bridges R1086-E114, R1090-D84, R1094-E80 and E84 and R1095-D50 and E54 from MD simulations. A stable salt bridge is expected to have a distance of about 5Å between the termini of oppositely charged amino acids.
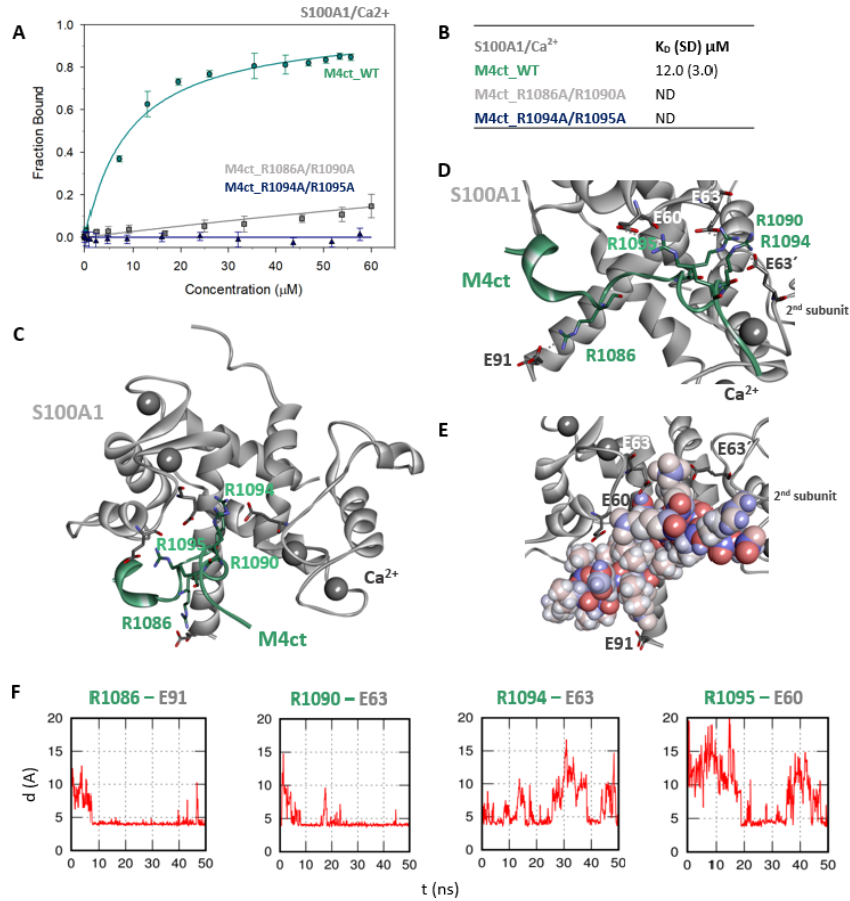
Figure 5. The M4ct/S100A1 complex. (**A**) The F_B of fluorescently labelled M4ct_WT (circles), M4ct_R1086A/R1090A (squares) and M4ct_R1094A/R1095A (up-triangles) as a function of S100A1 (grey) concentrations. M4ct peptides were titrated by S100A1, and F_B was calculated according to Equation (1); the solid lines represent the best fit to the binding isotherm from Equation (2) (Methods). (**B**) The equilibrium K_D of the M4ct-binding epitope in complexes with S100A1 obtained by steady-state FA. (**C**) M4ct/ S100A1 in the context of the whole S100A1 in the presence of Ca^{2+} as a result of MDs. The side chains of M4ct (ribbon representation, green colour) with displayed R1086, R1090, R1094 and R1095 basic residues involved in the interaction with S100A1 (ribbon representation, grey colour). (**D**) The M4ct/S100A1 complex in detailed view; the binding partners are shown in the same representation as in Figure 5C, with salt bridges in atomic detail displayed as sticks: R1086-E91, R1090-E63, R1094-E63 and R1095-E60 and R1090- and R1094-E63´ of the 2nd monomer. (**E**) The M4ct/S100A1 complex in detailed view; M4ct is shown in CPK (partial charge colouring) representation, S100A1 displayed with E60, E63 and N72 of the 1st monomer and E63´ of the 2nd S100A1 monomer, with negatively charged residues (sticks representation, grey colour) involved in the interactions with M4ct. Ca^{2+} displayed in a ball representation, grey colour. (**F**) Time-dependent geometry characteristics of the studied salt bridges R1086-E91, R1090-E63, R1094-E63 and R1095-E60 from MD simulations. A stable salt bridge is expected to have a distance of about 5Å between the termini of oppositely charged amino acids.

2.3. The Basic Amino Acids of M4nt_WT and M4ct_WT are Crucial for Binding to CaM and S100A1

Further, we examined the involvement of selected basic residues in interactions (presumably salt bridges) stabilising complexes of both peptides with CaM and S100A1. We were interested in the positional dependence of these interactions and their potential cooperativity. Therefore, several representative analogues of both peptides by alanine scanning mutagenesis were prepared (see Figure 1B: M4nt_R632A, M4nt_R640A, M4nt_R640A/R644A/R645A, M4ct_R1086A/R1090A and M4ct_R1094A/R1095A). For M4nt_R632, an approx. 20-fold decrease of binding affinity to CaM with K_D = 27.2 (SD 5) μM (Figure 2B) was observed. For M4nt_R640A, there was an approx. 13-fold decrease of binding affinity to CaM with K_D = 17 (SD 2) μM. The triple-mutant M4nt_R640A/R644A/R645A confirmed that basic amino acids work cooperatively, because about 62-fold higher K_D = 80 (SD 20) μM than in the case of M4nt_WT was determined. Moreover, the M4nt_R632A, M4nt_R640A and M4nt_R640A/R644A/R645A mutant peptides were not able to bind S100A1 at all (Figure 3B). Further, a total loss of M4ct_R1086A/R1090A and M4ct_R1094A/R1095A-binding to CaM and S100A1 were observed with $K_D \gg 250$ μM—i.e., in the "not determined" (ND) range (Figures 4B and 5B). The maximum concentrations of the proteins and peptides were, in some cases, limited by precipitation and their solubility; therefore, it was not possible to achieve the saturation (plateau), basically. To summarise, the FA measurements confirmed that all the studied basic amino acids of both peptides substantially stabilised their complexes with CaM and S100A1 (Figures 2A,B–5A,B).

2.4. The Binding Interfaces of M4nt_WT/CaM and M4ct_WT/CaM Complexes

The binding interfaces of M4nt_WT/CaM and M4ct_WT/CaM were studied in detail by in silico molecular modelling (i.e., by protein–protein docking and MD simulations). Initially, both peptides (preorganised into α-helices) were docked into various CaM structures that had originally been complexed with peptides carrying hydrophobic anchors in the canonical positions 1–10 (3SUI) [41], 1–14 (1CDL) [42] and 1–17 (2BCX) [43]. The amino acid sequences of M4nt_WT and M4ct_WT peptides contain many bulky hydrophobic amino acids that can serve as hydrophobic anchors orienting peptides properly with respect to CaM. Nevertheless, the phenylalanines at the N-termini of both peptides (i.e., F627 in M4nt_WT and F1079 in M4ct_WT) are best suited for this purpose. Therefore, antiparallel complexes where these N-terminal phenylalanines were buried into the hydrophobic cavity in the C-domain of CaM were selected as the most appropriate for the positioning. Subsequently, the M4nt_WT/CaM and M4ct_WT/CaM complexes were relaxed by means of extensive MD simulations.

More specifically, the protein–protein docking of M4nt_WT into the 1–17 (2BCX) structure of CaM provided two complexes that corresponded to the canonical hydrophobic binding motifs 1–14/1–17 and 1–10. The R632, R644 and R645 of M4nt_WT were involved in the salt bridges formed with E11, D50, E54 and E87 of CaM (according to conventional numbering). During the MD simulations, all the studied basic amino acids of M4nt_WT (i.e., R632, R640, R644 and R645) were significantly involved in the salt bridges with the acidic residues E11, D50, E54 and E87 of CaM (Figure 2C–F, Figure S1).

The protein–protein docking of M4ct_WT into the 1–14 (1CDL) structure of CaM resulted in a complex with the hydrophobic-binding motif 1–7/1–10. A similar complex was obtained by the docking of M4ct_WT into the 1–17 (2BCX) structure of CaM. However, only R1090 and R1094 of M4ct_WT formed salt bridges with their acidic counterparts of CaM. Nevertheless, within subsequent MD simulations, all the studied basic amino acids (i.e., R1086, R1090, R1094 and R1095) successfully found their acidic counterparts D50, E54, E80, E84 and E114 in CaM (Figure 4C–F, Figure S2).

To summarise, M4nt_WT/CaM and M4ct_WT/CaM complexes have been obtained. All the studied basic amino acids formed salt bridges with CaM (regardless of their initial conformation) during MD simulations. This indicates their importance, explored by alanine mutants, which lost their affinity, demonstrated by apparent increases in the K_D values.

2.5. The Binding Interfaces of M4nt_WT/S100A1 and M4ct_WT/S100A1 Complexes

In addition, both M4nt_WT and M4ct_WT peptides were docked into the S100A1 structures (2KBM and 2K2F) [44], which had originally been complexed with peptides representing the TRTK12 and RyRP12-binding epitopes.

The most reasonable complex identified by the ClusPro protein–protein docking process revealed that the M4nt_WT peptide was bound to the main binding site of S100A1 [40,43]. During subsequent MD simulations, M4nt_WT retained the canonical alpha-helical conformation, and numerous stabilising salt bridges were established (Figure 3C–F). The M4nt_WT R632 formed a salt bridge with E60 from the first monomer of S100A1. The same applied for the R640 and R644 of M4nt_WT, forming salt bridges with E63 from the first monomer of S100A1. Moreover, the R644 interaction with N72 from the first monomer of S100A1 was observed. There were two additional salt bridges between R645 and E60′ and E63′ of the second monomer of S100A1. This means that M4nt_WT was able to bridge both S100A1 subunits. Furthermore, the K56 of S100A1 from the first monomer was bound to the acidic E635 of M4nt_WT.

The M4ct_WT/S100A1 complex identified by the ClusPro web server was completely consistent with known crystal structures in the sense that the hydrophobic L1087 of M4ct_WT was directed to the binding site defined by the V57, L77 and L81 side chains of S100A1. It was similar to RyRP12 peptide binding in the 2K2F structure [44]. However, the number of stabilising salt bridges substantially increased within a subsequent MD run (Figure 5C–F). In fact, all the studied basic amino acids were found to be bound by salt bridges to the first monomer of S100A1: R1086-E91, R1090-E63, R1094-E63 and R1095-E60. Moreover, R1090 and R1094 also formed salt bridges with E63′ of the second monomer of S100A1.

Analogously to the previous binding of M4nt and M4ct to CaM, M4nt_WT/S100A1 and M4ct_WT/S100A1 complexes were obtained that led to the establishment of numerous salt bridges being stable during the simulation. In both cases studied, the importance of basic amino acids in the binding epitope was proved.

2.6. M4nt_WT and M4ct_WT Bind PIP$_2$

To identify the M4nt_WT/PIP$_2$ and M4ct_WT/PIP$_2$ complexes, we again used steady-state FA measurements with PIP2, labelled as TopFluor® PI (4, 5) P2 (Avanti polar lipids, Alabaster, Alabama 35007-9105, USA). The PIP$_2$ was titrated with increasing amounts of nonlabelled M4nt_WT or M4ct_WT, and FA was measured for each point of titration. The fraction bound (F_b) was calculated for M4nt_WT and M4ct_WT (Figure 6A). The complexes were characterised by the determination of K_D. The K_D of the M4nt_WT/PIP$_2$ complex was 18.0 (SD 4.0), whereas the K_D of the M4ct_WT/ PIP$_2$ complex was 0.9 (SD 0.2) µM (Figure 6B).

2.7. The Binding Interface of the PIP$_2$/M4ct_WT Complex

To determine the positioning of the PIP2 in the M4ct_WT/PIP$_2$ complex, ten independent MD runs were performed, each lasting 100 ns. The total length of the MD trajectories reached 1 µs. There was no interaction between the M4ct peptide and the PIP2 detected at the beginning of the MD simulations. M4ct_WT and PIP2 were separated by bulk water molecules. The first contacts between PIP$_2$ and M4ct_WT were established relatively quickly, usually after about 10 ns, and electrostatic interactions were substantially involved in this process. PIP$_2$ had three phosphate groups with a total charge of −5. M4ct_WT carried the exact opposite charge, +5. Additional stabilisation can originate from contacts of hydrophobic lipid tails of PIP$_2$ with hydrophobic amino acids of M4ct_WT. A typical result of the MD simulations is depicted in Figure 6C,D. In this particular case, salt bridges were formed between phosphate groups of PIP$_2$ and arginine side chains of M4ct_WT (R1090, R1094 and R1095—involved in CaM/S100A1 complexes).
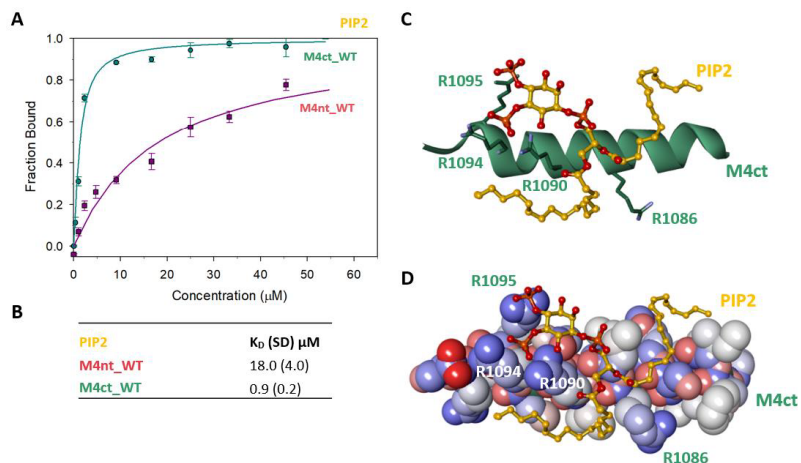
Figure 6. The M4nt/PIP$_2$ and M4ct/PIP2 complexes. (**A**) The F$_B$ of M4ct_WT (circles) and M4nt_WT (squares) as a function of PIP$_2$ (yellow) concentrations. The labelled PIP$_2$ was titrated by M4nt or M4ct peptides, and F$_B$ was calculated according to Equation (1); the solid lines represent the best fit to the binding isotherm from Equation (2) (Methods). (**B**) The equilibrium K$_D$ of PIP$_2$ in complexes with M4nt and M4ct peptides obtained by steady-state FA. (**C,D**) Spontaneous association of PIP$_2$ (ball and stick representation, yellow colour) and M4ct (sticks in green colour or CPK with a partial-charge representation) was observed within a 100-ns MD run. The salt bridges were formed between the phosphate groups of PIP$_2$ and R1090, R1094 and R1095 of M4ct (green colour, stick representation).

3. Discussion

The modulation of receptors by CaM and S100A1 is well-described in the scientific literature [20,39,43]. For the RyR1 receptor, two overlapping binding epitopes have been characterised for CaM and S100A1 [45]. The competition between CaM and S100A1 for the overlapping binding epitopes of TRPs and other receptors (e.g., RyR1) has already been investigated [39,44–47]. In vitro experiments have previously confirmed the competition of CaM and S100A1 at the very same concentration levels [46].

In the presented study, we have decided to investigate whether CaM, S100A1 and PIP$_2$ can also share binding epitopes in TRPM4. The Ca^{2+}-dependent formation of protein/peptide complexes has been described many times [39,47]. The in vitro Ca^{2+} concentrations used to stimulate the M4/CaM/S100A1 interactions were hence maintained at the same concentration level of 200 μM. Two potential binding epitopes for the endogenous modulators of TRPM4 have been identified in the N- and C-termini of TRPM4-representing peptides. The binding affinities of the M4nt_WT and M4ct_WT peptides to endogenous modulators were examined in vitro, which revealed a typical micromolar range of K$_D$ values [36,40,46–48]. The N-terminal binding site (M4nt_WT) is apparently able to bind CaM and S100A1; moreover, the C-terminal binding site (M4ct_WT) binds PIP$_2$ as well. The relative occupancy of endogenous modulators will depend on their actual concentration in the intracellular environment. Regarding the lower physiological concentrations of S100A1 as compared to the abundant CaM [49], we suppose that, in vivo, both potential binding epitopes in TRPM4 will be occupied predominantly by CaM.

Generally, the binding of CaM and S100A1 to epitopes involves two distinct driving forces. The first is mostly of long-range electrostatic and rather nonspecific character, resulting in salt bridges with the involvement of long and flexible arginine side chains acting in synergy. The second driving force is apparently of Van der Waals origin, in which the most important role is played by dispersion.

Ultimately, the so-called hydrophobic anchors of peptides are properly placed into the binding cavities of CaM and S100A1. Here, we have only addressed the importance of electrostatic forces by means of FA measurements and arginine-to-alanine mutagenesis. A set of representative basic amino acids and their combinations was used. Nevertheless, computer modelling was based on the profound bioinformatics analysis of both peptides to identify all potential hydrophobic anchors situated in well-known canonical positions. Based on that, we usually chose as reliable only those results of protein–protein docking where bulky hydrophobic anchors of M4nt_WT/M4ct_WT peptides were buried into the binding cavities of CaM/S100A1. Overall, our docking results showed that both M4ct_WT and M4nt_WT peptides bind to CaM in an antiparallel manner. Finally, we allowed all complexes to relax by means of extensive MD simulations. Thanks to this, we have obtained final models where all mutated basic amino acids of both peptides have found their acidic binding partners in CaM/S100A1/PIP2 endogenous modulators of TRPM4.

The currently known structures of TRPM4 obtained at the resolution of ∼2.88–3.8 Å [8,9,11] have suggested that the so-called TRP domain (i.e., W1058–R1098, which includes M4ctWT-P1078–1098) bridges the gating helix S6 and cytoplasmic C-terminal Rib helix. This domain is considered as a key determinant for signal transduction and channel gating [10]. The TRP domain is divided into two characteristic segments, the first of which is the helical stretch running parallel to the cytosolic surface of the membrane as an extension of S6, labelled as the TRP helix. The second TRP domain segment is a re-entrant loop and helix. The re-entrant loop (P1073–P1077) is embedded between helices S1 and S2 of the transmembrane S1–S4 sensor domain, whereas the re-entrant helix (P1078–R1098, i.e., M4ct) is located at the cytoplasmic side. The M4ct segment is thus perfectly positioned to interact with such membrane-embedded molecules as PIP_2. It has been also described that the TRPC3 C-terminal loop (connecting the re-entrant and Rib helix) affects channel gating by altering the allosteric coupling between the cytoplasmic and transmembrane domains [50]. Electrophysiological analyses have disclosed that the shortening of the length of the C-terminal loop increases TRPC3 activity and that the elongation of the length of the loop has the opposite effect. The C-terminal moiety of TRPM4 was proposed to be a target of CaM already in several previous studies [1,20,21]. However, all cryo-EM structures of TRPM4 show the re-entrant helix embedded in the membrane—i.e., not readily available for CaM. Nevertheless, the moiety is a common feature of TRPM, TRPC and TRPV channels. In several TRPC structures, this segment has not been resolved, which indicates conformational disorder [51]. More interestingly, a comparison of available TRPV2 structures (see the amino acids 675–684 in 5HI9 [51] and 6BWM [52]) shows that, under suitable conditions, the re-entrant moiety can be re-localised into the cytoplasm, and it is available for modulatory bindings. This probably allows interactions with endogenous modulators other than the membrane-anchored PIP_2 (including CaM and S100A1). The M4nt_WT is in proximal contact with the so-called Rib helix, which forms another binding site for CaM, confirmed by experiments in TRPM4 [1], as well as in structurally homologous TRPC channels [53]. An examination of the currently available TRPM4 structures has led us to the conclusion that the M4nt_WT and M4ct_WT segments are close enough to simultaneously bind one CaM molecule. This means that M4nt_WT might serve as a base for conformational changes stimulated by the CaM of the re-entrant moiety, which includes M4ct_WT.

The C-terminal segment of TRPM4 was previously designed as a target for PIP_2 [10]. Our results provide a detailed description of the binding interface. The structure of TRPV5-PIP_2 (PDB: 6DMU) discloses the binding site between the N-linker, S4-S5linker and S6-helix of TRPV5 [28]. These interactions with PIP_2 induce conformational rearrangements in the lower gate, resulting in channel activation. Furthermore, based on the TRPM4-SUR1-AQP4 complex, we assume that PIP_2 could potentially keep M4ct_WT and the TMD0 of SUR1 domains together, as seen in the Kir6.2-SUR1 complex [54]. Interestingly, the M4ct_WT-PIP_2 interactions could be physiologically relevant in a specialised cardiac conduction system and Purkinje fibres [55]. Mutations in the TRPM4 gene (including mutations in the C-terminal part of TRPM4) have been reported to cause familial cases of progressive cardiac conduction disease and heart block [5]. In particular, I1082S and R1086G mutants were

identified when a total of 330 cases of sudden, unexpected deaths were tested for cardiac channelopathy and cardiomyopathy genes [55].

4. Conclusions

Since TRPM4 has been designated as a functional agent of various diseases, including cancer and heart attack [3,5], it is necessary to describe in detail its function and modulation mechanisms. In this work, we describe two new binding sites at the N- and C-termini of the channel. In particular, the M4nt_WT and M4ct_WT intracellular segments of TRPM4 have been confirmed as shared binding epitopes for commonly known [26,46] endogenous modulators such as CaM, S100A1 and PIP$_2$. The shared, so-called promiscuous characters of some ligand-binding sites is a known feature of many proteins [56–59]. The receptor-binding segment exploits its disorder character to be more flexible and adaptable to bind different types of ligands. Each ligand with a diverse binding affinity to the receptor domain induces distinct structural changes in the channel, resulting in a different functional response and channel modulation. The novel TRPM4 N- and C-terminal promiscuous binding sites for CaM, S100A1 and PIP2 are promising candidates for the diverse modulation of the channel. Such ligands are commonly utilised by cells as activators and/or inhibitors of the functions of many receptors. The effect and strength of the regulation depends on the character of an acceptor (receptor) binding interface and the structural changes induced within. CaM, S100A1 and PIP2 have been proven as effective modulatory molecules of many receptors [20,26,39]. Moreover, the effect of the modulation can be multiplied across shared ligand-binding sites via more channel subunits [15], indicating a very complex regulatory process that occurs during receptor communication with the external environment. We suppose that these new M4nt/CaM-, M4nt/S100A1-, M4nt/PIP2-, M4ct/CaM-, M4ct/S100A1- and M4ct/PIP2-binding interfaces described in atomic detail will help to clarify multicomplex TRPM4 modulatory functions and will stimulate further functional studies of the whole TRPM4 by in vivo assays with the listed promising ligands.

5. Materials and Methods

5.1. Design of TRPM4 N- and C- Terminal Binding Epitopes

For the identification of novel CaM-binding motifs commonly defined by the hydrophobic positions 1-5-10 and 1-10-14 or by the IQ motif at the intracellular N- and C- termini of human TRPM4 (UniProtKB/Swiss-Prot: Q8TD43), we used the Calmodulin Target Database [34]. This tool was also utilised to identify a S100A1-binding epitope because it is known that this ligand recognises the binding motif at the receptor, very often overlapping with a CaM-binding site with the same or very similar hydrophobic positions [40,45]. Furthermore, we have also identified the potential PIP2-binding sites using PH-domain characteristics [60,61].

5.2. M4nt and M4ct Peptide Synthesis and Site-Directed Mutagenesis

M4nt and M4ct peptides and their alanine-scanning analogues were synthesised by solid-phase peptide synthesis according to the Nα-Fmoc protocol in our previous publication [40].

5.3. CaM, S100A1 Purification and PIP2 Preparation

CaM and S100A1 cDNAs were subcloned into the pET28b expression vector, and they were expressed and purified according to our standard purification protocol [40]. The fluorescently labelled PIP2, 1-oleoyl-2- {6- [4- (dipyrrometheneboron difluoride) butanoyl] amino}x hexanoyl-sn-glycero-3-phosphoinositol-4,5-bisphosphate, shortly TopFluor® PI(4,5)P2, was purchased from Avanti Polar Lipids, Inc. (Alabaster, AL, USA).

5.4. Steady-State Fluorescence Anisotropy

The experiments were performed on a K2 spectrofluorometer (ISS, Inc., Champaign, IL, USA) at 25 °C in a cuvette with a 2-mm path length. The FA-binding assays were performed in a 25-mM Tris-HCl (pH 7.5) buffer containing 250-mM NaCl and 200-μM CaCl$_2$. M4nt and M4ct peptides were labelled by carboxyfluorescein and titrated by small aliquots of the ligands (CaM and S100A1). In the opposite way, labelled PIP$_2$ was titrated with nonlabelled M4 peptides. Fluorescence was excited at 490 nm, and polarised emission components I_{II} and $I_\perp$, required for the construction of the emission anisotropy, were acquired and averaged quasi-simultaneously at 525 nm by repetitive switching of the emission polariser. Any residual scattered light was suppressed by a long-pass dielectric filter (520 nm) placed in front of the input slit of the emission monochromator. The anisotropy values r were calculated from the fluorescence intensities in the parallel (I_{II}) and perpendicular ($I_\perp$) directions according to the relationship $r = (I_{II} - GI_\perp)/(I_{II} + 2GI_\perp)$ [62], where G is a factor correcting for different transmittance of the detection channel for the two measured polarisations (I_{II} and $I_\perp$). The G factor was determined in a separate experiment. The measurements were repeated six times for each ligand concentration; the mean anisotropy value was calculated and used for further analysis. The fractions of bound ligands F_B were evaluated as [63]:

$$F_B = (r\text{obs} - r\text{min}) \,/\, [(r\text{max} - r\text{obs})Q + (r\text{obs} - r\text{min})], \tag{1}$$

where Q is the quantum-yield ratio of the bound to the free form of the labelled peptide; r_{max} is the anisotropy of the complex at saturation; r_{min} is the minimum anisotropy for free M4nt, M4ct or PIP$_2$ and r_{obs} is the measured anisotropy at any intermediate ligand concentration. The Q was evaluated for every binding experiment from the ratio of the fluorescence lifetimes of the bound to the free M4nt, M4ct or PIP$_2$: Q = τ_{bound}/τ_{free}. For the determination of the equilibrium dissociation constant (K$_D$), F_B was plotted as a function of the ligand concentration and fitted by [64]:

$$F_B = \frac{K_D + [P1] + [P2] - \sqrt{(K_D + [P1] + [P2])^2 - 4[P1][P2]}}{2[P1]}, \tag{2}$$

where [P1] represents the M4nt, M4ct or PIP$_2$ concentration, and [P2] is the ligand concentration. Nonlinear data fitting was performed using SigmaPlot 11.0 (Systat software, Inc., San Jose, CA 95110, USA).

5.5. Time-Resolved Fluorescence Measurements

Fluorescence lifetimes were evaluated at room temperature in a drop placed on a coverslip and inserted in an inverted confocal microscope IX83 (Olympus, Hamburg, Germany) equipped with TimeHarp 260 PICO time-correlated single-photon counting electronics and cooled GaAsP hybrid detectors (all PicoQuant, Berlin, Germany). The M4 peptides or PIP$_2$ fluorescence were excited at 485 nm by an LDH-485 picosecond laser head (PicoQuant, Berlin, Germany). Emission decays were collected in the epifluorescence mode using a combination of a 488-nm dichroic reflector (Olympus, Hamburg, Germany) and a Semrock 520/35 bandpass filter in the detection path. Fluorescence was assumed to decay multiexponentially according to the formula:

$$I(t) = \sum_i \alpha_i \times exp^{\left(\frac{-t}{\tau_i}\right)} \tag{3}$$

where τ_i are fluorescence lifetimes and α_i the corresponding amplitudes. The intensity-weighted mean fluorescence lifetime was calculated as:

$$\tau_{mean} = \sum_i \alpha_i \times \tau_i^2 \,/\, \sum_i \alpha_i \times \tau_i \tag{4}$$

The least-squares deconvolution fitting was performed by the SymPho Time 64 software (PicoQuant).

5.6. Protein–Protein Docking

The ClusPro web server was used for the docking of α-helical M4nt_WT/M4ct_WT peptides (created using the Molefacture module in VMD studio) [65] into the CaM and S100A1 structures. The ClusPro 2.0: protein-protein docking server was chosen based on the results of the community-wide contest called CAPRI (Critical Assessment of Predicted Interactions), in which ClusPro is traditionally doing well [66]. The quality of the very fast, fully automated and reproducible docking produced by ClusPro is very close to that of the best human predictor groups, which can use any type of information [67].

The ClusPro server performs rigid-body docking by sampling billions of conformations by means of the PIPER docking program [68], which is based on the Fourier transform (FFT) correlation approach. RMSD-based clustering of the 1000 lowest-energy structures generated makes it possible to find the centres of the largest clusters that represent the most likely models of the complex. Selected structures are refined using energy minimisation.

5.7. Molecular Dynamics Simulations

The protein–peptide complexes obtained by protein–protein docking were simulated by means of extensive MD sampling at different temperatures. The MD simulations of the selected complexes utilised the AMBER_ILDN (The Amber Project, San Francisko CA 94158-2517, USA) force field [69], and water molecules were modelled using the Transferable Intermolecular Potential 3-Point (TIP3P) water model [70]. Prior to the production of MD simulations, all systems were energy-equilibrated using the *pmemd* module of AMBER 14 [71]. MD runs (lasting for 50–1800 ns) were performed with the *pmemd.cuda.MPI* module of AMBER 14, which runs exclusively on GPUs at the equivalent speed of tens of standard processor cores [72]. The SPFP precision model was used, and periodic boundary conditions (PBC) were applied. The particle-mesh Ewald (PME) method was used for the calculation of electrostatic interactions [73]. A cut-off distance of 8 Å was applied for Lennard-Jones interactions. The temperature was maintained at 300K via Langevin dynamics with a friction factor of 5. The Monte Carlo barostat (a new addition to AMBER 14), which samples rigorously from the isobaric–isothermal ensemble, was used for the production phase. The covalent bonds involving hydrogen atoms were constrained using the SHAKE algorithm. For water molecules, a special "three-point" RATTLE algorithm was used [74]. The hydrogen mass repartitioning scheme allowed a timestep set to 4 fs [75]. Data were recorded every 100 ps.

The PIP_2-M4ct_WT complex was explored by long MD runs. The simulated complex was solvated using a (TIP3P) water model [70] to ensure at least 10 Å of solvent in the periodic box and neutralised in 0.5-M NaCl. This gave a periodic box with a size of ~ $60 \times 60 \times 60$ Å for a simulated system consisting of ~19,000 atoms. All-atom structure and topology files were generated using VMD [63]. Forces were computed using a CHARMM36 forcefield for proteins, lipids and ions [76]. MD simulations were produced by means of the software package NAMD2.13 [77], running on workstations equipped with NVIDIA graphics processing units. Simulated systems were energy-minimised and heated to 300 K. Langevin dynamics were used for temperature control, with the target temperature set to 300 K, and the Langevin piston method was applied to reach an efficient pressure control with a target pressure of 1 atm [77]. The production of the MD runs was 100 ns. The integration timestep was set to 2 fs. The SETTLE algorithm (tolerance, 1×10^{-8}) was applied to constrain the bonds in the water molecules [78]. The nonbonded cut-off was set to 11 Å. Data were recorded every 20 ps. All MD trajectories were visualised with the aid of the VMD 1.9 software package [65] and analysed by means of the CPPTRAJ module from the AMBER Tools suite [79]. The figures were produced using the Biovia Discovery Studio [80].

Abbreviations

ATP	Adenosine triphosphate
CaM	Calmodulin
EM	Electron microscopy
FA	Fluorescence anisotropy
FFT	Fourier transform
MD	Molecular dynamics
PBC	Periodic boundary conditions
PH	Pleckstrin homology
PIP_2	phosphatidylinositol 4, 5-bisphosphate
PME	particle mesh Ewald
S100A1	S100 calcium-binding protein A1
TRPs	transient receptor potential (channels)
TRPC	TRP canonical
TRPV	TRP vaniloid
TRPM4	TRP melastatin 4

References

1. Nilius, B.; Prenen, J.; Tang, J.; Wang, C.; Owsianik, G.; Janssens, A.; Voets, T.; Zhu, M.X. Regulation of the Ca^{2+} sensitivity of the nonselective cation channel TRPM4. *J. Biol. Chem.* **2005**, *280*, 6423–6433. [CrossRef]
2. Clapham, D.E.; Runnels, L.W.; Strübing, C. The TRP ion channel family. *Nat. Rev. Neurosci.* **2001**, *2*, 387. [CrossRef] [PubMed]
3. Ehara, T.; Noma, A.; Ono, K. Calcium-activated non-selective cation channel in ventricular cells isolated from adult guinea-pig hearts. *J. Physiol.* **1988**, *403*, 117–133. [CrossRef] [PubMed]
4. Launay, P.; Fleig, A.; Perraud, A.-L.; Scharenberg, A.M.; Penner, R.; Kinet, J.-P. TRPM4 is a Ca^{2+}-activated nonselective cation channel mediating cell membrane depolarization. *Cell* **2002**, *109*, 397–407. [CrossRef]
5. Tian, J.; An, X.; Fu, M. Transient receptor potential melastatin 4 cation channel in pediatric heart block. *Eur. Rev. Med. Pharmacol. Sci.* **2017**, *21*, 79–84. [PubMed]
6. Nilius, B.; Prenen, J.; Droogmans, G.; Voets, T.; Vennekens, R.; Freichel, M.; Wissenbach, U.; Flockerzi, V. Voltage dependence of the Ca^{2+}-activated cation channel TRPM4. *J. Biol. Chem.* **2003**, *278*, 30813–30820. [CrossRef] [PubMed]
7. Mathar, I.; Jacobs, G.; Kecskes, M.; Menigoz, A.; Philippaert, K.; Vennekens, R. Trpm4. In *Mammalian Transient Receptor Potential (TRP) Cation Channels*; Springer: Berlin, Germany, 2014; pp. 461–487.
8. Duan, J.; Li, Z.; Li, J.; Santa-Cruz, A.; Sanchez-Martinez, S.; Zhang, J.; Clapham, D.E. Structure of full-length human TRPM4. *Proc. Natl. Acad. Sci. USA* **2018**, *115*, 2377–2382. [CrossRef] [PubMed]
9. Autzen, H.E.; Myasnikov, A.G.; Campbell, M.G.; Asarnow, D.; Julius, D.; Cheng, Y. Structure of the human TRPM4 ion channel in a lipid nanodisc. *Science* **2018**, *359*, 228–232. [CrossRef]

10. Winkler, P.A.; Huang, Y.; Sun, W.; Du, J.; Lü, W. Electron cryo-microscopy structure of a human TRPM4 channel. *Nature* **2017**, *552*, 200. [CrossRef]

11. Guo, J.; She, J.; Zeng, W.; Chen, Q.; Bai, X.-c.; Jiang, Y. Structures of the calcium-activated, non-selective cation channel TRPM4. *Nature* **2017**, *552*, 205. [CrossRef] [PubMed]

12. Nilius, B.; Mahieu, F.; Prenen, J.; Janssens, A.; Owsianik, G.; Vennekens, R.; Voets, T. The Ca^{2+}-activated cation channel TRPM4 is regulated by phosphatidylinositol 4, 5-biphosphate. *EMBO J.* **2006**, *25*, 467–478. [CrossRef] [PubMed]

13. Zhang, Z.; Okawa, H.; Wang, Y.; Liman, E.R. Phosphatidylinositol 4, 5-bisphosphate rescues TRPM4 channels from desensitization. *J. Biol. Chem.* **2005**, *280*, 39185–39192. [CrossRef]

14. Vennekens, R.; Nilius, B. Insights into TRPM4 function, regulation and physiological role. In *Transient Receptor Potential (TRP) Channels*; Springer: Berlin, Germany, 2007; pp. 269–285.

15. Singh, A.K.; McGoldrick, L.L.; Twomey, E.C.; Sobolevsky, A.I. Mechanism of calmodulin inactivation of the calcium-selective TRP channel TRPV6. *Sci. Adv.* **2018**, *4*, eaau6088. [CrossRef] [PubMed]

16. De Groot, T.; Kovalevskaya, N.V.; Verkaart, S.; Schilderink, N.; Felici, M.; van der Hagen, E.A.; Bindels, R.J.; Vuister, G.W.; Hoenderop, J.G. The molecular mechanisms of calmodulin action on TRPV5 and the modulation by parathyroid hormone. *Mol. Cell. Biol.* **2011**, *31*, 2845–2853. [CrossRef]

17. Villalobo, A.; González-Muñoz, M.; Berchtold, M.W. Proteins with calmodulin-like domains: Structures and functional roles. *Cell. Mol. Life Sci.* **2019**, *76*, 2299–2328. [CrossRef] [PubMed]

18. Tabernero, L.; Taylor, D.A.; Chandross, R.J.; VanBerkum, M.F.; Means, A.R.; Quiocho, F.A.; Sack, J.S. The structure of a calmodulin mutant with a deletion in the central helix: Implications for molecular recognition and protein binding. *Structure* **1997**, *5*, 613–622. [CrossRef]

19. Rhoads, A.R.; Friedberg, F. Sequence motifs for calmodulin recognition. *FASEB J.* **1997**, *11*, 331–340. [CrossRef]

20. Zhu, M.X. Multiple roles of calmodulin and other Ca^{2+}-binding proteins in the functional regulation of TRP channels. *Pflügers Archiv.* **2005**, *451*, 105–115. [CrossRef]

21. Hasan, R.; Zhang, X. Ca^{2+} regulation of TRP ion channels. *Int. J. Mol. Sci.* **2018**, *19*, 1256. [CrossRef]

22. Rohacs, T.; Nilius, B. Regulation of transient receptor potential (TRP) channels by phosphoinositides. *Pflügers Archiv. Eur. J. Physiol.* **2007**, *455*, 157–168. [CrossRef]

23. Lemmon, M.A.; Ferguson, K.M.; O'Brien, R.; Sigler, P.B.; Schlessinger, J. Specific and high-affinity binding of inositol phosphates to an isolated pleckstrin homology domain. *Proc. Natl. Acad. Sci. USA* **1995**, *92*, 10472–10476. [CrossRef] [PubMed]

24. Yamaguchi, S.; Tanimoto, A.; Iwasa, S.; Otsuguro, K.-i. TRPM4 and TRPM5 Channels Share Crucial Amino Acid Residues for Ca^{2+} Sensitivity but Not Significance of PI (4, 5) P2. *Int. J. Mol. Sci.* **2019**, *20*, 2012. [CrossRef] [PubMed]

25. Bousova, K.; Jirku, M.; Bumba, L.; Bednarova, L.; Sulc, M.; Franek, M.; Vyklicky, L.; Vondrasek, J.; Teisinger, J. PIP2 and PIP3 interact with N-terminus region of TRPM4 channel. *Biophys. Chem.* **2015**, *205*, 24–32. [CrossRef] [PubMed]

26. Ufret-Vincenty, C.A.; Klein, R.M.; Hua, L.; Angueyra, J.; Gordon, S.E. Localization of the PIP2 sensor of TRPV1 ion channels. *J. Biol. Chem.* **2011**, *286*, 9688–9698. [CrossRef]

27. Yin, Y.; Le, S.C.; Hsu, A.L.; Borgnia, M.J.; Yang, H.; Lee, S.-Y. Structural basis of cooling agent and lipid sensing by the cold-activated TRPM8 channel. *Science* **2019**, *363*, eaav9334. [CrossRef]

28. Hughes, T.E.; Pumroy, R.A.; Yazici, A.T.; Kasimova, M.A.; Fluck, E.C.; Huynh, K.W.; Samanta, A.; Molugu, S.K.; Zhou, Z.H.; Carnevale, V. Structural insights on TRPV5 gating by endogenous modulators. *Nat. Commun.* **2018**, *9*, 4198. [CrossRef]

29. Fine, M.; Schmiege, P.; Li, X. Structural basis for PtdInsP 2-mediated human TRPML1 regulation. *Nat. Commun.* **2018**, *9*, 4192. [CrossRef]

30. Stokum, J.A.; Kwon, M.S.; Woo, S.K.; Tsymbalyuk, O.; Vennekens, R.; Gerzanich, V.; Simard, J.M. SUR1-TRPM4 and AQP4 form a heteromultimeric complex that amplifies ion/water osmotic coupling and drives astrocyte swelling. *Glia* **2018**, *66*, 108–125. [CrossRef]

31. Woo, S.K.; Kwon, M.S.; Ivanov, A.; Gerzanich, V.; Simard, J.M. The sulfonylurea receptor 1 (Sur1)-transient receptor potential melastatin 4 (Trpm4) channel. *J. Biol. Chem.* **2013**, *288*, 3655–3667. [CrossRef]

32. Pratt, E.B.; Tewson, P.; Bruederle, C.E.; Skach, W.R.; Shyng, S.-L. N-terminal transmembrane domain of SUR1 controls gating of Kir6. 2 by modulating channel sensitivity to PIP2. *J. Gen. Physiol.* **2011**, *137*, 299–314. [CrossRef]

33.　Galizia, L.; Pizzoni, A.; Fernandez, J.; Rivarola, V.; Capurro, C.; Ford, P. Functional interaction between AQP2 and TRPV4 in renal cells. *J. Cell. Biochem.* **2012**, *113*, 580–589. [CrossRef] [PubMed]

34.　Yap, K.L.; Kim, J.; Truong, K.; Sherman, M.; Yuan, T.; Ikura, M. Calmodulin target database. *J. Struct. Funct. Genom.* **2000**, *1*, 8–14. [CrossRef] [PubMed]

35.　Roche, J.V.; Törnroth-Horsefield, S. Aquaporin protein-protein interactions. *Int. J. Mol. Sci.* **2017**, *18*, 2255. [CrossRef] [PubMed]

36.　Bily, J.; Grycova, L.; Holendova, B.; Jirku, M.; Janouskova, H.; Bousova, K.; Teisinger, J. Characterization of the S100A1 protein binding site on TRPC6 C-terminus. *PLoS ONE* **2013**, *8*, e62677. [CrossRef]

37.　Grycova, L.; Holendova, B.; Bumba, L.; Bily, J.; Jirku, M.; Lansky, Z.; Teisinger, J. Integrative binding sites within intracellular termini of TRPV1 receptor. *PLoS ONE* **2012**, *7*, e48437. [CrossRef]

38.　Holakovska, B.; Grycova, L.; Bily, J.; Teisinger, J. Characterization of calmodulin binding domains in TRPV2 and TRPV5 C-tails. *Amino Acids* **2011**, *40*, 741–748. [CrossRef]

39.　Prosser, B.L.; Hernández-Ochoa, E.O.; Schneider, M.F. S100A1 and calmodulin regulation of ryanodine receptor in striated muscle. *Cell Calcium* **2011**, *50*, 323–331. [CrossRef]

40.　Bousova, K.; Herman, P.; Vecer, J.; Bednarova, L.; Monincova, L.; Majer, P.; Vyklicky, L.; Vondrasek, J.; Teisinger, J. Shared CaM-and S100A1-binding epitopes in the distal TRPM 4 N terminus. *FEBS J.* **2018**, *285*, 599–613. [CrossRef]

41.　Lau, S.-Y.; Procko, E.; Gaudet, R. Distinct properties of Ca^{2+}–calmodulin binding to N-and C-terminal regulatory regions of the TRPV1 channel. *J. Gen. Physiol.* **2012**, *140*, 541–555. [CrossRef]

42.　Meador, W.E.; Means, A.R.; Quiocho, F.A. Target enzyme recognition by calmodulin: 2.4 A structure of a calmodulin-peptide complex. *Science* **1992**, *257*, 1251–1255. [CrossRef]

43.　Maximciuc, A.A.; Putkey, J.A.; Shamoo, Y.; MacKenzie, K.R. Complex of calmodulin with a ryanodine receptor target reveals a novel, flexible binding mode. *Structure* **2006**, *14*, 1547–1556. [CrossRef] [PubMed]

44.　Wright, N.T.; Prosser, B.L.; Varney, K.M.; Zimmer, D.B.; Schneider, M.F.; Weber, D.J. S100A1 and calmodulin compete for the same binding site on ryanodine receptor. *J. Biol. Chem.* **2008**, *283*, 26676–26683. [CrossRef] [PubMed]

45.　Prosser, B.L.; Wright, N.T.; Hernandez-Ochoa, E.O.; Varney, K.M.; Liu, Y.; Olojo, R.O.; Zimmer, D.B.; Weber, D.J.; Schneider, M.F. S100A1 binds to the calmodulin-binding site of ryanodine receptor and modulates skeletal muscle excitation-contraction coupling. *J. Biol. Chem.* **2008**, *283*, 5046–5057. [CrossRef] [PubMed]

46.　Grycova, L.; Holendova, B.; Lansky, Z.; Bumba, L.; Jirku, M.; Bousova, K.; Teisinger, J. Ca^{2+} Binding Protein S100A1 Competes with Calmodulin and PIP2 for Binding Site on the C-Terminus of the TPRV1 Receptor. *ACS Chem. Neurosci.* **2014**, *6*, 386–392. [CrossRef]

47.　Holakovska, B.; Grycova, L.; Jirku, M.; Sulc, M.; Bumba, L.; Teisinger, J. Calmodulin and S100A1 protein interact with N terminus of TRPM3 channel. *J. Biol. Chem.* **2012**, *287*, 16645–16655. [CrossRef]

48.　Jirku, M.; Lansky, Z.; Bednarova, L.; Sulc, M.; Monincova, L.; Majer, P.; Vyklicky, L.; Vondrasek, J.; Teisinger, J.; Bousova, K. The characterization of a novel S100A1 binding site in the N-terminus of TRPM1. *Int. J. Biochem. Cell Biol.* **2016**, *78*, 186–193. [CrossRef]

49.　Uhlén, M.; Fagerberg, L.; Hallström, B.M.; Lindskog, C.; Oksvold, P.; Mardinoglu, A.; Sivertsson, Å.; Kampf, C.; Sjöstedt, E.; Asplund, A. Tissue-based map of the human proteome. *Science* **2015**, *347*, 1260419. [CrossRef] [PubMed]

50.　Sierra-Valdez, F.; Azumaya, C.M.; Romero, L.O.; Nakagawa, T.; Cordero-Morales, J.F. Structure–function analyses of the ion channel TRPC3 reveal that its cytoplasmic domain allosterically modulates channel gating. *J. Biol. Chem.* **2018**, *293*, 16102–16114. [CrossRef] [PubMed]

51.　Huynh, K.W.; Cohen, M.R.; Jiang, J.; Samanta, A.; Lodowski, D.T.; Zhou, Z.H.; Moiseenkova-Bell, V.Y. Structure of the full-length TRPV2 channel by cryo-EM. *Nat. Commun.* **2016**, *7*, 1–8. [CrossRef]

52.　Zubcevic, L.; Le, S.; Yang, H.; Lee, S.-Y. Conformational plasticity in the selectivity filter of the TRPV2 ion channel. *Nat. Struct. Mol. Biol.* **2018**, *25*, 405–415. [CrossRef]

53.　Zhu, M.X.; Tang, J. TRPC channel interactions with calmodulin and IP$_3$ receptors. *Novartis Found. Symp.* **2004**, *258*, 44–58. [CrossRef] [PubMed]

54.　Martin, G.M.; Yoshioka, C.; Rex, E.A.; Fay, J.F.; Xie, Q.; Whorton, M.R.; Chen, J.Z.; Shyng, S.-L. Cryo-EM structure of the ATP-sensitive potassium channel illuminates mechanisms of assembly and gating. *Elife* **2017**, *6*, e24149. [CrossRef] [PubMed]

55. Subbotina, E.; Williams, N.; Sampson, B.A.; Tang, Y.; Coetzee, W.A. Functional characterization of TRPM4 variants identified in sudden unexpected natural death. *Forensic Sci. Int.* **2018**, *293*, 37–46. [CrossRef]

56. Lindsay, C.; Sitsapesan, M.; Chan, W.M.; Venturi, E.; Welch, W.; Musgaard, M.; Sitsapesan, R. Promiscuous attraction of ligands within the ATP binding site of RyR2 promotes diverse gating behaviour. *Sci. Rep.* **2018**, *8*, 1–13. [CrossRef]

57. Kohda, D. "Multiple partial recognitions in dynamic equilibrium" in the binding sites of proteins form the molecular basis of promiscuous recognition of structurally diverse ligands. *Biophys. Rev.* **2018**, *10*, 421–433. [CrossRef]

58. Brix, J.; Dietmeier, K.; Pfanner, N. Differential recognition of preproteins by the purified cytosolic domains of the mitochondrial import receptors Tom20, Tom22, and Tom70. *J. Biol. Chem.* **1997**, *272*, 20730–20735. [CrossRef]

59. Hainzl, T.; Huang, S.; Meriläinen, G.; Brännström, K.; Sauer-Eriksson, A.E. Structural basis of signal-sequence recognition by the signal recognition particle. *Nat. Struct. Mol. Biol.* **2011**, *18*, 389. [CrossRef]

60. Hansen, S.B.; Tao, X.; MacKinnon, R. Structural basis of PIP 2 activation of the classical inward rectifier K+ channel Kir2. 2. *Nature* **2011**, *477*, 495. [CrossRef] [PubMed]

61. Suh, B.-C.; Hille, B. Regulation of ion channels by phosphatidylinositol 4, 5-bisphosphate. *Curr. Opin. Neurobiol.* **2005**, *15*, 370–378. [CrossRef]

62. Lakowicz, J.R.; Ray, K.; Chowdhury, M.; Szmacinski, H.; Fu, Y.; Zhang, J.; Nowaczyk, K. Plasmon-controlled fluorescence: A new paradigm in fluorescence spectroscopy. *Analyst* **2008**, *133*, 1308–1346. [CrossRef]

63. Harper, C.C.; Berg, J.M.; Gould, S.J. PEX5 binds the PTS1 independently of Hsp70 and the peroxin PEX12. *J. Biol. Chem.* **2003**, *278*, 7897–7901. [CrossRef] [PubMed]

64. Kohler, J.J.; Schepartz, A. Kinetic studies of fos- jun- DNA complex formation: DNA binding prior to dimerization. *Biochemistry* **2001**, *40*, 130–142. [CrossRef] [PubMed]

65. Humphrey, W.; Dalke, A.; Schulten, K. VMD: Visual molecular dynamics. *J. Mol. Graph.* **1996**, *14*, 33–38. [CrossRef]

66. Kozakov, D.; Hall, D.R.; Xia, B.; Porter, K.A.; Padhorny, D.; Yueh, C.; Beglov, D.; Vajda, S. The ClusPro web server for protein–protein docking. *Nat. Protoc.* **2017**, *12*, 255. [CrossRef] [PubMed]

67. Kozakov, D.; Beglov, D.; Bohnuud, T.; Mottarella, S.E.; Xia, B.; Hall, D.R.; Vajda, S. How good is automated protein docking? *Proteins Struct. Funct. Bioinform.* **2013**, *81*, 2159–2166. [CrossRef] [PubMed]

68. Kozakov, D.; Brenke, R.; Comeau, S.R.; Vajda, S. PIPER: An FFT-based protein docking program with pairwise potentials. *Proteins Struct. Funct. Bioinform.* **2006**, *65*, 392–406. [CrossRef]

69. Lindorff-Larsen, K.; Piana, S.; Palmo, K.; Maragakis, P.; Klepeis, J.L.; Dror, R.O.; Shaw, D.E. Improved side-chain torsion potentials for the Amber ff99SB protein force field. *Proteins Struct. Funct. Bioinform.* **2010**, *78*, 1950–1958. [CrossRef]

70. Jorgensen, W.L.; Chandrasekhar, J.; Madura, J.D.; Impey, R.W.; Klein, M.L. Comparison of simple potential functions for simulating liquid water. *J. Chem. Phys.* **1983**, *79*, 926–935. [CrossRef]

71. Salomon-Ferrer, R.; Götz, A.W.; Poole, D.; Le Grand, S.; Walker, R.C. Routine microsecond molecular dynamics simulations with AMBER on GPUs. 2. Explicit solvent particle mesh Ewald. *J. Chem. Theory Comput.* **2013**, *9*, 3878–3888. [CrossRef]

72. Le Grand, S.; Götz, A.W.; Walker, R.C. SPFP: Speed without compromise—A mixed precision model for GPU accelerated molecular dynamics simulations. *Comput. Phys. Commun.* **2013**, *184*, 374–380. [CrossRef]

73. Cheatham, T.I.; Miller, J.; Fox, T.; Darden, T.; Kollman, P. Molecular dynamics simulations on solvated biomolecular systems: The particle mesh Ewald method leads to stable trajectories of DNA, RNA, and proteins. *J. Am. Chem. Soc.* **1995**, *117*, 4193–4194. [CrossRef]

74. Miyamoto, S.; Kollman, P.A. Settle: An analytical version of the SHAKE and RATTLE algorithm for rigid water models. *J. Comput. Chem.* **1992**, *13*, 952–962. [CrossRef]

75. Feenstra, K.A.; Hess, B.; Berendsen, H.J. Improving efficiency of large time-scale molecular dynamics simulations of hydrogen-rich systems. *J. Comput. Chem.* **1999**, *20*, 786–798. [CrossRef]

76. Vanommeslaeghe, K.; MacKerell, A., Jr. CHARMM additive and polarizable force fields for biophysics and computer-aided drug design. *Biochim. Biophys. Acta (BBA)-Gen. Subj.* **2015**, *1850*, 861–871. [CrossRef]

77. Phillips, J.C.; Braun, R.; Wang, W.; Gumbart, J.; Tajkhorshid, E.; Villa, E.; Chipot, C.; Skeel, R.D.; Kale, L.; Schulten, K. Scalable molecular dynamics with NAMD. *J. Comput. Chem.* **2005**, *26*, 1781–1802. [CrossRef]

78. Ryckaert, J.-P.; Ciccotti, G.; Berendsen, H.J. Numerical integration of the cartesian equations of motion of a system with constraints: Molecular dynamics of n-alkanes. *J. Comput. Phys.* **1977**, *23*, 327–341. [CrossRef]

79. Roe, D.R.; Cheatham, T.E., III. PTRAJ and CPPTRAJ: Software for processing and analysis of molecular dynamics trajectory data. *J. Chem. Theory Comput.* **2013**, *9*, 3084–3095. [CrossRef]

80. Biovia, D.S. *Discovery Studio Modeling Environment*; Release 2017; Dassault Systèmes: San Diego, CA, USA, 2016.